

# Interactions of Ammonia with Platinum and Ruthenium Surfaces

Thesis by  
Wilman Tsai

In Partial Fulfillment of the Requirements  
for the Degree of  
Doctor of Philosophy

California Institute of Technology  
Pasadena, California

1987

(Submitted January 29, 1987)

吾生也者  
 涯  
 而  
 知也  
 豈  
 涯  
 以  
 有  
 涯  
 也  
 豈  
 涯  
 孰  
 也

**To my loving wife, Wen-Hsing**

## Acknowledgments

John Vajo worked with me during most of my years at Caltech and we coauthored five papers that are presented in this thesis. He gave me much insights into experimentations and problems solving. I appreciated his friendship as well.

Jim Engstrom also worked with me in many of the experiments and we coauthored one paper in the appendix. We have frequent discussions about research in Rm 123 and I am grateful for many of his helpful inspirations.

Yong-Kui Sun also helped me in one of my works and I am thankful for his assistance.

My advisor, William Henry Weinberg, allowed me much freedom in choosing my research. He always gave me new ideas to try, valuable resources and encouragement. I am grateful to him for all these qualities and for his continuous financial support for all these years.

Others that aided me were—secretary Kathy Lewis, machinists "Chic" Nakawatase and electronics fellows Tom Dunn and John Yehle.

## Abstract

Specific reaction rates ( $\text{cm}^{-2}\text{-s}^{-1}$ ) of the catalytic decomposition of ammonia, the isotopic exchange between ammonia and deuterium, and the inhibition of the decomposition of ammonia by hydrogen (with ammonia to hydrogen partial pressure ratios varying from 1:1 to 1:4) on a polycrystalline platinum wire have been measured in a continuous stirred tank microreactor at pressures between  $5 \times 10^{-7}$  and 0.6 Torr and temperatures between 400 and 1200 K. At relatively low temperatures and/or high pressures, nitrogen adatoms are the dominant surface species, and the recombinative desorption of nitrogen controls the rate of decomposition of ammonia. At relatively high temperatures and/or low pressures, the surface coverage of all species is low, and a competition between the desorption of molecular ammonia and the cleavage of an N-H bond of molecularly adsorbed ammonia controls the rate of reaction. The kinetics of decomposition of ammonia as well as the results for the  $\text{NH}_3 + \text{D}_2$  exchange reaction are described quantitatively by a mechanistic model employing independently measured adsorption-desorption parameters of  $\text{NH}_3$  and  $\text{H}_2$ , and desorption parameters of  $\text{N}_2$ . The model was extended to incorporate the nitrogen coverage-dependence of the rate coefficient of hydrogen desorption to describe the inhibition of the decomposition by hydrogen. The hydrogenation of  $\text{NH}_2(\text{a})$  to produce molecularly adsorbed ammonia is predicted to be the dominant factor in the inhibition of the decomposition of ammonia.

The kinetics of adsorption and desorption of deuterium have been studied on Pt(110)-(1x2) surfaces on which various fractional coverages of nitrogen adatoms were deposited via the decomposition of ammonia at 400 K. Nitrogen

selectively blocks the high temperature  $\beta_2$ -state of deuterium prior to poisoning the low temperature  $\beta_1$ -state. No evidence of a 'long-range' electronic perturbation of the surface by the nitrogen adatoms was found. The adsorption kinetics of deuterium on both clean and nitrogen-precovered Pt(110)-(1x2) surfaces were Langmuirian. Nitrogen modifies the preexponential factor and the activation energy of desorption of deuterium on Pt(110)-(1x2) by essentially rescaling the effective coverage of the deuterium. The results are consistent with findings from previous studies of the inhibition of the decomposition of ammonia by hydrogen on polycrystalline platinum.

Steady-state specific reaction rates have also been measured for the catalytic decomposition of ammonia on a Ru(001) surface at pressures of  $10^{-6}$  and  $2 \times 10^{-6}$  Torr and temperatures between approximately 500 and 1250 K. Qualitatively, the kinetics are similar to those observed for ammonia decomposition on the polycrystalline platinum surface. Based on thermal desorption measurements during the steady-state decomposition of ammonia at  $2 \times 10^{-6}$  Torr, nitrogen adatoms are the dominant surface species, and the recombinative desorption of nitrogen is the major (and probably the only) elementary reaction that produces molecular nitrogen. The mechanistic model developed previously describes accurately the pressure and temperature dependence of both the decomposition kinetics and the measured steady-state coverage of nitrogen adatoms.

The isotopic exchange reaction between  $^{15}\text{NH}_3$  and deuterium at steady-state has been studied on Ru(001) for a partial pressure ratio of ammonia to deuterium of 4:1 with a total pressure of  $2.5 \times 10^{-6}$  Torr at temperatures between 380 and 720 K. All three exchange products were observed, and a dissociative ex-

change mechanism was found to describe quantitatively the experimental data. This mechanistic model is discussed in terms of a potential energy diagram that describes the catalytic decomposition (or *synthesis*) of ammonia on Ru(001). The energy levels of and the activation barriers separating the chemisorbed intermediates in the ammonia decomposition and synthesis reactions, namely,  $\text{NH}_3$ ,  $\text{NH}_2 + \text{H}$ ,  $\text{NH} + 2\text{H}$ ,  $\text{N} + 3\text{H}$  are determined, and the dissociative chemisorption of molecular nitrogen on Ru(001) is found to be activated with an activation energy estimated to be approximately  $5 \text{ kcal}\cdot\text{mol}^{-1}$  in the limit of zero surface coverage of nitrogen adatoms. Direct comparison between the estimated barrier for the dissociative adsorption of nitrogen on polycrystalline platinum and Ru(001) surfaces indicates clearly that ruthenium is a superior catalyst to platinum for the synthesis of ammonia.

# Contents

Acknowledgements	ii
Abstract	iii
Chapter 1: Introduction	1
Chapter 2: Inhibition by Hydrogen of the Heterogeneous Decomposition of Ammonia on Platinum	9
Chapter 3: Perturbations in the Surface Chemistry of Hydrogen by Nitrogen Adatoms on Pt(110)-(1x2)	17
Chapter 4: Steady-State Decomposition of Ammonia on the Ru(001) Surface	58
Chapter 5: "Steady-State" Thermal Desorption Mass Spectrometry	90
Chapter 6: Isotopic Exchange between Ammonia and Deuterium on the Ru(001) Surface	114
Chapter 7: Conclusions	143
Appendix 1: Versatile Microreactor for Studies of Gas-Surface Catalytic Reactions between $10^{-7}$ and 1000 Torr	145
Appendix 2: Mechanistic Details of the Heterogeneous Decomposition of Ammonia on Platinum	150
Appendix 3: The Chemisorption of Hydrogen on the (111) and (110)-(1x2) Surfaces of Iridium and Platinum	160
Appendix 4: Steady-State Decomposition of Ammonia on the Pt(110)-(1x2) Surface	228
Appendix 5: Data Acquisition and Real-time Control Computer Station	234

**Chapter 1.**

**Introduction**

The catalytic synthesis of ammonia via the Haber process [1], developed in Germany between 1908 and 1913, has probably been studied more extensively than any other catalytic reaction. Studies of the mechanism of ammonia synthesis have been extraordinarily productive as they have led to an array of new techniques and new concepts, many of which are due to Paul Emmett and his collaborators. These techniques and concepts have found their way into the theory and practice of heterogeneous catalysis [2]. Among the techniques are the BET method of surface area determination [3], selective chemisorption for surface analysis [4] and the use of isotopes in kinetic and catalytic studies [5]. Among the concepts are activated adsorption, rate-determining step, textural promotion and chemical promotion [6]. Thus for over 70 years, ammonia synthesis has provided a fertile ground for new ideas in catalysis. However, there remain many unanswered questions concerning the mechanism of ammonia synthesis [6,7] such as the energetics of individual reaction steps and the dependence of the reaction on the electronic and structural properties of different metal catalysts. Further research is needed in order to have a full understanding of this important catalytic reaction.

The motivation for this thesis was to further our understanding of the interactions of ammonia, hydrogen and nitrogen with transition-metal surfaces by studying the catalytic decomposition of ammonia, a reaction which is directly related by microscopic reversibility to the synthesis of ammonia from hydrogen and nitrogen. The catalysts chosen are a polycrystalline surface of platinum and single crystalline surfaces of platinum and ruthenium. Platinum is known to be a relatively 'poor' synthesis catalyst [8], while ruthenium (4.5 wt-%) supported on

active carbon and promoted by potassium (3.2 wt-%) is the most active catalyst for ammonia synthesis [9,10]. The methodology followed in this study consists of the following: (1) measuring overall steady-state kinetics over a wide range of pressures and temperatures, (2) independently determining the energetics of specific elementary steps such as the adsorption and desorption of reactants and products, (3) microscopically locating various binding states for adatoms and admolecules, (4) identifying the chemical nature of the adspecies, (5) measuring surface coverages of adspecies *during* the steady-state reaction, (6) numerically modeling these elementary steps via a proposed mechanism over the wide range of pressures and temperatures.

In order to have a complete understanding of any catalytic reaction, it is essential to investigate the reaction in different pressure regimes. At relatively high pressures, near or above atmospheric pressure, a reaction may be studied under conditions that resemble those in actual commercial catalytic chemical processes. In contrast, under ultrahigh vacuum (UHV), the surface composition and structures of a catalyst may be well-characterized. In addition, the energetics of elementary steps such as adsorption and desorption can be readily measured on catalytic surfaces and reaction intermediates can be often isolated and identified under these UHV conditions.

The pressure gap between these two limiting regimes is considered the most serious problem in heterogeneous catalysis. One solution to the problem is the development of high pressure cells [11-13] which allow the reaction to be studied under atmospheric (or even higher) pressures and to analyze the surface afterwards under UHV conditions without exposure to air. However, the kinetics

of catalytic reactions will be primarily determined by the surface concentration rather than by the partial pressure, and higher coverages can also be achieved by lowering the temperature instead of raising the pressure. Furthermore, it would be incorrect to assume that catalytic reactions will always proceed at high surface concentration: the steady-state coverage of a certain species will, in general, be determined by the kinetics of various parallel, consecutive or competitive reaction steps and may thus be rather low even if high pressures are applied. Information on the reaction mechanism may further be obtained by studying the reverse reaction (at low pressure) since the catalyst will only accelerate the rate by which the equilibrium is established and since forward and backward reactions necessarily proceed through the same microscopic steps.

In this thesis, the catalytic decomposition of ammonia, the isotopic exchange reaction of ammonia with deuterium and the inhibition of the decomposition of ammonia by hydrogen on polycrystalline platinum were studied at steady-state, both at low and high pressures, using mass spectrometry. In addition, the adsorption-desorption of ammonia and hydrogen, the desorption of nitrogen, and the steady-state decomposition of ammonia were investigated under UHV conditions on Pt(110)-(1x2) and Ru(001) surfaces via various surface-sensitive techniques. These techniques include thermal desorption mass spectrometry (TDMS), low-energy electron diffraction (LEED), Auger electron spectroscopy (AES), contact potential difference (CPD) measurements and X-ray photoelectron spectroscopy (XPS). Utilizing this kinetic information, a mechanistic model based on elementary steps was developed which contained *very few* adjustable parameters and yielded specific reaction rates and surface coverages over a wide

range of experimental variables thus effectively bridging the "pressure gap" between fundamental surface science studies conducted under UHV conditions and catalytic studies conducted at high pressures [14-16].

In order to measure specific reaction rates over a wide range of pressures, a microreactor system was specially designed to measure steady-state kinetics of heterogeneous catalytic reactions at pressures between  $10^{-7}$  and 1000 Torr, and this is described in Appendix 1. This experimental system was used to study the catalytic decomposition of ammonia and the isotopic exchange reaction of ammonia with deuterium on a polycrystalline platinum surface.

The approach discussed above was implemented in Chapter 2 of this thesis to develop a steady-state, non-equilibrium model for describing the steady-state decomposition of ammonia, the isotopic exchange reaction of ammonia with deuterium and the inhibition of the decomposition of ammonia by hydrogen on polycrystalline platinum. Specific rates have been obtained for these reactions at total pressures from  $5 \times 10^{-7}$  to 0.5 Torr and at temperatures between 400 and 1200 K. The specific rates have been used together with independent experimental results regarding the adsorption-desorption of  $\text{NH}_3$  and  $\text{H}_2$ , and the desorption of  $\text{N}_2$  and reaction intermediates  $\text{NH}$  and  $\text{NH}_2$  to develop a mechanistic model that describes the reaction rates over the complete range of conditions studied. The success of this model attests to the general utility of the approach outlined above, namely, analyzing kinetic data obtained over a wide range of experimental conditions by using kinetic parameters determined independently from UHV measurements.

The kinetics of adsorption and desorption of deuterium have been studied on a nitrogen-precovered Pt(110)-(1x2) surface, and this work is presented in Chapter 3. The modification of the desorption rate coefficients of deuterium on Pt(110)-(1x2) by the nitrogen adatoms was measured quantitatively. The results were found to be consistent with findings from previous studies of the inhibition of the decomposition of ammonia by hydrogen. Furthermore, the energetics of nitrogen desorption from Pt(110)-(1x2) are in agreement with those determined during the steady-state decomposition of ammonia on the same surface, as described in Appendix 4.

The steady-state decomposition of ammonia has also been studied on the Ru(001) surface at pressures of approximately  $10^{-6}$  Torr and temperatures between 500 and 1250 K, and this is described in Chapter 4. The surface composition and the desorption rate coefficients of the product nitrogen have been determined during steady-state decomposition. Together with independently measured rate parameters for the adsorption-desorption of ammonia and hydrogen, the same mechanistic model used for the decomposition of ammonia on platinum was found to be successful in describing the interactions of ammonia with Ru(001).

The transient experimental technique used in Chapter 4 to measure the surface coverage of adspecies *during* the steady-state reaction is described in detail in Chapter 5. By monitoring the partial pressure rise of an adspecies as a function of a linear temperature program *during* the steady-state reaction, useful kinetic parameters can be extracted as a function of surface coverages. In addition, important mechanistic details can be also revealed concerning the

rate-limiting step of the overall reaction.

Finally, the isotopic exchange between ammonia and deuterium together with the decomposition of ammonia have been investigated on a Ru(001) surface at approximately  $10^{-6}$  Torr and temperatures between 380 and 720 K. The results were used to evaluate both the energy levels of and the activation barriers separating the chemisorbed intermediates in the ammonia decomposition and synthesis reactions, namely,  $\text{NH}_3$ ,  $\text{NH}_2 + \text{H}$ ,  $\text{NH} + 2\text{H}$ ,  $\text{N} + 3\text{H}$ , and the activation energy for the dissociative adsorption of nitrogen on Ru(001) in the limit of zero surface coverage via mechanistic modeling. A direct comparison between platinum and ruthenium in activity in the *synthesis* of ammonia was made, and this is presented in Chapter 6.

## References

- [1] F. Haber and G. van Oordt, *Z. Anorg. Chem.*, **43**, 111 (1904); **44**, 341 (1905); S.A. Topham, in *Catalysis, Science and Technology*, Eds., Anderson J.R. and Boudart M., Vol. 7 (Springer-Verlag, Heidelberg, 1986), p. 1.
- [2] M. Boudart, *Chemtech*, **8**, 4 (1978)
- [3] P.H. Emmett and S. Brunauer, *J. Am. Chem. Soc.*, **59**, 1553 (1937)
- [4] P.H. Emmett and R.W. Harkness, *J. Am. Chem. Soc.*, **57**, 1631 (1935)
- [5] Y. Morikawa, A. Ozaki, *J. Catal.* **12**, 145 (1968).
- [6] M. Boudart, *Catal. Rev. Sci. Eng.*, **23**, 1 (1981)
- [7] M. Grunze in *The Chemical Physics of Solid Surfaces and Heterogeneous Catalysis*, D.A. King and D.P. Woodruff, Eds., Vol.4, Elsevier Amsterdam, 1982, p. 143
- [8] G.C. Bond, in *The Physical Basis for Heterogeneous Catalysis*, Eds., E. Drauglis and R.I. Jaffee, (Plenum, New York 1975), p. 53.
- [9] K. Aika, *Angew. Chem. Int. Ed. Engl.* **25**, 558 (1986).
- [10] S. Uchiyama, Y. Hattori, A. Ozaki and K. Aika, *Chem. Letters* 1463 (1981).
- [11] D.W. Goodman, R.D. Kelly, T.E. Madey and J.T. Yates, *J. Catal.* **63**, 226 (1980).
- [12] H.J. Krebs, H.P. Bonzel and G. Gafner, *Surface Sci.* **88**, 269 (1979).
- [13] J. Goschnick and M. Grunze, *J. Vac. Sci. Technol.* **18**, 561 (1981).
- [14] Se.H. Oh, G.B. Fisher, J.E. Carpenter and D.W. Goodman, *J. Catal.* **100**, 360 (1986).
- [15] P. Stoltze and J.K. Norskov, *Phys. Rev. Letters* **55**, 2502 (1985).
- [16] R.D. Kelly and D.W. Goodman in *The Chemical Physics of Solid Surfaces and Heterogeneous Catalysis*, D.A. King and D.P. Woodruff, Eds., Vol.4, Elsevier Amsterdam, 1982, p. 427

**Chapter 2.**

Inhibition by Hydrogen of the Heterogeneous

Decomposition of Ammonia on Platinum

[Chapter 2 consists of an article coauthored with J.J. Vajo and W.H. Weinberg, which appeared in the *Journal of Physical Chemistry* **1985**, 89, 4926.]

## Inhibition by Hydrogen of the Heterogeneous Decomposition of Ammonia on Platinum

W. Tsai, J. J. Vajo, and W. H. Weinberg\*

*Division of Chemistry and Chemical Engineering, California Institute of Technology, Pasadena, California 91125 (Received: May 28, 1985)*

Absolute reaction rates have been measured in a continuous flow microreactor for the inhibition by hydrogen of the heterogeneous decomposition of ammonia over a polycrystalline platinum wire at pressures between  $10^{-3}$  and 0.6 torr, with ammonia to hydrogen partial pressure ratios varying from 1:1 to 1:4 and temperatures between 400 and 1200 K. Inhibition of the decomposition is observed at relatively high total pressures (0.2–0.6 torr) for all temperatures studied. The reaction orders with respect to hydrogen and ammonia are  $-1.5$  and  $1.0$ , respectively, with an apparent activation energy of 38 kcal/mol. For relatively low total pressures ( $10^{-3}$ – $5 \times 10^{-3}$  torr), inhibition is only observed at temperatures below 650 K, where the activation energy varies from 33 to 55 kcal/mol and the reaction order with respect to hydrogen approaches  $-1.5$  at low temperatures. The decomposition becomes uninhibited at high temperatures and the activation energy is 4.5 kcal/mol. The kinetics of this reaction as well as previous results for the  $\text{NH}_3 + \text{D}_2$  exchange reaction are described quantitatively by a mechanistic model employing independently measured adsorption–desorption parameters of  $\text{NH}_3$ ,  $\text{N}_2$ , and  $\text{H}_2$ , where the rate coefficient for hydrogen desorption is a function of the fractional surface coverage of nitrogen adatoms. The hydrogenation of  $\text{NH}_2(\text{a})$  to produce molecularly adsorbed ammonia is predicted to be the dominant factor in the inhibition of the ammonia decomposition.

### 1. Introduction

The catalytic synthesis of ammonia is one of the most important heterogeneous processes ever developed. There have been numerous studies and reviews regarding the mechanism of ammonia synthesis, the kinetics of the reaction, and the characterization of the catalytic surface.<sup>1–9</sup> The catalytic decomposition of ammonia on transition metals has also been investigated extensively, presumably due both to its (apparent) simplicity and its relevance to the synthesis of ammonia. Although the decomposition has been studied widely on platinum,<sup>10–13</sup> a complete mechanism, which describes the reaction over a wide range of experimental conditions in terms of elementary steps, has not been available until recently.<sup>14</sup> In conjunction with the decomposition of pure ammonia, the inhibition by hydrogen of the decomposition reaction has also been examined frequently.<sup>13,15–17</sup> Classical kinetic studies of ammonia decomposition on platinum filaments and evaporated films have been investigated in batch reactors with large excesses of hydrogen in the feed stream ( $P_{\text{H}_2}/P_{\text{NH}_3}$  varying from 3 to 6) at atmospheric pressure and temperatures between 600 and 1000 K. The reaction order with respect to hydrogen under these conditions was reported to vary from  $-1.3$  to  $-1.83$  in different experiments,<sup>15–17</sup> and the apparent activation energy was found to vary over a wide range from 30.1 to 59 kcal/mol.

Loffler and Schmidt studied the inhibition of ammonia decomposition by hydrogen on a platinum wire in a flow reactor at

ammonia partial pressures from 0.05 to 0.65 torr and partial pressures of hydrogen from 0.15 to 0.68 torr in the temperature range between 600 and 1600 K.<sup>13</sup> Using a Langmuir–Hinshelwood (L-H) rate expression, they determined that the reaction order with respect to hydrogen was  $-1.5 \pm 0.3$  and that the activation energy approaches 32 kcal/mol asymptotically at low temperatures. They were able to fit the L-H rate expression to within 20% of their experimental data over the complete range of temperatures and pressures that they studied. While the Langmuir–Hinshelwood rate expression provides a consistent framework for discussion of a heterogeneous reaction, it gives no microscopic information concerning the energetics and the mechanistic details of the reaction, and the lack of kinetic parameters for the adsorption and desorption of  $\text{NH}_3$ ,  $\text{H}_2$ , and  $\text{N}_2$  precluded a critical evaluation of particular kinetic models.

The presence of hydrogen in the reactant stream can influence the decomposition of ammonia in the following two ways: (1) adsorbed hydrogen may react chemically, by hydrogenating intermediates generated during the decomposition; and (2) chemisorbed hydrogen may block surface sites that are necessary for ammonia adsorption. Each of these inhibition mechanisms has been observed previously.<sup>18–21</sup> Apel'baum and Temkin determined from their kinetic measurements at low temperatures and 0.01 torr total pressure that during ammonia decomposition on a platinum wire, the surface coverage of nitrogen decreases with an increase in the partial pressure of hydrogen.<sup>18</sup> This observation is consistent with both a hydrogenation reaction and a site blocking mechanism. However in a recent review, Grunze, considering the results of Loffler and Schmidt,<sup>13</sup> attributed the inhibition of the decomposition of ammonia by hydrogen to the reverse reaction, the hydrogenation reaction to reform ammonia.<sup>19</sup> In addition, using laser-induced fluorescence,<sup>20</sup> Selwyn and Lin showed that the addition of hydrogen ( $\leq 0.15$  torr) to 0.1 torr of ammonia at 1200–1400 K enhances the yield of NH radicals desorbing from a polycrystalline platinum wire. They suggested that this is due to a surface reaction that converts  $\text{N}(\text{a})$  to  $\text{NH}(\text{a})$ . Thermal desorption mass spectrometry experiments showed that the amount of ammonia adsorbed on a ruthenium (0001) surface previously saturated with hydrogen is diminished when compared to ammonia

- (1) Boudart, M. *Catal. Rev.-Sci. Eng.* **1981**, *23*, 1.
- (2) Grunze, M.; Bozso, F.; Ertl, G. "Proceedings of the 7th International Vacuum Congress, Vienna, 1977"; Dobrozemsky: Vienna, 1977; p 1137.
- (3) Boudart, M. In "Physical Chemistry: An Advanced Treatise"; Eyring, H., Ed.; Academic Press: New York, 1975; p 1.
- (4) Ertl, G. *Catal. Rev.-Sci. Eng.* **1980**, *21*, 201.
- (5) Emmett, P. H.; Brunauer, S. *J. Am. Chem. Soc.* **1934**, *56*, 35.
- (6) Emmett, P. H. In "The Physical Basis for Heterogeneous Catalysis"; Drauglis, E.; Jaffee, R. I., Eds.; Plenum Press: New York, 1975; pp 3–34.
- (7) Boudart, M. In "Proceedings of the 6th International Congress on Catalysis, London, 1976"; Royal Society of Chemistry: Letchworth, U.K., 1977; Vol. 1.
- (8) Love, K. S.; Emmett, P. H. *J. Am. Chem. Soc.* **1941**, *63*, 3297.
- (9) Emmett, P. H.; Kummer, J. T. *Ind. Eng. Chem.* **1943**, *35*, 677.
- (10) Melton, C. E.; Emmett, P. H. *J. Phys. Chem.* **1964**, *68*, 3318.
- (11) Gland, J. L.; Kollin, E. B. *Surf. Sci.* **1981**, *104*, 478.
- (12) Loffler, D. G.; Schmidt, L. D. *Surf. Sci.* **1976**, *59*, 195.
- (13) Loffler, D. G.; Schmidt, L. D. *J. Catal.* **1976**, *41*, 440.
- (14) Vajo, J. J.; Tsai, W.; Weinberg, W. H. *J. Phys. Chem.* **1985**, *89*, 3243.
- (15) Dixon, J. K. *J. Am. Chem. Soc.* **1931**, *53*, 2071.
- (16) Logan, S. R.; Kemball, C. *Trans. Faraday Soc.* **1960**, *56*, 144.
- (17) Robertson, A. J. B.; Willhoft, E. M. A. *Trans. Faraday Soc.* **1967**, *63*, 476.

- (18) Apel'baum, L. O.; Temkin, M. I. *Russ. J. Phys. Chem.* **1959**, *33*, 585.
- (19) Grunze, M. In "The Chemical Physics of Solid Surfaces and Heterogeneous Catalysis"; King, D. A., Woodruff, D. P., Eds.; Elsevier: Amsterdam, 1982; Vol. 4, p 150.
- (20) Selwyn, G. S.; Lin, M. C. *Chem. Phys.* **1982**, *67*, 213.
- (21) Danielson, L. R.; Dresser, M. J.; Donaldson, E. E.; Dickinson, J. T. *Surf. Sci.* **1978**, *71*, 599.

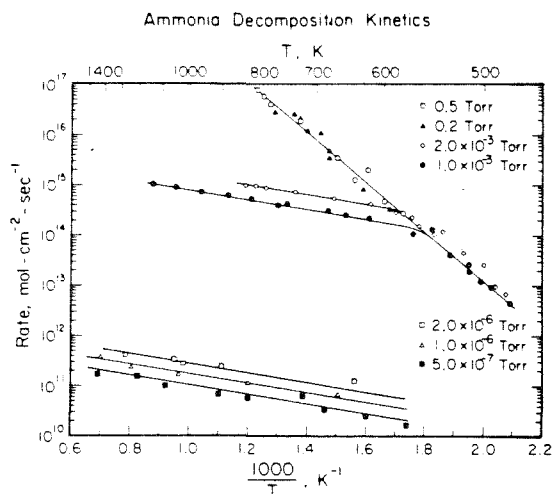


**Figure 1.** Arrhenius plots of the rate of ammonia decomposition on platinum for ammonia pressures of 0.5, 0.2,  $2 \times 10^{-3}$ ,  $1 \times 10^{-3}$ ,  $2 \times 10^{-6}$ ,  $1 \times 10^{-6}$ , and  $5 \times 10^{-7}$  torr. Lines have been drawn through the data points as a visual aid.

adsorption on the clean surface, although no detailed calibration was made to determine the reduction quantitatively.<sup>21</sup> Similar qualitative results were obtained by preadsorbing deuterium on a Pt(111) surface.<sup>11</sup> Apparently, hydrogen adatoms either block the surface sites necessary for ammonia adsorption or indirectly affect the nature of the ammonia adsorption sites, thereby reducing the amount adsorbed.

In a recent study in our laboratory of the steady-state decomposition of  $\text{NH}_3$  and  $\text{ND}_3$  over polycrystalline platinum at pressures between  $5 \times 10^{-7}$  and 0.5 torr and temperatures between 400 and 1200 K, the energetics of the reaction mechanism were clarified by employing a steady-state nonequilibrium model to describe the experimental results in terms of elementary surface reactions.<sup>14</sup> It was found that ammonia decomposes with zero-order kinetics at low temperatures and/or high pressures. Under these conditions the reaction rate is controlled by the desorption of the product nitrogen. A first-order dependence on ammonia pressure was observed at high temperatures and/or low pressures, where the rate of decomposition is controlled by a surface reaction involving the cleavage of an N-H bond. These data are summarized in the form of an Arrhenius plot in Figure 1. In addition, the isotopic exchange reaction,  $\text{NH}_3 + \text{D}_2$ , produced all three exchange products through a mechanism involving dissociative adsorption of both  $\text{NH}_3$  and  $\text{D}_2$ . In particular, reasonable agreement with the experimental data was obtained from model calculations by assuming that  $\text{ND}_3$  results from the deuteration of nitrogen adatoms. Furthermore, during the course of a  $\text{NH}_3 + \text{D}_2$  exchange experiment at a total pressure of  $1.2 \times 10^{-3}$  torr, inhibition of the decomposition reaction was observed at low temperatures.<sup>14</sup>

The various reaction steps included in the model to describe the decomposition and the isotopic exchange reaction are the following:

1. The adsorption and desorption of the reactants,  $\text{NH}_3$  and  $\text{D}_2$ , and the desorption of the products  $\text{N}_2$ ,  $\text{H}_2$ ,  $\text{HD}$ ,  $\text{NH}_2\text{D}$ , and  $\text{ND}_3$  from the surface. (Note that in order to simplify the calculation of the steady-state reaction rates, the surface species  $\text{NH}(\text{a})$  and  $\text{ND}(\text{a})$  were omitted from the model. Consequently, the production of  $\text{NHD}_2$ , which would have resulted from deuteration of  $\text{NH}(\text{a})$ , is not included.)

2. The surface reaction of deuterium adatoms with  $\text{NH}_2(\text{a})$  and  $\text{ND}_2(\text{a})$  to form  $\text{NH}_2\text{D}(\text{a})$  and  $\text{ND}_3(\text{a})$ .

3. The surface reaction of nitrogen with deuterium adatoms to form the intermediate  $\text{ND}_2(\text{a})$ . Hydrogenation of the intermediates  $\text{N}(\text{a})$  and  $\text{NH}_2(\text{a})$  was omitted because the rate of hydrogenation was found to be an order of magnitude lower than

the rate of deuteration under our experimental conditions.

By formulating the model in terms of elementary surface reactions, no assumption was made concerning any chemisorption equilibrium on the catalytic surface, as is implicit in the L-H approach. Moreover, it should be emphasized that all the kinetic parameters used in the model are coverage-independent, and the success of the model in predicting absolute decomposition rates indicates the relative insensitivity of the rate parameters to surface coverages. This can be understood as follows. At high temperatures, where the surface coverage of all species is low, the model is sensitive only to the kinetic parameters for the surface reaction and ammonia desorption, although in this case the nitrogen desorption parameters approach the low coverage limiting values. Similarly, at low temperatures, where the surface coverage of nitrogen approaches unity, the model is sensitive only to the nitrogen desorption parameters. However, thermal desorption studies of nitrogen desorption from a polycrystalline platinum wire indicate that the activation energy as well as the preexponential factor of the nitrogen desorption rate coefficient are rather constant over a range of surface coverage from 0.1 to 0.9.<sup>22</sup> On the other hand, the variation with surface coverage of the desorption rate coefficient of hydrogen is irrelevant since the backward surface reaction is negligible during the decomposition of pure ammonia under differential conditions.

In the work described here, we have studied the inhibition of ammonia decomposition by hydrogen over polycrystalline platinum at total pressures from  $10^{-3}$  to 0.6 torr with ammonia to hydrogen partial pressure ratios varying from 1:1 to 1:4, and at temperatures between 400 and 1200 K. On the basis of our measured absolute rates, we have extended our previous mechanistic model to describe accurately the inhibition reaction over the full range of experimental conditions studied and to improve the agreement between the model calculations and the exchange data.

The organization of this paper is the following. Experimental details are described in section 2, and the experimental data are presented in section 3. A refined mechanistic model is developed in section 4 and discussed in section 5. Finally, the results are summarized in section 6.

## 2. Experimental Procedures

The experiments were performed over a range of total pressures from  $10^{-3}$  to 0.6 torr in a steady-state flow microreactor that has been described previously.<sup>14,23</sup> The catalyst was a 20-cm length of 0.0125-cm-diameter high purity (99.99%) polycrystalline platinum wire. Ammonia (99.99%, anhydrous grade) and hydrogen (99.995%, research grade) were initially mixed in a manifold system in the various partial pressure ratios. The reaction products, which leaked through a capillary tube from the main chamber of the reactor, were monitored continuously by an EA1 1200 quadrupole mass spectrometer in a high vacuum section with a base pressure of approximately  $10^{-8}$  torr. The reactor is shown schematically in Figure 2. Calibration of the mass spectrometer was achieved by adding different pressures of nitrogen to the feed (ammonia + hydrogen) representing conversions of less than 10% and monitoring the product nitrogen signal. The average residence time in the reactor was established via experiments that determined the absolute pumping speed for various mixtures of ammonia and hydrogen. Absolute reaction rates were then obtained by using the continuous stirred tank reactor (CSTR) equation. The reactor was well characterized as a CSTR from a series of step-response experiments.<sup>23</sup>

Prior to the decomposition experiments, the platinum wire was heated in  $10^{-3}$ –0.1 torr of oxygen (99.99%) at 1100 K for 4 h and then reduced in  $10^{-3}$ –0.1 torr of hydrogen (99.995%) under the same conditions. The actual pressures corresponded to the pressure at which the decomposition of ammonia was carried out subsequently. This treatment led to reproducible decomposition rates of ammonia.

(22) Wilf, M.; Dawson, P. T. *Surf. Sci.* **1976**, *60*, 561.

(23) Vajo, J. J.; Tsai, W.; Weinberg, W. H. *Rev. Sci. Instrum.*, in press.

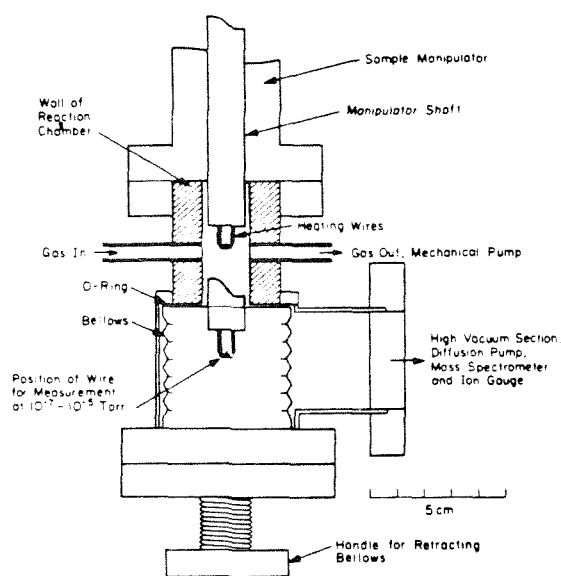


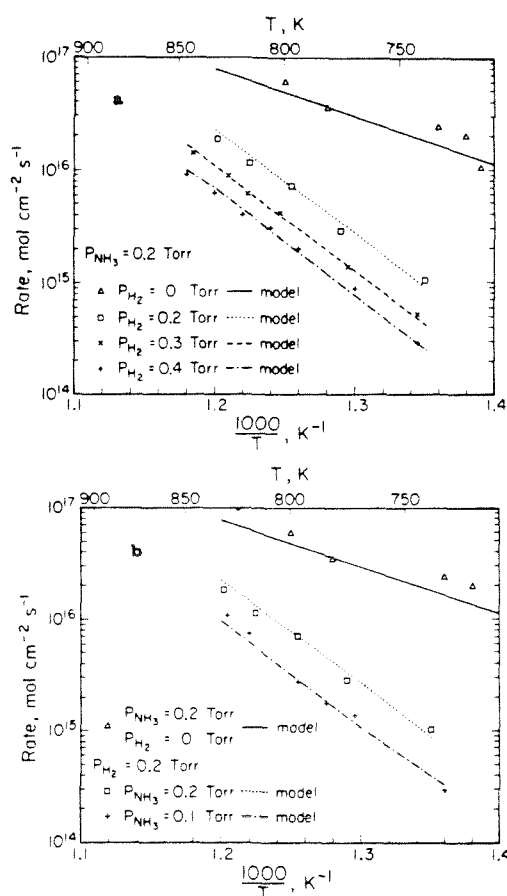
**Figure 2.** Cross section of microreactor body showing the wire in position for experiments at both  $10^{-3}$ - and  $10^{-5}$ -torr. Ports for pressure measurement and the leak to the high-vacuum section, which are orthogonal to the inlet and outlet flow ports, are not shown. The volume of the baratron and the access ports together with the shaded region is the reactor volume,  $30 \text{ cm}^3$ . The sample manipulator is described in detail elsewhere.<sup>23</sup>

### 3. Experimental Results

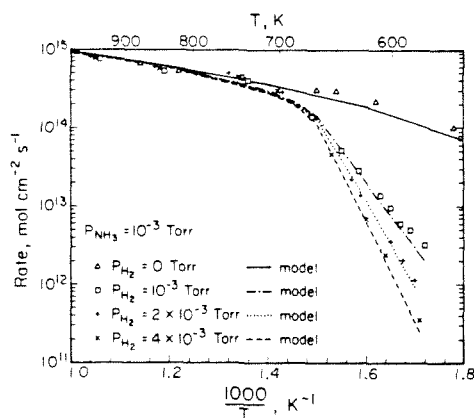
Absolute reaction rates for the decomposition of ammonia with hydrogen inhibition are shown in Figures 3 and 4 as a function of reciprocal temperature for total pressures from  $10^{-3}$  to 0.6 torr with ammonia to hydrogen partial pressure ratios varying from 1:1 to 1:4. (The curves in Figures 3 and 4 designate results of model calculations which will be discussed in the next section.) Pronounced inhibition of ammonia decomposition is observed for total pressures between 0.3 torr ( $P_{\text{H}_2}/P_{\text{NH}_3} = 2$ ) and 0.6 torr ( $P_{\text{H}_2}/P_{\text{NH}_3} = 2$ ) over the whole range of temperatures studied, as may be seen in Figure 3 parts a and b. Inhibition was observed at low temperatures, below approximately 650 K, for pressures between  $2 \times 10^{-3}$  torr ( $P_{\text{H}_2}/P_{\text{NH}_3} = 1$ ) and  $5 \times 10^{-3}$  torr ( $P_{\text{H}_2}/P_{\text{NH}_3} = 4$ ), as may be seen in Figure 4. The degree of inhibition is indicated by the magnitude of the difference in reaction rates between pure ammonia and an ammonia-hydrogen mixture with the same partial pressure of ammonia (Figure 3 and 4). The reaction order with respect to hydrogen between 0.3 and 0.6 torr total pressure is  $-1.5 \pm 0.3$  (Figure 3a) and that with respect to ammonia is  $1.0 \pm 0.2$  (Figure 3b). These results are in agreement with earlier results of Loffler and Schmidt for similar conditions.<sup>13</sup> Between  $2 \times 10^{-3}$  and  $5 \times 10^{-3}$  torr total pressure, the reaction order with respect to hydrogen also approaches  $-1.5$  at low temperatures (Figure 4). The apparent activation energy is  $38 \pm 2$  kcal/mol at pressures between 0.3 and 0.6 torr, and varies from  $33 \pm 3$  kcal/mol for  $2 \times 10^{-3}$  torr ( $P_{\text{H}_2}/P_{\text{NH}_3} = 1$ ) to  $55 \pm 4$  kcal/mol for  $5 \times 10^{-3}$  torr ( $P_{\text{H}_2}/P_{\text{NH}_3} = 4$ ) total pressures. For high temperatures, between  $2 \times 10^{-3}$  and  $5 \times 10^{-3}$  torr, the decomposition becomes uninhibited, and the kinetic order with respect to hydrogen increases continuously to zero. The absolute rates in this limit agree quantitatively with our previous data for the decomposition of pure ammonia,<sup>14</sup> as is shown explicitly in Figure 4. The apparent activation energy is  $4.5 \pm 0.2$  kcal/mol under these conditions.

### 4. Mechanistic Modeling

In our previous work, a mechanistic model based on elementary reactions was developed to describe the kinetics of ammonia decomposition and the isotopic exchange reaction with deuterium

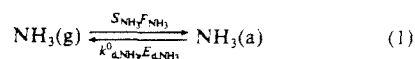


**Figure 3.** Arrhenius plots of the rate of ammonia decomposition with hydrogen inhibition on platinum and the comparison of calculations based on the mechanistic model described in the text with the experimental data. (a)  $P_{\text{NH}_3} = 0.2$  torr,  $P_{\text{H}_2} = 0, 0.2, 0.3,$  and  $0.4$  torr. (b)  $P_{\text{NH}_3} = 0.2$  torr,  $P_{\text{H}_2} = 0, 0.2$  torr, and  $P_{\text{NH}_3} = 0.1$  torr,  $P_{\text{H}_2} = 0.2$  torr.



**Figure 4.** Arrhenius plots of the rate of ammonia decomposition with hydrogen inhibition on platinum and the comparison of model calculations with the experimental data.  $P_{\text{NH}_3} = 10^{-3}$  torr,  $P_{\text{H}_2} = 0, 10^{-3}, 2 \times 10^{-3},$  and  $4 \times 10^{-3}$  torr.

to produce  $\text{NH}_2\text{D}$  and  $\text{ND}_3$ . The reaction mechanism is formulated as follows:



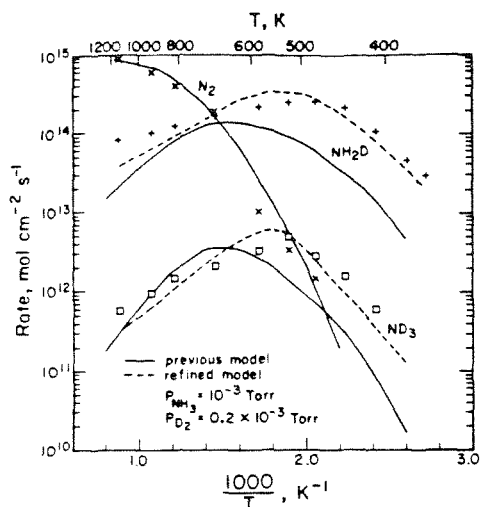


**Figure 5.** Comparison of model calculations with the experimental exchange data for  $N_2$ ,  $NH_2D$ , and  $ND_3$  for  $P_{NH_3} = 10^{-3}$  and  $P_{D_2} = 0.2 \times 10^{-3}$  torr. Previous model calculations are also shown to indicate the improvement of the model prediction.

In addition, as may be seen in Figure 5, there is improved agreement between the model calculations and the exchange data when compared with the previously calculated results using a constant rate coefficient for hydrogen desorption.<sup>14</sup> Specifically, the maxima in the absolute rates of production of  $NH_2D$  and  $ND_3$  are shifted to lower temperatures in qualitative agreement with experiment. In addition, the low-temperature apparent activation energy for the production of  $NH_2D$  is calculated to be 8.7 kcal/mol compared to the experimental value of  $8.4 \pm 0.4$  kcal/mol, while it was estimated to be 10.1 kcal/mol previously.<sup>14</sup> The high-temperature activation energy is determined to be 3.9 kcal/mol compared to measured value of  $2.2 \pm 0.1$  kcal/mol (formerly estimated to be 5.1 kcal/mol). For the production of  $ND_3$ , the low-temperature apparent activation energy is calculated to be 4.4 kcal/mol compared to the observed value of  $4.0 \pm 0.4$  kcal/mol (previously calculated to be 5.9 kcal/mol), and the high-temperature activation energy is calculated to be 8.9 kcal/mol compared to the experimental value of  $8.7 \pm 0.6$  kcal/mol (formerly calculated to be 9.5 kcal/mol).

As discussed previously, the model results are relatively insensitive to a variation in the nitrogen desorption rate coefficient with coverage. This insensitivity arises at high temperatures because the rate of decomposition of ammonia with and without hydrogen present in the feed is controlled by the surface reaction and desorption of ammonia. Under these conditions the nitrogen desorption parameters approach the low coverage limiting values. Since there is experimental evidence that the desorption parameters of nitrogen do not vary appreciably over a wide range of surface coverages,<sup>22</sup> a single coverage-independent set of nitrogen desorption parameters is expected to suffice, even for low temperatures where the reaction rates are sensitive to the rate of desorption of nitrogen. This has been confirmed by the quantitative agreement between calculated and measured values for the decomposition of ammonia at low temperatures.<sup>14</sup> Although it appears that the nitrogen desorption parameters are coverage-independent, they have been varied as well as the surface reaction parameters for eq 2 and 3, with a functional form similar to eq 6. It was found that none of these parameters, when varied, could give an accurate description of both the inhibition and the exchange chemistry, compared to varying the hydrogen desorption rate parameters with coverage.

## 5. Discussion

The model results indicate that  $\theta_N$  varies from 0.2 to 0.6 between 0.3 and 0.6 torr total pressure and from 0.02 to 0.15 between  $2 \times 10^{-3}$  and  $5 \times 10^{-3}$  torr. Obviously, varying the hydrogen de-

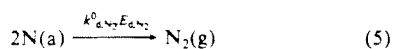
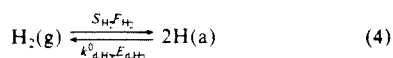
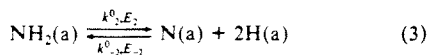
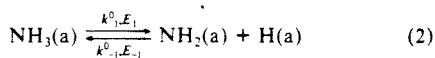
sorption parameters with  $\theta_N$  in eq 6 has a more pronounced effect for pressures between 0.3 and 0.6 torr where the nitrogen coverage is relatively high, than for pressures near  $10^{-3}$  torr where the nitrogen coverage is low. For the same reason, it is clear why the original set of coverage-independent parameters is capable of predicting reaction rates near  $10^{-3}$  torr while failing between 0.3 and 0.6 torr total pressure. Furthermore, the variation of the nitrogen coverage with temperature between 0.3 and 0.6 torr total pressure is rather constant for all partial pressure ratios of hydrogen and ammonia studied. For example  $\theta_N$  varies from 0.58 to 0.32 for  $P_{H_2}/P_{NH_3} = 1$  between 740 and 833 K, and from 0.34 to 0.18 for  $P_{H_2}/P_{NH_3} = 2$  within the same temperature range. This is manifest by the relatively constant apparent activation energy of 38 kcal/mol for the inhibited decomposition. Since the rate of decomposition of ammonia is given by

$$R_{NH_3} = 2k_{d,N_2}^0(n_4\theta_N)^2 \exp(-E_{d,N_2}/kT) \quad (7)$$

a constant change in  $\theta_N$  with temperature will result in a constant apparent activation energy. In contrast, the variation of nitrogen coverage within the temperature range studied at pressures between  $2 \times 10^{-3}$  and  $5 \times 10^{-3}$  torr is relatively large compared to the variation at higher pressures, and, in addition, it is strongly dependent on the partial pressure of hydrogen. For example,  $\theta_N$  varies from 0.15 to 0.06 for  $P_{H_2}/P_{NH_3} = 1$  between 580 and 720 K, while it changes from 0.15 to 0.015 for  $P_{H_2}/P_{NH_3} = 4$ . This results in an increase in the apparent activation energy from 33 to 55 kcal/mol as the partial pressure ratio of hydrogen to ammonia increases from 1 to 4.

Two possible pathways of inhibition were suggested in the introduction, namely, hydrogenation of surface intermediates to re-form ammonia and blocking of ammonia adsorption sites by dissociatively adsorbed hydrogen. An analysis of the reaction model will provide insight concerning the contributions from each of these mechanisms. Although preadsorbed hydrogen is known to block the adsorption of ammonia at low surface temperatures,<sup>11,21</sup> the contribution from this inhibition mechanism is minor in our work because the maximum fractional coverage of hydrogen on the surface under the reaction conditions studied is approximately  $8 \times 10^{-3}$ . Thus the hydrogenation of surface intermediates is predicted to be the primary mechanism for the inhibition of ammonia decomposition. A detailed understanding regarding the nature of the backward (hydrogenation) reactions may be obtained by considering the exchange reactions between ammonia and deuterium. From our proposed dissociative exchange mechanism,<sup>14</sup>  $NH_2D$  is produced from a reaction between  $NH_2(a)$  and deuterium adatoms, and  $ND_3$  is produced from the successive deuteration of nitrogen adatoms. Similarly,  $NHD_2$  is believed to be produced by reaction of deuterium adatoms with  $NH(a)$ , although this reaction is not included in the model. Therefore, a comparison of the measured relative rates of production of  $NH_2D$ ,  $NHD_2$ , and  $ND_3$  indicates directly the contribution from hydrogenation of  $NH_2(a)$ ,  $NH(a)$ , and nitrogen adatoms to the inhibition of ammonia decomposition.

Previously it was determined that for a partial pressure ratio of deuterium to ammonia of 1:5 with a total pressure of  $1.2 \times 10^{-3}$  torr, the ratio of the rates of production of  $NH_2D$ ,  $NHD_2$ , and  $ND_3$ , measured at the temperature corresponding to the maximum value of the rates, is 1:0.17:0.02, respectively.<sup>14</sup> For a total pressure of  $2 \times 10^{-3}$  torr ( $P_{D_2}/P_{NH_3} = 1$ ), the ratio of the maximum rates is 1:0.5:0.07 for  $NH_2D$ ,  $NHD_2$ , and  $ND_3$ , respectively. Clearly, an increase in the deuterium partial pressure enhances the rate of hydrogenation of surface nitrogen relative to the rate of hydrogenation of  $NH_2(a)$ . However, at these pressures, hydrogenation of  $NH_2(a)$  remains the dominant pathway of inhibition compared to the hydrogenation of  $NH(a)$  and nitrogen adatoms, which form  $NHD_2$  and  $ND_3$ , respectively. This experimental result is supported by the model calculations which predict the ratio of the maximum rates of production of  $NH_2D$  and  $ND_3$  to be 1:0.09 for  $P_{D_2}/P_{NH_3} = 1$  at  $2 \times 10^{-3}$  torr and 1:0.17 for  $P_{D_2}/P_{NH_3} = 4$  at  $5 \times 10^{-3}$  torr total pressure. Thus the calculated ratio agrees to within 20% with the observed ratio at  $2 \times 10^{-3}$  torr, the highest pressure at which the exchange



The steady-state mass balance equations for the reactants and the products were solved by employing an iterative scheme. Since independently measured rate parameters were used to describe the adsorption and desorption of ammonia, nitrogen, and hydrogen on the platinum surface, the only adjustable parameters introduced were the activation energies and preexponential factors for the surface reactions, eq 2 and 3. These were varied within reasonable limits in order to obtain the best agreement between the calculations and the experimental results. To model the inhibition kinetics, the same mechanism with the same set of kinetic parameters was found to predict the observed kinetics reasonably well between  $2 \times 10^{-3}$  and  $5 \times 10^{-3}$  torr total pressure. However, the calculated rates between 0.3 and 0.6 torr are approximately 2 orders of magnitude lower than the measured rates, and the predicted reaction order with respect to hydrogen is -3, compared to -1.5 observed experimentally (cf. section 3).

In the previous modeling of the exchange reaction, which also exhibited inhibition of the decomposition reaction for a total pressure of  $1.2 \times 10^{-3}$  torr ( $P_{\text{D}_2}/P_{\text{NH}_3} = 0.2$ ), it was suggested that the deviations between the model predictions and the experimental results (the calculated values for the rate of formation of NH<sub>2</sub>D and ND<sub>3</sub> are shifted to higher temperatures with respect to the data) indicate that it may be necessary to allow a variation of certain kinetic parameters with surface coverages in the model.<sup>14</sup> Hence, in view of the failure of the model to predict inhibition rates between 0.3 and 0.6 torr, one immediately suspects a possible variation in one or more of the kinetic parameters with the surface coverages of ammonia, hydrogen and/or nitrogen.

The effect of  $\theta_{\text{NH}_3}$ , the fractional surface coverage of ammonia, on any rate parameters will be small because the maximum ammonia coverage on the platinum surface under the reaction conditions employed is found to be  $10^{-3}$ ,<sup>14</sup> and the influence of hydrogen adatoms is also small since the fractional coverage of hydrogen adatoms under reaction conditions is estimated to be less than  $8 \times 10^{-3}$ . However, the fractional surface coverage of nitrogen adatoms, which is on the order of 0.1 to unity,<sup>14</sup> may be important in modifying the various kinetic parameters present in the model. An initial adjustment of the model has been made for the desorption rate coefficient of hydrogen. This rate coefficient is particularly important during the inhibition reaction since the backward hydrogenation step is not negligible when hydrogen is present in the reactant feed, although it is not important in the decomposition of pure ammonia. In general, the activation energy and the preexponential factor of any heterogeneous reaction rate coefficient may be a function of surface coverage. In particular, there are many examples in the literature where the activation energy and the preexponential factor of the hydrogen desorption rate coefficient decrease as a function of surface coverage (see the discussion below and ref 24-30). Consequently, the rate of desorption of hydrogen may be represented as

$$R_{\text{d,H}_2} = 2k_{\text{d,H}_2}^0(\theta)(n_{\text{H}}\theta_{\text{H}})^2 \exp[-E_{\text{d}}(\theta)/kT] \quad (6a)$$

where

$$k_{\text{d,H}_2}^0(\theta) = k_{\text{d,H}_2}^0 \exp(-\alpha\theta) \quad (6b)$$

$$E_{\text{d}}(\theta) = E_{\text{d}} - \beta\theta \quad (6c)$$

In this case  $\theta$ , the fractional surface coverage, is given essentially by  $\theta_{\text{N}}$ , the fractional surface coverage of nitrogen. Here  $\alpha$  and  $\beta$  are allowed to vary such that a physically reasonable range of rate parameters for hydrogen desorption is obtained. Note that the model is modified to accommodate the change of only these two parameters, while retaining the same set of parameters

TABLE I: Model Parameters for the Decomposition Reactions of Ammonia on Platinum

	parameter	value	ref
$k_{\text{d,NH}_3}^0$	ammonia desorption preexponential	$1 \times 10^{14} \text{ s}^{-1}$	11, 35
$E_{\text{d,NH}_3}$	ammonia desorption energy	12 kcal/mol	11, 35
$S_{\text{NH}_3}^0$	ammonia probability of adsorption	1	11, 35
$k_{\text{d,N}_2}^0$	nitrogen desorption preexponential	$4 \times 10^{-8} \text{ cm}^2 \text{ s}^{-1}$	22
$E_{\text{d,N}_2}$	nitrogen desorption energy	22 kcal/mol	22
$k_{\text{d,H}_2}^0$	hydrogen desorption preexponential	$0.01 \text{ cm}^2 \text{ s}^{-1}$	36, 37
$E_{\text{d,H}_2}$	hydrogen desorption energy	19 kcal/mol	36, 37
36, 37	hydrogen probability of adsorption	0.1	36, 37
$k_{\text{e}_1}^0, k_{\text{e}_2}^0$	surface reaction preexponentials	$1.5 \times 10^{12} \text{ s}^{-1}$	
$E_1$	surface reaction activation energy	16 kcal/mol	
$k_{\text{e}_{-2}}^0$	hydrogenation reaction preexponential	$3 \times 10^{-17} \text{ cm}^4 \text{ s}^{-1}$	
$E_{-2}$	surface hydrogenation activation energy	28 kcal/mol	
$k_{\text{e}_{-1}}^0$	exchange reaction preexponential	$0.05 \text{ cm}^2 \text{ s}^{-1}$	
$E_{\text{eff}}$	$E_2 - E_{-1}$	4 kcal/mol	
$n_{\text{H}}$	surface atom density	$1 \times 10^{15} \text{ cm}^{-2}$	
$\alpha$	parameter for hydrogen desorption	5	
$\beta$	parameter for hydrogen desorption	14 kcal/mol	

successfully used previously in all other cases. These parameters are summarized in Table I.

The model results indicate that values of  $\alpha$  and  $\beta$  which are able to describe the inhibition data are not unique. For instance, for both sets of parameters  $\alpha = 5$ ,  $\beta = 14$  kcal/mol and  $\alpha = 6$ ,  $\beta = 8$  kcal/mol, there is close agreement between the model calculations and the observed experimental values. In order to discriminate between these and other sets of  $\alpha$  and  $\beta$  which accurately describe the inhibition data, Equation 6 was used to calculate rates of production of NH<sub>2</sub>D and ND<sub>3</sub> for a partial pressure ratio of deuterium to ammonia of 1:5 with a total pressure of  $1.2 \times 10^{-3}$  torr. Comparison of these calculations with the previous experimental results<sup>14</sup> indicates that not all of the sets  $\alpha$  and  $\beta$  which describe the inhibition results can also describe the exchange results. Indeed,  $\alpha$  and  $\beta$  are unique within experimental uncertainties, and their values are found to be  $\alpha = 5$  and  $\beta = 14$  kcal/mol. A sensitivity analysis of the model with respect to  $\alpha$  and  $\beta$  indicates that the agreement with the measured values degrades considerably if  $\alpha$  and  $\beta$  are varied by more than  $\pm 0.5$ . For  $\alpha = 5$  and  $\beta = 14$  kcal/mol, the variation in the activation energy and preexponential factor for hydrogen desorption is from 19 to 10.6 kcal/mol and  $10^{-2}$  to  $5 \times 10^{-4} \text{ cm}^2 \text{ s}^{-1}$ , for nitrogen coverages from zero to 0.6, respectively. (The maximum fractional surface coverage of nitrogen under reaction conditions is calculated to be 0.6.)

The calculated results based on these parameters are shown in Figures 3 and 4. The correct reaction orders, -1.5 for hydrogen and 1.0 for ammonia, are predicted under the conditions where these values are observed experimentally. Each of the calculated activation energies of the reaction also agree to within  $\pm 2$  kcal/mol with the experimental values. In general, the inhibition decreases as the temperature increases and the hydrogen coverage decreases. The model calculations agree perfectly with the data near 690 K between  $2 \times 10^{-3}$  and  $5 \times 10^{-3}$  torr, where the rate of decomposition approaches the rate characteristic of pure ammonia. Furthermore, the measured rates, which are also in qualitative agreement with the model between 0.3 and 0.6 torr total pressure, do not approach the noninhibited rate due to an insufficiently high temperature in this case. However, our data and model (which predicts that the inhibition should become negligible near 1090 K) are both consistent with previous results of Loffler and Schmidt<sup>13</sup> which indicate that the inhibition does indeed become negligible under these high-pressure conditions between 1000 and 1100 K.

experiment was conducted. Furthermore, an extrapolation of this calculation for the exchange reaction to 0.4 torr total pressure ( $P_{\text{D}_2}/P_{\text{NH}_3} = 1$ ) indicates that the ratio of the rates is 1:0.23 for  $\text{NH}_2\text{D}$  and  $\text{ND}_3$  production, respectively. Hence, ratios of the calculated rates, together with the experimentally observed values, indicate that the hydrogenation of  $\text{NH}_3(\text{a})$  is the predominant inhibition pathway over the whole range of pressures studied. To summarize, the inhibition of ammonia decomposition is believed to occur predominantly through the hydrogenation of  $\text{NH}_3(\text{a})$  to produce molecularly adsorbed ammonia. This results in a reduction of nitrogen adatom coverage on the surface and consequently the observed inhibition.

The functional form given by eq 6, which describes the desorption of hydrogen, is an example of the so-called compensation effect. Hence, the activation energy and the preexponential factor vary in sympathy with coverage, reducing the observed change in the value of the desorption rate. With  $\alpha = 5$  and  $\beta = 14$  kcal/mol in eq 6, the value of the preexponential factor of the hydrogen desorption rate coefficient at zero nitrogen coverage is  $k_{\text{d,H}_2}^0(\theta) = 10^{-2} \text{ cm}^2 \text{ s}^{-1}$ , and  $E_{\text{d,H}_2}(\theta) = 19$  kcal/mol; while the values at high coverage ( $\theta_{\text{N}} = 0.6$ ) are  $k_{\text{d,H}_2}^0(\theta) = 5 \times 10^{-4} \text{ cm}^2 \text{ s}^{-1}$  and  $E_{\text{d,H}_2}(\theta) = 10.6$  kcal/mol. This variation appears physically reasonable since similar variations have been found experimentally for the desorption rate coefficients of hydrogen as a function of coverage.<sup>24-30</sup> For example, studies of the adsorption and desorption of hydrogen from Ni(100), Ni(100)-p(2×2)S, and Ni(100)-c(2×2)S surfaces<sup>24</sup> indicate that the presence of sulfur reduces the values of the desorption rate parameters which characterize hydrogen recombination. The activation energy of desorption of 21.3 kcal/mol and the preexponential factor of  $5 \times 10^{-2} \text{ cm}^2 \text{ s}^{-1}$  on clean Ni(100) are reduced to 17.4 kcal/mol and  $4 \times 10^{-4} \text{ cm}^2 \text{ s}^{-1}$  on the p(2×2)S surface, and to 10 kcal/mol and  $3 \times 10^{-8} \text{ cm}^2 \text{ s}^{-1}$  on the c(2×2)S surface. The low value for  $k_{\text{d,H}_2}^0$  on the surface with half a monolayer of sulfur present, which gives rise to the compensation effect, was suggested to originate from severe steric hindrance to hydrogen recombination.<sup>24</sup> The same effect occurs except to a lesser extent in the case of a quarter monolayer of sulfur. A similar change in hydrogen desorption kinetics was observed when carbon was present on the Ni(100) surface.<sup>25</sup> For the Ni(100) surface with 0.25 monolayer carbon, the activation energy for hydrogen desorption was 9.5 kcal/mol with a preexponential factor of  $10^{-8} \text{ cm}^2 \text{ s}^{-1}$  in contrast to the clean surface values of 21.3 kcal/mol and  $5 \times 10^{-2} \text{ cm}^2 \text{ s}^{-1}$ . In addition, the compensation effect has also been observed for hydrogen desorption from Rh(111),<sup>26</sup> where the activation energy of hydrogen desorption was observed to decrease linearly by almost 10 kcal/mol, while the preexponential factor was found to decrease by 5 orders of magnitude for hydrogen coverages varying from 0 to 0.5. This variation was attributed to the involvement of a mobile precursor state of molecular hydrogen during desorption, as described by Gorte and Schmidt.<sup>31</sup> A similar precursor state for hydrogen desorption, which occurs during ammonia decomposition with finite nitrogen coverages, is certainly reasonable.

Compensatory behavior has also been attributed to multiple adsorption states and to repulsive lateral interactions.<sup>32,33</sup> Evidence for these mechanisms may be obtained by analyzing thermal desorption measurements of hydrogen on platinum. A recent study of hydrogen desorption from the Pt(110)-(1×2) surface has revealed the existence of two dissociatively adsorbed states.<sup>34</sup> At

low coverages, hydrogen desorbs from a single state with a peak temperature of approximately 360 K. This state becomes saturated at higher coverages and a second peak in the thermal desorption spectrum appears, initially with a peak temperature of approximately 260 K.<sup>34</sup> Although an analysis in terms of activation energies and preexponential factors has not been conducted, we can compare these data on Pt(110) with thermal desorption spectra generated for surfaces with different precoverages of nitrogen using eq 6b,c to obtain the kinetic parameters for the desorption of hydrogen. Thermal desorption spectra can be calculated by integrating the rate equation describing the desorption reaction, i.e.

$$R_{\text{d,H}_2} = n_{\text{s}}(d\theta_{\text{H}}/dt) = 2k_{\text{d,H}_2}^0(n_{\text{s}}\theta_{\text{H}})^2 \exp(-E_{\text{d,H}_2}/kT)$$

where  $k_{\text{d,H}_2}^0$  and  $E_{\text{d,H}_2}$  are the preexponential factor and the activation energy appropriate for a given nitrogen coverage. Thermal desorption spectra were calculated for two surfaces, both with a small fractional coverage ( $\theta_{\text{H}} = 0.01$ ) of hydrogen: a surface with no nitrogen coverage,  $\theta_{\text{N}} = 0$ , and a surface with  $\theta_{\text{N}} = 0.6$ . For  $\theta_{\text{N}} = 0$  ( $k_{\text{d,H}_2}^0 = 0.01 \text{ cm}^2 \text{ s}^{-1}$  and  $E_{\text{d,H}_2} = 19$  kcal/mol), the calculated hydrogen desorption peak temperature is 370 K, while for  $\theta_{\text{N}} = 0.6$  ( $k_{\text{d,H}_2}^0 = 5 \times 10^{-4} \text{ cm}^2 \text{ s}^{-1}$  and  $E_{\text{d,H}_2} = 10.6$  kcal/mol), the peak temperature is 250 K. The agreement of these results with the thermal desorption measurements on Pt(110)<sup>34</sup> is consistent with both multiple adsorption states and repulsive lateral interactions. In the former case, adsorbed nitrogen blocks the adsite for hydrogen which desorbs at 360 K. Therefore, as the nitrogen coverage increases, the fraction of hydrogen adsorbed in the high-temperature adstate decreases, while the fraction in the low-temperature adstate increases. In the latter case, repulsive interactions between nitrogen and hydrogen adatoms reduce the hydrogen desorption energy, which mimics population of the low-temperature hydrogen adstate and the depopulation of the high-temperature adstate. In addition, our calculations are consistent with thermal desorption measurements of hydrogen from Pt(111),<sup>30</sup> which indicate two adsorption states with peak temperatures of approximately 380 and 270 K. Since compensatory behavior may be attributed to many different mechanisms, further work is being conducted in our laboratory to characterize the mechanism of hydrogen desorption from nitrogen-covered platinum surfaces.

In summary, the mechanistic model given by eq 1-5 together with eq 6 is able to describe quantitatively the decomposition of ammonia, the isotopic exchange reaction of ammonia with deuterium, and the inhibition of the decomposition of ammonia by hydrogen over a pressure range which spans 7 orders of magnitude and over a temperature range of 800 K. The success of the model attests to the general utility of analyzing kinetic data obtained over a wide range of experimental conditions by using kinetic parameters determined independently from UHV measurements. Finally, an accurate description of the interaction of ammonia with platinum up to a pressure of approximately 1 torr has been obtained without hypothesizing any mechanistic steps or processes which cannot be directly investigated at pressures amenable to modern surface science techniques.

## 6. Conclusions

The results of this study can be summarized as follows:

1. Inhibition of ammonia decomposition is observed for total pressures between 0.3 torr ( $P_{\text{H}_2}/P_{\text{NH}_3} = 2$ ) and 0.6 torr ( $P_{\text{H}_2}/P_{\text{NH}_3} = 2$ ) and for temperatures between 740 and 850 K. Under these conditions, the apparent activation energy is  $38 \pm 2$  kcal/mol, and the reaction orders with respect to hydrogen and ammonia are  $-1.5 \pm 0.3$  and  $1.0 \pm 0.2$ , respectively.

2. For total pressures between  $2 \times 10^{-3}$  torr ( $P_{\text{H}_2}/P_{\text{NH}_3} = 1$ ) and  $5 \times 10^{-3}$  torr ( $P_{\text{H}_2}/P_{\text{NH}_3} = 4$ ), inhibition is observed at temperatures below approximately 650 K, where the reaction order with respect to hydrogen approaches  $-1.5 \pm 0.3$  at low temper-

- (24) Johnson, S.; Madix, R. J. *Surf. Sci.* **1981**, *108*, 77.  
 (25) Ko, E. I.; Madix, R. J. *Appl. Surf. Sci.* **1979**, *3*, 236.  
 (26) Yates, Jr., J. T.; Thiel, P. A.; Weinberg, W. H. *Surf. Sci.* **1979**, *84*, 427.  
 (27) Christmann, K.; Ertl, G.; Pignet, T. *Surf. Sci.* **1976**, *54*, 365.  
 (28) Ibbotson, D. E.; Wittig, T. S.; Weinberg, W. H. *J. Chem. Phys.* **1980**, *72*, 4885.  
 (29) Engstrom, J. R.; Tsai, W.; Weinberg, W. H., in preparation.  
 (30) McCabe, R. W.; Schmidt, L. D. *Surf. Sci.* **1977**, *65*, 189.  
 (31) Gorte, R.; Schmidt, L. D. *Surf. Sci.* **1978**, *76*, 559.  
 (32) Galwey, A. K. *Adv. Catal.* **1977**, *26*, 247 and references therein.  
 (33) Goymour, C. G.; King, D. A. *J. Chem. Soc., Faraday Trans. 1* **1973**, *69*, 749.  
 (34) Szuromi, P. D.; Engstrom, J. R.; Weinberg, W. H. *J. Phys. Chem.* **1985**, *89*, 2497.

- (35) Gland, J. L. *Surf. Sci.* **1978**, *71*, 327.  
 (36) Poelsema, B.; Mechttersheimer, G.; Comsa, G. *Surf. Sci.* **1981**, *111*, 519.  
 (37) Poelsema, B.; Mechttersheimer, G.; Comsa, G. *Surf. Sci.* **1981**, *111*, L728.

atures. The activation energy varies from  $33 \pm 3$  kcal/mol for  $2 \times 10^{-3}$  torr to  $55 \pm 4$  kcal/mol for  $5 \times 10^{-3}$  torr total pressure. The decomposition becomes uninhibited at high temperatures, and the apparent activation energy is  $4.5 \pm 0.2$  kcal/mol.

3. The observed kinetics for the reaction of ammonia and hydrogen on platinum are described quantitatively by a model employing elementary surface reactions, where the rate coefficient for hydrogen desorption is a function of the fractional surface coverage of nitrogen adatoms.

4. The hydrogenation of  $\text{NH}_2(\text{a})$  to produce molecularly adsorbed ammonia is the dominant factor in the inhibition of ammonia decomposition.

*Acknowledgment.* We gratefully acknowledge the financial support of the Army Research Office under Grant No. DAAG29-83-K-0094, and the Central Research and Development Department of E.I. du Pont de Nemours and Co.

**Registry No.**  $\text{NH}_3$ , 7664-41-7;  $\text{H}_2$ , 1333-74-0; Pt, 7440-06-4.

**Chapter 3.**

Perturbations in the Surface Chemistry of Hydrogen

by Nitrogen Adatoms on Pt(110)-(1x2)

[Chapter 3 consists of an article coauthored with J.J. Vajo and W.H. Weinberg.]

### Abstract

The kinetics of adsorption and desorption of deuterium have been studied on Pt(110)-(1x2) surfaces on which various fractional coverages of nitrogen adatoms are present. The nitrogen was adsorbed via the decomposition of ammonia at 400 K, at which temperature the initial probability of dissociative adsorption is approximately  $4 \times 10^{-3}$ . Nitrogen selectively blocks the high temperature  $\beta_2$ -state of deuterium prior to poisoning the low temperature  $\beta_1$ -state. No evidence of a 'long-range' electronic perturbation of the surface by the nitrogen adatoms was found. The adsorption kinetics of deuterium on both clean and nitrogen-precovered Pt(110)-(1x2) surfaces were Langmuirian. In particular, adsorption into the  $\beta_2$ -state was first-order with respect to the fraction of vacant surface sites, and adsorption into the  $\beta_1$ -state was second-order in all cases. The modification of the desorption rate coefficients of deuterium on Pt(110)-(1x2) by the nitrogen adatoms was measured quantitatively. Nitrogen modifies the preexponential factor and the activation energy of desorption of deuterium on Pt(110)-(1x2) by essentially rescaling the effective coverage of the deuterium. For the  $\beta_2$ -state, the activation energy and the preexponential factor of the rate coefficient of deuterium desorption from both clean and nitrogen-precovered Pt(110)-(1x2) display a compensation effect. The activation energy of desorption of nitrogen from Pt(110)-(1x2) was determined to be 24 kcal-mol<sup>-1</sup> and relatively independent of coverage, whereas the preexponential factor decreases from approximately  $5 \times 10^{-5}$  cm<sup>2</sup>-s<sup>-1</sup> at low coverages ( $\theta_N \leq 0.15$ ) to approximately  $5 \times 10^{-7}$  cm<sup>2</sup>-s<sup>-1</sup> at higher coverages ( $\theta_N \geq 0.3$ ).

## I. Introduction

Solid surfaces are frequently modified chemically by adsorbed species for various applications in vacuum technology [1], corrosion prevention [2], adhesion [3] and heterogeneous catalysis [4-15]. An important aspect of practical heterogeneous catalysis is that the addition of an electropositive or an electronegative additive can have a profound effect on the activity, the selectivity, and/or the resistance to poisoning of the catalyst [4]. For example, alkali metal compounds are routinely used as promoters for supported iron catalysts in both ammonia synthesis [5-7] and the hydrogenation of carbon monoxide to hydrocarbons [8-11]. On the other hand, the introduction of sulfur, a prototypical 'poison' of nickel catalysts, increases dramatically the *selectivity* of these catalysts for the partial hydrogenation of acetylene to ethylene [12], of polyolefins and cyclic polyenes to the corresponding monoolefins [13,14], and of nitrobenzene to aniline [15].

These chemical additives can perturb the electronic structure of the metal surface and thereby alter both the nature of the bonding of adsorbed species as well as the rates and mechanisms of chemisorption, desorption and surface reactions. In order to have an accurate description of the mechanism by which the catalytic chemistry is modified by poisons and promoters, it is essential to have a complete understanding of the effects of chemical additives on the chemisorbed reactants. There have been a number of experimental [16-20] and theoretical [21,22] studies concerning the effects of chemical modification of surfaces on the chemisorption of hydrogen, and the mechanisms by which surfaces are either poisoned or promoted.

Ertl and coworkers [16] have examined the interaction of nitrogen and hydrogen on Fe(110) and have observed that nitrogen adatoms block sites for the dissociative chemisorption of hydrogen. However, no quantitative evaluation was reported concerning perturbations by the nitrogen on the binding energy or the kinetics of adsorption and desorption of the hydrogen. Kiskinova and Goodman [17] have investigated the effect of nitrogen adatoms, deposited by the dissociative adsorption of hydrazine, on the chemisorption of hydrogen on the Ni(100) surface. A reduction in both the uptake of hydrogen and its binding energy was observed. The variation of the "initial" probability of adsorption of hydrogen with nitrogen precoverage was found to be described by

$$\lim_{\theta_H \rightarrow 0} S^{(0)}(\theta_N) = (1 - 4\theta_N)^2 S^{(0)}(\theta_N = 0) \quad (1)$$

for  $\theta_N \leq 0.25$ , where  $\theta_N$  is the fractional surface coverage of nitrogen.

From studies of hydrogen chemisorption on sulfur-precovered Ru(001) surfaces, Schwarz [18] has shown that the effect of sulfur coverage  $\theta_S$  on the amount of hydrogen that can be adsorbed at saturation  $\theta_H^{sat}$  is given by

$$\theta_H^{sat} = 1 - 4\theta_S \quad (2)$$

for  $\theta_S \leq 0.25$ . On the clean surface the activation energy of desorption decreased linearly with hydrogen coverage, indicating repulsive adatom-adatom interactions. Furthermore, for each hydrogen coverage, both the activation energy and the logarithm of the preexponential factor of the rate coefficient of desorption of

hydrogen decreased nonlinearly with sulfur precoverage. It was concluded that sulfur acts to block sites for the dissociative adsorption of hydrogen as well as sites for the recombinative desorption of hydrogen.

Kiskinova and Goodman [19] have carried out similar studies on the Ni(100) surface and found that  $\theta_H^{sat}$  decreases rapidly and nonlinearly with  $\theta_S$ . They suggested that at low sulfur coverages long-range electronic effects are important in inhibiting the chemisorption of hydrogen. The variation of the initial probability of adsorption of hydrogen with sulfur precoverage was found to be identical to that for nitrogen given by Eq. (1). The binding energy of hydrogen was also reduced, and this was attributed to a reduction of the surface electron density of states due to the presence of electronegative sulfur adatoms, and possibly to repulsive adatom-adatom interactions also. Johnson and Madix [20] observed in their studies of the interaction of hydrogen with the Ni(100), the Ni(100)-p(2x2)S ( $\theta_S=0.25$ ) and the Ni(100)-c(2x2)S ( $\theta_S=0.5$ ) surfaces that the presence of sulfur reduces the values of both of the hydrogen desorption rate parameters. The activation energy of desorption of  $21.3 \text{ kcal-mol}^{-1}$  and the pre-exponential factor of the desorption rate coefficient of  $5 \times 10^{-2} \text{ cm}^2\text{-s}^{-1}$  on clean Ni(100) are reduced to  $17.4 \text{ kcal-mol}^{-1}$  and  $4 \times 10^{-4} \text{ cm}^2\text{-s}^{-1}$  on the p(2x2)S surface, and to  $10 \text{ kcal-mol}^{-1}$  and  $3 \times 10^{-8} \text{ cm}^2\text{-s}^{-1}$  on the c(2x2)S surface. The low values of the preexponential factor were suggested to originate from steric hindrance to the recombination of hydrogen on these sulfur-precovered surfaces.

In the present work, we have studied the chemisorption of hydrogen on nitrogen precovered Pt(110)-(1x2) surfaces, where the nitrogen adatoms were deposited via the decomposition of ammonia. Perturbations by the nitrogen

adatoms on the adsorption and desorption of hydrogen have been examined quantitatively, and a connection is made between these results and measurements of the decomposition of ammonia and the inhibition in the decomposition of ammonia by hydrogen on a polycrystalline platinum surface [23,24]. In addition, the rate coefficient of the recombinative desorption of nitrogen from the Pt(110)-(1x2) surface has been evaluated as a function of surface coverage of nitrogen adatoms.

## II. Experimental Procedures

The experiments reported here were carried out in an ion pumped, stainless steel ultrahigh vacuum system that has been described in detail previously [25]. The base pressure of the system is below  $1 \times 10^{-10}$  Torr of reactive gases. Facilities are available for experimental studies involving mass spectrometry, low-energy electron diffraction (LEED), Auger electron spectroscopy, and X-ray and UV-photoelectron spectroscopies.

The Pt(110) crystal was oriented and cut from a single crystalline boule of platinum, polished to within  $\frac{1}{2}^\circ$  of the (110) orientation using standard metallographic techniques, and etched briefly in hot aqua regia. The crystal was mounted by spotwelding to two 10 mil tantalum support wires; and it was heated resistively, and cooled conductively by liquid nitrogen. The temperature was measured by a W/5%Re-W/26%Re thermocouple that was spotwelded to the back of the crystal. The Pt(110) surface was cleaned *in situ* by argon ion sputtering, and heating in  $5 \times 10^{-7}$  Torr of oxygen (at 800 K) followed by high temperature annealing (at 1400 K). The cleanliness of the surface was

established by both Auger electron spectroscopy and X-ray photoelectron spectroscopy. Special care was taken to reduce the concentration of silicon impurity in the sample to a negligible level, since it has been shown that its presence is related to the formation of a "subsurface oxide" on Pt(111) [26]. After cleaning and annealing, the (1x2) LEED pattern characteristic of the clean, reconstructed surface was observed. The structure of reconstructed Pt(110) is a surface with every other row of surface atoms missing in the [001] direction [27-29], similar to that of the Ir(110)-(1x2) surface [30].

The ammonia exposures were carried out with a directional beam doser consisting of a multichannel array of capillaries [31]. During adsorption the crystal was positioned approximately 3 mm from the doser face, providing a beam pressure-to-background pressure ratio that is greater than 20:1. These exposures were calibrated in Langmuir units ( $1 \text{ Langmuir} \equiv 1 \text{ L} \equiv 10^{-6} \text{ Torr-s}$ ) by a comparison of thermal desorption spectra obtained both by backfilling the belljar and by employing the doser.

Automated data acquisition [32] and substrate temperature control [33] were achieved by using an IBM-XT computer station with a Data-Translation 2801-A board. All thermal desorption mass spectra were measured with a UTI-100C quadrupole mass spectrometer, enclosed in a glass envelope to discriminate against desorption from surfaces other than the oriented front of the crystal [34]. The protocol used in the mass spectrometric measurements was the following. The clean Pt(110)-(1x2) surface was precovered with atomic nitrogen by decomposing ammonia from the directional beam doser at surface temperatures between 350 and 400 K. Deuterium was adsorbed subsequently at a surface tem-

perature of 120 K. The quadrupole mass spectrometer was multiplexed for the detection of both deuterium (mass 4) and nitrogen (mass 14). By varying the heating rate (from 3 to 25 K/s), both the activation energy of desorption and the preexponential factor of the desorption rate coefficient of deuterium were determined independently as a function of the fractional coverages of deuterium and nitrogen adatoms.

Ammonia,  $^{14}\text{NH}_3$  (99.99%, anhydrous grade), deuterated ammonia  $^{15}\text{ND}_3$  (99 atom%  $^{15}\text{N}$ , 99 atom% deuterium) and deuterium (99.995%, research grade) were obtained from Matheson and were used without further purification. The purity of each reagent was verified *in situ* mass spectrometrically.

### III. Results

#### 1. Molecular Chemisorption of Ammonia at Low Temperature

Thermal desorption spectra following various exposures (1.5 to 10 L) of deuterated ammonia ( $^{15}\text{ND}_3$ ) on the clean Pt(110)-(1x2) surface at 120 K are shown in Fig. 1. There is no detectable dissociation of the chemisorbed ammonia, either at 120 K or during the heating ( $5\text{ K}\cdot\text{s}^{-1}$ ) to record the thermal desorption spectra. The desorption of chemisorbed ammonia is observed at temperatures greater than approximately 200 K. In the limit of low surface coverages the peak temperature of the thermal desorption spectra is near 360 K. The downshift in the temperature of desorption with increasing surface coverage is largely due to perturbations in the platinum substrate originated from the electron donor bond that chemisorbed ammonia forms with the surface. The activation energy of the desorption of ammonia is estimated to be 12.8-23.1 kcal-

$\text{mol}^{-1}$ , assuming a preexponential factor of the rate coefficient of desorption of  $10^{14} \text{ s}^{-1}$  [35]. The peak at approximately at 165 K, with a binding energy of approximately 9.8-10.6  $\text{kcal}\cdot\text{mol}^{-1}$ , is due to a "second layer" of adsorbed ammonia, as has been observed previously for ammonia adsorption on Pt(111) [36] and Ru(001) [37] surfaces. Approximately equal amounts of ammonia are adsorbed in the first two layers following a saturation exposure at 120 K (cf., Fig. 1). In separate experiments at a lower adsorption temperature (approximately 100 K), the zeroth-order multilayer desorption peak of ammonia is observed at approximately 110 K with an estimated binding energy of 6.5-7.0  $\text{kcal}\cdot\text{mol}^{-1}$  [38]. The initial probability of adsorption of ammonia on this surface at 120 K is approximately unity.

## **2. Dissociative Chemisorption of Ammonia at High Temperature**

Although there was no detectable dissociative chemisorption of ammonia after adsorption at 120 K followed by heating, dissociation could be effected by exposing the Pt(110)-(1x2) surface to ammonia at temperatures near 400 K. The probability of dissociative adsorption was found to be approximately  $4 \times 10^{-3}$  in the limit of zero coverage at this surface temperature. The coverage dependence of the probability of dissociative adsorption will be discussed further in Sect. IV. No desorption of hydrogen was observed following the dissociative adsorption of ammonia at 400 K, implying that neither  $\text{NH}_2$  nor  $\text{NH}$  species are stable on the surface at this temperature. (The desorption of surface hydrogen is complete below 350 K.)

The thermal desorption spectra of nitrogen from the Pt(110)-(1x2) surface, shown parametric in ammonia exposure in Fig. 2, were used to evaluate the coverage-dependent rate coefficient of the desorption of nitrogen. The rate ( $\text{cm}^{-2}\text{-s}^{-1}$ ) of the second-order recombinative desorption reaction may be written in a Polanyi-Wigner form as

$$R_{d,N_2} = n_s^2 \theta_N^2 k_{d,N_2}^{(0)}(\theta_N) e^{-E_{d,N_2}(\theta_N)/k_B T}, \quad (3)$$

where  $E_{d,N_2}(\theta_N)$  and  $k_{d,N_2}^{(0)}(\theta_N)$ , which may be functions of the fractional surface coverage of atomic nitrogen  $\theta_N$ , are the activation energy and the preexponential factor of the rate coefficient of desorption of molecular nitrogen, and  $n_s$  is the concentration of surface sites.

The saturation coverage of nitrogen adatoms was determined by calibration against the saturation coverage of molecularly adsorbed carbon monoxide. The surface coverage at saturation of CO on Pt(110)-(1x2) is known to be  $9.2 \times 10^{14}$  molecules- $\text{cm}^{-2}$  [39], and the CO overlayer forms an ordered  $\text{p}1\text{g}1(2\text{x}1)$  superstructure. Time-integrated areas of desorption traces of saturated nitrogen overlayers were compared to those of carbon monoxide. After correcting for mass spectrometric sensitivities and pumping time constants, the saturation coverage of atomic nitrogen on Pt(110)-(1x2), deposited via ammonia decomposition, was found to be approximately  $1.4 \times 10^{15}$  atoms- $\text{cm}^{-2}$ . This value of the fractional nitrogen coverage is defined to be  $\theta_N=1$ . It should be emphasized that the accuracy of the *relative* coverages discussed later is greater than that of this absolute coverage, which may be uncertain by approximately  $\pm 50\%$ . The

(1x2) LEED structure of the substrate was not observed to be influenced by the presence of the nitrogen overlayer, nor were any ordered superstructures due to the nitrogen adatoms observed at any coverage or annealing temperature.

By varying the heating rate, both the activation energy and the preexponential factor of the desorption rate coefficient of nitrogen were evaluated independently as a function of nitrogen coverage [40]. For a rapidly pumped system in which the desorption rate is proportional to the ion current of the mass spectrometer, the coverage at any point in a desorption spectrum is determined by integrating the product signal with respect to time. By varying the heating rate at a fixed initial coverage, the thermal desorption spectra can be used to construct "desorption isotherms", i.e.,  $R_{d,N_2}$  as a function of  $\theta_N$  at various constant temperatures. By extracting isosteric (constant coverage) data from the desorption isotherms, one can construct Arrhenius plots of  $\ln R_{d,N_2}$  as a function of reciprocal temperature at constant coverage of which the slopes are  $-E_{d,N_2}(\theta_N)/k_B$  and the intercepts are  $\ln [n_s^2 \theta_N^2 k_{d,N_2}^{(0)}(\theta_N)]$ . Consequently, the values of  $E_{d,N_2}(\theta_N)$  and  $k_{d,N_2}^{(0)}(\theta_N)$  can be determined if the absolute coverage is known.

The calculated activation energy of desorption and the preexponential factor of the desorption rate coefficient are shown as a function of nitrogen coverage in Fig. 3. The activation energy of desorption decreases only slightly with surface coverage from an initial value of approximately  $24 \text{ kcal-mol}^{-1}$ , while the preexponential factor decreases precipitously from approximately  $5 \times 10^{-5} \text{ cm}^2\text{-s}^{-1}$  at low coverages ( $\theta_N \leq 0.15$ ) to approximately  $5 \times 10^{-7} \text{ cm}^2\text{-s}^{-1}$  at higher coverages ( $\theta_N \geq 0.3$ ).

### 3. Adsorption Kinetics of Deuterium on Clean and Nitrogen-precovered Pt(110)-(1x2) Surfaces

Thermal desorption spectra of deuterium adsorbed on the initially clean Pt(110)-(1x2) surface are shown in Fig. 4(a), parametric in exposure [41]. These spectra are in good agreement with those published previously by Ferrer and Bonzel [42]. The (1x2) LEED structure of the substrate was not influenced visually by the presence of the deuterium overlayer [43]. The  $\beta_2$ -state that desorbs near 300 K has a considerably higher probability of adsorption than does the  $\beta_1$ -state which desorbs at a lower temperature. The coverage-exposure relation indicates that the  $\beta_2$ -state follows first-order Langmuir adsorption kinetics with an initial probability of adsorption  $S^{(0)}$  of 0.46, whereas the  $\beta_1$ -state obeys second-order Langmuir adsorption kinetics with an  $S^{(0)}$  of 0.024. The saturation coverage of the  $\beta_2$ -state is approximately half that of the  $\beta_1$ -state.

The saturation coverage of deuterium on the initially clean Pt(110)-(1x2) surface at 170 K is known to be  $1.1 \times 10^{15}$  atoms-cm<sup>-2</sup> [44], and the saturation coverage at 120 K is estimated to be  $1.6 \times 10^{15}$  atoms-cm<sup>-2</sup> [41]. The saturation coverage of the low temperature  $\beta_1$ -state at an adsorption temperature of 120 K was found to be  $1.1 \times 10^{15}$  atoms-cm<sup>-2</sup>, whereas the high temperature  $\beta_2$ -state saturated at  $5.2 \times 10^{14}$  atoms-cm<sup>-2</sup> [41].

The influence of nitrogen adatoms upon the chemisorption of deuterium on the Pt(110)-(1x2) surface at 120 K is shown in the three sets of thermal desorption spectra in Fig. 4(b)-(d) for nitrogen fractional coverages of 0.13, 0.26 and 0.4. It is obvious that the high temperature  $\beta_2$ -state of deuterium is

poisoned prior to the  $\beta_1$ -state by the nitrogen adatoms. The maximum fractional surface coverages of both states  $\theta_{D,i}^{max}$  are plotted as a function of the fractional surface coverage of nitrogen in Fig. 5. Note that the fractional surface coverage of each adstate of deuterium was normalized independently to its own saturation coverage. By extrapolating the linear dependence of  $\theta_{D,\beta_2}^{max}$  on  $\theta_N$  to  $\theta_{D,\beta_2}^{max} = 0$ , it is seen that this state (saturation coverage on the clean surface of  $5.2 \times 10^{14}$  atoms-cm $^{-2}$ ) is poisoned completely by nitrogen at  $\theta_N \approx \frac{1}{3}$  or  $4.7 \times 10^{14}$  atoms-cm $^{-2}$ . The linear decrease of  $\theta_{D,\beta_2}^{max}$  with  $\theta_N$  is suggestive of geometrical site blocking.

There is negligible poisoning of deuterium in the  $\beta_1$ -state for  $\theta_N \leq 0.3$ . The decrease of  $\theta_{D,\beta_1}^{max}$  with  $\theta_N$  (for  $\theta_N > 0.3$ ) can be approximated as a linear function, as shown in Fig. 5, with the  $\beta_1$ -state (saturation coverage on the clean surface of  $1.1 \times 10^{15}$  atoms-cm $^{-2}$ ) completely poisoned by a saturation precoverage of nitrogen. The concentration of nitrogen adatoms that poisons the  $\beta_1$ -state of deuterium completely is approximately  $9.3 \times 10^{14}$  atoms-cm $^{-2}$ , and the linear decrease of  $\theta_{D,\beta_1}^{max}$  with  $\theta_N$  is again indicative of geometrical site blocking.

The adsorption kinetics of deuterium on Pt(110)-(1x2) with various nitrogen precoverages are shown in Fig. 6(a) and (b) for the  $\beta_2$ - and the  $\beta_1$ -states. Both the Langmuir model and models which include precursor-mediated adsorption kinetics [45,46] were employed to describe the measured data. The incorporation of the influence of the nitrogen adatoms on the adsorption of deuterium in these models is straightforward by rescaling the observed linear poisoning of deuterium adstates by nitrogen adatoms. In the case of Langmuir kinetics, the rates of first-order and second-order adsorption are proportional,

respectively, to

$$\left(\frac{\partial\theta_{D,i}}{\partial\hat{\epsilon}_{D_2}}\right)_{T,P_{D_2},\theta_N} = (\theta_{D,i}^{max} - \theta_{D,i})S^{(0)}, \quad (4a)$$

and

$$\left(\frac{\partial\theta_{D,i}}{\partial\hat{\epsilon}_{D_2}}\right)_{T,P_{D_2},\theta_N} = (\theta_{D,i}^{max} - \theta_{D,i})^2 S^{(0)}, \quad (4b)$$

where

$$\hat{\epsilon}_{D_2} \equiv \frac{P_{D_2}t}{n_s(2\pi m_{D_2}kT)^{1/2}}, \quad (4c)$$

and  $\theta_{D,i}^{max}$ , the maximum fractional coverage of deuterium in state "i", is a function of the nitrogen precoverage (cf., Fig. 5).

For the case of precursor-mediated adsorption, the rates of first- and second-order adsorption are proportional, respectively, to [32]

$$\left(\frac{\partial\theta_{D,i}}{\partial\hat{\epsilon}_{D_2}}\right)_{T,P_{D_2},\theta_N} = \frac{(\theta_{D,i}^{max} - \theta_{D,i})S^{(0)}}{\kappa + \theta_{D,i}(\kappa - 1) + \theta_{D,i}^{max}(1 - \kappa)}, \quad (5a)$$

and

$$\left(\frac{\partial\theta_{D,i}}{\partial\hat{\epsilon}_{D_2}}\right)_{T,P_{D_2},\theta_N} = \frac{(\theta_{D,i}^{max} - \theta_{D,i})^2 S^{(0)}}{\theta_{D,i}^{max} - \theta_{D,i} + (1 - \theta_{D,i}^{max} + \theta_{D,i})\kappa + (1 - \theta_{D,i}^{max} + \theta_{D,i})^2 S^{(0)}}, \quad (5b)$$

where  $\kappa$  is a parameter that is inversely proportional to the lifetime of the precursor state on the surface [45,46]. For first-order adsorption, for example,  $\kappa$  is the ratio of the probability of desorption of a precursor molecule over a filled site to the sum of the probabilities of chemisorption and desorption of a precursor molecule above an empty site.

These models were fit to the experimental data by optimizing both the initial probability of adsorption  $S^{(0)}$  and the parameter  $\kappa$  (cf., Table 1). All second-order models failed to describe the observed adsorption kinetics of the  $\beta_2$ -state of deuterium, and the first-order models cannot describe the experimental data for the  $\beta_1$ -state, as on the clean surface. As may be seen in Fig. 6, all of the experimental data are consistent with the Langmuir models, and, therefore, it is not *necessary* to invoke the (two-parameter) precursor models. These results do not preclude, however, the existence of a molecular "precursor" to the dissociative adsorption of deuterium on these surfaces. Rather, they suggest that the (integral) measurements are insensitive to unambiguous manifestations of the precursor state.

#### 4. Desorption Kinetics of Deuterium from Clean and Nitrogen-precovered Pt(110)-(1x2) Surfaces

The thermal desorption spectra of  $D_2$ , adsorbed on Pt(110)-(1x2) at 120 K with various nitrogen precoverages (cf., Fig. 4) were also used to evaluate the coverage-dependent rate coefficients of desorption of deuterium. An analysis similar to that described in Sect. III.2 yields the activation energy and the preexponential factor of the desorption rate coefficient as a function of deuterium coverage for  $\theta_N$ =zero, 0.13, 0.26 and 0.4. These results are shown in Fig. 7(a) and (b).

On the clean surface, the desorption rate parameters of the  $\beta_2$ -state ( $\theta_D \leq 0.33$ ) are strongly dependent on deuterium coverage, whereas those of the  $\beta_1$ -state ( $\theta_D > 0.33$ ) are weak functions of coverage. For the  $\beta_2$ -state of deu-

terium, the activation energy of desorption increases from a low coverage limit of  $19 \text{ kcal-mol}^{-1}$  to a maximum value of  $26 \text{ kcal-mol}^{-1}$  at  $\theta_D=0.15$ , and then decreases with increasing  $\theta_D$ . Similarly, the preexponential factor of the desorption rate coefficient increases from a low coverage limit of  $3 \times 10^{-4} \text{ cm}^2\text{-s}^{-1}$  to a maximum value of  $0.3 \text{ cm}^2\text{-s}^{-1}$  at  $\theta_D=0.15$ , and then decreases with increasing  $\theta_D$ .

Likewise, for  $\theta_N=0.13$ , the kinetic parameters for desorption of the  $\beta_2$ -state of deuterium are functions of surface coverage of deuterium and obey a compensation effect, i.e., the activation energy of desorption and the preexponential factor increase with deuterium coverage up to maximum values at  $\theta_{D,\beta_2}^{max}/2$ , as for the clean surface, and then decrease with increasing  $\theta_D$ . The compensatory behavior of the desorption kinetic parameters of the  $\beta_2$ -state of deuterium on clean and nitrogen precovered Pt(110)-(1x2) ( $\theta_N=0.13$ ) is similar to that which was observed for hydrogen on Ir(110)-(1x2) [47]. At higher coverages of nitrogen, the behavior of the kinetic parameters for the  $\beta_2$ -state of deuterium is obscured, since the nitrogen adatoms selectively poison the  $\beta_2$ -state prior to the  $\beta_1$ -state (cf., Fig. 5).

On the clean surface, the activation energy of desorption of the  $\beta_1$ -state decreases approximately linearly with increasing coverage from a value of  $19 \text{ kcal-mol}^{-1}$  at  $\theta_D = 0.33$  to a value of  $13 \text{ kcal-mol}^{-1}$  at  $\theta_D = 0.65$ , whereas the preexponential factor of the desorption rate coefficient decreases from  $1.5 \times 10^{-3} \text{ cm}^2\text{-s}^{-1}$  at  $\theta_D = 0.33$  to  $1.5 \times 10^{-4} \text{ cm}^2\text{-s}^{-1}$  at  $\theta_D = 0.65$ . The effect of the nitrogen adatoms on the kinetic parameters of deuterium in the  $\beta_1$ -state is similar to that observed in the  $\beta_2$ -state, i.e., the kinetic parameters are modified

by approximately rescaling the effective coverage of deuterium.

The effects of  $\theta_N$  on both the activation energy  $E_{d,D_2}(\theta)$  and the preexponential factor  $k_{d,D_2}^{(0)}$  in the limit of low  $\theta_D$  are shown in Fig. 8. The variation with  $\theta_N$  of both the activation energy and the logarithm of the preexponential factor is approximately linear. These functional dependences can be described by

$$E_{d,D_2}(\theta_N) = E_{d,D_2}^{(0)} - 17\theta_N \text{ kcal} - \text{mol}^{-1}, \quad (6a)$$

and

$$k_{d,D_2}^{(0)}(\theta_N) = k_{d,D_2}^{(0)} e^{-9\theta_N}, \quad (6b)$$

the significance of which will be addressed in Sect. IV.

#### IV. Discussion

As may be seen from the thermal desorption spectra of ammonia in Fig. 1, there is a broad distribution of binding energies of ammonia on Pt(110)-(1x2) ranging from approximately 23.1 kcal-mol<sup>-1</sup> in the limit of zero coverage to approximately 12.8 kcal-mol<sup>-1</sup> at saturation coverage of the chemisorbed overlayer. This may be due to the fact that the electron donor bond is strongest initially at low coverage and becomes progressively weaker at higher coverages as the charge transfer per ammonia admolecule to the surface has decreased, as demonstrated from recent work function measurements of ammonia on Ru(001) [37]. The second-layer of adsorbed ammonia, characterized by a relatively sharp thermal desorption peak at 165 K, is hydrogen-bonded to the chemisorbed ammonia

monolayer. As may be seen in Fig. 1, the second-layer of ammonia begins to form prior to saturation of the chemisorbed monolayer. This is a consequence of the similar binding energies of the first- and second-layers of ammonia near saturation coverages. This bi-layer structure of ammonia on Pt(110)-(1x2), Pt(111) [36] and Ru(001) [37] is analogous to that of water on Ru(001) [48]. Furthermore, the thermal desorption spectra of molecularly adsorbed ammonia from the Pt(110)-(1x2) surface are similar to those that were measured on the Ru(001) [37] and Pt(111) surfaces [49], where the activation energy of desorption for ammonia was estimated to be 12-21 kcal-mol<sup>-1</sup> in the chemisorbed overlayer [37], and 8.6 kcal-mol<sup>-1</sup> in the second-layer [49].

The probability of dissociative adsorption of ammonia of  $4 \times 10^{-3}$  in the limit of zero coverage on the Pt(110)-(1x2) surface at 400 K is consistent with the value estimated during a separate study of the steady-state decomposition of ammonia on the same surface [50]. The probability of dissociation  $P_r$ , which is, in general, a function of the surface coverage, is defined as the ratio of the rate of dissociation  $R_r$  to the rate of desorption  $R_d$ , i.e., in the limit of zero coverage, it is defined as

$$P_r^{(0)} = \frac{R_r}{R_r + R_d}, \quad (7)$$

where

$$R_r = n_s \theta_{NH_3} k_r^{(0)} e^{-E_r/k_B T}, \quad (8)$$

$$R_d = n_s \theta_{NH_3} k_d^{(0)} e^{-E_d/k_B T}, \quad (9)$$

and  $k_r^{(0)}$ ,  $E_r$  and  $k_d^{(0)}$ ,  $E_d$  are the preexponential factors and the activation energies for dissociation and desorption, respectively. Using kinetic parameters that were determined from mechanistic modeling of the *steady-state* decomposition of ammonia on Pt(110)-(1x2) [50] ( $k_r^{(0)} = 5 \times 10^{11} \text{ s}^{-1}$ ,  $k_d^{(0)} = 10^{14} \text{ s}^{-1}$  and  $E_r - E_d = 0.5 \text{ kcal-mol}^{-1}$ ), the expected value of  $P_r^{(0)}$  at 400 K is approximately  $3 \times 10^{-3}$ , which is in good agreement with the present transient measurement. In the case of finite surface coverages, the rate of dissociation in Eq. (8) is given by  $n_s \theta_{NH_3} (1 - \theta) k_r^{(0)} e^{-E_r/k_B T}$ , where  $\theta$  is the sum of  $\theta_N$ ,  $\theta_{NH_3}$  and  $\theta_H$ . The probability of dissociation at  $\theta_N = 0.99$  and 400 K, for instance (using the same set of kinetic parameters) is calculated to be  $4 \times 10^{-6}$ , which is also consistent with steady-state measurements on this surface when  $\theta_N$  is close to unity [50].

The measured activation energy of desorption of nitrogen from Pt(110)-(1x2) is consistent with the value determined during the steady-state decomposition of ammonia on the same surface [50]. Whereas an activation energy of  $22 \text{ kcal-mol}^{-1}$  and a preexponential factor of  $4 \times 10^{-8} \text{ cm}^2\text{-s}^{-1}$  were reported for the desorption of nitrogen at low temperatures and/or high pressures, from studies of steady-state decomposition of ammonia on a polycrystalline platinum wire at pressures between  $5 \times 10^{-7}$  and 0.5 Torr and temperatures between 400 and 1200 K. [23]. The similarity of the kinetic parameters for the desorption of nitrogen on Pt(110)-(1x2) and polycrystalline platinum surfaces at *high* surface coverages of nitrogen adatoms, indicates the desorption of nitrogen under these conditions is at most, only slightly sensitive to the structure of the platinum surface [51,52].

From Figs. 4 and 5, it is clear that nitrogen adatoms selectively poison

the  $\beta_2$ -state of deuterium prior to poisoning the  $\beta_1$ -state. This suggests an initial occupation of the pseudo-fourfold hollow sites by nitrogen adatoms [53,54] where hydrogen is thought to chemisorb in the  $\beta_2$ -state on both Ir(110)-(1x2) and Pt(110)-(1x2) surfaces [41,47]. The structure of the Pt(110)-(1x2) surface may be thought of as (111) microfacets, which are three atomic rows in width and which are inclined at an angle of  $109.5^\circ$  with respect to one another (cf., Fig. 9). The probable binding sites of hydrogen on this surface are indicated in Fig. 9 [41,47,55], where "A" is a pseudo-fourfold hollow site for the  $\beta_2$ -state of hydrogen, and "B" and "C" are the inequivalent threefold binding sites for the  $\beta_1$ -state. The agreement of the experimental data with Eqs. 4(a) and (b) for the two adstates and the linear decrease of  $\theta_{D,\beta_2}^{max}$  with  $\theta_N$  for  $\theta_N < \frac{1}{3}$  and of  $\theta_{D,\beta_1}^{max}$  with  $\theta_N$  for  $\theta_N > \frac{1}{3}$  (cf., Fig. 5) indicate that the adsorption kinetics of deuterium (or hydrogen) on the nitrogen precovered surfaces follow a site-blocking mechanism. Within experimental uncertainty, one nitrogen adatom blocks the adsorption of one deuterium adatom (cf., Fig. 5). Furthermore, the linear and independent poisoning of both the  $\beta_2$ - and  $\beta_1$ -states of deuterium by nitrogen adatoms implies the absence of 'long-range' electronic perturbations of the surface by the nitrogen insofar as the chemisorption of hydrogen is concerned. This behavior is in contrast to the nonlinear (or non-geometric) poisoning in the coadsorption of hydrogen and sulfur, and hydrogen and nitrogen on the Ni(100) surface [17,19]. Long-range electronic effects due to the sulfur and nitrogen adatoms were invoked to explain the observed large deviation from geometrical site-blocking. In addition, the variation of the "initial" probability of adsorption of hydrogen with nitrogen and sulfur precoverages on Ni(100) was found to be described by Eq. (1) [17,19], whereas this probability is approximately the same

on both the nitrogen-precovered and the clean Pt(110)-(1x2) surfaces (cf., Table 1).

The adsorption kinetics of deuterium on clean and nitrogen precovered Pt(110)-(1x2) are described well by Langmuir models for the entire range of coverages studied, when the observed linear poisoning of the two deuterium adstates by the nitrogen adatoms is taken into account. The orders of reaction for the adsorption of deuterium on the nitrogen precovered surfaces are the same as those on the clean surface, namely, first-order for the  $\beta_2$ -state and second-order for the  $\beta_1$ -state. Furthermore, the influence of any molecular precursor state on the dissociative adsorption of deuterium on either clean or nitrogen precovered Pt(110)-(1x2) is not manifest in the thermal desorption data.

In addition to blocking sites for the adsorption of deuterium, the nitrogen adatoms modify the activation energy and the preexponential factor of the desorption rate coefficient of deuterium on Pt(110)-(1x2) by "rescaling" the fractional coverage of deuterium adatoms to a higher effective value (cf., Fig. 7(a)). This effect of a modified activation energy of desorption has been observed also with the coadsorption of hydrogen and sulfur, and hydrogen and nitrogen on Ni(100) and Ru(001) surfaces [17-20], where downshifts of peak temperature of desorption of hydrogen were observed and the presence of the preadsorbed adatoms was assumed to reduce the local electron density of states of the substrate, resulting in a weakening of the substrate-hydrogen chemisorption bond.

On the clean surface,  $E_{d,D_2}(\theta)$  for the  $\beta_2$ -state increases with deuterium coverage up to  $\theta_{D,\beta_2}^{max}/2$  due to next-nearest neighbor attractive interactions be-

tween deuterium adatoms (approximately  $3.5 \text{ kcal-mol}^{-1}$  per adatom) and decreases at higher coverages due to nearest neighbor repulsive interactions (approximately  $3.5 \text{ kcal-mol}^{-1}$  per adatom) [56]. The same behavior is observed for the nitrogen-precovered surface ( $\theta_N=0.13$ ), except in a compressed range of coverages (cf., Fig. 7). The decrease of  $E_{d,D_2}(\theta)$  for the  $\beta_1$ -state on the clean surface is more gradual compared to the  $\beta_2$ -state, and only (net) repulsive interactions are present over the whole range of coverages.

Recently, a mechanistic model consisting of elementary surface reactions was introduced that describes accurately experimentally measured rates of the steady-state decomposition of ammonia from  $10^{-7}$  to 0.5 Torr on polycrystalline platinum [23,24]. The measured inhibition of ammonia decomposition by hydrogen suggested that the desorption kinetics of hydrogen were modified by the presence of nitrogen adatoms, compared to those appropriate for the clean surface [24]. In particular, if the rate of recombinative desorption of hydrogen is written in the form of Eq. (3), it was found that the preexponential factor and the activation energy of the desorption rate coefficient of hydrogen obeyed the following functional relationships:

$$k_{d,H_2}^{(0)}(\theta) = k_{d,H_2}^{(0)} e^{-\alpha\theta}, \quad (10a)$$

and

$$E_{d,H_2}(\theta) = E_{d,H_2}^{(0)} - \beta\theta, \quad (10b)$$

where  $\theta$  is the fractional surface coverage (essentially that of nitrogen adatoms, the dominant surface species during the ammonia decomposition reaction), and

$\alpha$  and  $\beta$  are empirical constants. It was proposed that this compensation effect occurs under reaction conditions when the nitrogen coverage is high ( $0.1 < \theta_N$ ) and the hydrogen coverage is low ( $\theta_H \leq 0.01$ ) [24]. A comparison with Eqs. (6a,b) shows that these are the exact functional forms that were deduced from the mechanistic modeling of ammonia decomposition with hydrogen inhibition [24].

## V. Conclusions

Ammonia chemisorbs molecularly on Pt(110)-(1x2) at 120 K, with binding energies ranging from 23.1 kcal-mol<sup>-1</sup> in the limit of zero coverage to 12.8 kcal-mol<sup>-1</sup> at saturation coverage. The probability of dissociative adsorption of ammonia on Pt(110)-(1x2) at 400 K is  $4 \times 10^{-3}$  in the limit of zero coverage. The activation energy of the recombinative desorption of nitrogen from Pt(110)-(1x2) is approximately 24 kcal-mol<sup>-1</sup>, while the preexponential factor of the desorption rate coefficient ranges from approximately  $5 \times 10^{-5}$  cm<sup>2</sup>-s<sup>-1</sup> at low coverages ( $\theta_N \leq 0.15$ ) to approximately  $5 \times 10^{-7}$  cm<sup>2</sup>-s<sup>-1</sup> at higher coverages ( $\theta_N \geq 0.3$ ).

Nitrogen adatoms selectively poison the  $\beta_2$ -state of deuterium prior to poisoning the  $\beta_1$ -state without any 'long-range' electronic perturbations of the surface. The kinetics of chemisorption of both states of deuterium on clean and nitrogen precovered Pt(110)-(1x2) obey Langmuir models, and the modification of the adsorption kinetics of deuterium by nitrogen adatoms is governed by site blocking. Nitrogen adatoms modify the preexponential factor and the activation energy of desorption of deuterium on Pt(110)-(1x2) by rescaling the effective

coverage of the deuterium adatoms.

*Acknowledgment.* This research was supported by the National Science Foundation under Grant No. CHE-8516615.

## References

- [1] O' Hanlon J.F., *A User's Guide to Vacuum Technology* (John Wiley & Sons, Inc., New York 1980).
- [2] Baer D.R. , *Appl. Surface Sci.* **1984**, *19*, 382.
- [3] Dodiuk H., Yaniv A.E., Klein I.E., Fin N. and Drori L., *Appl. Surface Sci.* **1986**, *25* 137.
- [4] Martin G.A., in *Metal-Support and Metal-Additive Effects in Catalysis*, Eds., Imelik B., Naccache C., Coudurier G., Praliaud H., Meriaudeau P., Gallezot P., Martin G.A. and Vedrine J.C. (Elsevier, New York, 1982), p. 315.
- [5] Boudart M., *Catal. Rev.-Sci. Eng.* **1981**, *23*, 1.
- [6] Ertl G., in *Catalysis, Science and Technology*, Eds., Anderson J.R. and Boudart M., Vol. 4 (Springer, Berlin, 1983), p. 210.
- [7] Ertl G., Lee S.B. and Weiss M., *Surface Sci.* **1981**, *111*, 584.
- [8] Campbell C.T. and Goodman D.W., *Surface Sci.* **1982**, *123*, 413.
- [9] Dry M.E., *Brennst.-Chem.* **1969**, *50*, 193.
- [10] Bonzel H.P. and Krebs H.J., *Surface Sci.* **1981**, *109*, L527.
- [11] Benzinger J. and Madix R.J., *Surface Sci.* **1980**, *94*, 119.
- [12] Kirkpatrick W.J., in *Advances in Catalysis*, Eds., Frankenberg W., Komarewski V.I. and Rideal E.K. (Academic, New York, 1951), p. 329.
- [13] Takeuchi A., Tanaka K., Toyoshima K.I. and Miyahara K., *Chem. Phys. Letters* **1974**, *25*, 411.
- [14] Takeuchi A., Tanaka K., Toyoshima K.I. and Miyahara K., *J. Catal.* **1974**, *40*, 94.
- [15] Greensfelder B.S. and Patterson W.R., U.S. Patent No.2 **1946**, 402, 493.
- [16] Ertl G., Huber M., Lee S.B., Paal Z. and Weiss M., *Appl. Surface Sci.* **1981**, *8*, 373.
- [17] Kiskinova M. and Goodman D.W., *Surface Sci.* **1981**, *109*, L555.
- [18] Schwarz J.A., *Surface Sci.* **1979**, *87*, 525.
- [19] Kiskinova M. and Goodman D.W., *Surface Sci.* **1981**, *108*, 64.

- [20] Johnson S. and Madix R.J., Surface Sci. **1981**, 108, 77.
- [21] Feibelman P.J. and Hamann D.R., Phys. Rev. Letters **1984**, 52, 61.
- [22] Lang N.D., Holloway S. and Norskov J.K., Surface Sci. **1985**, 150, 24.
- [23] Vajo J.J., Tsai W. and Weinberg W.H., J. Phys. Chem. **1985**, 89, 3243.
- [24] Tsai W., Vajo J.J. and Weinberg W.H., J. Phys. Chem. **1985**, 89, 4926.
- [25] Taylor J.L., Ibbotson D.E. and Weinberg W.H., J. Chem. Phys. **1978**, 69, 4298.
- [26] Niehus H. and Comsa G., Surface Sci. , **1981**, 102, L14; Niehus H. and Comsa G., Surface Sci. **1980**, 93, L147.
- [27] Lahee A.M., Allison W., Willis R.F. and Rieder K.H., Surface Sci. **1983**, 126, 654.
- [28] Niehus H., Surface Sci. **1984**, 145, 407.
- [29] Kellogg G.L., Phys. Rev. Letters **1985**, 55, 2168.
- [30] Chan C.M., Van Hove M.A., Weinberg W.H. and Williams E.D., Solid State Commun. **1979**, 30, 47; Chan C.M., Van Hove M.A., Weinberg W.H. and Williams E.D., Surface Sci. **1980**, 91, 430.
- [31] Ibbotson D.E., Wittrig T.S. and Weinberg W.H., Surface Sci. **1981**, 110, 294.
- [32] Tsai W., PhD Thesis, California Institute of Technology **1987**.
- [33] Engstrom J.R. and Weinberg W.H., Rev. Sci. Instrum. **1984**, 55, 404.
- [34] Feulner P. and Menzel D., J. Vacuum Sci. Technol. **1980**, 17, 662.
- [35] Redhead P.A., Vacuum **1962**, 12, 203.
- [36] Sexton B.A., and Mitchell G.E., Surface Sci. **1980**, 99, 523.
- [37] Benndorf C., and Madey T.E., Surface Sci. **1983**, 135, 164.
- [38] The heat of sublimation of ammonia is estimated to be approximately 6.9 kcal-mol<sup>-1</sup>; *Lange's Handbook of Chemistry*, 13th Ed., Eds., Lange N.A. and Forker G.M. (Handbook of Publishers, Sandusky, 1984), p. 300.
- [39] Unertl W.N., Jackman T.E., Norton P.R., Jackson D.P. and Davies J.A., J. Vacuum Sci. Technol. **1982**, 20, 607.
- [40] Taylor J.L. and Weinberg W.H., Surface Sci. **1978**, 78, 259.

- [41] Engstrom J.R., Tsai W. and Weinberg W.H. (in preparation).
- [42] Ferrer S. and Bonzel H.P., *Surface Sci.* **1982**, 119, 234.
- [43] The behavior of hydrogen on this surface is identical to that of deuterium [41].
- [44] Jackman T.E., Davies J.A., Jackson D.P., Unertl W.N. and Norton P.R., *Surface Sci.* **1982**, 120, 389.
- [45] Kisliuk P., *J. Phys. Chem. Solids* **1957**, 3, 95.
- [46] Kisliuk P., *J. Phys. Chem. Solids* **1958**, 5, 78.
- [47] Ibbotson D.E., Wittrig T.S. and Weinberg W.H., *J. Chem. Phys.* **1980**, 72, 4885.
- [48] Thiel P.A., Hoffmann F.M. and Weinberg W.H., *J. Chem. Phys.* **1981**, 75, 5556.
- [49] Gland J.L. and Kollin E.B., *Surface Sci.* **1981**, 104, 478.
- [50] Vajo J.J., Tsai W. and Weinberg W.H., *J. Phys. Chem.* **1986**, 90, 6531.
- [51] The structure of polycrystalline platinum has been shown to consist of mostly (111)-oriented microfacets from extensive annealing of a polycrystalline platinum ribbon at 1400 K for 12 h [52].
- [52] Lambert, R.M. and Comrie, C.M., *Surface Sci.* **1974**, 46, 61.
- [53] It was suggested that the preferred binding site for nitrogen adatoms on Fe(100) is a fourfold hollow site [54].
- [54] Grunze M., in *The Chemical Physics of Solid Surfaces and Heterogeneous Catalysis*, King D.A. and Woodruff D.P., Eds., Vol.4, Elsevier Amsterdam, 1982, p143.
- [55] Doyen G. and Ertl G., *J. Chem. Phys.* **1978**, 68, 5417.
- [56] For the Pt(110)-(1x2) surface, the saturation density of the  $\beta_2$ - adstate is approximately equal to the density of the "trough" sites, i.e., one hydrogen adatom per reconstructed primitive unit cell.

TABLE 1. ADSORPTION KINETICS OF DEUTERIUM ON CLEAN  
AND NITROGEN-PRECOVERED Pt(110)-(1x2) SURFACES

	<u><math>\beta_2</math>-state (first-order)</u>		<u><math>\beta_1</math>-state (second-order)</u>	
	<u>Langmuir</u> $S^{(0)}$	<u>Kisliuk</u> $S^{(0)}, \kappa$	<u>Langmuir</u> $S^{(0)}$	<u>Kisliuk</u> $S^{(0)}, \kappa$
$\theta_N=0$	0.46	0.44, 0.5	0.024	0.015, 0.5
$\theta_N=0.13$	0.75	0.46, 0.5	-	-
$\theta_N=0.26$	0.46	0.44, 0.5	-	-
$\theta_N=0.40$	-	-	0.020	0.015, 0.5

### Figure Captions

- Fig. 1: Thermal desorption spectra of deuterated ammonia ( $^{15}\text{ND}_3$ ) from Pt(110)-(1x2), parametric in ammonia exposure: (a), 1.5 L; (b), 3.5 L; (c), 5.5 L; (d), 7.5 L; and (e), 10 L. The temperature of adsorption is 120 K, and the heating rate is  $5.0 \text{ K-s}^{-1}$ .
- Fig. 2: Thermal desorption spectra of nitrogen from Pt(110)-(1x2) parametric in ammonia ( $^{14}\text{NH}_3$ ) exposure: (a), 10 L,  $\theta_N=0.13$ ; (b), 30 L,  $\theta_N=0.17$ ; (c), 90 L,  $\theta_N=0.26$ ; (d), 300 L,  $\theta_N=0.4$ ; and (e), 400 L,  $\theta_N=0.45$ . The temperature of adsorption is approximately 400 K, and the heating rate is  $5.0 \text{ K-s}^{-1}$ .
- Fig. 3: Activation energy  $E_{d,N_2}(\theta_N)$  and preexponential factor  $k_{d,N_2}^{(0)}(\theta_N)$  of the rate coefficient of desorption of nitrogen from Pt(110)-(1x2) as a function of the fractional surface coverage of nitrogen.
- Fig. 4: Thermal desorption spectra of deuterium from Pt(110)-(1x2) parametric in deuterium exposure with various fractional coverages of nitrogen: (a), zero; (b), 0.13; (c), 0.26; and (d), 0.4. The temperature of adsorption is 120 K, and the heating rate is  $5.0 \text{ K-s}^{-1}$ .
- Fig. 5: The maximum fractional surface coverages of the  $\beta_2$ -adstate ( $\theta_{D,\beta_2}^{max}$ ) and the  $\beta_1$ -adstate ( $\theta_{D,\beta_1}^{max}$ ) of deuterium as a function of the fractional surface coverage of nitrogen.
- Fig. 6: The coverage-exposure relation for deuterium on Pt(110)-(1x2) together with analytic fits to the adsorption kinetics with Langmuir and precursor models. (a)  $\beta_2$ -state (first-order); and (b)  $\beta_1$ -state (second-order).
- Fig. 7: (a) Activation energy  $E_{d,D_2}(\theta_D)$  and (b) preexponential factor  $k_{d,D_2}^{(0)}(\theta_D)$  for deuterium desorption from Pt(110)-(1x2) as a function of fractional coverage of deuterium for  $\theta_N = \text{zero}, 0.13, 0.26$  and  $0.4$ .
- Fig. 8: Activation energy  $E_{d,D_2}(\theta_N)$  and preexponential factor  $k_{d,D_2}^{(0)}(\theta_N)$  for deuterium desorption from Pt(110)-(1x2) as a function of the fractional surface coverage of nitrogen for  $\theta_D=0.05$ .

Fig. 9: Probable locations of hydrogen on Pt(110)-(1x2). "A" represents the probable location for the  $\beta_2$ -adstate of hydrogen, which is a pseudo-fourfold hollow site. "B" and "C" represent the probable binding sites for the  $\beta_1$ -adstate of hydrogen, which are inequivalent threefold hollow sites.

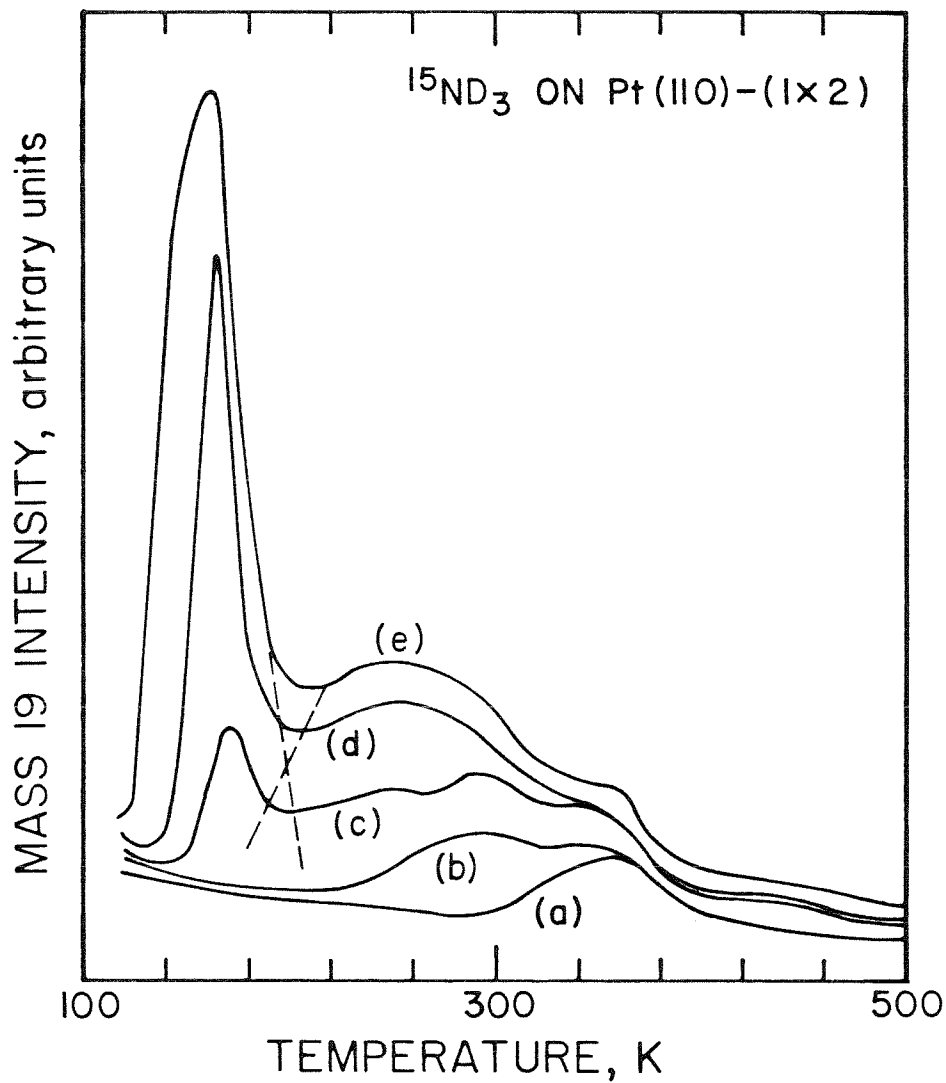


Figure 1

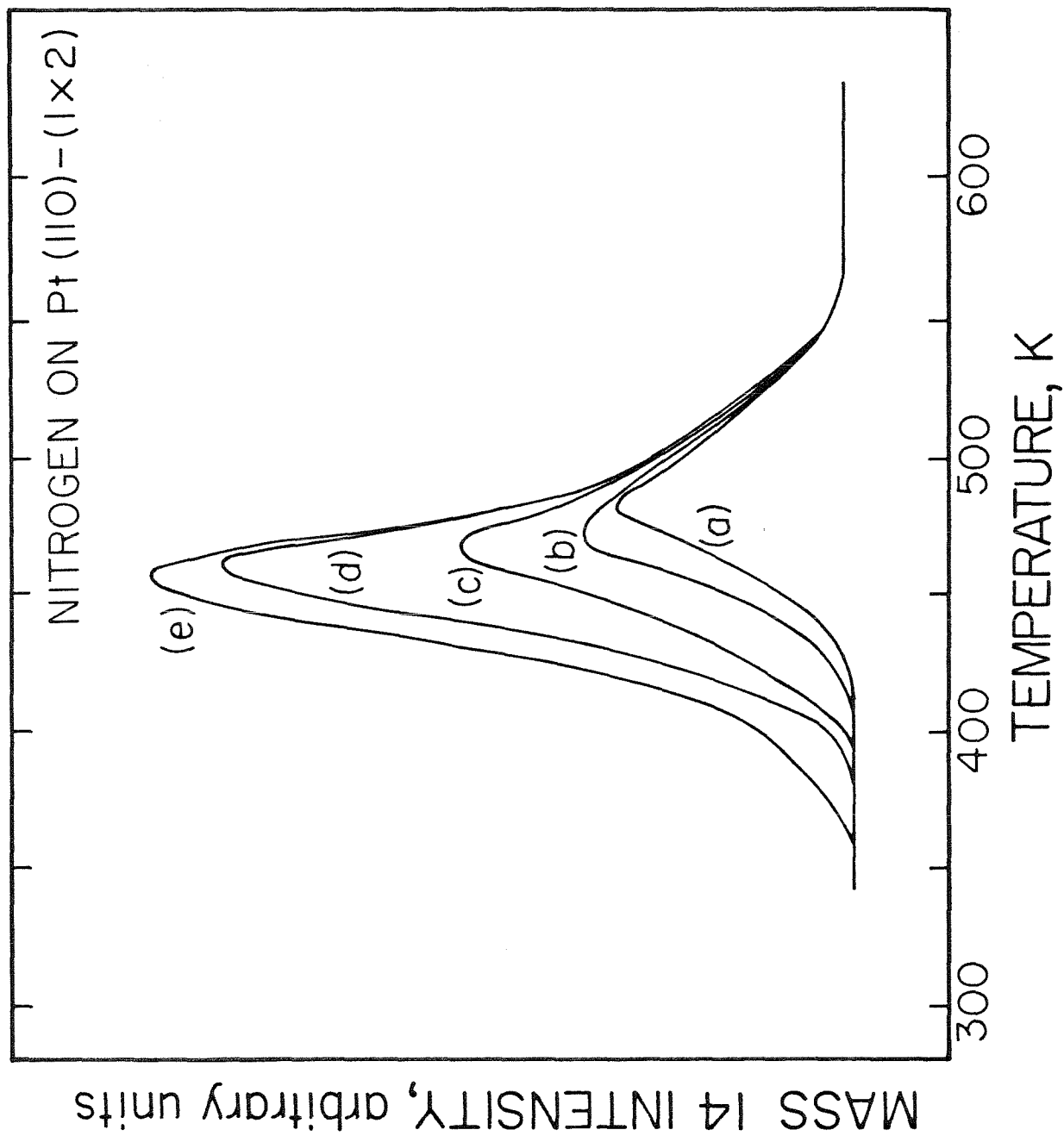


Figure 2

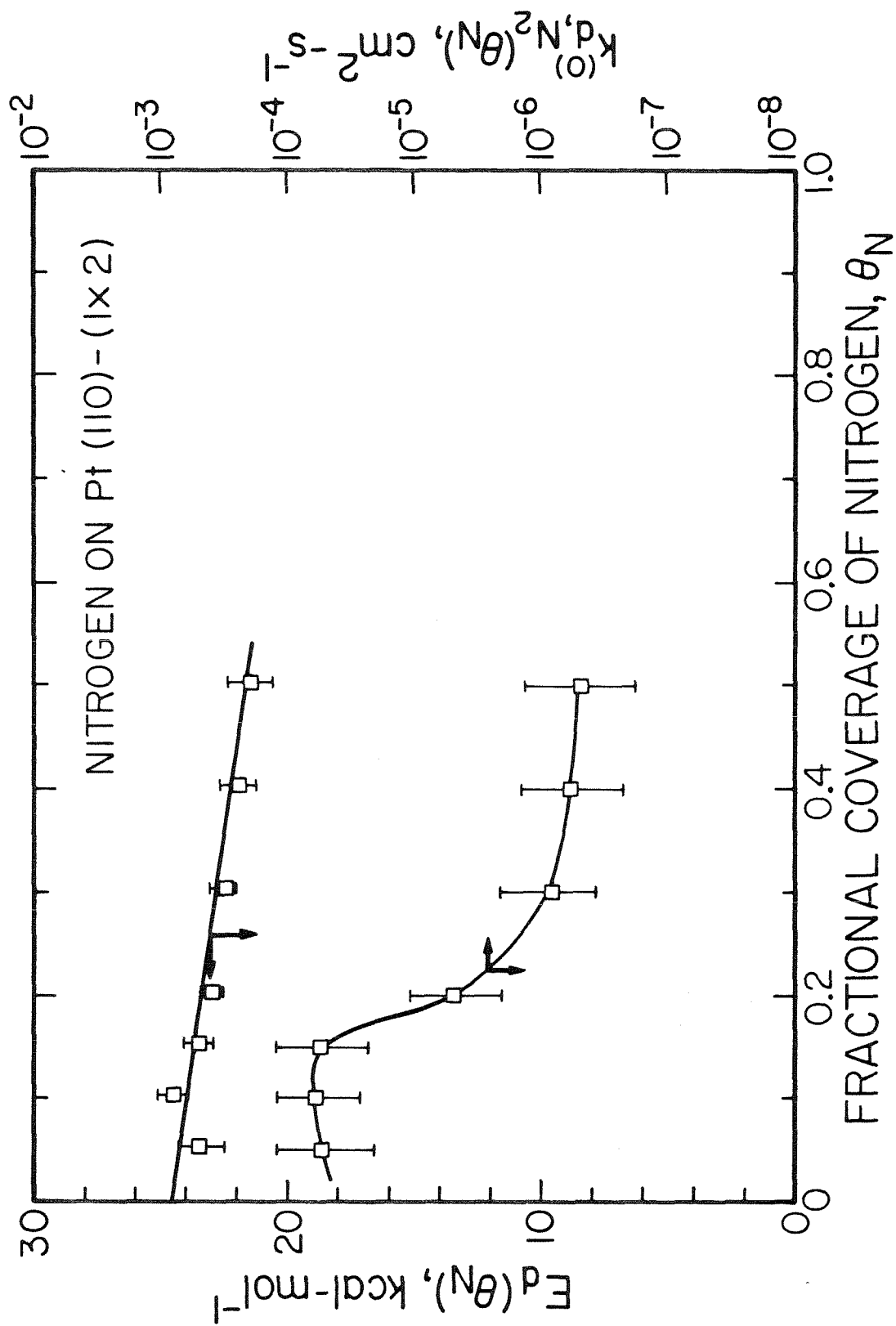


Figure 3

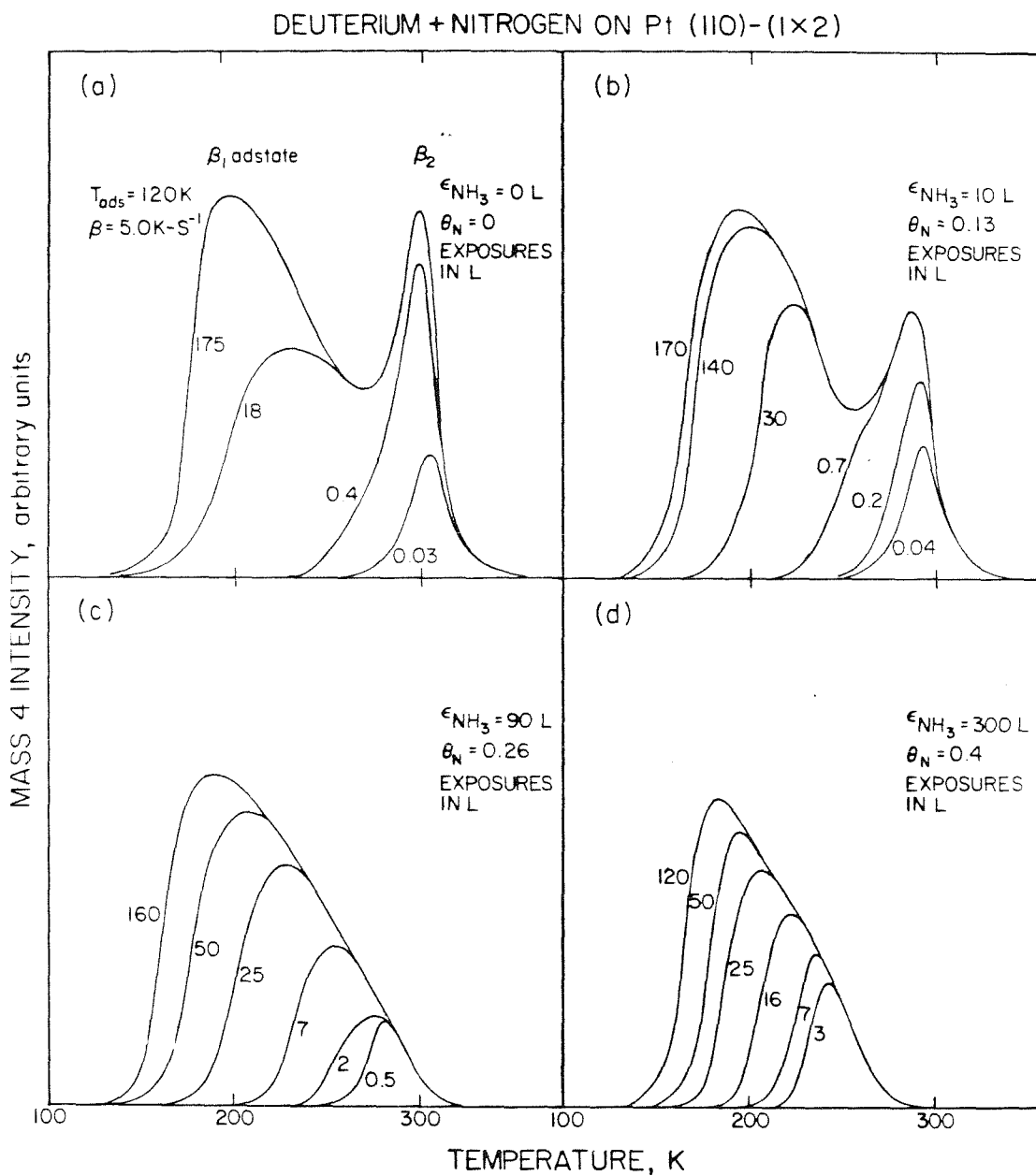


Figure 4

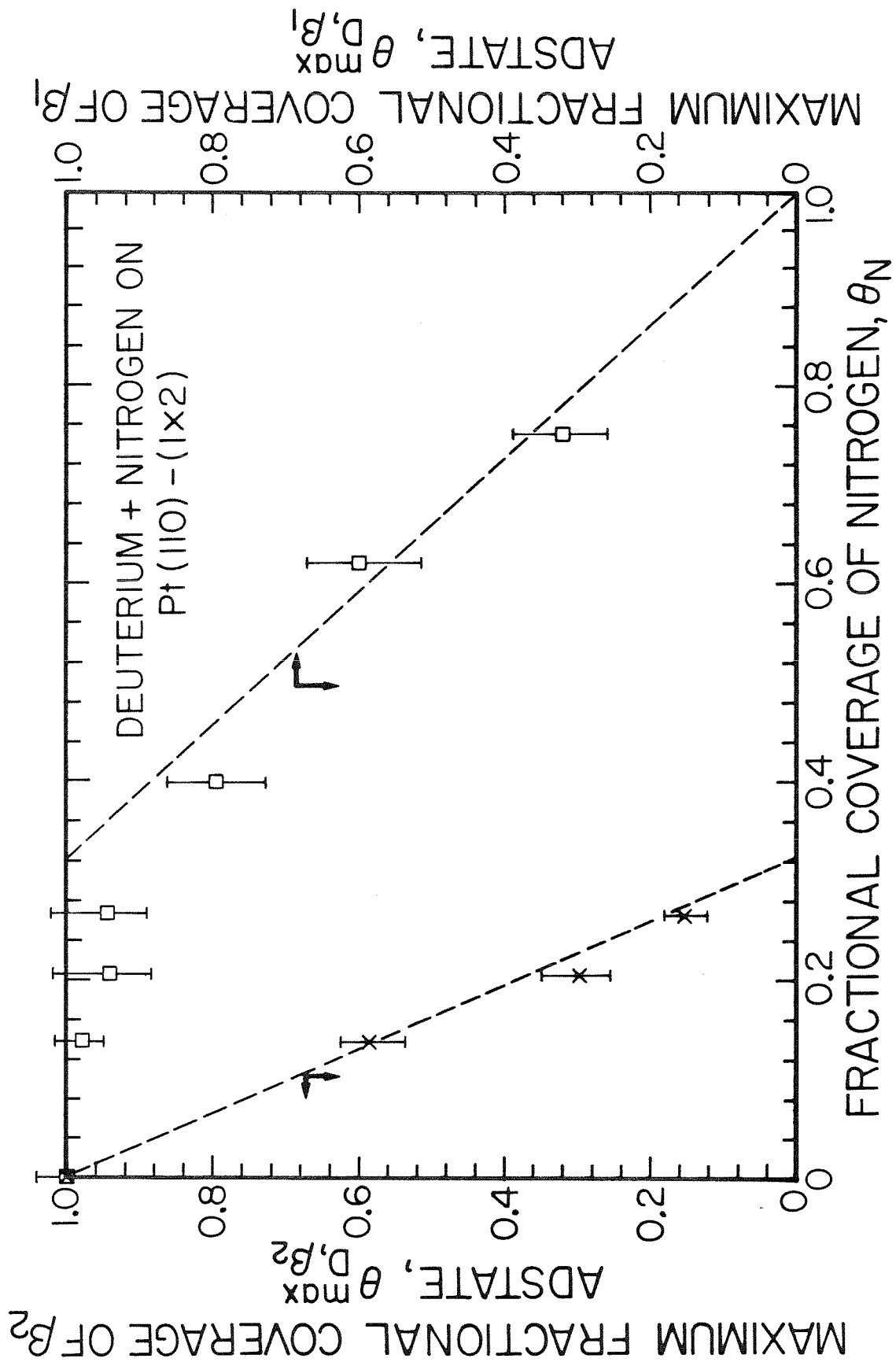


Figure 5

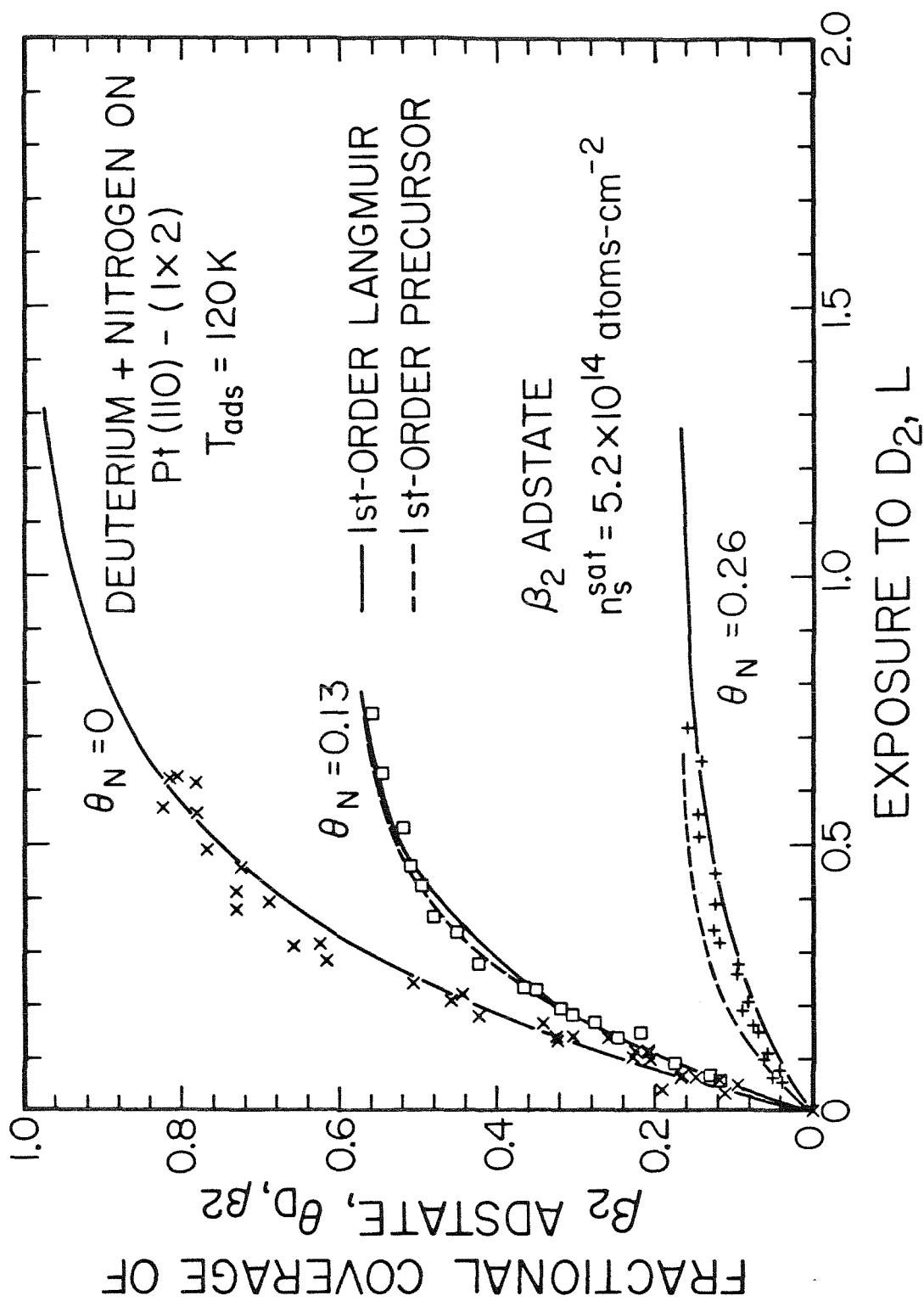


Figure 6(a)

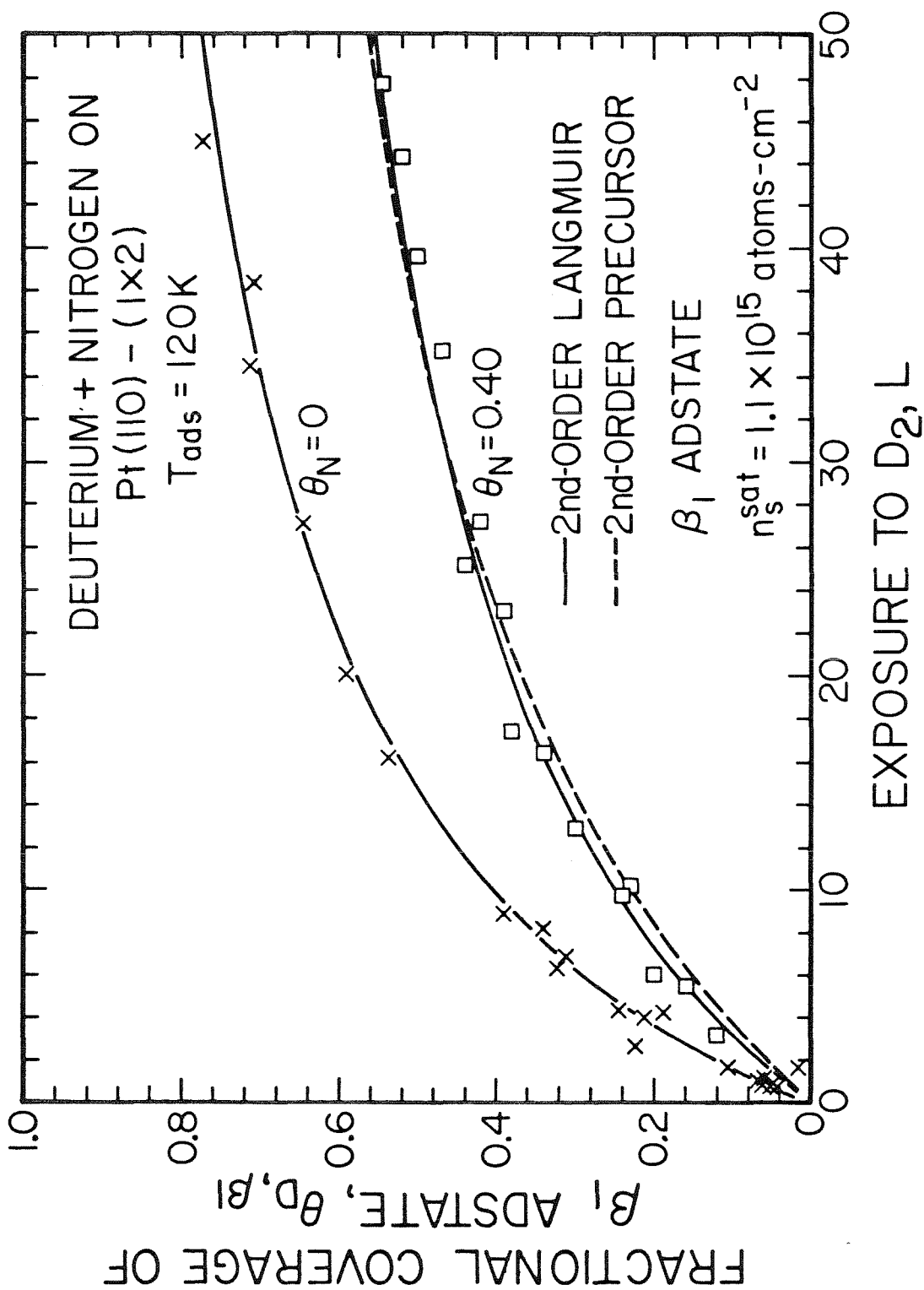


Figure 6(b)

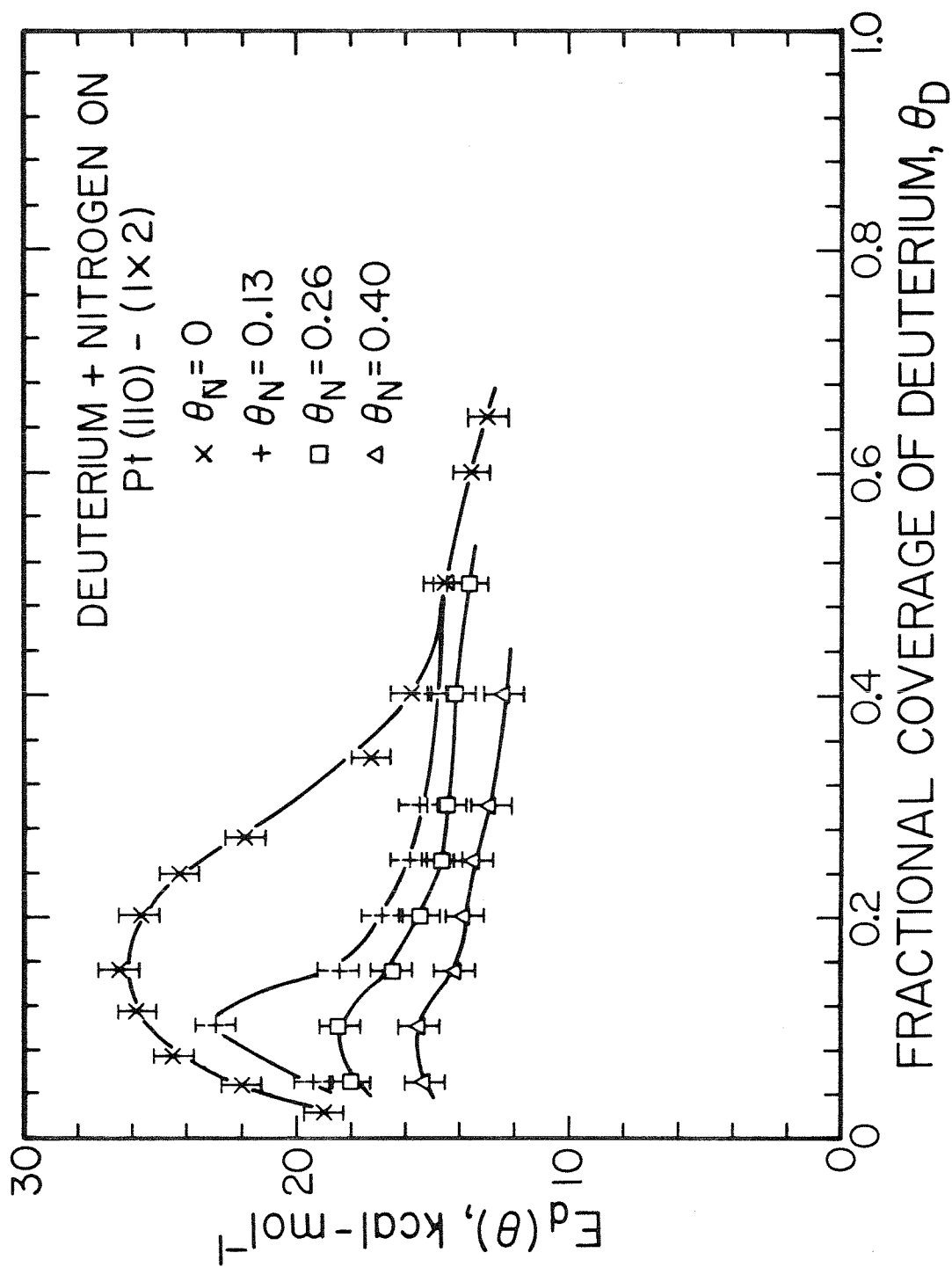


Figure 7(a)

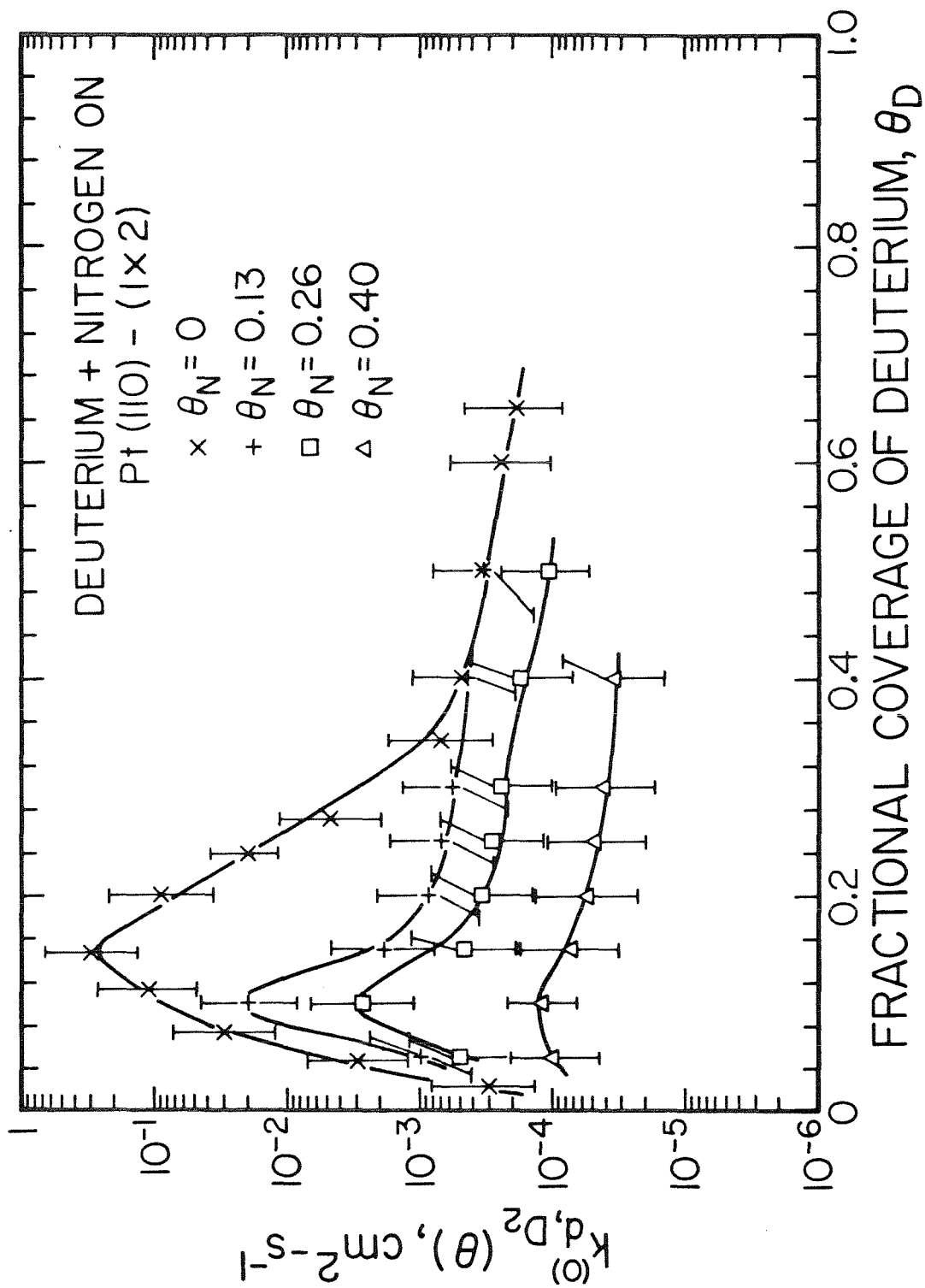


Figure 7(b)

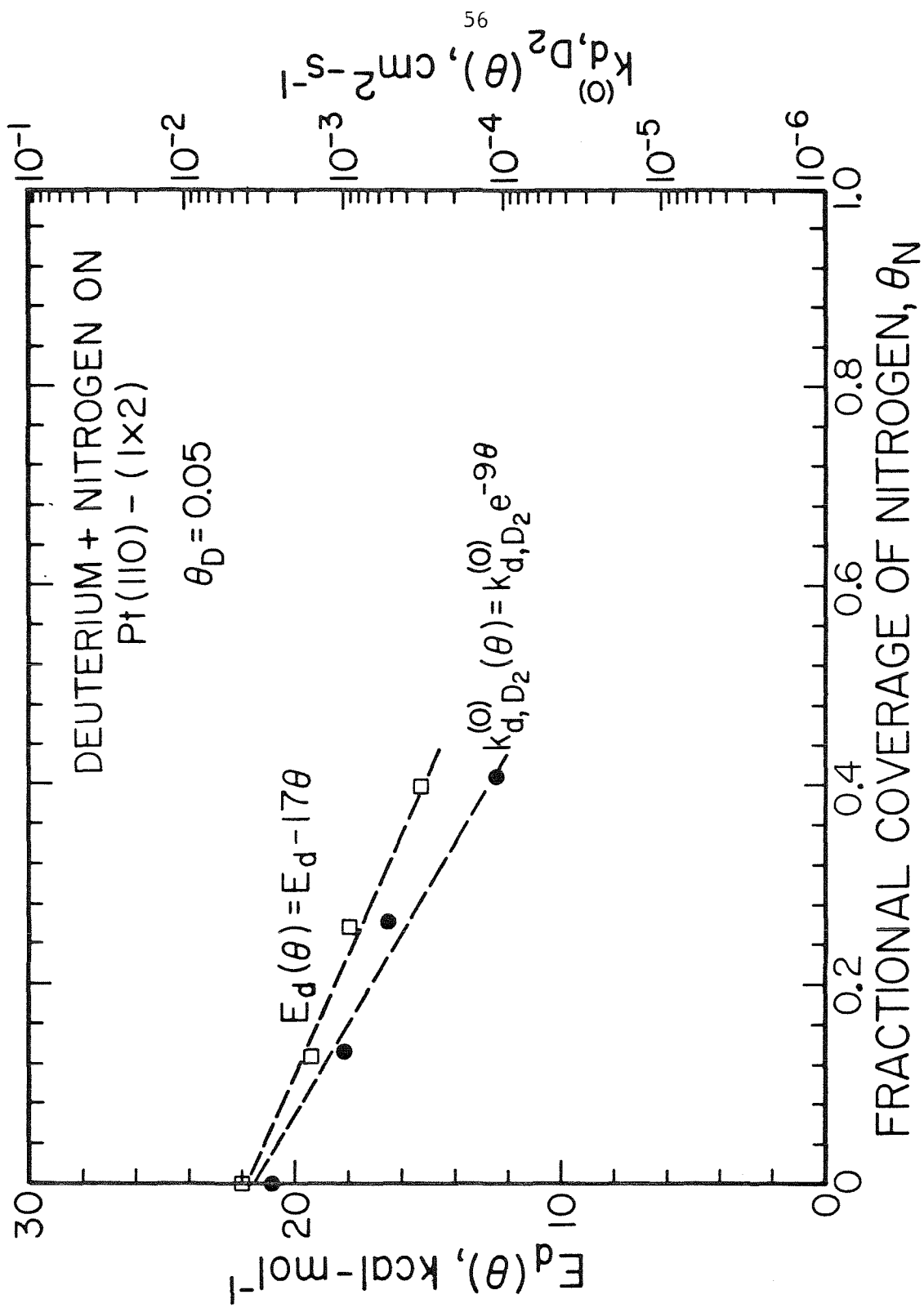


Figure 8

Pt (110) - (1x2)

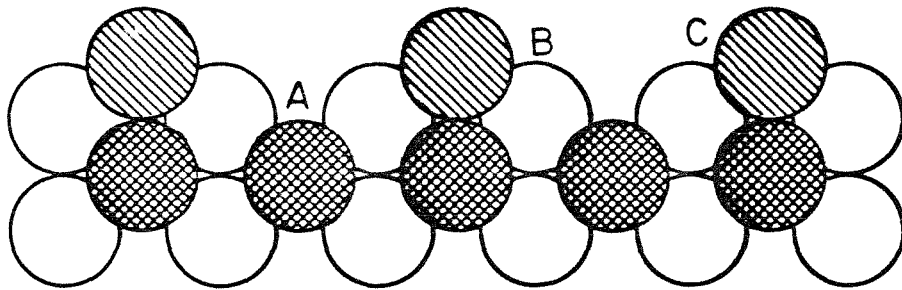
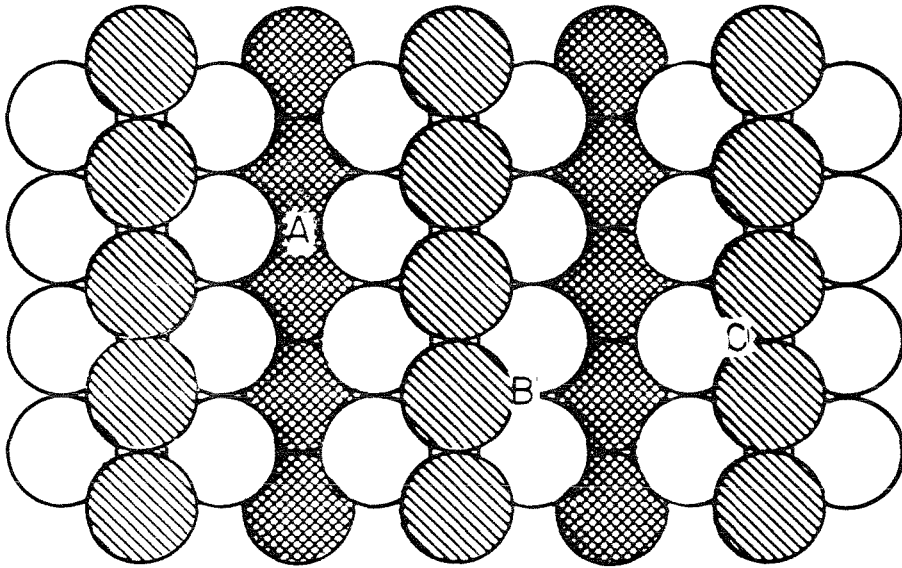


Figure 9

**Chapter 4.**

Steady-State Decomposition of Ammonia on the Ru(001) Surface

[Chapter 4 consists of an article coauthored with W.H. Weinberg.]

### Abstract

Steady-state specific reaction rates for the catalytic decomposition of ammonia at pressures of  $1 \times 10^{-6}$  and  $2 \times 10^{-6}$  Torr have been measured on the Ru(001) surface at temperatures between approximately 500 and 1250 K. For temperatures above 750 K, the reaction rate approaches first-order in ammonia pressure, and the apparent activation energy is  $5.0 \pm 0.3$  kcal-mol<sup>-1</sup>. A kinetic isotope effect is observed at these high temperatures, and the activation energy for the decomposition of deuterated ammonia is  $6.6 \pm 0.3$  kcal-mol<sup>-1</sup>. This apparent activation energy is associated with the difference in activation energies between that of the cleavage of a nitrogen-hydrogen (nitrogen-deuterium) bond in chemisorbed ammonia and that of the desorption of molecularly chemisorbed ammonia. At lower temperatures, the reaction rate is independent of ammonia pressure, and the apparent activation energy is  $43 \pm 3$  kcal-mol<sup>-1</sup> which is associated with the recombinative desorption of nitrogen. From independent measurements, the activation energy of the desorption of nitrogen on Ru(001) was found to be  $44.0 \pm 0.5$  kcal-mol<sup>-1</sup>, and the preexponential factor of the desorption rate coefficient is  $1.3 \pm 0.6 \times 10^{-3}$  cm<sup>2</sup>-s<sup>-1</sup>. Based on thermal desorption measurements during the steady-state decomposition of ammonia at  $2 \times 10^{-6}$  Torr, nitrogen adatoms are the dominant surface species at these experimental conditions. A mechanistic model that has been introduced previously [J.J. Vajo, W. Tsai and W.H. Weinberg, *J. Phys. Chem.* **1985**, 89, 3243] was found to describe accurately the pressure and temperature dependence of both the measured decomposition kinetics and steady-state coverage of nitrogen adatoms.

## I. Introduction

The synthesis of ammonia from nitrogen and hydrogen on iron catalysts (the Haber process [1]) is one of the more important catalytic processes that has been developed, and there have been numerous subsequent investigations aimed at determining the mechanism of ammonia synthesis on transition metal surfaces, including both measurements of the reaction kinetics as well as a characterization of the catalytic surface [2-6]. Ruthenium (4.5 wt-%) supported on active carbon and promoted by potassium (3.2 wt-%) has been reported to be a better catalyst for ammonia synthesis than the doubly-promoted iron catalyst ( $\text{Fe-K}_2\text{O-Al}_2\text{O}_3$ ) [7-10]. The rate of synthesis of ammonia on the ruthenium catalyst is 4-10 times greater than that on the iron catalyst at temperatures between 520 and 590 K, and a total pressure of 600 Torr of a stoichiometric mixture of hydrogen and nitrogen [7]. Indeed, ammonia synthesis was observed to proceed at a rate of 0.011 mmol per day and per gram of catalyst on potassium-promoted ruthenium supported on active carbon at room temperature and one atmosphere total pressure [9].

Studies of the catalytic decomposition of ammonia on transition metal surfaces are directly relevant (via detailed balance) to a better understanding of the mechanism of ammonia synthesis. There have been numerous studies of the decomposition of ammonia on surfaces of iron [11-14], nickel [15], platinum [16-19], ruthenium [20] and rhodium [21]. A detailed mechanism of the ammonia decomposition reaction on polycrystalline platinum and Pt(110)-(1x2) surfaces at pressures between  $5 \times 10^{-7}$  and 0.5 Torr and temperatures between 400 and 1200 K has been put forward recently [17-19]. This mechanistic model

that is embodied by a series of elementary reactions describes successfully both steady-state specific reaction rates and surface coverages over the wide range of pressures and temperatures that were studied. The model indicates that at relatively low temperatures and/or high pressures, nitrogen adatoms are the dominant surface species, and the recombinative desorption of nitrogen controls the rate of decomposition of ammonia. At relatively high temperatures and/or low pressures, however, the surface coverage of all species is low, and a competition between the desorption of molecular ammonia and the cleavage of an N-H bond in molecularly adsorbed ammonia controls the rate of the decomposition reaction.

The steady-state decomposition of ammonia on Ru(001) has been studied previously for ammonia pressures between  $10^{-7}$  and  $10^{-5}$  Torr and surface temperatures from 400 to 800 K [20]. It was reported that at low temperatures the reaction rate is limited by the recombination of nitrogen adatoms, whereas at high temperatures the reaction rate is linearly dependent on ammonia pressure and independent of hydrogen and nitrogen pressures. These data were not interpreted, however, in terms of a mechanistic model. Recombinative desorption of nitrogen was observed during the steady-state decomposition of ammonia on Ru(001) with a maximum rate of desorption at 750 K [20,32]. The recombinative desorption of nitrogen was observed at temperatures between 600 and 800 K on Raney-Ru and Ru powder. [33].

The adsorption and decomposition of ammonia on Ru(001) has also been investigated by X-ray and UV-photoelectron spectroscopy [22]. At 120 K, molecularly adsorbed ammonia exhibits a nitrogen 1s core level at 400.0 eV, and valence orbitals at 6.7 and 11.0 eV corresponding to the  $3a_1$  and  $1e$  molecular

orbitals of ammonia. After large exposures (900 L, where 1 L = 1 Langmuir  $\equiv 10^{-6}$  Torr-s) of ammonia at 500 K, atomic nitrogen was formed, which exhibits a nitrogen 1s level at 397.3 eV and a peak at 5.6 eV in the valence band. Recent high-resolution electron energy loss spectroscopic studies of the adsorption and decomposition of ammonia on Ru(001) have also indicated that nitrogen adatoms are the only detectable species present on the surface during ammonia decomposition at temperatures above 400 K [23]. However, a small concentration of NH species was detected between 300 and 400 K on the Ru(001) surface.

The molecular adsorption of ammonia on Ru(001) at 80 K has been investigated by Auger electron spectroscopy, low-energy electron diffraction (LEED), thermal desorption mass spectrometry, and electron stimulated desorption ion angular distributions (ESDIAD) [24-27]. The thermal desorption spectra of ammonia are characterized by the desorption of chemisorbed ammonia between 180 and 320 K with associated activation energies of desorption of approximately 12-21 kcal-mol<sup>-1</sup>, and a lower temperature feature at 140 K which is attributed to a second layer of adsorbed ammonia [26]. At relatively low coverages of ammonia ( $\theta_{NH_3} \leq 0.15$ ), ESDIAD provides evidence of randomly (azimuthally) oriented or freely rotating ammonia monomers, bonded to the surface via the lone pair of electrons on the nitrogen atoms with the hydrogen atoms pointing away from the surface [26]. Dissociation of ammonia on Ru(001) was observed at higher temperatures (above 500 K), which gave rise to a (2x2) LEED pattern characteristic of an overlayer of nitrogen adatoms [24].

The chemisorption of hydrogen on Ru(001) has been investigated by thermal desorption mass spectrometry [28-31]. Second-order desorption of hydrogen

was observed with an activation energy of desorption of  $22 \text{ kcal}\cdot\text{mol}^{-1}$  and a pre-exponential factor of the desorption rate coefficient of  $10^{-3} \text{ cm}^2\cdot\text{s}^{-1}$  in the limit of zero coverage [28]. Both the activation energy and the preexponential factor of the desorption rate coefficient were found to decrease with an increasing surface coverage of hydrogen [28-31].

In the work reported here, specific reaction rates ( $\text{cm}^{-2}\cdot\text{s}^{-1}$ ) of the catalytic decomposition of  $^{15}\text{NH}_3$  and  $^{15}\text{ND}_3$  on the Ru(001) surface have been measured at pressures of  $10^{-6}$  and  $2 \times 10^{-6}$  Torr, and temperatures between approximately 500 and 1250 K. Transient "thermal desorption" experiments were conducted *during* the steady-state reaction, and these results were utilized to determine both surface coverages and desorption kinetics of the surface species that are present during the decomposition of ammonia. The previously proposed reaction mechanism for ammonia decomposition on platinum [17-19] was found to be successful in describing the decomposition on ruthenium also. This observation allows detailed comparisons to be made between the activity of ruthenium and that of platinum for the catalytic decomposition of ammonia.

## II. Experimental Procedures

The measurements reported here were carried out in an ion pumped, stainless steel ultrahigh vacuum chamber that has been described in detail previously [34]. The base pressure of the system is below  $1 \times 10^{-10}$  Torr of reactive gases. Facilities are available for experimental studies involving mass spectrometry, LEED, Auger electron spectroscopy, and X-ray and UV-photoelectron spectroscopies.

The Ru(001) crystal was oriented and cut from a single crystalline boule of ruthenium, polished to within  $\frac{1}{2}^{\circ}$  of the (001) orientation using standard metallographic techniques, and etched briefly in hot aqua regia. The crystal was mounted by spotwelding to two 15 mil tantalum support wires; and it was heated resistively, and cooled conductively by liquid nitrogen. The temperature was measured by a W/5%Re-W/26%Re thermocouple that was spotwelded to the back of the crystal. The Ru(001) surface was cleaned *in situ* by argon ion sputtering, and heating cycles in  $5 \times 10^{-7}$  Torr of oxygen (600-1000 K) followed by high temperature annealing (at 1600 K) to remove all chemisorbed oxygen [35]. The cleanliness of the surface was established by both Auger electron spectroscopy and X-ray photoelectron spectroscopy. After cleaning and annealing, the (1x1) LEED pattern characteristic of the clean surface was observed.

Since the decomposition of ammonia occurred on the hot filament of the mass spectrometer, the steady-state decomposition experiments were carried out with a directional beam doser consisting of a multichannel array of capillaries [36]. During the decomposition reaction, the crystal was positioned approximately 3 mm from the doser face, providing a beam pressure-to-background pressure ratio that was greater than 20:1. In addition, the crystal manipulator was cooled to approximately 100 K with liquid nitrogen, which reduced further the background pressure of ammonia. Absolute "beam" fluxes were determined by measuring the rate of pressure decrease in the doser reservoir. Specific reaction rates were determined by replacing the ammonia in the doser reservoir with nitrogen (the reaction product), and calibrating the mass spectrometer using the known flux from the capillary array.

Automated data acquisition [28] and substrate temperature control [37] for both the thermal desorption as well as the steady-state reaction rate measurements were achieved by using an IBM-XT computer station with a Data-Translation 2801-A board. Both  $^{15}\text{NH}_3$  (99 atom%  $^{15}\text{N}$ ) and  $^{15}\text{ND}_3$  (99 atom%  $^{15}\text{N}$ , 99 atom % deuterium) were obtained from Matheson and were used without further purification. The purity of each reagent was verified *in situ* mass spectrometrically.

### III. Results

#### 1. Steady-State Decomposition of $^{15}\text{NH}_3$ and $^{15}\text{ND}_3$

Specific reaction rates for the decomposition of  $^{15}\text{NH}_3$  on the Ru(001) surface are shown in Fig. 1 as a function of reciprocal temperature at effective pressures of ammonia of  $10^{-6}$  and  $2 \times 10^{-6}$  Torr. These data were measured by exposing the clean surface at 1250 K to a continuous flux of  $^{15}\text{NH}_3$ . The surface was then cooled at a rate of 2-3 K-s $^{-1}$  while recording the  $^{15}\text{N}_2$  mass spectrometric intensity [19,38]. Identical results were obtained by monitoring the hydrogen product. For temperatures above approximately 750 K, the dependence of the reaction rate on ammonia pressure is nearly first-order, while for temperatures below 650 K, the reaction rate becomes zero-order in ammonia pressure. These two different kinetic regimes, which have very different apparent activation energies, are qualitatively similar to previous results for ammonia decomposition on polycrystalline iron [13,14], polycrystalline nickel [15], and both polycrystalline platinum and Pt(110)-(1x2) surfaces [16-19]. For temperatures below 650 K, the apparent activation energy of the decomposition reaction is  $43 \pm 3$  kcal-mol $^{-1}$ . At higher temperatures, the activation energy decreases, becoming approximately

$5.0 \pm 0.3$  kcal-mol<sup>-1</sup> for temperatures above 750 K.

Figure 2 shows the rate of decomposition of deuterated ammonia  $^{15}\text{ND}_3$ , together with the data for  $^{15}\text{NH}_3$ , both at  $2 \times 10^{-6}$  Torr. The rates converge at low temperatures, and the kinetics for  $^{15}\text{ND}_3$  decomposition become identical to those for  $^{15}\text{NH}_3$ . However, at higher temperatures, the activation energy for decomposition of  $^{15}\text{ND}_3$  is  $6.6 \pm 0.3$  kcal-mol<sup>-1</sup>, compared to  $5.0 \pm 0.3$  kcal-mol<sup>-1</sup> for  $^{15}\text{NH}_3$ . This difference in the activation energy is direct evidence of a primary isotope effect [39]. This result implies that in the high temperature (low activation energy) regime, a surface reaction involving the cleavage of a N-H bond is rate-limiting. The same behavior has been observed previously on a polycrystalline platinum surface [17].

## 2. Surface Composition and Coverage during Ammonia Decomposition

The measured  $^{15}\text{N}_2$  mass spectrometric intensity is shown as a function of temperature in Fig. 3 for several cooling and heating cycles during a continuous exposure of the Ru(001) surface to  $^{15}\text{NH}_3$  at a pressure of  $2 \times 10^{-6}$  Torr. For each cycle, the surface was cooled at a rate of 2-3 K-s<sup>-1</sup> from an initial temperature of 950 K to a specified temperature which was maintained for approximately 15 s. Thereafter, the surface temperature was increased at a rate of 5 K-s<sup>-1</sup> to 950 K. The cooling traces describe the steady-state rate of decomposition of  $^{15}\text{NH}_3$ , while the heating traces describe both the steady-state reaction rate *and* the transient thermal desorption of nitrogen from the surface [19]. The results shown in Fig. 3 are essentially independent of cooling rate for rates less than 25 K-s<sup>-1</sup>, and this indicates the steady-state is established rapidly

compared to these rates of *cooling*. During the heating cycles, however, the depletion of an accumulated surface coverage of nitrogen gives rise to a thermal desorption trace superposed upon the steady-state rate of reaction. As proposed previously [19] and demonstrated in recent simulations [40], the area between the heating and cooling traces reflects the concentration of nitrogen adatoms present on the surface during the steady-state decomposition of ammonia at the particular temperature at which the heating traces were begun. The measured fractional surface coverage of nitrogen adatoms (with normalization to the saturation coverage obtained at temperatures below 550 K) present during ammonia decomposition at  $2 \times 10^{-6}$  Torr is shown in Fig. 4 as a function of reciprocal temperature.

Similarly, the  $H_2$  mass spectrometric signal (or that of  $D_2$  during the decomposition of  $^{15}ND_3$ ) was also monitored for the cooling and heating cycles during the decomposition of ammonia. Only the steady-state decomposition rate was observed regardless of whether the surface was being heated or cooled. This is direct evidence that the fractional coverage of hydrogen is negligible *during* the steady-state decomposition of ammonia [19].

By varying the heating rate (from 3 to 25  $K\cdot s^{-1}$ ), both the activation energy and the preexponential factor of the desorption rate coefficient of nitrogen may be evaluated independently as a function of fractional nitrogen coverage [41,42]. The heating rate was varied at a fixed initial coverage, i.e., a particular initial steady-state temperature, and the thermal desorption spectra were used to construct "desorption isotherms", i.e., the rate of desorption as a function of nitrogen coverage at constant temperature. By extracting isosteric data from

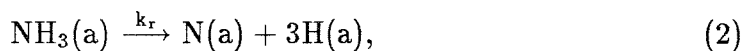
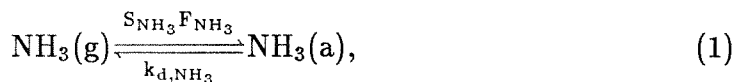
the desorption isotherms, Arrhenius plots of the desorption rate at constant coverages were constructed from which the coverage dependence of both the activation energy and the preexponential factor of the desorption rate coefficient was evaluated. The results of this procedure, using a saturation surface coverage of nitrogen adatoms of  $7.3 \times 10^{14}$  atoms-cm<sup>-2</sup> (see below), are shown in Fig. 5(a) and (b), where  $\theta_N$  is the *relative* fractional coverage of nitrogen normalized to saturation. For  $\theta_N \geq 0.1$ , the activation energy  $E_{d,N_2}(\theta_N)$  is very nearly constant with a least-squares value of  $44.0 \pm 0.5$  kcal-mol<sup>-1</sup>. Likewise, the preexponential factor  $k_{d,N_2}^{(0)}(\theta_N)$  has the essentially constant value of  $1.3 \pm 0.6 \times 10^{-3}$  cm<sup>2</sup>-s<sup>-1</sup>. At low coverages of nitrogen ( $\theta_N \leq 0.1$ ), the variation of the activation energy of desorption and the preexponential factor with coverage is consistent with the presence of a small concentration of defect sites at which the nitrogen adatoms are bound more strongly on the surface. These results suggest that this Ru(001) surface may have a defect density on the order of or less than approximately 5%. Similar observations have been reported from studies of the chemisorption of hydrogen on Pt[9(111)x(111)] [43], and Ir(111) surfaces [44] where defect densities of 2.5-10% were found.

Consistent with a previous report [24], a (2x2) LEED pattern was observed during ammonia decomposition at temperatures between 450 and 750 K, which is due to an ordered overlayer of nitrogen adatoms. This ordered nitrogen superstructure was formed by exposing the Ru(001) surface to a continuous flux of ammonia at a pressure of  $2 \times 10^{-6}$  Torr and annealing to temperatures between 450 and 750 K, which corresponds to a range of fractional nitrogen coverages between 0.26 and unity (relative to saturation). The saturation coverage of nitrogen adatoms was estimated by comparison with the saturation cover-

age of molecularly adsorbed carbon monoxide, the latter of which is known to be  $1.04 \times 10^{15}$  molecules-cm<sup>-2</sup> [35,45,46]. In particular, time-integrated areas of desorption traces of saturated nitrogen overlayers were compared to those of carbon monoxide. After correcting for mass spectrometric sensitivities and pumping time constants, the saturation coverage of nitrogen on Ru(001), deposited via ammonia decomposition, was found to be approximately  $7.3 \times 10^{14}$  atoms-cm<sup>-2</sup>. This is consistent with a fractional surface coverage of 0.47 and implies that the "(2x2)" LEED pattern observed at saturation is due to three independent p(1x2) domains rotated 120° with respect to one another [46-48].

### 3. Mechanistic Modeling

A non-equilibrium, steady-state mechanistic model has been proposed to describe the decomposition of ammonia on polycrystalline platinum and Pt(110)-(1x2) surfaces in terms of elementary (or "almost elementary") reactions [17-19]. In its simplest form, the reaction mechanism is the following:



and



where  $S_{\text{NH}_3}$  is the probability of molecular adsorption of ammonia,  $F_{\text{NH}_3}$  is the flux of ammonia to the surface, and  $k_{\text{d,NH}_3}$ ,  $k_r$ ,  $k_{\text{d,N}_2}$  and  $k_{\text{d,H}_2}$  are the rate coefficients of the four surface reactions. Each of these rate coefficients can be written as

$$k_i = k_i^{(0)} e^{-E_i/k_B T}, \quad (5)$$

where  $k_i^{(0)}$  and  $E_i$  are (assumed) coverage-independent preexponential factors and activation energies, respectively. The steady-state rate of the decomposition of ammonia is determined by solving the governing material balances for each adsorbed species [17]. Independently measured kinetic parameters are used in this calculation for describing the adsorption and desorption of ammonia [24,26], and the desorption of hydrogen [28] and nitrogen (cf., Fig. 5). Thus, the model contains only two *adjustable* parameters, namely, the surface reaction preexponential factor  $k_r^{(0)}$  and activation energy  $E_r$ , both of which are obtained by comparison with the experimental data.

The analytical form of the rate of decomposition of ammonia in the low and high temperature limits is given by [17]

$$R_{\text{NH}_3} = 2k_{\text{d,N}_2}^{(0)} \theta_N^2 n_s^2 e^{-E_{\text{d,N}_2}/k_B T}, \quad (6)$$

and

$$R_{\text{NH}_3} = \frac{k_r^{(0)} S_{\text{NH}_3} F_{\text{NH}_3} e^{-E_r/k_B T}}{k_{\text{d,NH}_3}^{(0)} e^{-E_{\text{d,NH}_3}/k_B T} + k_r^{(0)} e^{-E_r/k_B T}}, \quad (7)$$

respectively, where  $n_s$  is the surface atom density. At high temperatures, the apparent activation energy of reaction is given by  $E_r - E_{\text{d,NH}_3}$  since  $k_{\text{d,NH}_3}^{(0)} e^{-E_{\text{d,NH}_3}/k_B T} \gg$

$k_r^{(0)}e^{-E_r/k_B T}$  (cf., Table 1). At low temperatures, on the other hand, the apparent activation energy of reaction is equal to the activation energy of desorption of nitrogen,  $E_{d,N_2}$ . This model description of the measured specific rates of ammonia decomposition is shown in Figs. 1 and 2. The calculations are in excellent agreement with the experimental data, which suggests that this reaction mechanism for the decomposition of ammonia applies to ruthenium as well as to platinum surfaces [17-19]. In order to describe the data for  $^{15}\text{ND}_3$  accurately, it is necessary that  $E_{r,\text{ND}_3} - E_{d,\text{ND}_3} = 6.6 \text{ kcal-mol}^{-1}$ , (using the same value for  $k_r^{(0)}$ ) compared to  $5.0 \text{ kcal-mol}^{-1}$  for  $^{15}\text{NH}_3$ . This increase of  $1.6 \text{ kcal-mol}^{-1}$  in the value of  $E_{r,\text{ND}_3}$  is consistent with the theoretically estimated value of  $1.3 \text{ kcal-mol}^{-1}$  [39].

The assumption of coverage-independent preexponential factors and activation energies of the rate coefficients is acceptable since the model is not sensitive to  $k_{d,\text{NH}_3}$ ,  $k_r$  and  $k_{d,\text{H}_2}$  at low temperatures where decomposition is controlled by the recombinative desorption of nitrogen, and  $k_{d,N_2}$  is essentially independent of coverage (cf., Fig. 5). On the other hand, the model is sensitive to  $k_r$  and  $k_{d,\text{NH}_3}$  only at high temperatures where all surface coverages are small.

The model calculations also yield the steady-state coverages of each adsorbed species. The calculated fractional coverages of both adsorbed ammonia ( $< 10^{-9}$ ) and hydrogen ( $< 8 \times 10^{-3}$ ) are negligible, as expected, for all the reaction conditions studied. The calculated fractional surface coverage of nitrogen adatoms is shown in Fig. 4 as a function of reciprocal temperature. The agreement between the model prediction and the measured nitrogen coverage is excellent, and this provides direct evidence for the fact that recombinative

desorption of nitrogen is the dominant pathway of nitrogen production *during* the steady-state decomposition of ammonia [19].

#### IV. Discussion

It is of interest to compare the activity of ruthenium, an active ammonia synthesis catalyst [7-10], with that of platinum, which is known to be a poor catalyst for the synthesis reaction [4,10], in the catalytic decomposition of ammonia. The specific rate of decomposition of ammonia at a pressure of  $2 \times 10^{-6}$  Torr measured on three surfaces—Ru(001), polycrystalline platinum [17,18] and Pt(110)-(1x2) [19]—are shown in Fig. 6. At high temperatures ( $T \geq 650$  K), Ru(001) is more active than either of the platinum surfaces in the decomposition of ammonia, for example, by a factor of 50-100 at 1000 K. The apparent activation energy of decomposition at high temperatures  $E_r - E_{d, \text{NH}_3}$  of 5.0 kcal-mol<sup>-1</sup> on Ru(001) is similar to those that were determined on polycrystalline platinum (4.0 kcal-mol<sup>-1</sup>) [17] and Pt(110)-(1x2) (0.5 kcal-mol<sup>-1</sup>) [19]. However, the surface reaction preexponential factor  $k_r^{(0)}$  of  $5 \times 10^{13}$  s<sup>-1</sup> for Ru(001) is approximately 30-400 times greater than those for the polycrystalline platinum ( $1.5 \times 10^{12}$  s<sup>-1</sup>) [17,18] and the Pt(110)-(1x2) surfaces ( $1.3 \times 10^{11}$  s<sup>-1</sup>) [19]. This large difference in the values of  $k_r^{(0)}$  is reflected directly in the difference in the specific reaction rates in the high temperature limit, where the surface reaction is limiting the rate of decomposition of ammonia. In particular, the specific reaction rate on Ru(001) as  $T \rightarrow \infty$  approaches  $3.3 \times 10^{14}$  cm<sup>-2</sup>-s<sup>-1</sup>, while those on the polycrystalline platinum and the Pt(110)-(1x2) surfaces approach  $1.4 \times 10^{13}$  cm<sup>-2</sup>-s<sup>-1</sup> and  $1.3 \times 10^{12}$  cm<sup>-2</sup>-s<sup>-1</sup>, respectively. The decomposition kinetics at high temperatures "roll-over" to the low temperature regime at approximately

680 K for Ru(001) and 480 K for Pt(110)-(1x2) at a ammonia pressure of  $2 \times 10^{-6}$  Torr. In the low temperature regime where the desorption of nitrogen is rate-limiting, Pt(110)-(1x2) is more active in the decomposition of ammonia than Ru(001), since nitrogen adatoms are bound more strongly on the Ru(001) surface.

The nature of the measured heating and cooling traces during the steady-state decomposition of ammonia can be understood quantitatively through mathematical modeling [40]. The mass balances on the surface species were integrated with respect to time when the surface is subjected to a (linear) temperature ramp in an ultrahigh vacuum system with a "high" pumping speed such that  $T^*/\beta\tau \gg 0.5$ , where  $T^* \equiv 1$  K,  $\beta$  is the heating rate, and  $\tau$  is the pumping time constant of the system [49]. The simulated *heating* traces of nitrogen ( $\beta > 0$ ) are observed to be strong functions of  $\beta$ , whereas the *cooling* traces ( $\beta < 0$ ) are relatively weak functions of  $\beta$ . However, the families of curves for both  $\beta < 0$  and  $\beta > 0$  approach the *steady-state* curve asymptotically as  $|\beta| \rightarrow 0$ . The deviation of the cooling curves from the steady-state curve is small for  $|\beta| < 25 \text{ K}\cdot\text{s}^{-1}$ , as observed experimentally (cf., Fig. 3). Physically, the heating traces describe the (relatively) slow process of nitrogen desorption during the steady-state decomposition of ammonia, and the desorption of nitrogen that has accumulated on the surface at lower temperatures gives rise to the relatively strong dependence on the heating rate. On the other hand, the cooling traces describe the effect of a finite cooling rate on the fast process of the steady-state reaction, *i.e.* nitrogen is accumulating on rather than desorbing from the surface. Thus, for the same rate of change of temperature, there is a significantly larger deviation from the steady-state reaction rate in the case of heating compared to cooling, when the

gauge of the rate of the decomposition reaction is the appearance of nitrogen in the gas phase. Simulations of the heating and cooling curves of hydrogen, however, give solutions essentially identical to the steady-state curve [40]. This indicates that the hydrogen coverage is negligible ( $< 8 \times 10^{-3}$ ) on the surface at temperatures above 500 K with a pressure of ammonia of  $2 \times 10^{-6}$  Torr. Hence, the rate of desorption of hydrogen during the decomposition of ammonia reflects the steady-state reaction rate which is independent of heating rate ( $|\beta| < 25 \text{ K-s}^{-1}$ ) for initial temperatures above 500 K [50]. This result is not surprising in view of the respective activation energies of desorption of hydrogen and nitrogen from the Ru(001) surface (cf., Table 1). In addition, an estimate of the individual values of  $E_r$  and  $E_{d,\text{NH}_3}$  can be obtained from an analysis of these transient desorption traces [40], whereas such a direct separation is not possible from the steady-state kinetics of the ammonia decomposition reaction [51]. The surface reaction activation energy  $E_r$  is estimated to be  $24 \text{ kcal-mol}^{-1}$ , while the activation energy of desorption of ammonia  $E_{d,\text{NH}_3}$  is found to be  $19 \text{ kcal-mol}^{-1}$ . The latter is consistent with previous thermal desorption measurements of ammonia on Ru(001), where the activation energy of desorption of ammonia was found to be  $21 \text{ kcal-mol}^{-1}$  in the low coverage limit [26].

The desorption of  $\text{N}_2^*$  with  $20 \text{ kcal-mol}^{-1}$  of vibrational excitation has been observed in threshold ionization studies of ammonia decomposition on a polycrystalline platinum ribbon at a pressure of 0.1-1.4 Torr and temperatures between 773-1373 K [52]. Based on these results, it was suggested that the bimolecular reaction of two adsorbed NH species is the dominant reaction producing molecular nitrogen and limiting the rate of ammonia decomposition. However, from the present thermal desorption experiments conducted *during*

the steady-state decomposition of ammonia at temperatures between 500 and 950 K, it has been demonstrated conclusively that nitrogen adatoms are the predominant surface species during ammonia decomposition at  $2 \times 10^{-6}$  Torr on Ru(001), and the recombinative desorption of nitrogen is the major reaction producing molecular nitrogen during the steady-state decomposition of ammonia [53].

The measured activation energy of desorption of nitrogen on Ru(001) is consistent with the observation of a maximum rate of desorption at 750 K for thermal desorption of atomic nitrogen during the steady-state decomposition of ammonia on the same surface [20,54]. On Raney-Ru and Ru powder, activation energies of the desorption of nitrogen have been estimated to be between 36 and 53 kcal-mol<sup>-1</sup> from thermal desorption measurements [33]. Furthermore, the behavior of the activation energy of desorption of nitrogen on Ru(001) for  $\theta_N \geq 0.1$ , (cf., Fig. 5(a)) suggests that *both* the activation barrier for the dissociative adsorption of nitrogen and the binding energy of nitrogen adatoms on Ru(001) vary as a function of surface coverage [55]. In particular, the binding energy of nitrogen decrease with coverage while the activation barrier for the dissociative adsorption of nitrogen increase with coverage, and maintaining approximately a constant activation energy of desorption. A similar behavior of the activation energy of desorption of nitrogen was observed for the recombinative desorption of nitrogen during steady-state decomposition of ammonia on a Pt(110)-(1x2) surface [19].

In order to assess the difference in activity between ruthenium and platinum in ammonia *synthesis*, it is essential to evaluate the reactivity of the two

different metals for the dissociative chemisorption of nitrogen, which is known to be the rate-limiting step in ammonia synthesis [2,3]. From recent studies of the decomposition of ammonia and the isotopic exchange between  $\text{NH}_3$  and deuterium from  $5 \times 10^{-7}$  to 0.5 Torr on polycrystalline platinum, an activation barrier for the dissociative adsorption of nitrogen of  $16 \text{ kcal}\cdot\text{mol}^{-1}$  was predicted in the limit of zero surface coverage [17]. Similar studies are currently in progress for the Ru(001) surface to determine the predicted activation barrier for the dissociative adsorption of nitrogen [56].

## V. Conclusions

The steady-state decomposition kinetics of ammonia on Ru(001) are controlled at high temperatures by a competition between the desorption of ammonia and a surface reaction involving the dissociation of a N-H bond in molecularly chemisorbed ammonia. The apparent activation energy in this regime is  $5.0 \pm 0.3 \text{ kcal}\cdot\text{mol}^{-1}$ , and the rate of decomposition, which is first-order in ammonia pressure, exhibits a primary kinetic isotope effect. At low temperatures, the steady-state decomposition kinetics are controlled by the desorption of nitrogen, and the rate is independent of ammonia pressure. The apparent activation energy in this regime is  $43 \pm 3 \text{ kcal}\cdot\text{mol}^{-1}$  and is equal to the measured activation energy of desorption of nitrogen. The previously proposed reaction mechanism for ammonia decomposition on platinum describes quantitatively the decomposition on ruthenium. Nitrogen adatoms are the dominant surface species during the decomposition of ammonia at  $2 \times 10^{-6}$  Torr, and the nitrogen overlayer gives rise to a (2x2) LEED pattern which corresponds to an absolute fractional surface coverage of 0.47 at saturation. The activation energy of the recombinative

desorption of nitrogen on the Ru(001) surface is  $44.0 \pm 0.5$  kcal-mol<sup>-1</sup>, and the preexponential factor of the desorption rate coefficient is  $1.3 \pm 0.6 \times 10^{-3}$  cm<sup>2</sup>-s<sup>-1</sup>. Both rate parameters are approximately independent of surface coverage.

*Acknowledgment.* This research was supported by the National Science Foundation under Grant No. CHE-8516615.

## References

- [1] Haber F. and van Oordt G., *Z. Anorg. Chem.*, **1904**, 43, 111; **1905**, 44, 341.
- [2] Boudart M., *Catal. Rev.-Sci. Eng.* **1981**, 23, 1.
- [3] Ertl G., in *Catalysis, Science and Technology*, Eds., Anderson J.R. and Boudart M., Vol. 4 (Springer-Verlag, Heidelberg, 1983), p. 210.
- [4] Emmett P.H., in *The Physical Basis for Heterogeneous Catalysis*, Eds., Drauglis E. and Jaffee R.I., (Plenum, New York 1975), p. 3.
- [5] Boudart M. and Loffler D.F., *J. Phys. Chem.* **1984**, 88, 5763.
- [6] Ertl G., Weiss M. and Lee S.B., *Chem. Phys. Letters* **1979**, 60, 391.
- [7] Ozaki A., Aika K. and Hori H., *Bull. Chem. Soc. Japan* **1971**, 44, 3216.
- [8] Uchiyama S., Hattori Y., Ozaki A. and K. Aika, *Chem. Letters* **1981** 1463.
- [9] Aika K., *Angew. Chem. Int. Ed. Engl.* **1986**, 25, 558.
- [10] Bond G.C., in *The Physical Basis for Heterogeneous Catalysis*, Eds., E. Drauglis and R.I. Jaffee, (Plenum, New York 1975), p. 53.
- [11] Grunze M., Bozso F., Ertl G. and Weiss M., *Appl. Surface Sci.* **1978**, 1, 241.
- [12] Weiss M., Ertl G. and Nitschke F., *Appl. Surface Sci.* **1979**, 2, 614.
- [13] Ertl G. and Huber M., *J. Catal.* **1980**, 61, 537.
- [14] Loffler D.G. and Schmidt L.D., *J. Catal.* **1976**, 44, 244.
- [15] McCabe R.W., *J. Catal.* **1983**, 79, 445.
- [16] Loffler D.G. and Schmidt L.D., *J. Catal.* **1976**, 41, 440.
- [17] Vajo J.J., Tsai W. and Weinberg W.H., *J. Phys. Chem.* **1985**, 89, 3243.
- [18] Tsai W., Vajo J.J. and Weinberg W.H., *J. Phys. Chem.* **1985**, 89, 4926.
- [19] Vajo J.J., Tsai W. and Weinberg W.H., *J. Phys. Chem.* **1986**, 90, 6531.
- [20] Egawa C., Nishida T., Naito S. and Tamaru K., *J. Chem. Soc., Faraday Trans.* **1984**, 80, 1595.
- [21] Vavere A. and Hansen R.S., *J. Catal.* **1981**, 69, 158.
- [22] Egawa C., Naito S. and Tamaru K., *Surface Sci.* **1984**, 138, 279.

- [23] Parmeter J.E., Schwalke U. and Weinberg W.H. (in preparation).
- [24] Danielson L.R., Dresser M.J., Donaldson E.E. and Dickinson J.T., Surface Sci. **1978**, 71, 599.
- [25] Danielson L.R., Dresser M.J., Donaldson E.E. and Dickinson J.T., Surface Sci. **1978**, 71, 615.
- [26] Benndorf C. and Madey T.E., Surface Sci. **1983**, 135, 164.
- [27] Benndorf C. and Madey T.E., Chem. Phys. Letters **1983**, 101, 59.
- [28] Tsai W., PhD Thesis, California Institute of Technology **1987**.
- [29] Schwarz J.A., Surface Sci. **1979**, 87, 525.
- [30] Shimizu H., Christmann K. and Ertl G., J. Catal. **1980**, 61, 412.
- [31] Feulner P. and Menzel D., Surface Sci. **1985**, 154, 465.
- [32] Nishida T., Egawa C., Naito S. and Tamaru K., J. Chem. Soc., Faraday Trans. **1984**, 80, 1567.
- [33] Ogata Y., Aika K. and Onishi T., Surface Sci. **1984**, 140, L285.
- [34] Taylor J.L., Ibbotson D.E. and Weinberg W.H., J. Chem. Phys. **1978**, 69, 4298.
- [35] Thomas G.E. and Weinberg W.H., J. Chem. Phys. **1979**, 70, 1437.
- [36] Ibbotson D.E., Wittrig T.S. and Weinberg W.H., Surface Sci. **1981**, 110, 294.
- [37] Engstrom J.R. and Weinberg W.H., Rev. Sci. Instrum. **1984**, 55, 404.
- [38] In independent measurements, it was shown that *steady-state* rates of decomposition are maintained at these *cooling* rates.
- [39] A simple calculation assuming a vibrational frequency of  $3400\text{ cm}^{-1}$  for the N-H bond predicts an increased activation energy of  $1.3\text{ kcal}\cdot\text{mol}^{-1}$ .
- [40] Tsai W. and Weinberg W.H. (in preparation).
- [41] Taylor J.L. and Weinberg W.H. Surface Sci. **1978**, 78, 259.
- [42] Since the fractional surface coverage of ammonia, hydrogen, and  $\text{NH}_2$  and  $\text{NH}$  intermediates is negligible, this procedure yields the variation of the desorption rate coefficient of nitrogen with the fractional coverage of *nitrogen adatoms*.
- [43] Christmann K. and G. Ertl, Surface Sci. **1976**, 60, 365.

- [44] Engstrom J.R., Tsai W. and Weinberg W.H. (in preparation).
- [45] Williams E.D. and Weinberg W.H., *Surface Sci.* **1979**, 82, 93.
- [46] Madey T.E., Engelhardt H.A. and Menzel D., *Surface Sci.* **1975**, 48, 304; Pfnur H. and Menzel D., *J. Chem. Phys.* **1983**, 79, 2400; Pfnur H. and Menzel D., *J. Chem. Phys.* **1983**, 79, 4613.
- [47] Rahman T.S., Anton A.B., Avery N.R. and Weinberg W.H., *Phys. Rev. Letters* **1983**, 51, 1979.
- [48] In the case of an overlayer of oxygen adatoms, a p(2x2) superstructure transforms into three p(1x2) domains at fractional coverages between 0.25 and 0.5 [46,47].
- [49] Chan C.M. and Weinberg W.H., *Appl. Surface Sci.* **1978**, 1, 377.
- [50] The rate of desorption of hydrogen during the decomposition of ammonia is dependent on the heating rate for  $\beta \geq 300 \text{ K-s}^{-1}$  [40].
- [51] The surface reaction activation energy  $E_r$  can only be obtained from steady-state decomposition kinetics with an independent measurement of the activation energy of desorption of ammonia  $E_{d,\text{NH}_3}$ .
- [52] Foner S.N. and Hudson R.L., *J. Chem. Phys.* **1984**, 80, 518.
- [53] The same conclusion was drawn from the previous studies of decomposition of ammonia on the Pt(110)-(1x2) surface [19].
- [54] An activation energy of desorption of nitrogen can be estimated to be approximately  $45 \text{ kcal-mol}^{-1}$  assuming a "normal" preexponential factor of the rate coefficient of desorption of  $10^{-2} \text{ cm}^2\text{-s}^{-1}$ .
- [55] The binding energy of nitrogen is given by  $(E_b + Q_{\text{ads}})/2$  where  $E_b$  is the strength of a nitrogen-nitrogen bond ( $226 \text{ kcal-mol}^{-1}$ ) and  $Q_{\text{ads}}$  is the heat of adsorption of nitrogen on the surface. An activation energy of dissociative adsorption of nitrogen was estimated to be  $5 \text{ kcal-mol}^{-1}$  on Ru(001) in the limit of zero surface coverage [56].
- [56] Tsai W. and Weinberg W.H. (in preparation).

TABLE 1. Kinetic Parameters for the Decomposition of  
Ammonia on Ru(001)

	Parameter	Value	Ref.
$S_{\text{NH}_3}^0$	Ammonia probability of adsorption	1	24,26
$k_{\text{d,NH}_3}^{(0)}$	Ammonia desorption preexponential factor	$1 \times 10^{14} \text{ s}^{-1}$	24,26
$k_{\text{d,H}_2}^{(0)}, k_{\text{d,D}_2}^{(0)}$	Hydrogen desorption preexponential factor	$1 \times 10^{-3} \text{ cm}^2\text{-s}^{-1}$	28
$E_{\text{d,H}_2}, E_{\text{d,D}_2}$	Hydrogen desorption activation energy	$22 \text{ kcal-mol}^{-1}$	28
$k_{\text{d,N}_2}^{(0)}$	Nitrogen desorption preexponential factor	$1.3 \times 10^{-3} \text{ cm}^2\text{-s}^{-1}$	
$E_{\text{d,N}_2}$	Nitrogen desorption activation energy	$44.0 \text{ kcal-mol}^{-1}$	
$k_{\text{r}}^{(0)}$	Surface reaction preexponential factor	$5 \times 10^{13} \text{ s}^{-1}$	
$E_{\text{r}}-E_{\text{d,NH}_3}$	Difference between surface reaction and desorption activation energies	$5.0 \text{ kcal-mol}^{-1}$	
$E_{\text{r}}-E_{\text{d,ND}_3}$	Difference between surface reaction and desorption activation energies	$6.6 \text{ kcal-mol}^{-1}$	
$n_{\text{s}}$	Surface atom density	$1.56 \times 10^{15} \text{ cm}^{-2}$	

### Figure Captions

- Fig. 1: Steady-state decomposition of  $^{15}\text{NH}_3$  on Ru(001) at ammonia pressures of  $1 \times 10^{-6}$  and  $2 \times 10^{-6}$  Torr. The circles and crosses represent experimental measurements, and the dashed and dotted curves are calculated results based on the model described in the text.
- Fig. 2: Steady-state decomposition of  $^{15}\text{NH}_3$  and  $^{15}\text{ND}_3$  on Ru(001) at ammonia pressures of  $2 \times 10^{-6}$  Torr. The circles and curves represent experimental measurements, and the dashed and dotted curves are calculated results based on the model described in the text.
- Fig. 3: Thermal desorption of  $^{15}\text{N}_2$  from Ru(001) during the steady-state decomposition of  $^{15}\text{NH}_3$  at  $2 \times 10^{-6}$  Torr. The temperatures indicated in the figure represent the temperatures at which the desorption was begun.
- Fig. 4: Steady-state fractional coverage of nitrogen adatoms (relative to the saturation coverage) on Ru(001) as a function of reciprocal temperature during the decomposition of  $^{15}\text{NH}_3$  at  $2 \times 10^{-6}$  Torr. The circles represent experimental measurements, and the dot-dashed curve represents the calculated values based on the model described in the text.
- Fig. 5: (a) Activation energy  $E_{d,N_2}(\theta_N)$  and (b) preexponential factor  $k_{d,N_2}^{(0)}(\theta_N)$  of the rate coefficient of desorption of nitrogen from Ru(001) as a function of the fractional surface coverage of nitrogen (relative to the saturation coverage).
- Fig. 6: Steady-state decomposition rate of  $^{15}\text{NH}_3$  on Ru(001), Pt(110)-(1x2) and polycrystalline platinum surfaces at ammonia pressures of  $2 \times 10^{-6}$  Torr.

## Ammonia Decomposition Kinetics

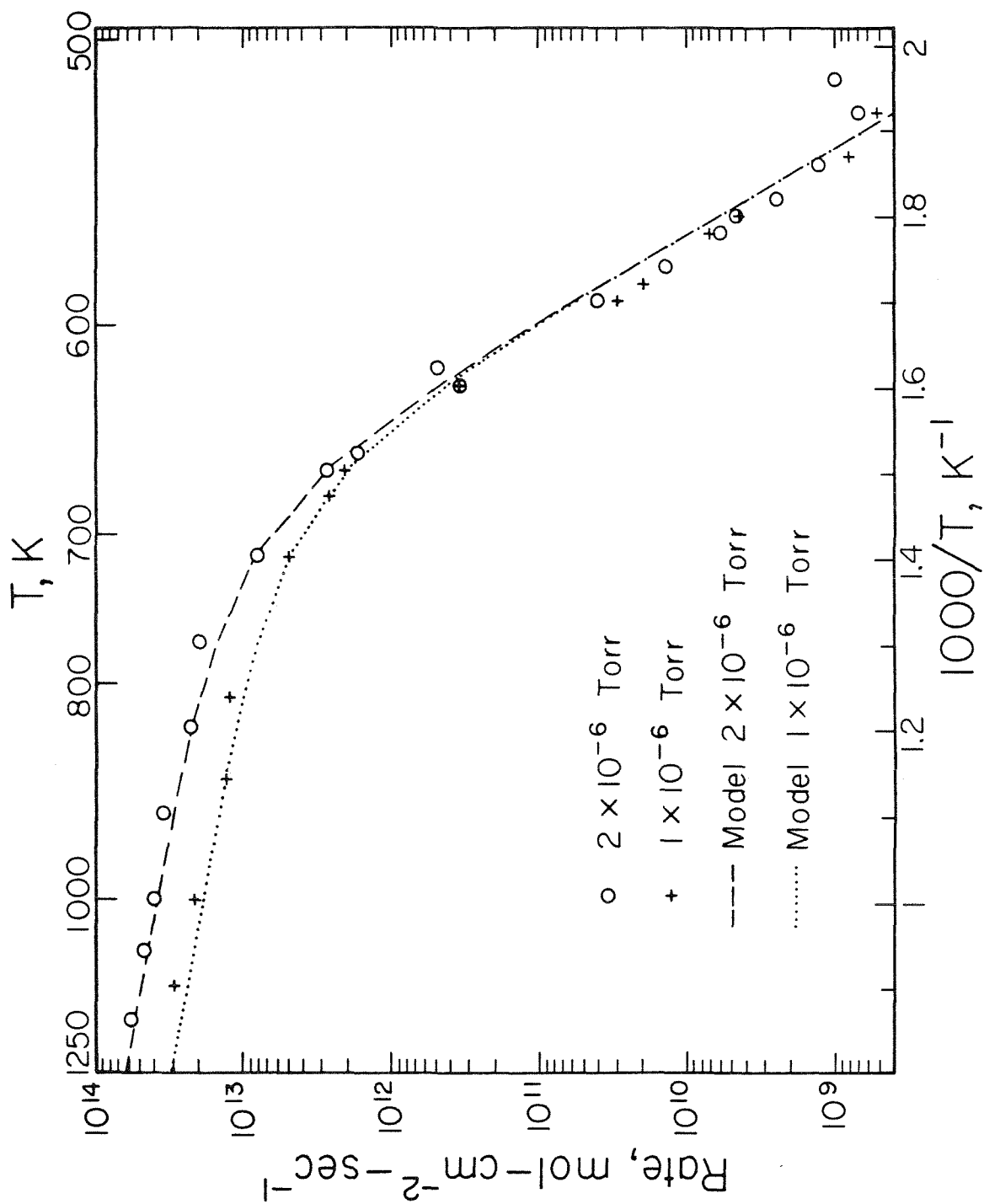


Figure 1

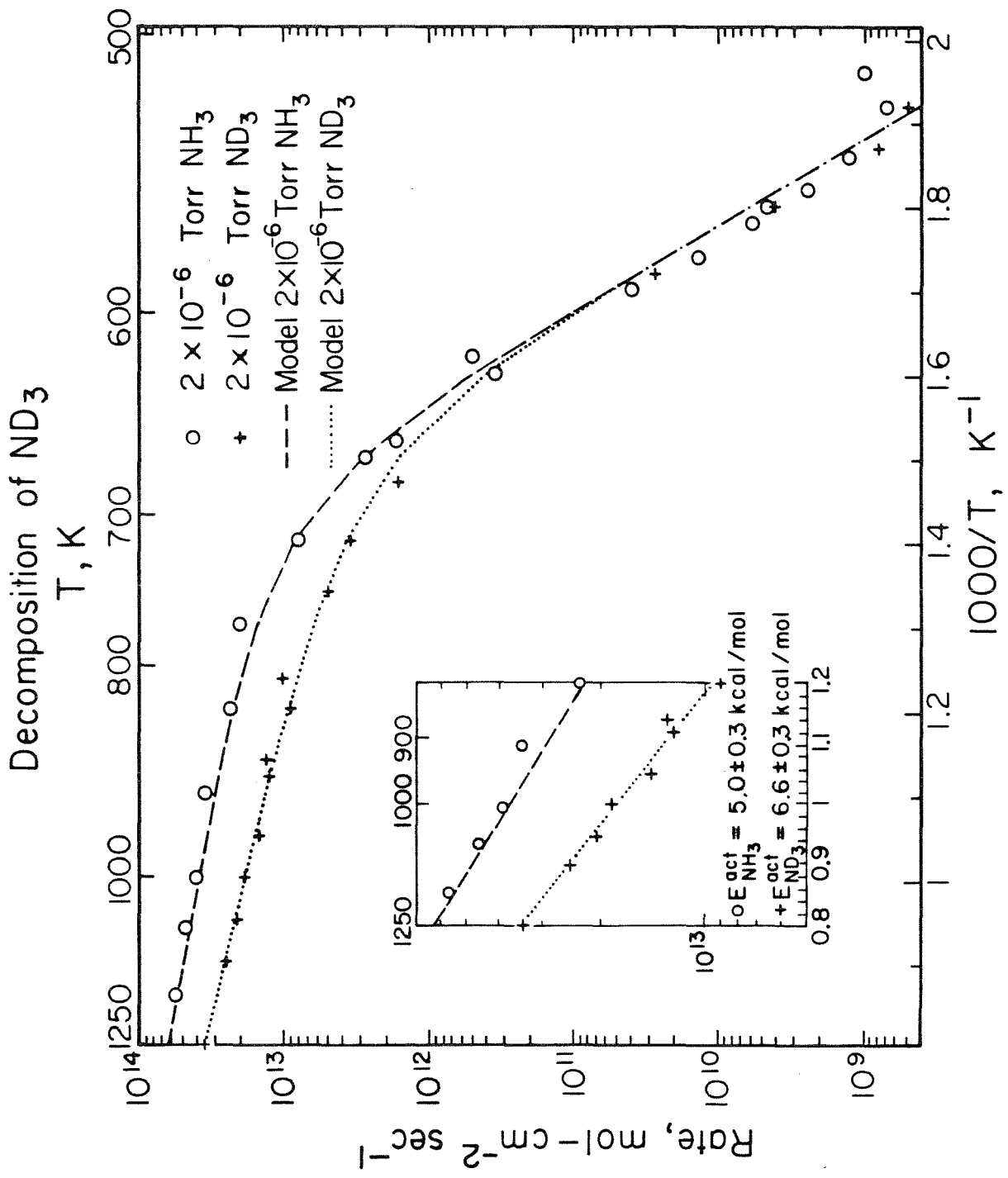


Figure 2

## Nitrogen Desorption During Steady-State Decomposition

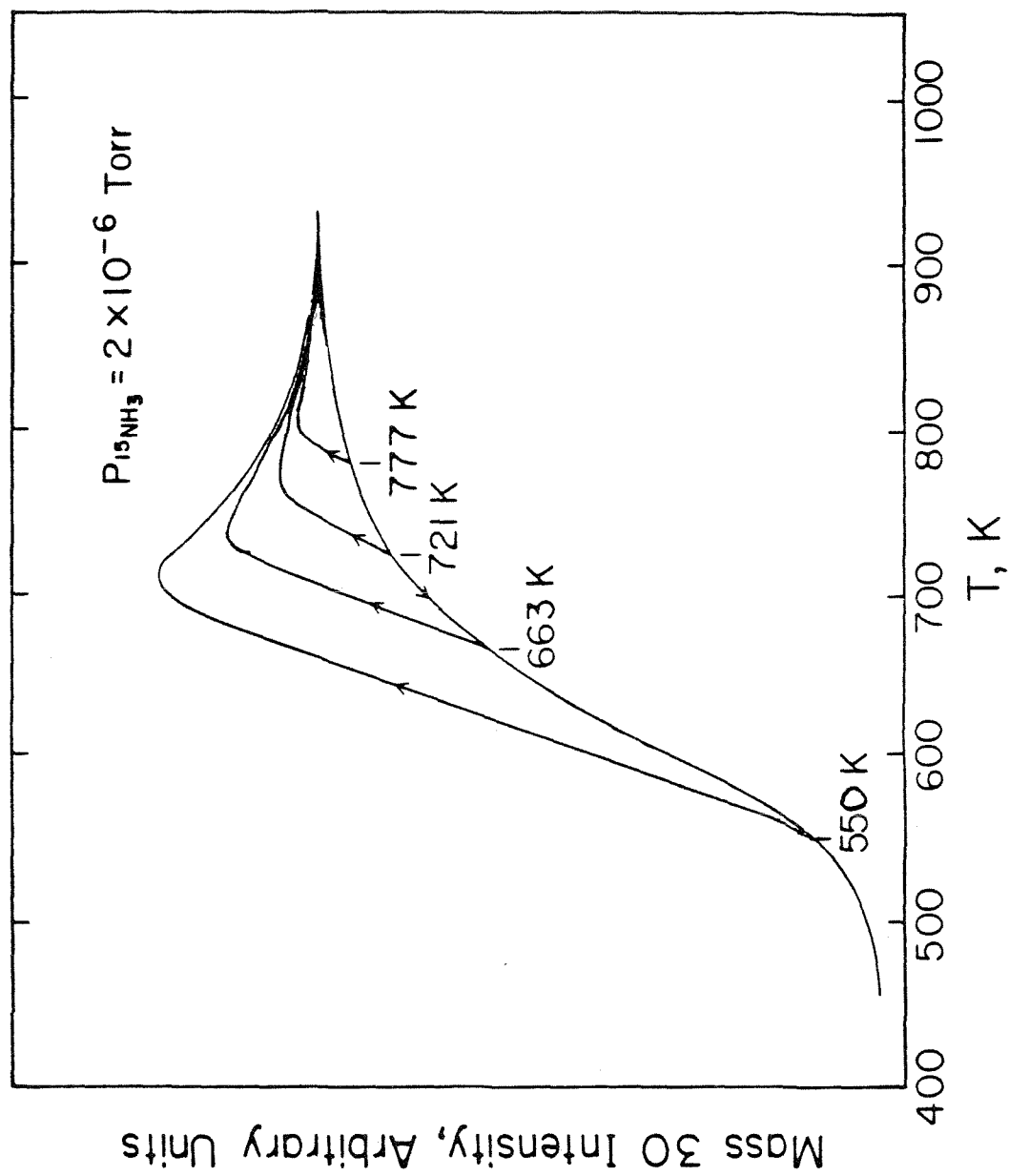


Figure 3

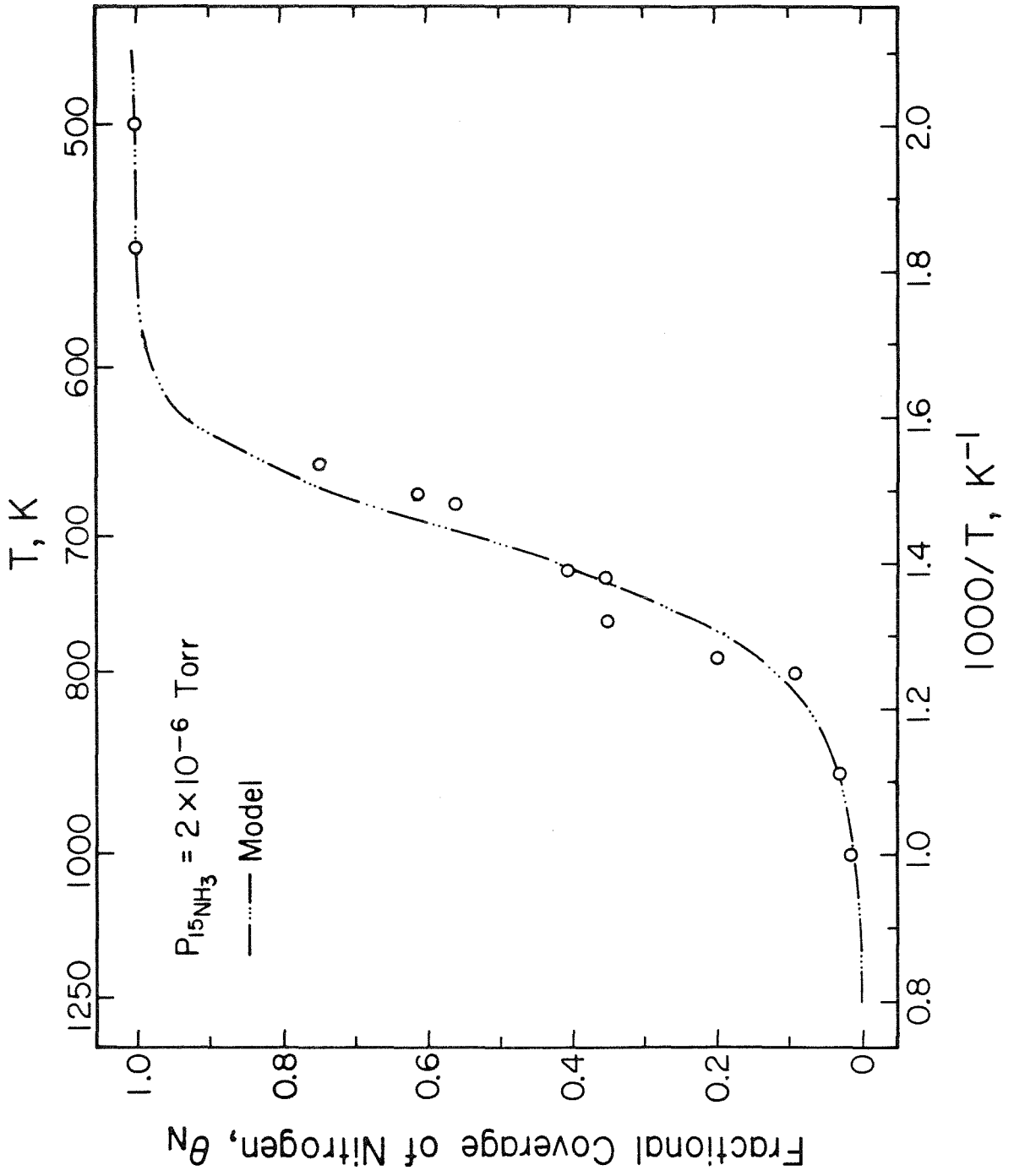


Figure 4

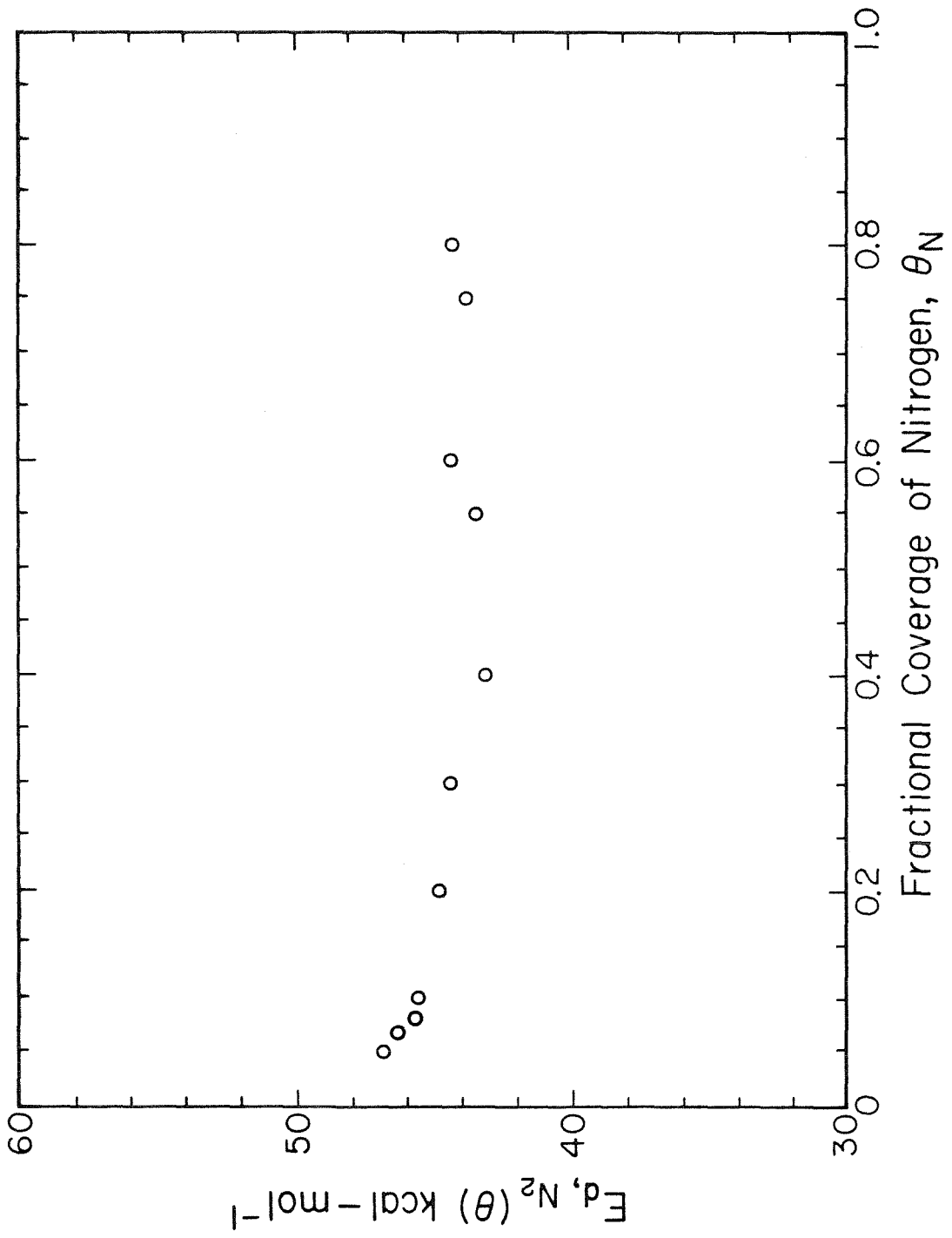


Figure 5(a)

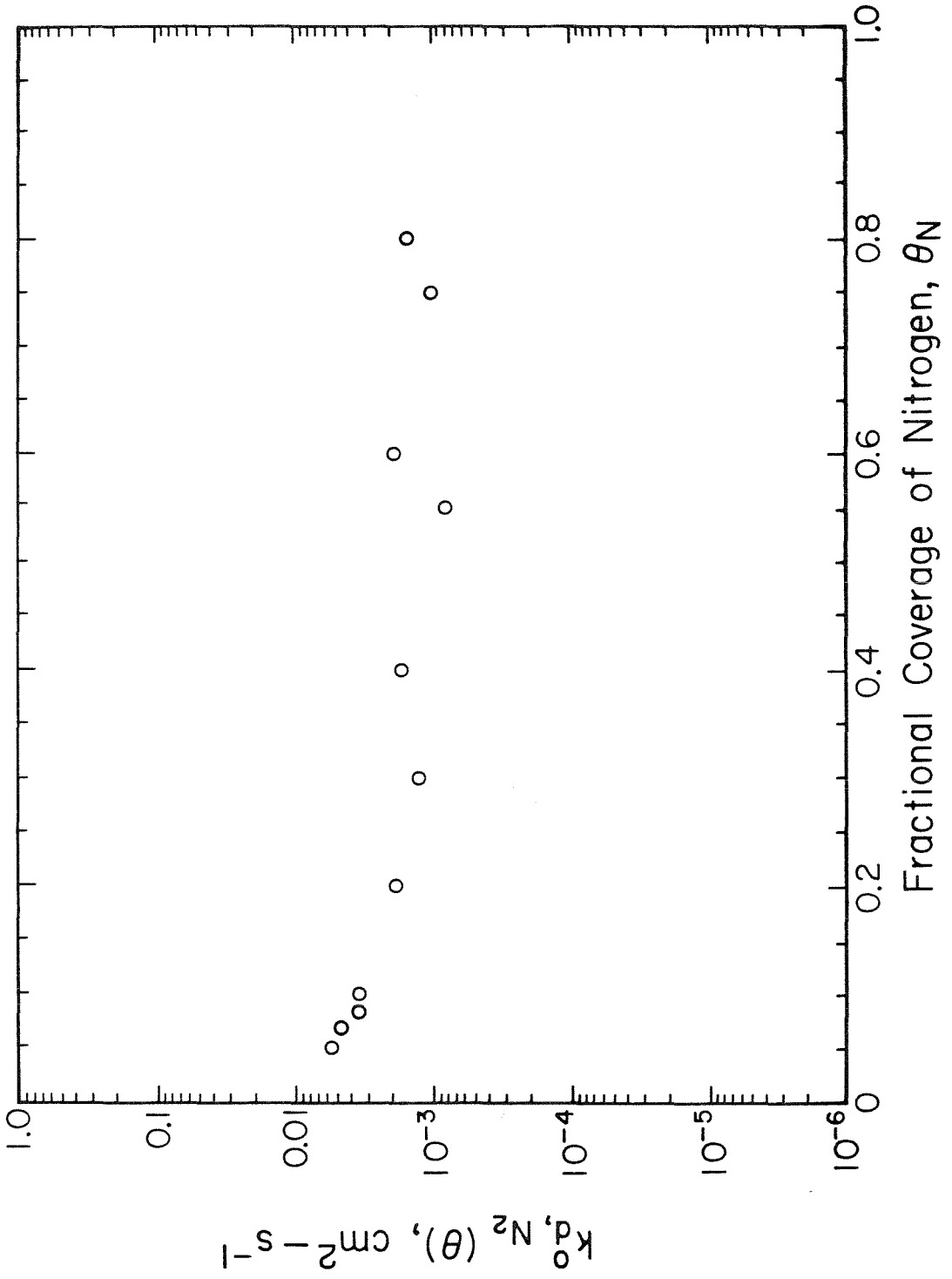


Figure 5(b)

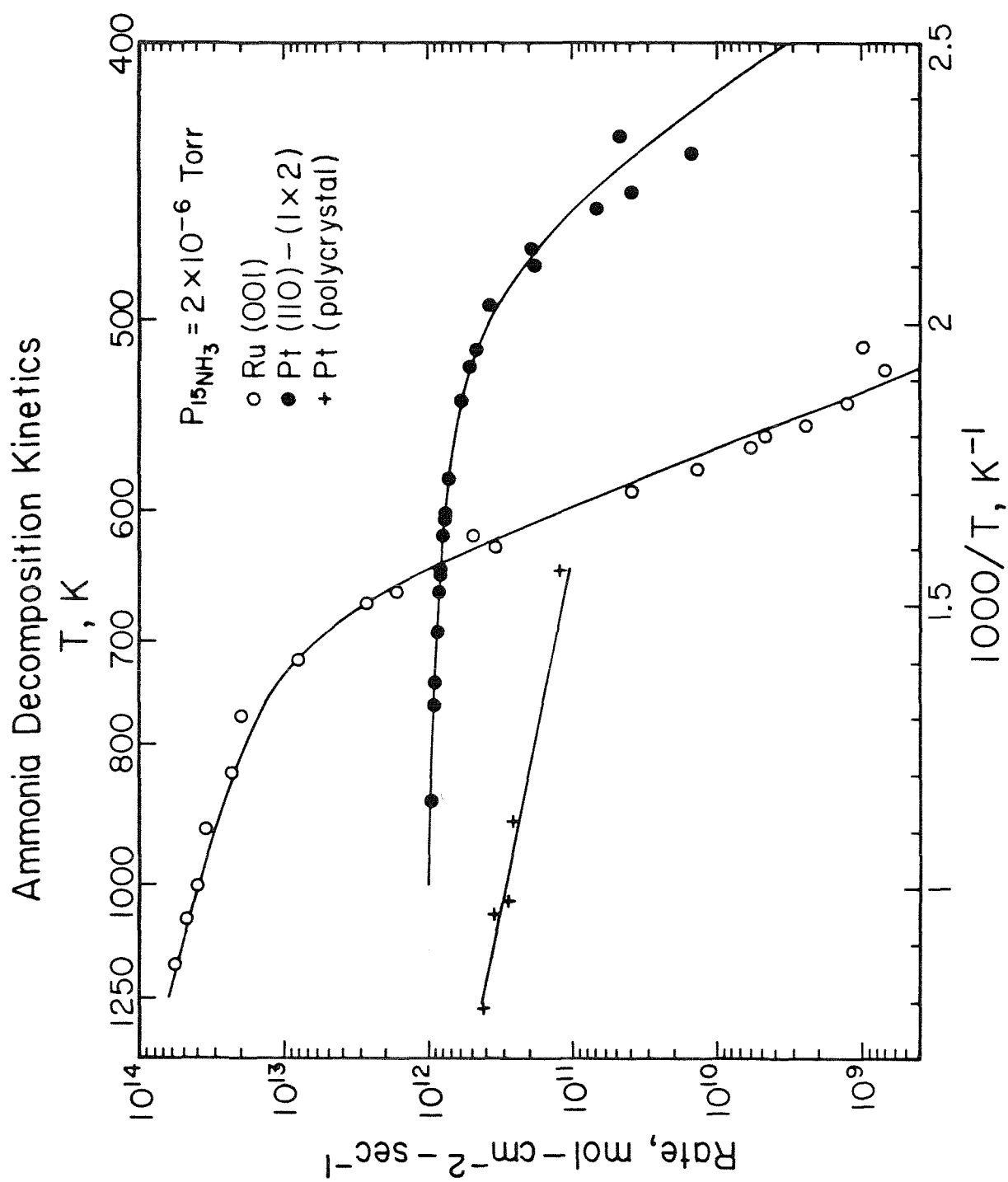


Figure 6

**Chapter 5.**

"Steady-State" Thermal Desorption Mass Spectrometry

[Chapter 5 consists of an article coauthored with W.H. Weinberg.]

**Abstract**

A thermal desorption mass spectrometric technique is described here that allows an examination of the energetics of adspecies present on catalytic surfaces *during* a steady-state reaction. The technique has been utilized to study the catalytic decomposition of ammonia on the Pt(110)-(1x2) surface at a pressure of  $2 \times 10^{-6}$  Torr and temperatures between 400 and 900 K. Close agreement was obtained between the calculated and observed thermal desorption traces of nitrogen, the dominant surface adspecies during the steady-state decomposition of ammonia. The fractional coverage of nitrogen adatoms present on the surface during steady-state reaction was obtained as a function of temperature. The nonlinear kinetic system was decoupled to yield the activation energy of the surface reaction ( $\text{NH}_3(\text{a}) \longrightarrow 3\text{H}(\text{a}) + \text{N}(\text{a})$ ),  $E_r \leq 20.0 \text{ kcal-mol}^{-1}$  and the activation energy of desorption of ammonia  $E_{\text{d,NH}_3} \leq 19.5 \text{ kcal-mol}^{-1}$  on the Pt(110)-(1x2) surface.

## I. Introduction

The study of the rates of chemical reactions on catalytic surfaces under transient conditions is of fundamental importance since it frequently can provide complementary information to measurements carried out under steady-state conditions [1-15]. Steady-state data can be interpreted frequently by a number of different kinetic models, whereas results of transient experiments are normally so rich that a detailed mechanistic model is sufficient to explain the data [6]. Various transient techniques are capable of investigating the kinetics of gas-surface reactions, such as measurements of the gas phase reaction product response to step or pulse perturbations in one of the experimental variables such as surface temperature or partial pressure of reactants [6,7]. Numerous *in situ* techniques involving electronic [8,9] and vibrational [10,11] spectroscopies have been developed to measure directly the time evolution of surface species. In addition, thermal desorption mass spectrometry has been employed advantageously to study the rates of adsorption, desorption and chemical reactions on solid surfaces [12-15]. This technique involves a (usually linear) perturbation of the surface temperature *after* the introduction of various fractional coverages of adsorbates onto the surface. The desorbed species are monitored in the gas phase as a function of the surface temperature (and time).

A transient experimental technique is described here that allows an investigation of the energetics of adsorption, desorption and chemical reactions of species present on catalytic surfaces *during* a steady-state reaction. The technique is basically a thermal desorption mass spectrometric measurement. By linearly ramping the surface temperature, desorption traces of those species

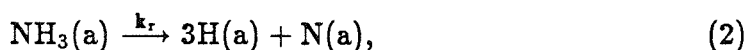
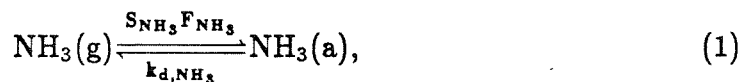
present on the surface during the steady-state reaction at the initial temperature can be analyzed to yield kinetic parameters of the heterogeneous reaction as a function of surface coverages. Important mechanistic details can be also revealed concerning the rate-limiting step of the chemical reaction. A similar experimental technique has been described previously [16,17] to investigate the transient kinetics of surface reactions under steady-state conditions. These data were not analyzed, however, to obtain the kinetic parameters of the reaction as a function of surface coverage.

As a pedagogic example, the technique is developed for the special case of a unimolecular surface reaction in which the decomposition of the reactant gives rise to two product species. A generalization of the technique to other classes of surface reactions is straightforward. The utility of the methodology is illustrated by a specific consideration of the decomposition of ammonia on the Pt(110)-(1x2) surface [18].

## II. Results

### 1. System of Equations

We shall consider the catalytic decomposition of ammonia, the mechanism of which may be written in its simplest form as follows [18,19]:





and



where  $S_{\text{NH}_3}$  is the probability of molecular adsorption of ammonia,  $F_{\text{NH}_3}$  is the flux of ammonia to the surface, and  $k_{\text{d},\text{NH}_3}$ ,  $k_r$ ,  $k_{\text{d},\text{H}_2}$  and  $k_{\text{d},\text{N}_2}$  are the rate coefficients of the four surface reactions. Each of these rate coefficients can be written as

$$k_i = k_i^{(0)} e^{-E_i/k_{\text{B}}T}, \quad (5)$$

where  $k_i^{(0)}$  and  $E_i$  are (assumed) coverage-independent preexponential factors and activation energies, respectively. The three governing material balances are

$$\frac{d\theta_{\text{NH}_3}}{dt} = S_{\text{NH}_3}^0 F_{\text{NH}_3} (1 - \theta_{\text{N}}) / n_s - \theta_{\text{NH}_3} k_r^{(0)} e^{-E_r/k_{\text{B}}T} - \theta_{\text{NH}_3} k_{\text{d},\text{NH}_3}^{(0)} e^{-E_{\text{d},\text{NH}_3}/k_{\text{B}}T}, \quad (6)$$

$$\frac{d\theta_{\text{H}}}{dt} = 3\theta_{\text{NH}_3} k_r^{(0)} e^{-E_r/k_{\text{B}}T} - 2n_s \theta_{\text{H}}^2 k_{\text{d},\text{H}_2}^{(0)} e^{-E_{\text{d},\text{H}_2}/k_{\text{B}}T}, \quad (7)$$

and

$$\frac{d\theta_{\text{N}}}{dt} = \theta_{\text{NH}_3} k_r^{(0)} e^{-E_r/k_{\text{B}}T} - 2n_s \theta_{\text{N}}^2 k_{\text{d},\text{N}_2}^{(0)} e^{-E_{\text{d},\text{N}_2}/k_{\text{B}}T}, \quad (8)$$

where  $S_{\text{NH}_3}^0$  is the zero coverage limit of the probability of molecular adsorption of ammonia,  $\theta_i$  is the fractional coverage of species "i" and  $n_s$  is the surface atom

density. A linear temperature ramp  $T=T_0+\beta t$  is applied to the surface ( $T_0$  is the initial temperature,  $t$  is time, and  $\beta$  is the heating rate) in an ultrahigh vacuum system with an "high" pumping speed such that  $T^*/\beta\tau_p \gg 0.5$ , where  $T^* \equiv 1$  K and  $\tau_p$  is the pumping time constant of the system [20]. The dependence of surface vacant sites is neglected in the rate of dissociation of ammonia (cf., Eq. (6) and (8)) since all surface coverages are small at high temperatures, and the kinetics of decomposition of ammonia is controlled by the recombinative desorption of nitrogen at low temperatures [18].

Nondimensionalizing Eqs. (6)-(8) gives

$$\frac{d\theta_{\text{NH}_3}}{d\tau} = F(1 - \theta_{\text{N}}) - R(\tau)\theta_{\text{NH}_3} - D(\tau)\theta_{\text{NH}_3}, \quad (9)$$

$$\frac{d\theta_{\text{H}}}{d\tau} = 3R(\tau)\theta_{\text{NH}_3} - 2N(\tau)\theta_{\text{H}}^2, \quad (10)$$

and

$$\frac{d\theta_{\text{N}}}{d\tau} = R(\tau)\theta_{\text{NH}_3} - 2M(\tau)\theta_{\text{N}}^2, \quad (11)$$

where

$$\tau \equiv t/t_c, \quad (12)$$

$$F = S_{\text{NH}_3}^0 F_{\text{NH}_3} t_c / n_s, \quad (13)$$

$$R(\tau) = t_c k_r^{(0)} e^{-E_r/k_B T}, \quad (14)$$

$$D(\tau) = t_c k_{d,NH_3}^{(0)} e^{-E_{d,NH_3}/k_B T}. \quad (15)$$

$$N(\tau) = n_s t_c k_{d,H_2}^{(0)} e^{-E_{d,H_2}/k_B T}, \quad (16)$$

$$M(\tau) = n_s t_c k_{d,N_2}^{(0)} e^{-E_{d,N_2}/k_B T}, \quad (17)$$

and  $t_c$  is a characteristic time [21]. To evaluate the transient behavior of each individual species present on the catalytic surface during the steady-state reaction, this dimensionless system of equations must be solved numerically with all of the kinetic parameters having been either determined or estimated *a priori*.

## 2. Solutions

The catalytic decomposition of ammonia has been studied on the Pt(110)-(1x2) surface at a pressure of  $2 \times 10^{-6}$  Torr and temperatures between 400 and 900 K [18]. A steady-state, non equilibrium mechanistic model was put forward to describe the measured specific reaction rates and fractional surface coverages during the ammonia decomposition reaction [cf., Eqs. (1)-(8)]. It should be emphasized that there are only two adjustable kinetic parameters ( $k_r^{(0)}$  and  $E_r - E_{d,NH_3}$ ) in the steady-state mechanistic model (cf., Table 1). Each of the others was determined independently. The fractional surface coverages of

adsorbed ammonia  $\theta_{NH_3} \sim O(10^{-7})$  and hydrogen  $\theta_H \sim O(10^{-4})$  were found to be negligible compared to that of nitrogen  $\theta_N \sim O(1)$  for temperatures between 400 and 900 K. The influence of both ammonia and hydrogen coverages on the adsorption of ammonia during the steady-state decomposition reaction are thus insignificant compared to that of nitrogen (cf., Eq. (6)).

The rate of desorption of nitrogen during the steady-state decomposition of ammonia at a pressure of  $2 \times 10^{-6}$  Torr was calculated as a function of heating rate using Gear's algorithm [23,24] with the kinetic parameters listed in Table 1 for  $E_r \leq 20.0$  kcal-mol $^{-1}$  and  $E_{d,NH_3} \leq 19.5$  kcal-mol $^{-1}$  [25]. The results, shown in Fig. 1, are in excellent agreement with those measured experimentally on the Pt(110)-(1x2) surface [18]. The solution of Eqs. (9)-(11) for  $E_r > 20.0$  kcal-mol $^{-1}$  and  $E_{d,NH_3} > 19.5$  kcal-mol $^{-1}$  will be discussed in Sec. II.3.

With an initial condition of  $\theta_N=0.995$ ,  $\theta_H=3.5 \times 10^{-4}$  and  $\theta_{NH_3}=9.0 \times 10^{-8}$  at  $T_0=400$  K [26], the calculated *heating* curves ( $\beta > 0$ ) of Fig. 1 are found to be a strong function of  $\beta$ . On the other hand, the *cooling* curves ( $\beta < 0$ ) are relatively weak functions of  $\beta$  with an initial condition of  $\theta_N=0.0032$ ,  $\theta_H=7.9 \times 10^{-6}$  and  $\theta_{NH_3}=1.2 \times 10^{-10}$  at  $T_0=900$  K. The families of curves for both  $\beta < 0$  and  $\beta > 0$  approach asymptotically the *steady-state* curve as  $|\beta| \rightarrow 0$ . (The steady-state curve is obtained from the solution of Eqs. (9)-(11) where LHS is set to zero.)

Simulation of the heating and cooling curves of hydrogen, however, gives solutions essentially identical to the steady-state curve. The fact that the heating and cooling curves of hydrogen are *not* a function of heating or cooling rates

is direct evidence that the coverage of hydrogen is negligible ( $\theta_H \sim O(10^{-4})$ ) during the steady-state reaction for temperatures above 400 K [18]. Under these conditions, the rate of desorption of hydrogen reflects the steady-state rate of decomposition which is independent of the heating rate (for  $|\beta| < 25 \text{ K-s}^{-1}$ ) [27]. This result is not surprising in view of the respective desorption rate coefficients of hydrogen and nitrogen (cf., Table 1) on the Pt(110)-(1x2) surface under the reaction conditions studied.

Similar calculations were carried out with different initial temperatures (i.e., different initial coverages) to obtain heating traces of nitrogen during the steady-state reaction. The results are shown in Fig. 2 for  $\beta=5 \text{ K-s}^{-1}$ . By integrating the area between the heating curve of nitrogen and the steady-state curve, one can obtain the surface coverage of nitrogen that is present *during* the steady-state reaction at the particular temperature where the heating begins. The results of this integration are in excellent agreement ( $\pm 2\%$ ) with the steady-state coverage of nitrogen obtained by solving Eqs. (9)-(11) under steady-state conditions.

It is also of interest to determine the time constants of relaxation from the heating and cooling curves to the steady-state curve at a specific temperature  $T=T_s$ . The simulation of such a decay process was achieved by integrating Eqs. (9)-(11) at  $T=T_s$  (with initial coverages determined from the solution of Eqs. (9)-(11) for  $T_0=400 \text{ K}$  and  $\beta=5 \text{ K-s}^{-1}$ ). The result of such a calculation for  $T_s=520 \text{ K}$  is shown in Fig. 3(a), where the 'relaxation' of the fractional coverage of nitrogen is plotted as a function of time. By fitting to an exponential function, it was found that a time constant of approximately  $2.5t_c$  (25 s) describes the

relaxation from the initial 'state' on the heating curve to the final 'state' on the steady-state curve. A similar calculation for the cooling curve indicates that the time constant of this relaxation process is approximately  $0.08t_c$  (0.8 s) for  $\beta = -15 \text{ K}\cdot\text{s}^{-1}$  (cf., Fig. 3b) [28].

### 3. Decoupling of Kinetic Parameters

For a coupled nonlinear kinetic system such as Eqs. (9)-(11), the determination of the kinetic parameters of individual elementary reactions is usually difficult, if not impossible, from steady-state rate measurements. For example, a separation of the activation energy of the surface reaction  $E_r$  and the activation energy of desorption of ammonia  $E_{d,\text{NH}_3}$  is not possible from the measured steady-state kinetics of decomposition of ammonia. Only the difference  $E_r - E_{d,\text{NH}_3}$  is accessible in the high temperature and/or low pressure limit [18,19]. However, the decoupling of a nonlinear kinetic system is usually possible via transient measurements [2-6].

For  $E_r > 20.0 \text{ kcal}\cdot\text{mol}^{-1}$  and  $E_{d,\text{NH}_3} > 19.5 \text{ kcal}\cdot\text{mol}^{-1}$  (with  $E_r - E_{d,\text{NH}_3} = 0.5 \text{ kcal}\cdot\text{mol}^{-1}$ ) the solutions of Eqs. (9)-(11) indicate the occurrence of a second 'state' of nitrogen at higher temperatures. This is demonstrated explicitly by the heating curves that are shown in Fig. 4 ( $\beta = 5 \text{ K}\cdot\text{s}^{-1}$ ). As  $E_r$  and  $E_{d,\text{NH}_3}$  increase, the "new" maximum in the rate of desorption of nitrogen shifts to higher temperatures, while the "original" desorption peak at approximately 550 K shifts slightly to lower temperatures. On the other hand, for  $E_r \leq 20.0 \text{ kcal}\cdot\text{mol}^{-1}$  and  $E_{d,\text{NH}_3} \leq 19.5 \text{ kcal}\cdot\text{mol}^{-1}$ , (with  $E_r - E_{d,\text{NH}_3} = 0.5 \text{ kcal}\cdot\text{mol}^{-1}$ ), the solution 'converges' to a unique trace that is in agreement with that which is

observed experimentally [18]. The transient behavior of the fractional ammonia and nitrogen surface coverages as a function of temperature for  $\beta=5 \text{ K-s}^{-1}$  with  $E_r > 20.0 \text{ kcal-mol}^{-1}$  and  $E_{d,\text{NH}_3} > 19.5 \text{ kcal-mol}^{-1}$  are shown in Figs. 5 and 6. By increasing both  $E_r$  and  $E_{d,\text{NH}_3}$  while maintaining  $E_r - E_{d,\text{NH}_3} = 0.5 \text{ kcal-mol}^{-1}$ , the population of adsorbed ammonia increases with increasing temperatures, and the coverage goes through a maximum (cf., Fig. 5). The decomposition of this 'state' of adsorbed ammonia produces the 'reaction-limited' nitrogen that desorbs at high temperatures. (cf., Fig. 4). Consistent with the results of Fig. 4, the surface coverage of nitrogen is decreased at 'low' temperatures with respect to those determined for  $E_r \leq 20.0 \text{ kcal-mol}^{-1}$  and  $E_{d,\text{NH}_3} \leq 19.5 \text{ kcal-mol}^{-1}$ , while it is increased at 'high' temperatures where adsorbed ammonia decomposes to produce the 'reaction-limited' nitrogen (cf., Fig. 6). The transient behaviors described above is essentially unchanged when other heating rate ( $\beta < 25 \text{ K-s}^{-1}$ ) is used in the calculations.

### III. Discussion

The calculated heating traces of nitrogen (cf., Fig. 1), and hydrogen during the steady-state decomposition of ammonia are in excellent agreement with those measured on the Pt(110)-(1x2) surface [18]. The observed behaviors of the heating and cooling traces of nitrogen during the steady-state decomposition of ammonia are successfully simulated. The deviation of the cooling curves of nitrogen from the steady-state curve is small for  $|\beta| < 25 \text{ K-s}^{-1}$  (cf., Fig. 1), as observed experimentally. Physically, the heating traces describe the (relatively) slow process of nitrogen desorption during the steady-state decomposition of ammonia for  $T \geq 400 \text{ K}$  and a pressure of  $2 \times 10^{-6} \text{ Torr}$ , and the desorption of

nitrogen that has accumulated on the surface at lower temperatures gives rises to the strong dependence on the heating rate. The fractional surface coverage of nitrogen on the heating curve is always greater than that on the steady-state curve due to the fact that more nitrogen adatoms desorbs from a surface that is being heated at a finite heating rate ( $\beta > 0$ ) than a surface at steady-state reaction condition ( $\beta = 0$ ). On the other hand, the cooling traces describe the effect of a finite cooling rate on the fast process of the steady-state reaction. The fractional coverage of nitrogen on the cooling curve (produced from the decomposition of ammonia) is always less than that obtained at the steady-state (cf., Fig. 1), since there is insufficient time to allow the full extent of reaction that occurs at steady-state when the surface is cooled at a finite rate ( $\beta < 0$ ). Thus, for the same rate of change of temperature, there is a significantly larger deviation from the steady-state reaction rate in the case of heating compared to cooling, when the gauge of the rate of the decomposition reaction is the appearance of nitrogen in the gas phase.

The fractional coverages of nitrogen on Pt(110)-(1x2) surfaces *during* steady-state decomposition of ammonia was obtained by integrating the area between the heating curves of nitrogen and the steady-state curve [18]. The previous claim of such coverages are accurate representations of actual concentrations of nitrogen adatoms during steady-state reaction is justified from the present calculations. (Sect. II.2). With these fractional coverage of nitrogen *during* ammonia decomposition determined, the kinetic parameters of desorption of nitrogen were evaluated as a function of coverage from the nitrogen heating curves [18]. From these results, the rate-limiting step of the decomposi-

tion of ammonia on Pt(110)-(1x2) surfaces at low temperatures is identified to be the recombinative desorption of nitrogen adatoms.

From the separation of  $E_r$  and  $E_{d,NH_3}$  in the solution of Eqs. (9)-(11), the values of  $E_r = 20.0 \text{ kcal-mol}^{-1}$  and  $E_{d,NH_3} = 19.5 \text{ kcal-mol}^{-1}$  were found to be the maximum values of the activation energies of the surface reaction and the desorption of ammonia, respectively. This value of the activation energy of desorption of ammonia is consistent with thermal desorption measurements of ammonia on Pt(110)-(1x2), where the activation energy was found to be 23  $\text{kcal-mol}^{-1}$  in the low coverage limit [22].

#### IV. Conclusions

The *steady-state* thermal desorption mass spectrometric measurement was developed for the investigation of the energetics of adspecies present on the Pt(110)-(1x2) surface during decomposition of ammonia at a pressure of  $2 \times 10^{-6}$  Torr and temperatures between 400 and 900 K. Nitrogen adatoms are the dominant surface species while the coverage of hydrogen adatoms is negligible during steady-state decomposition. The activation energy of the surface reaction  $E_r$  and the activation energy of desorption of ammonia  $E_{d,NH_3}$  were determined to be  $20.0 \text{ kcal-mol}^{-1}$  and  $19.5 \text{ kcal-mol}^{-1}$ , respectively.

*Acknowledgment.* This research was supported by the National Science Foundation under Grant No. CHE-8516615.

## References

- [1] M. Eigen, *Discuss. Faraday Soc.* **17**, 194 (1954); M. Eigen and L. Maeyer, *Technique of Organic Chemistry*, Vol 8, Pt.2,A. Weissberger Ed., Wiley, N.Y., 1963, p.895.
- [2] M. Feinberg, in *Dynamics and Modeling of Reactive Systems*, Eds., W.E. Stewart, W.H. Ray and C.C. Conley, Academic Press, New York, 1986, p. 59.
- [3] J.E. Bailey, in *Chemical Reactor Theory, A Review*, Eds., L. Lapidus and N.R. Amundson, Prentice-Hall, Englewood Cliffs, New Jersey 1977, p. 758.
- [4] P. Schuster, in *Stochastic Phenomena and Chaotic Behavior in Complex Systems*, Springer-Verlag, Heidelberg-New York, 1984, p. 1.
- [5] W. Morton, in *Catalysis*, Eds., P.G. Ashmore (Specialist Periodical Reports), The Chemical Society, London, 1982, p. 1.
- [6] C.O. Bennett, in *Catalysis under Transient Conditions*, ACS Symp. Ser. **178** (1982), p. 1.
- [7] M. Kobayashi and H. Kobayashi, *J. Catal.* **27**, 108 (1972).
- [8] M. Balooch, D.R. Olander, J. Abrefah and W.J. Siekhaus, *Surface Sci.* **149**, 285 (1985).
- [9] G.W. Rubloff, *Surface Sci.* **89**, 566 (1979).
- [10] W. Ho., *J. Vacuum Sci. Technol.* **A3**, 1432 (1985); B.A. Gurney and W. Ho, *J. Vacuum Sci. Technol.* **A3**, 1541 (1985).
- [11] D.A. Mantell, S.B. Ryali and G.L. Haller, *Chem. Phys. Letters* **102**, 37 (1983); D.A. Mantell, K. Kunimori, S.B. Ryali and G.L. Haller, *Am. Chem. Soc. Div. Pet. Chem. Prep.* **29**, 904 (1984).
- [12] J.T. Yates, Jr., in *Methods of Experimental Physics*, Vol 22, Eds., R.L. Park and M.G. Lagally, Academic Press, New York, 1985, p. 425.
- [13] D. Menzel, in *Chemistry and Physics of Solid Surfaces IV*, Eds., R. Vanselow and R. Howe, Springer-Verlag, Heidelberg-New York, 1982, p. 389.
- [14] R.J. Madix, *Catal. Rev. Sci. Eng.* **26**, 281 (1984).
- [15] J.L. Falconer and J.A. Schwarz, *Catal. Rev. Sci. Eng.* **25**, 428 (1983).
- [16] M.J. Mummey and L.D. Schmidt, *Surface Sci.* **109**, 29 (1981).

- [17] M.J. Mummey and L.D. Schmidt, *Surface Sci.* **109**, 43 (1981).
- [18] J.J. Vajo, W. Tsai and W.H. Weinberg, *J. Phys. Chem.* **90**, 6531 (1986).
- [19] J.J. Vajo, W. Tsai and W.H. Weinberg, *J. Phys. Chem.* **89**, 3243 (1985).
- [20] C.M. Chan and W.H. Weinberg, *Appl. Surface Sci.* **1**, 377 (1978).
- [21] A value of 10 s is used for  $t_c$  in the present calculations.
- [22] W. Tsai, J.J. Vajo and W.H. Weinberg, *J. Phys. Chem.* (submitted).
- [23] C.W. Gear, *Numerical Initial Value Problems in Ordinary Differential Equations*, Prentice-Hall, Englewood Cliffs, New Jersey 1971.
- [24] The magnitude of  $\theta_{NH_3}$  as well as that of  $\theta_H$  are rescaled with respect to that of  $\theta_N$  in order to avoid any inherent round-off problems. In particular,  $\theta_{NH_3}$  is multiplied by  $10^{10}$  and  $\theta_H$  by  $10^4$  in the calculational algorithm.
- [25] For  $E_r \leq 20.0 \text{ kcal-mol}^{-1}$  and  $E_{d,NH_3} \leq 19.5 \text{ kcal-mol}^{-1}$ , the calculated rate of desorption of nitrogen is unique, and is independent of the individual values of each activation energy (with  $E_r - E_{d,NH_3} = 0.5 \text{ kcal-mol}^{-1}$ ).
- [26] The initial coverages were determined from solutions of Eqs. (9)-(11) under steady-state conditions.
- [27] The rate of desorption of hydrogen during the decomposition of ammonia is found to be dependent on the heating rate for  $\beta \geq 300 \text{ K-s}^{-1}$ .
- [28] A typical pumping time constant of the ultrahigh vacuum system is approximately 0.08 s.

TABLE 1. Kinetic Parameters for the Decomposition of  
Ammonia on Pt(110)-(1x2)

Parameter	Value	Ref.
$S_{\text{NH}_3}^0$	Ammonia probability of adsorption 1	18,19
$k_{\text{d,NH}_3}^{(0)}$	Ammonia desorption preexponential factor $1 \times 10^{14} \text{ s}^{-1}$	18,19
$k_{\text{d,H}_2}^{(0)}$	Hydrogen desorption preexponential factor $3 \times 10^{-4} \text{ cm}^2\text{-s}^{-1}$	22
$E_{\text{d,H}_2}$	Hydrogen desorption activation energy $19.0 \text{ kcal-mol}^{-1}$	22
$k_{\text{d,N}_2}^{(0)}$	Nitrogen desorption preexponential factor $4 \times 10^{-8} \text{ cm}^2\text{-s}^{-1}$	18
$E_{\text{d,N}_2}$	Nitrogen desorption activation energy $24.5 \text{ kcal-mol}^{-1}$	18
$k_{\text{r}}^{(0)}$	Surface reaction preexponential factor $1.3 \times 10^{11} \text{ s}^{-1}$	18
$E_{\text{r}}-E_{\text{d,NH}_3}$	Difference between surface reaction and desorption activation energies $0.5 \text{ kcal-mol}^{-1}$	18
$n_{\text{s}}$	Surface atom density $1 \times 10^{15} \text{ cm}^{-2}$	

### Figure Captions

- Fig. 1: Rates of desorption of nitrogen on Pt(110)-(1x2) during steady-state decomposition of ammonia at a pressure of  $2 \times 10^{-6}$  Torr with  $E_r - E_{d,NH_3} = 0.5$  kcal-mol $^{-1}$ ;  $E_r \leq 20.0$  kcal-mol $^{-1}$  and  $E_{d,NH_3} \leq 19.5$  kcal-mol $^{-1}$ , parametric in heating rate: a, 20 K-s $^{-1}$ ; b, 5 K-s $^{-1}$ ; c, 2.5 K-s $^{-1}$ ; d, 0 K-s $^{-1}$  (steady-state); e, -7 K-s $^{-1}$ ; and f, -15 K-s $^{-1}$ . The circles represent the experimental data with a heating rate of 5 K-s $^{-1}$ .
- Fig. 2: Rates of desorption of nitrogen on Pt(110)-(1x2) during steady-state decomposition of ammonia with different initial temperatures for a heating rate of 5 K-s $^{-1}$ . The temperatures indicated in the figure represent the temperatures at which the desorption was begun.
- Fig. 3: a, Relaxation of nitrogen coverage from a heating curve ( $\beta = 5$  K-s $^{-1}$ ) to the steady-state curve at 520 K; and b, Relaxation of nitrogen coverage from a cooling curve ( $\beta = -15$  K-s $^{-1}$ ) to the steady-state curve at 520 K. The fit of the data to exponential functions is shown in dash lines.
- Fig. 4: Rates of desorption of nitrogen on Pt(110)-(1x2) during steady-state decomposition of ammonia at a pressure of  $2 \times 10^{-6}$  Torr for a heating rate of 5 K-s $^{-1}$  with  $E_r - E_{d,NH_3} = 0.5$  kcal-mol $^{-1}$  and a,  $E_r = 20.0$  kcal-mol $^{-1}$ ,  $E_{d,NH_3} = 19.5$  kcal-mol $^{-1}$ ; b,  $E_r = 22.0$  kcal-mol $^{-1}$ ,  $E_{d,NH_3} = 21.5$  kcal-mol $^{-1}$ ; c,  $E_r = 22.5$  kcal-mol $^{-1}$ ,  $E_{d,NH_3} = 22.0$  kcal-mol $^{-1}$ ; d,  $E_r = 23.0$  kcal-mol $^{-1}$ ,  $E_{d,NH_3} = 22.5$  kcal-mol $^{-1}$ ; and e,  $E_r = 24.0$  kcal-mol $^{-1}$ ,  $E_{d,NH_3} = 23.5$  kcal-mol $^{-1}$ .
- Fig. 5: Transient behavior of the fractional coverages of ammonia on Pt(110)-(1x2) ( $\beta = 5$  K-s $^{-1}$ ) with a,  $E_r = 20.0$  kcal-mol $^{-1}$ ,  $E_{d,NH_3} = 19.5$  kcal-mol $^{-1}$ ; b,  $E_r = 22.0$  kcal-mol $^{-1}$ ,  $E_{d,NH_3} = 21.5$  kcal-mol $^{-1}$ ; c,  $E_r = 22.5$  kcal-mol $^{-1}$ ,  $E_{d,NH_3} = 22.0$  kcal-mol $^{-1}$ ; d,  $E_r = 23.0$  kcal-mol $^{-1}$ ,  $E_{d,NH_3} = 22.5$  kcal-mol $^{-1}$ ; and e,  $E_r = 24.0$  kcal-mol $^{-1}$ ,  $E_{d,NH_3} = 23.5$  kcal-mol $^{-1}$ .
- Fig. 6: Transient behavior of the fractional coverages of nitrogen on Pt(110)-(1x2) ( $\beta = 5$  K-s $^{-1}$ ) with a,  $E_r = 20.0$  kcal-mol $^{-1}$ ,  $E_{d,NH_3} = 19.5$  kcal-mol $^{-1}$ ; b,  $E_r = 23.0$  kcal-mol $^{-1}$ ,  $E_{d,NH_3} = 22.5$  kcal-mol $^{-1}$ ; and c,  $E_r = 24.0$  kcal-mol $^{-1}$ ,  $E_{d,NH_3} = 23.5$  kcal-mol $^{-1}$ .

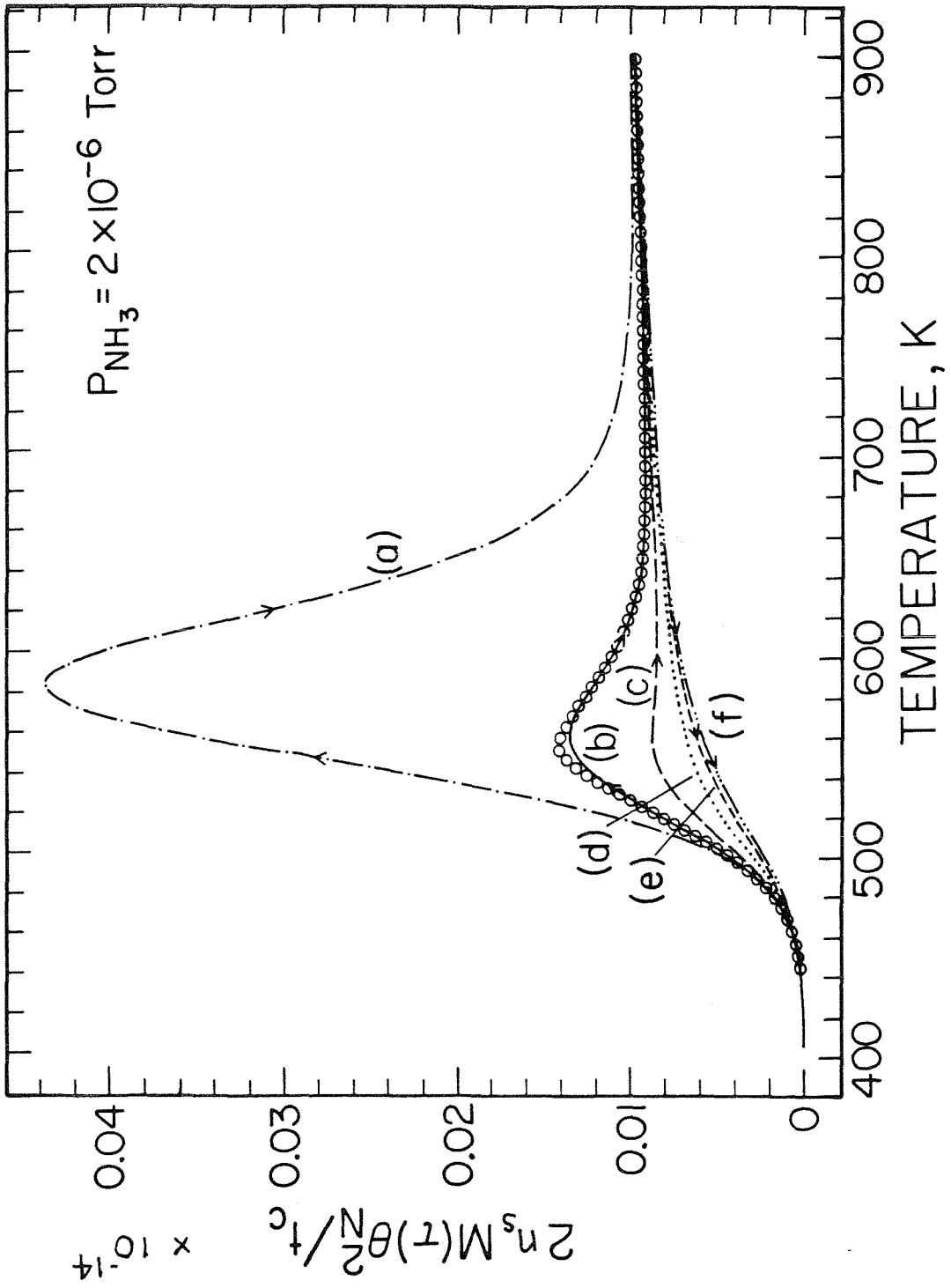


Figure 1

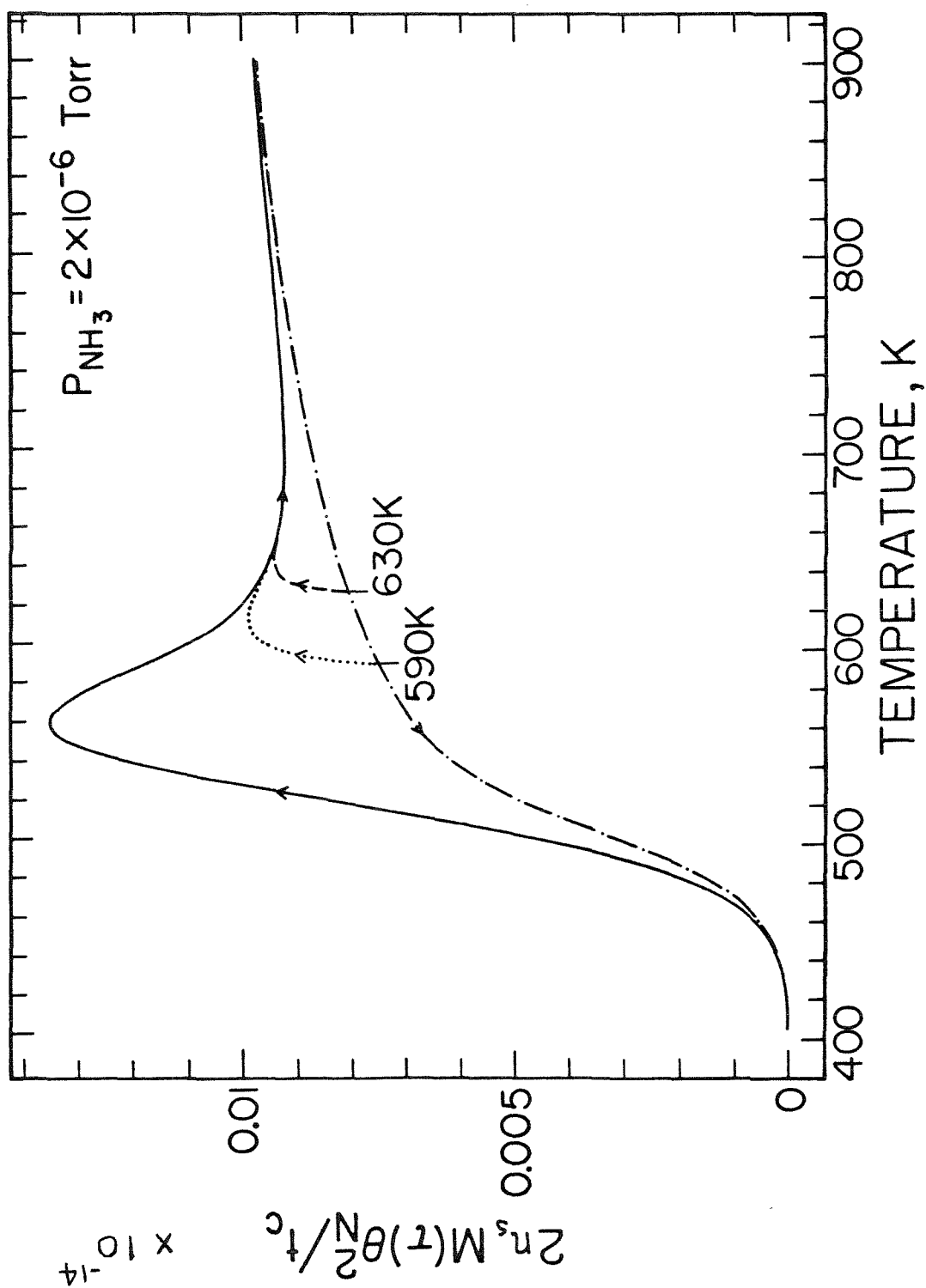


Figure 2

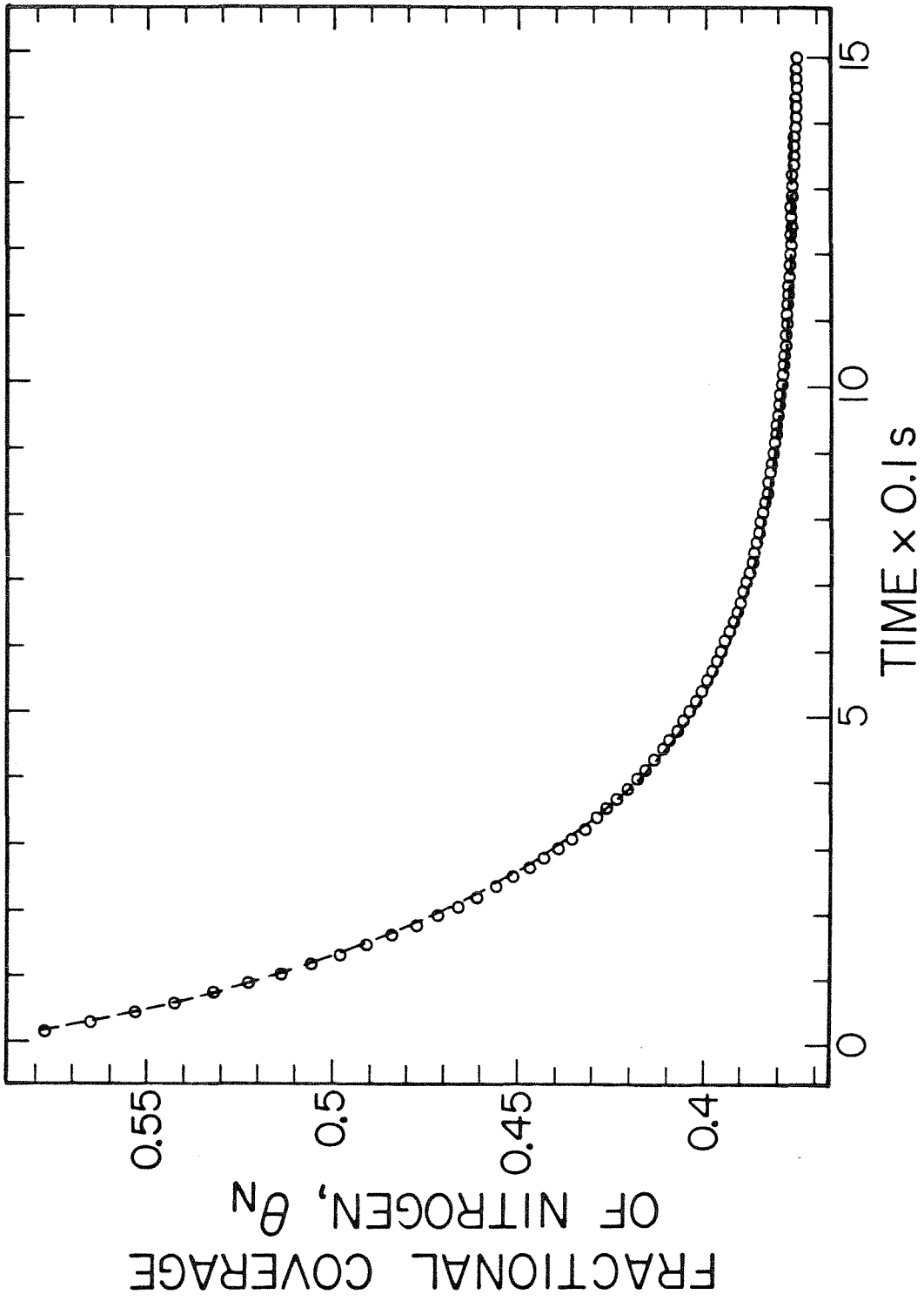


Figure 3(a)

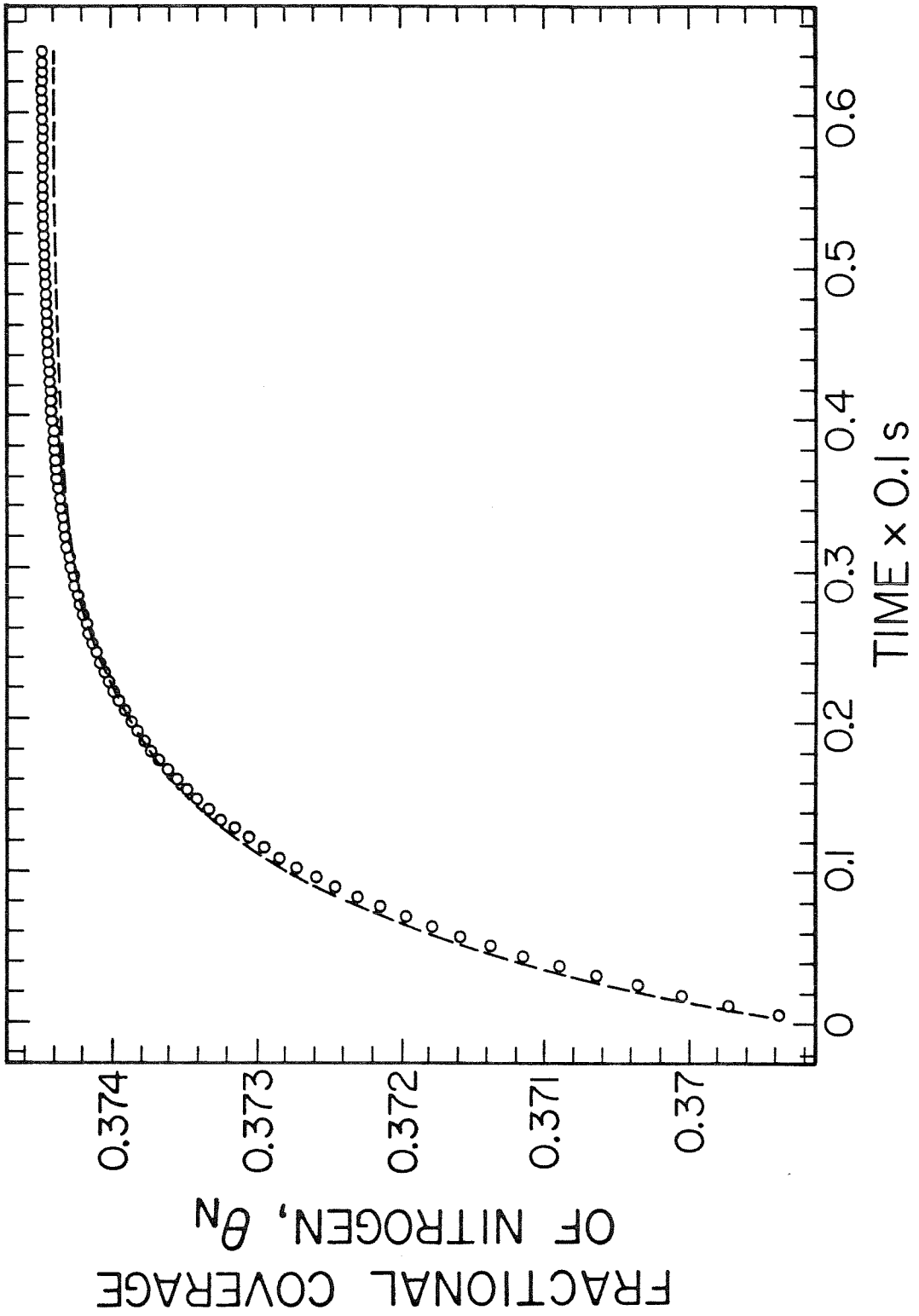


Figure 3(b)

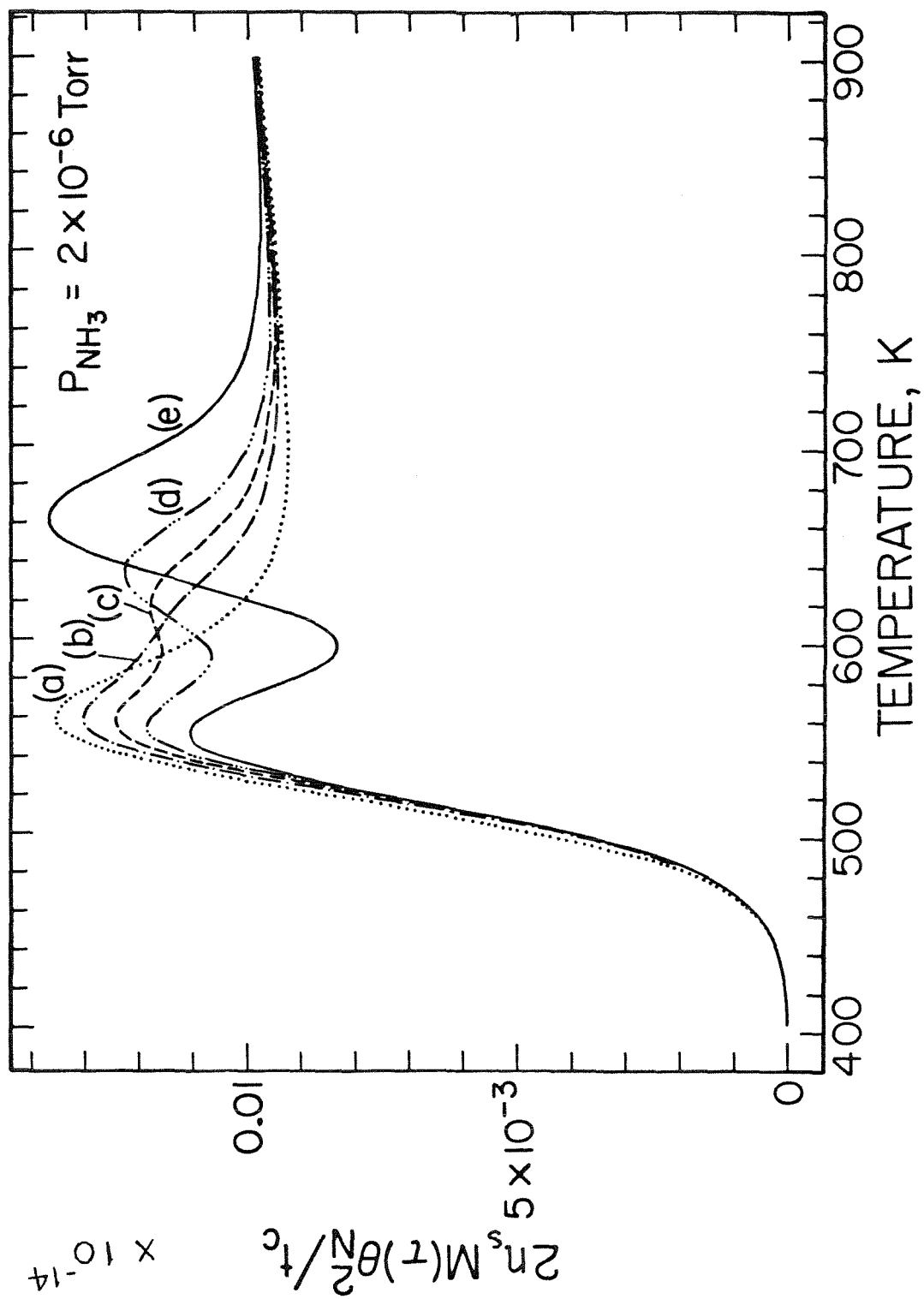


Figure 4

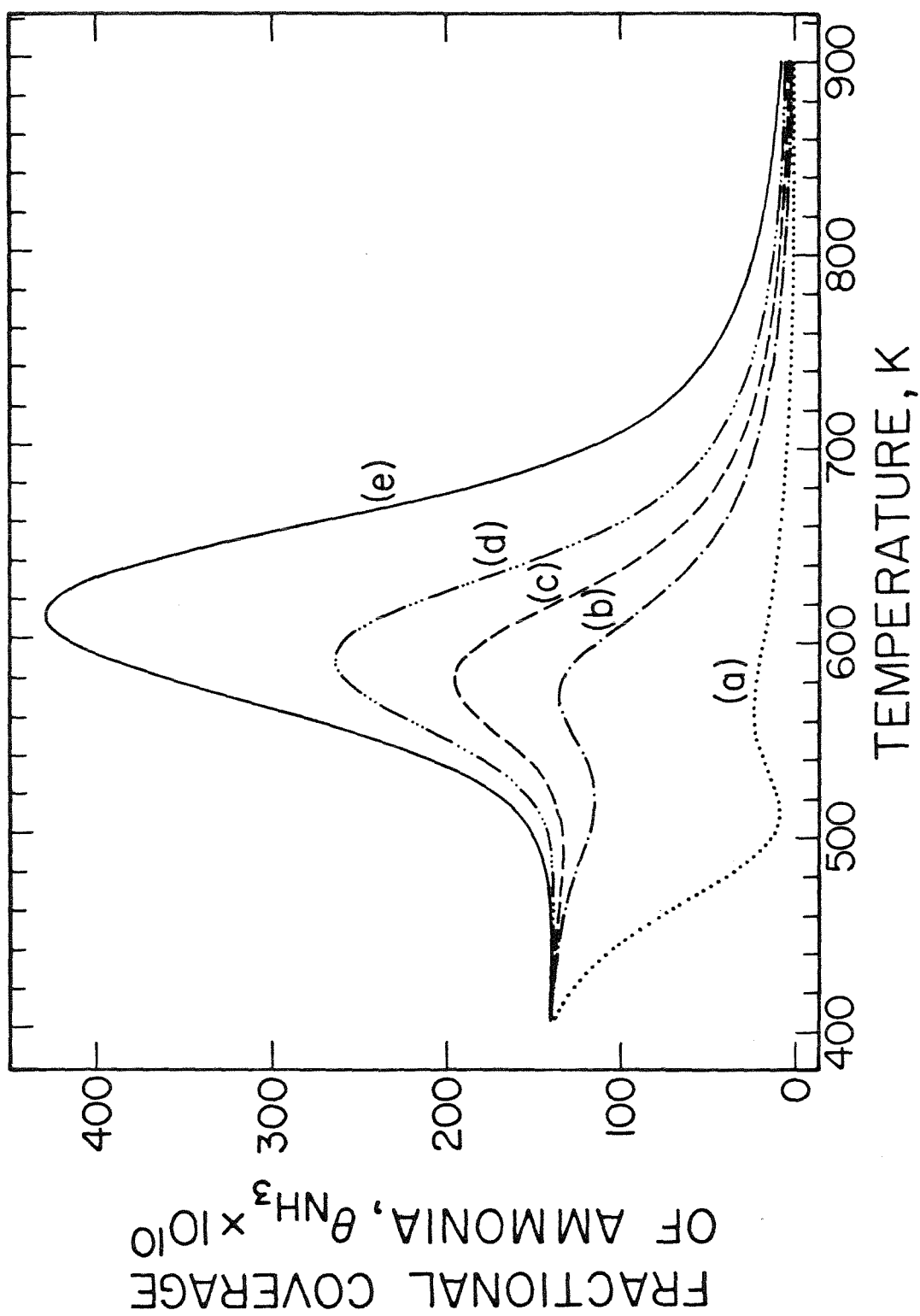


Figure 5

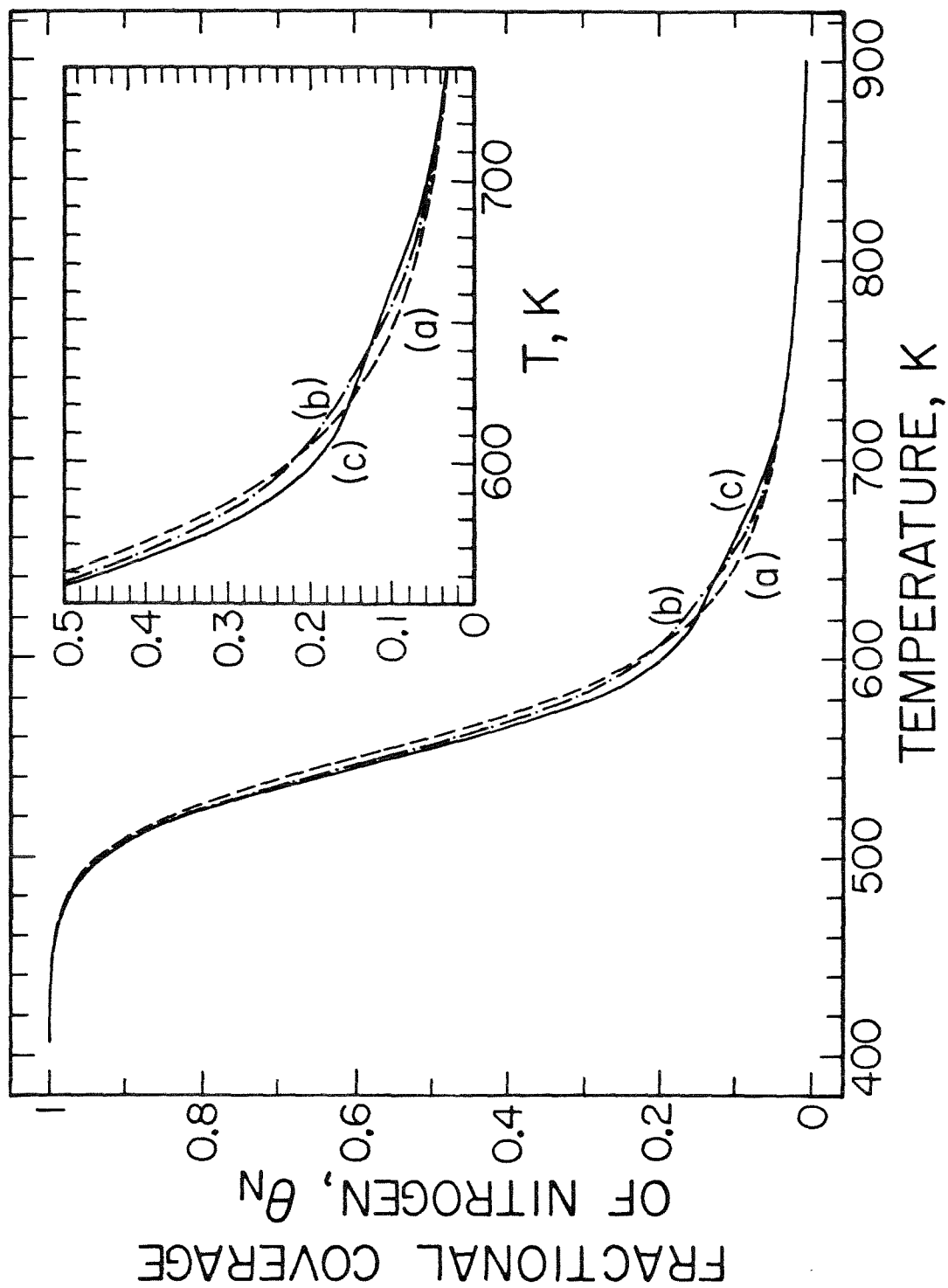


Figure 6

**Chapter 6.**

Isotopic Exchange between Ammonia and Deuterium  
on the Ru(001) Surface

[Chapter 6 consists of an article coauthored with W.H. Weinberg.]

**Abstract**

The isotopic exchange reaction between  $^{15}\text{NH}_3$  and deuterium, as well as the decomposition of  $^{15}\text{NH}_3$  have been studied at steady-state on Ru(001) at temperatures between 380 and 720 K for a partial pressure ratio of ammonia to deuterium of 4:1 and a total pressure of  $2.5 \times 10^{-6}$  Torr. All three exchange products were observed, and the exchange mechanism is dissociative as opposed to a concerted mechanism. A mechanistic model proposed previously for ammonia and deuterium on a polycrystalline platinum surface was found to describe the experimental data on the Ru(001) surface also. This model is discussed in terms of a potential energy diagram for the catalytic decomposition (or *synthesis*) of ammonia on Ru(001), where the energy levels of and the activation barriers separating the chemisorbed intermediates, namely,  $\text{NH}_3$ ,  $\text{NH}_2 + \text{H}$ ,  $\text{NH} + 2\text{H}$ ,  $\text{N} + 3\text{H}$  are evaluated. In particular, the energy level of  $\text{NH}_2(\text{a}) + \text{H}(\text{a})$ ,  $\text{NH}(\text{a}) + 2\text{H}(\text{a})$  and  $\text{N}(\text{a}) + 3\text{H}(\text{a})$  is estimated with respect to nitrogen and hydrogen in their standard states, to be  $-18 \text{ kcal}\cdot\text{mol}^{-1}$ ,  $-37 \text{ kcal}\cdot\text{mol}^{-1}$  and  $-52.5 \text{ kcal}\cdot\text{mol}^{-1}$ , respectively. The dissociative chemisorption of molecular nitrogen on Ru(001) is predicted to be activated, with an activation energy estimated to be approximately  $5 \text{ kcal}\cdot\text{mol}^{-1}$  in the limit of zero surface coverage of nitrogen adatoms.

## I. Introduction

Ruthenium (4.5 wt-%) supported on active carbon and promoted by potassium (3.2 wt-%) is an extremely active catalyst for the synthesis of ammonia from hydrogen and nitrogen [1,2]. Accordingly, there have been numerous studies aimed at understanding the mechanistic details of the synthesis reaction on and the nature of these catalytic surfaces [3-7]. In addition, the catalytic decomposition of ammonia, which is of direct relevance (via detailed balance) to the synthesis of ammonia, has been investigated on a Ru(001) surface at a pressure of approximately  $10^{-6}$  Torr and temperatures between 500 and 1250 K [8]. It was found that at high temperatures (above approximately 650 K), the steady-state decomposition kinetics of ammonia on Ru(001) are controlled by a competition between the desorption of molecular ammonia and a surface reaction involving the dissociation of an N-H bond in the chemisorbed ammonia, and the reaction rate is linearly dependent on ammonia pressure. At lower temperatures, on the other hand, the kinetics of decomposition of ammonia are controlled by the recombinative desorption of nitrogen adatoms, and the rate is independent of ammonia pressure. The mechanistic model that had been proposed previously for ammonia decomposition on both polycrystalline platinum and Pt(110)-(1x2) surfaces [9-11] was found to describe accurately the observed specific reaction rates as well as surface coverages during the steady-state decomposition reaction on Ru(001) [8].

In the work reported here, the isotopic exchange between  $^{15}\text{NH}_3$  and deuterium as well as the decomposition of  $^{15}\text{NH}_3$  were investigated on Ru(001) at a total pressure of  $2.5 \times 10^{-6}$  Torr, a partial pressure of ammonia to deuterium

of 4:1, and temperatures between 380 and 720 K. The objective of these measurements is to evaluate both the energy levels of and the activation barriers separating the chemisorbed intermediates in the ammonia decomposition and synthesis reactions, namely,  $\text{NH}_3$ ,  $\text{NH}_2 + \text{H}$ ,  $\text{NH} + 2\text{H}$ ,  $\text{N} + 3\text{H}$ . In the construction of this potential energy diagram along the reaction coordinate, a prediction is also made concerning the activation energy of the dissociative adsorption of nitrogen on the Ru(001) surface. A similar construction of such a thermochemical kinetics profile has been carried out for the synthesis of ammonia on iron surfaces [12-14]. However, many of the energy levels of and the activation barriers separating the chemisorbed intermediates in the synthesis reaction on iron are unknown [15], due to a lack of detailed mechanistic modeling of data for ammonia decomposition and synthesis, and the isotopic exchange between ammonia and deuterium. The development of this potential energy diagram is of fundamental importance to the understanding of reaction mechanism of the synthesis of ammonia since the mechanistic details of the reaction is *not* a function of pressure, as indicated by results of the studies of ammonia decomposition on polycrystalline platinum at total pressures from  $5 \times 10^{-7}$  to 0.5 Torr and at temperatures between 400 and 1200 K [9]. Furthermore, the elementary kinetics involved in this ammonia synthesis potential energy diagram can be extrapolated to industrially relevant temperatures ( $\sim 723$  K) and pressures ( $> 100$  atmospheres) to calculate specific reaction rates and surface coverages for the purpose of the design of the actual process [16].

In order to assess the difference in activity between different transition metals in ammonia synthesis, it is necessary to evaluate the activation energy

for the dissociative chemisorption of nitrogen, which is known to be the rate-limiting step in ammonia synthesis [15,17]. Using Auger electron spectroscopy, low-energy electron diffraction (LEED) and thermal desorption mass spectrometry, the activation energy for dissociative adsorption of nitrogen on Fe(111) was found to increase from an initial value of approximately zero kcal-mol<sup>-1</sup> at zero coverage to 0.96 kcal-mol<sup>-1</sup> at  $\theta_N=0.2$  [13]. On the Fe(100) surface, the activation energy was found to increase from an initial value of 5 kcal-mol<sup>-1</sup> at zero coverage to 10 kcal-mol<sup>-1</sup> at  $\theta_N=0.2$ , and an activation energy of 6.5 kcal-mol<sup>-1</sup> was reported on the Fe(110) surface at low coverages [14]. These activation energies determined on single crystalline iron surfaces compare favorably with results for singly-promoted iron catalysts (Fe-Al<sub>2</sub>O<sub>3</sub>) on which an activation energy of adsorption of 5.2 kcal-mol<sup>-1</sup> was found in the limit of zero surface coverage, increasing with coverage to 23 kcal-mol<sup>-1</sup> at  $\theta_N=0.2$  [18]. For ruthenium supported on alumina, an activation energy of dissociative adsorption of 11 kcal-mol<sup>-1</sup> was reported at temperatures between 650 and 720 K from isotopic equilibration studies of nitrogen at pressures between 40 and 200 Torr [6]. An activation barrier of 16 kcal-mol<sup>-1</sup> for the dissociative adsorption of nitrogen was predicted in the limit of zero surface coverage on a polycrystalline platinum surfaces, from studies of the decomposition of ammonia and the isotopic exchange between ammonia and deuterium [9].

## II. Experimental Procedures

The measurements reported here were carried out in an ion pumped, stainless steel ultrahigh vacuum chamber that has been described in detail previously [19]. The base pressure of the system is below  $1 \times 10^{-10}$  Torr of reactive

gases. Facilities are available for experimental studies involving mass spectrometry, LEED, Auger electron spectroscopy, and X-ray and UV-photoelectron spectroscopies. The Ru(001) surface was cleaned *in situ* by argon ion sputtering, and heating cycles in  $5 \times 10^{-7}$  Torr of oxygen (600-1000 K) followed by high temperature annealing (at 1600 K) to remove all chemisorbed oxygen [20]. The cleanliness of the surface was established by both Auger electron spectroscopy and X-ray photoelectron spectroscopy. Both  $^{15}\text{NH}_3$  (99 atom%  $^{15}\text{N}$ ) and deuterium (99.995% research grade) were obtained from Matheson and were used without further purification. The purity of each reagent was verified *in situ* mass spectrometrically.

Since the decomposition of ammonia occurred on the hot filament of the mass spectrometer, experiments were carried out with a directional beam doser consisting of a multichannel array of capillaries [21]. During the reactions, the crystal was positioned approximately 3 mm from the doser face, providing a beam pressure-to-background pressure ratio that was greater than 20:1. Absolute "beam" fluxes were determined by measuring the rate of pressure decrease in the doser reservoir. Specific decomposition rates were determined by replacing the ammonia in the doser reservoir with nitrogen (the reaction product), and calibrating the mass spectrometer using the known flux from the capillary array. Specific rates of production of the exchanged products were determined relative to the specific rate of nitrogen production by comparing the mass spectrometric sensitivity for nitrogen and ammonia, and then using that value for the deuterated ammonia products. Additional experimental details have been reported elsewhere [8,11].

### III. Results

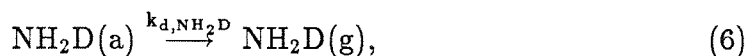
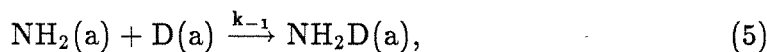
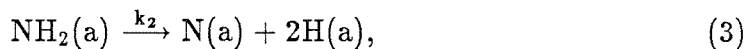
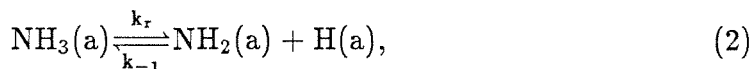
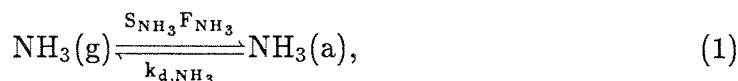
The results of the isotopic exchange experiments are shown in Fig. 1 for a partial pressure ratio of ammonia to deuterium of 4:1 with a total pressure of  $2.5 \times 10^{-6}$  Torr. Each of the three possible exchange products ( $^{15}\text{NH}_2\text{D}$ ,  $^{15}\text{NHD}_2$  and  $^{15}\text{ND}_3$ ) is observed. The ratio of the rates of production of  $^{15}\text{NH}_2\text{D}$ ,  $^{15}\text{NHD}_2$  and  $^{15}\text{ND}_3$ , measured at the temperature corresponding approximately to the maximum value of the rates (500 K), is 1:0.22:0.023. The specific reaction rate for each of the exchange products was obtained by monitoring the parent peak intensity, and the intensity of mass 19 was corrected for contributions due to cracking fragments of  $^{15}\text{ND}_3$  and  $^{15}\text{NHD}_2$ . At high temperatures the apparent activation energy, for the production of the three exchange products determined by a least-squares analysis, is  $-2.8 \pm 0.3$  kcal-mol $^{-1}$ . At low temperatures, these apparent activation energies are  $10.0 \pm 0.5$ ,  $8.8 \pm 0.5$  and  $9.3 \pm 0.6$  kcal-mol $^{-1}$  for  $^{15}\text{NH}_2\text{D}$ ,  $^{15}\text{NHD}_2$  and  $^{15}\text{ND}_3$ , respectively. The rate of ammonia decomposition, as determined from the rate of production of nitrogen, during the exchange reaction is also shown in Fig. 1. It should be noted that approximately 3-5 minutes were required to establish the steady-state for the exchange reactions, as was observed previously on the polycrystalline platinum surface [9]. On the other hand, the steady-state rates for the decomposition of pure ammonia were, achieved in all cases, in less than a second [8-11].

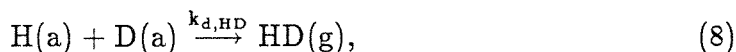
### IV. Mechanistic Modeling

A non-equilibrium, steady-state mechanistic model has been proposed that describes the decomposition of ammonia on polycrystalline platinum, Pt(110)-

(1x2) and Ru(001) surfaces in terms of elementary (or "almost elementary") reactions [8,9,11]. This model was extended to describe the isotopic exchange between ammonia and deuterium on the polycrystalline platinum surface [10]. The similarity of the kinetics of production of the exchange products on ruthenium (cf., Fig. 1) to those observed previously on platinum [9] indicates that the isotopic exchange between ammonia and deuterium proceeds through a dissociative mechanism as opposed to a concerted mechanism [22,23]. From mechanistic modeling of the exchange reactions, information concerning the energy levels and stabilities of the intermediates in the ammonia decomposition reaction can be obtained. Since  $^{15}\text{NH}_2\text{D}$  is the major product of the exchange reaction, the mechanistic model is developed initially to describe only the production of  $^{15}\text{NH}_2\text{D}$ , whereas the production of  $^{15}\text{ND}_3$  is treated as a perturbation in the mathematical modeling. The modeling of the production of  $^{15}\text{NHD}_2$  requires additional considerations and will be addressed later in this section.

Hence, the reaction mechanism considered initially is the following:





and



where  $S_i$  and  $F_i$  are the probability of adsorption and the incident flux of species "i", respectively. Each of the surface reaction rate coefficients  $k_i$  is written as

$$k_i = k_i^{(0)} e^{-E_i/k_B T}, \quad (10)$$

where  $k_i^{(0)}$  and  $E_i$  are (assumed) coverage-independent preexponential factors and activation energies, respectively.

Independently measured (i.e., nonadjustable) kinetic parameters were used in the calculation to describe the rates of adsorption and desorption of ammonia [24,25] and hydrogen [26,27], and the rate of desorption of nitrogen [8] (cf., Table 1). The first-order surface reaction preexponential factor  $k_1^{(0)}$  and the apparent activation energy of the decomposition reaction at high temperatures  $E_r - E_{d,\text{NH}_3}$  were obtained by comparison with the measured steady-state decomposition rates [8]. Assuming the activation energies of desorption and the preexponential factors of the desorption rate coefficients for  $^{15}\text{NH}_2\text{D}$  and deuterium are the same as for  $^{15}\text{NH}_3$  and hydrogen, respectively, the mechanism delineated in Eqs. (1)-(9) only introduces two new parameters,  $k_{-1}^{(0)}/k_2^{(0)}$  and  $E_{-1} - E_2$ , compared to the previous mechanistic model describing the decomposition of pure ammonia. [8,9,11]. The mass balance equations indicate that the rate coefficients  $k_{-1}$  and  $k_2$  are always coupled, and the rate of the exchange

reaction depends only on  $k_{\text{eff}}^{(0)} \equiv k_{-1}^{(0)}/k_2^{(0)}$  and  $E_{\text{eff}} \equiv E_{-1}-E_2$ . In addition, the kinetic parameter  $k_{-1}$  of Eq. (2) is considered to be identical to that of Eq. (5).

Rates of production of  $^{15}\text{NH}_2\text{D}$  and decomposition of  $^{15}\text{NH}_3$  were determined by solving iteratively the steady-state mass balance equations for  $\theta_{\text{NH}_3}$ ,  $\theta_{\text{D}}$ ,  $\theta_{\text{H}}$  and  $\theta_{\text{N}}$ . To describe both the exchange data and the associated decomposition data, only  $k_{\text{eff}}^{(0)}$  and  $E_{\text{eff}}$  were allowed to vary. Both the calculated and the experimentally determined rates of  $^{15}\text{NH}_2\text{D}$  production, and the rate of decomposition during the exchange reaction are shown in Fig. 2 with  $n_s k_{\text{eff}}^{(0)} = 3000$  and  $E_{\text{eff}} = 6 \text{ kcal-mol}^{-1}$ . (The permissible variation in the  $E_{\text{eff}}$  is only approximately  $1 \text{ kcal-mol}^{-1}$ .) It can be seen that the rate of production of  $^{15}\text{NH}_2\text{D}$  is reproduced reasonably well by the model calculations. However, the calculated rates are shifted to higher temperatures with respect to the experimental data, as was observed in the case of the polycrystalline platinum surface [9]. It was suggested previously that the temperature shift and also the deviation of model from the data at low temperatures is a consequence of assuming coverage-independent preexponential factors and activation energies of the rate coefficients [9], and it was demonstrated subsequently that a coverage-dependent preexponential factor and activation energy of the rate coefficient of the desorption of hydrogen is sufficient to describe accurately both the exchange data and the inhibition of the decomposition of ammonia by hydrogen on polycrystalline platinum [10]. Furthermore, such a coverage-dependence of the rate coefficient of the desorption of hydrogen was experimentally observed from studies of chemisorption of deuterium on nitrogen-precovered Pt(110)-(1x2) surface [28]. Inhibition of the decomposition by deuterium is observed to a small extent from the experimental

data during the exchange reactions.

The steady-state rate of production of  $^{15}\text{NH}_2\text{D}$  is given by

$$R_{\text{NH}_2\text{D}} = \frac{k_{\text{eff}}k_r\theta_{\text{NH}_3}\theta_{\text{D}}n_s^2}{1 + k_{\text{eff}}(\theta_{\text{D}} + \theta_{\text{H}})n_s}, \quad (11)$$

where  $k_{\text{eff}}=k_{-1}/k_2$ . At high temperatures  $k_{\text{eff}}(\theta_{\text{D}} + \theta_{\text{H}})n_s \ll 1$ , and the rate expression becomes

$$R_{\text{NH}_2\text{D}} = k_{\text{eff}}k_r\theta_{\text{NH}_3}\theta_{\text{D}}n_s^2. \quad (12)$$

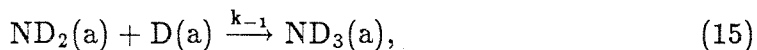
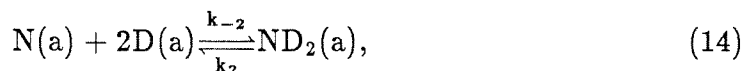
The calculated values of  $\theta_{\text{NH}_3}$  and  $\theta_{\text{D}}$  indicate that both ammonia and deuterium are within 0.06% of their respective adsorption-desorption equilibrium values. Therefore, the negative apparent activation energies observed at high temperatures result from decreasing equilibrium coverages of ammonia and deuterium as the temperature is increased. At low temperatures, it was found that  $k_{\text{eff}}(\theta_{\text{D}} + \theta_{\text{H}})n_s \gg 1$  and  $\theta_{\text{D}} > 10\theta_{\text{H}}$ , and the rate of production of  $\text{NH}_2\text{D}$  becomes

$$R_{\text{NH}_2\text{D}} = k_r\theta_{\text{NH}_3}n_s \quad (13)$$

From Eq. (13), the rate of exchange at low temperatures would be expected to show a primary isotope effect.

The production of  $^{15}\text{ND}_3$  proceeds via the deuteration of nitrogen adatoms on the ruthenium surface. Hydrogenation can be neglected since  $\theta_{\text{D}} > 10\theta_{\text{H}}$ , which implies that the rate of addition of a hydrogen adatom will be more

than an order of magnitude lower than that of addition of a deuterium adatom. Furthermore, since the rate of production of  $^{15}\text{NH}_2\text{D}$  exceeds that of  $^{15}\text{ND}_3$  by approximately a factor of 40, the formation of  $^{15}\text{ND}_3$  via the deuteration of nitrogen adatoms may be treated as a perturbation on the exchange mechanism discussed above, and the calculated values of  $\theta_{\text{NH}_3}$ ,  $\theta_{\text{D}}$  and  $\theta_{\text{N}}$  will not be affected significantly by including the production of  $^{15}\text{ND}_3$ . The mechanism can be written as



and



where the slight possibility that adsorbed  $^{15}\text{ND}_3$  will decompose has been neglected [29]. The rate of formation of  $^{15}\text{ND}_3$  is given by

$$R_{\text{ND}_3} = \frac{k_{\text{eff}}k_{-2}\theta_{\text{N}}\theta_{\text{D}}^3n_{\text{s}}^4}{1 + k_{\text{eff}}\theta_{\text{D}}n_{\text{s}}}, \quad (17)$$

which, at high temperatures ( $T > 670$  K), becomes

$$R_{\text{ND}_3} = k_{\text{eff}}k_{-2}\theta_{\text{N}}\theta_{\text{D}}^3n_{\text{s}}^4. \quad (18)$$

Taking the derivative of the logarithm of  $R_{\text{ND}_3}$  with respect to  $\beta \equiv 1/k_{\text{B}}T$  gives

$$E_{-2} = -E_{\text{eff}} + \frac{d(\ln\theta_N)}{d\beta} + 3\frac{d(\ln\theta_D)}{d\beta} - \frac{d(\ln R_{\text{ND}_3})}{d\beta}. \quad (19)$$

Using the previously determined value of  $E_{\text{eff}}$  (6 kcal-mol<sup>-1</sup>), the experimentally measured values of  $R_{\text{ND}_3}$ , and the calculated values of  $\theta_N$  and  $\theta_D$ , it was found that  $E_{-2}=43$  kcal-mol<sup>-1</sup>. A similar analysis for the low temperature ( $T < 410$  K) data gives  $E_{-2}=38$  kcal-mol<sup>-1</sup>. These results suggest that  $E_{-2}$  is a function of surface coverage ( $\simeq \theta_N + \theta_D$ ), and an average value of  $E_{-2}=40.5$  kcal-mol<sup>-1</sup> is used in calculating the rate of production of <sup>15</sup>ND<sub>3</sub>. Using a value of  $3 \times 10^{-17}$  cm<sup>4</sup>-s<sup>-1</sup> for the hydrogenation reaction preexponential  $k_{-2}^{(0)}$ , and values of  $\theta_N$  and  $\theta_D$  that were calculated from the exchange model, the calculated rate of production of <sup>15</sup>ND<sub>3</sub> is shown in Fig. 2. The good agreement between the model predictions and the experimental data is further evidence that <sup>15</sup>ND<sub>3</sub> is produced via deuteration of nitrogen adatoms.

Above perturbation approach cannot be used to describe the production of <sup>15</sup>NHD<sub>2</sub>, since the ratio of the rate of formation of <sup>15</sup>NHD<sub>2</sub> to that of <sup>15</sup>NH<sub>2</sub>D is not negligible. A dissociative exchange mechanism for *both* the production of <sup>15</sup>NH<sub>2</sub>D and <sup>15</sup>NHD<sub>2</sub> is described in the Appendix. Due to coupling of the mass balances, independent knowledge of the rate coefficients  $k_{-1}$ ,  $k_3$ ,  $k_{-3}$ , and  $k_4$  is required in order to calculate the rates of isotopic exchange between <sup>15</sup>NH<sub>3</sub> and deuterium. Note that the surface reaction rate coefficient  $k_2$  in Eq. (3) is the same as the rate coefficient  $k_3$  in Eq. (22) [30]. Using the result that  $n_s k_{\text{eff}}^{(0)} = 3000$  and  $E_{\text{eff}} = 6$  kcal-mol<sup>-1</sup> from above, and the values of the preexponential factors  $k_{-1}^{(0)}$ ,  $k_3^{(0)}$ ,  $k_{-3}^{(0)}$  and  $k_4^{(0)}$  in Table 1 [31], the remaining kinetic parameters (the activation energies) were adjusted to obtain the best agreement with the exper-

imental data. More than one set of activation energies was found to 'fit' the observed rates of production of  $^{15}\text{NH}_2\text{D}$  and  $^{15}\text{NHD}_2$ . However, only *one* set of activation energies is consistent with recent high-resolution electron energy loss spectroscopic (HREELS) studies of the adsorption and decomposition of ammonia on Ru(001) [32]. For example, values of the activation energies  $E_{-3}=37$  kcal-mol $^{-1}$  and  $E_4=35$  kcal-mol $^{-1}$  are not consistent with the HREELS observation of the decomposition of a stable NH intermediate on Ru(001) near 400 K. Similarly, values of the activation energies  $E_{-1}=28$  kcal-mol $^{-1}$  and  $E_3=22$  kcal-mol $^{-1}$  are not consistent with the absence of a stable  $\text{NH}_2$  intermediate on Ru(001) during the decomposition of ammonia. The calculated rates of production of  $^{15}\text{NH}_2\text{D}$  and  $^{15}\text{NHD}_2$  using  $k_{-1}^{(0)}=0.3$  cm $^2$ -s $^{-1}$ ,  $k_3^{(0)}=10^{11}$  s $^{-1}$ ,  $k_{-3}^{(0)}=0.01$  cm $^2$ -s $^{-1}$ ,  $k_4^{(0)}=10^{13}$  s $^{-1}$ ,  $E_{-1}=12$  kcal-mol $^{-1}$ ,  $E_3=6$  kcal-mol $^{-1}$ ,  $E_{-3}=25$  kcal-mol $^{-1}$ , and  $E_4=23$  kcal-mol $^{-1}$  are shown in Fig. 2. The calculated rate of production of  $^{15}\text{NH}_2\text{D}$  is within 1% of the rate calculated from the previous mechanism including only the production of  $^{15}\text{NH}_2\text{D}$  [Eqs. (1)-(9)].

## V. Discussion

The potential energy diagram that describes the decomposition (or synthesis) of ammonia on Ru(001) is shown in Fig. 3. This diagram was constructed using activation energies determined from the mechanistic modeling of the isotopic exchange and decomposition reactions, and independently measured kinetic parameters for the adsorption and desorption of ammonia and hydrogen, and the desorption of nitrogen. An activation energy for the desorption of ammonia of 19 kcal-mol $^{-1}$  was used [8], and this is consistent with previous thermal desorption measurements of ammonia on Ru(001) [25]. This implies that the

value of  $E_r$ , defined by Eq. (2), is equal to  $24 \text{ kcal-mol}^{-1}$  [33], and the energy level of the activation barrier to dissociation of the first hydrogen from ammonia with respect to nitrogen and hydrogen in their standard states is at  $-6 \text{ kcal-mol}^{-1}$  (cf., Fig. 3). Since the surface activation energy  $E_{-1}$  is estimated to be  $12 \text{ kcal-mol}^{-1}$ , the energy level of  $\text{NH}_2(\text{a}) + \text{H}(\text{a})$  is at  $-E_{-1}-6 = -18 \text{ kcal-mol}^{-1}$ . Since the heat of formation of  $\text{NH}_2$  is  $44 \text{ kcal-mol}^{-1}$  [34], the potential energy level of  $\text{NH}_2(\text{g})+\text{H}(\text{a})$  is  $33 \text{ kcal-mol}^{-1}$ , and the heat of adsorption of the  $\text{NH}_2$  radical on the ruthenium surface is  $E_{-1}+6+33 = 51 \text{ kcal-mol}^{-1}$ .

Since  $E_3$ , the activation energy for the dehydrogenation of  $\text{NH}_2(\text{a})$  to  $\text{NH}(\text{a})+\text{H}(\text{a})$ , is  $6 \text{ kcal-mol}^{-1}$ , the energy level at the barrier separating  $\text{NH}_2(\text{a})+\text{H}(\text{a})$  from  $\text{NH}(\text{a})+2\text{H}(\text{a})$  is  $-12 \text{ kcal-mol}^{-1}$ . Furthermore, the energy level of  $\text{NH}(\text{a})+2\text{H}(\text{a})$  is  $-E_{-3}-12 = -37 \text{ kcal-mol}^{-1}$ , where  $E_{-3}$  is the activation energy of the hydrogenation of  $\text{NH}(\text{a})$  to  $\text{NH}_2(\text{a})$ . Employing a value of  $85 \text{ kcal-mol}^{-1}$  for the heat of formation of  $\text{NH}$  [35], the potential energy level of  $\text{NH}(\text{g})+2\text{H}(\text{a})$  is  $63 \text{ kcal-mol}^{-1}$ . Consequently, the activation energy for the desorption of  $\text{NH}$  radicals is  $E_{-3}+12+63 = 100 \text{ kcal-mol}^{-1}$ . From the energy levels of  $\text{NH}_2(\text{a}) + \text{H}(\text{a})$  and  $\text{NH}(\text{a})+2\text{H}(\text{a})$  (cf., Fig. 3), the  $\text{NH}$  radical is clearly more stable than the  $\text{NH}_2$  radical on  $\text{Ru}(001)$ , as has been suggested by HREELS studies of decomposition of ammonia on  $\text{Ru}(001)$  [32]. The presence of the  $\text{NH}$  radical as a reaction intermediate has been detected by laser-induced fluorescence experiments during ammonia decomposition on polycrystalline platinum and iron surfaces at 0.1 Torr of ammonia and temperatures between 1200 and 1400 K [36,37]. However, the presence of  $\text{NH}_2$  radicals was not observed under these conditions, in agreement with the relative instability of the  $\text{NH}_2$  radical (compared to the  $\text{NH}$

radical) on transition-metal surfaces.

The activation energy for the hydrogenation of surface nitrogen to  $\text{NH}_2(\text{a})$ ,  $E_{-2} = 40.5 \text{ kcal}\cdot\text{mol}^{-1}$ , and that of the hydrogenation of surface nitrogen to  $\text{NH}(\text{a})$ ,  $38.5 \text{ kcal}\cdot\text{mol}^{-1}$ , are shown also in Fig. 3. Compared to the estimated activation energy of hydrogenation of nitrogen adatoms to  $\text{NH}_2(\text{a})$ ,  $E_{-2} = 28 \text{ kcal}\cdot\text{mol}^{-1}$ , on the polycrystalline platinum surface [9], the hydrogenation of surface nitrogen is more difficult on ruthenium since both the nitrogen and hydrogen adatoms are more strongly bonded. Hydrogenation of surface nitrogen to form ammonia has been studied previously on supported  $\text{Ru}/\text{Al}_2\text{O}_3$  and  $\text{Ru}/\text{SiO}_2\text{-Al}_2\text{O}_3$  catalysts at atmospheric pressure by the reaction of dissociatively adsorbed nitric oxide and hydrogen [38,39]. Though an activation energy for the hydrogenation was not determined, these data for the production of ammonia at a partial pressure ratio of hydrogen to nitric oxide of three are very similar to the data for  $^{15}\text{ND}_3$  production shown in Fig. 1. The maximum rate of production of ammonia occurs at approximately 600-620 K on the supported ruthenium catalysts. The similarity between the kinetics of ammonia production from  $\text{NO} + \text{H}_2$  [38,39] and the kinetics for  $^{15}\text{ND}_3$  production from  $^{15}\text{NH}_3 + \text{D}_2$  further suggested the formation of  $^{15}\text{ND}_3$  from deuteration of surface nitrogen.

Completion of the potential energy diagram using  $E_{-2} = 40.5 \text{ kcal}\cdot\text{mol}^{-1}$ ,  $\frac{3}{2}E_{\text{d,H}_2} = 33 \text{ kcal}\cdot\text{mol}^{-1}$  and  $\frac{1}{2}E_{\text{d,N}_2} = 22 \text{ kcal}\cdot\text{mol}^{-1}$  implies an activation barrier for the dissociative adsorption of nitrogen of  $5 \text{ kcal}\cdot\text{mol}^{-1}$  ( $2.5 \text{ kcal}\cdot\text{mol}^{-1}$  on an atom basis). Hence the heat of dissociative chemisorption of a nitrogen molecule is predicted to be exothermic by  $39 \text{ kcal}\cdot\text{mol}^{-1}$  on  $\text{Ru}(001)$ . The heat of adsorption of nitrogen on potassium-promoted ruthenium powder was estimated previously

to be exothermic by 40 kcal-mol<sup>-1</sup> [6].

This estimate of the activation barrier for the dissociative adsorption of nitrogen on Ru(001) in the limit of zero coverage is consistent with a previous estimate of 11 kcal-mol<sup>-1</sup> for ruthenium supported on alumina [6]. The latter was based on isotopic equilibration studies of <sup>15</sup>N<sub>2</sub> and <sup>14</sup>N<sub>2</sub> at pressures between 40 and 200 Torr and temperatures between 650 and 720 K. Assuming the dissociative chemisorption of nitrogen to be mediated by a molecular precursor: (N<sub>2</sub>(g)  $\xrightleftharpoons[k_d]{k_a}$  N<sub>2</sub>(a), and N<sub>2</sub>(a)  $\xrightarrow{k_c}$  2N(a)) the fractional coverage of nitrogen on the supported ruthenium under these conditions is estimated to be 0.27 using a preexponential factor of the initial probability of dissociative adsorption of 10<sup>-7</sup> for nitrogen [40,41]. In addition, it is known that platinum is a poor catalyst for the synthesis of ammonia [42,43], and the present result indicates clearly that ruthenium is a superior catalyst for ammonia synthesis than platinum, where an activation barrier for the dissociative adsorption of 16 kcal-mol<sup>-1</sup> for nitrogen was predicted in the limit of zero surface coverage for polycrystalline platinum surfaces using the identical mechanistic model [9]. Furthermore, the predicted activation energy for the dissociative adsorption of nitrogen on Ru(001) of 5 kcal-mol<sup>-1</sup> is similar to those measured on single crystalline surfaces of iron (0-6.5 kcal-mol<sup>-1</sup>) [13,14], and the activation energy was observed to increase with nitrogen coverage on both metals [6,13,14,18]. However, the influence of hydrogen coverage on the dissociative chemisorption of nitrogen is dominant over that of the nitrogen coverage during the catalytic synthesis of ammonia. The apparent activation energies of the ammonia synthesis reaction on supported iron [44-46] and supported ruthenium [5] catalysts are also very similar (20-22

kcal-mol<sup>-1</sup>). This suggests that the reported higher activity of ruthenium catalysts [1,2] in ammonia synthesis could be due to a higher preexponential factor of the apparent reaction rate coefficient.

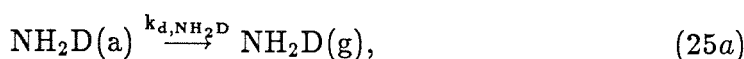
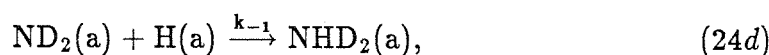
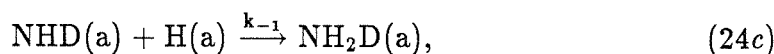
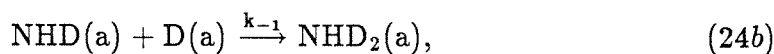
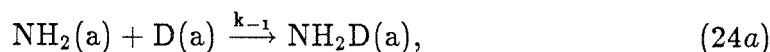
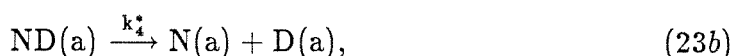
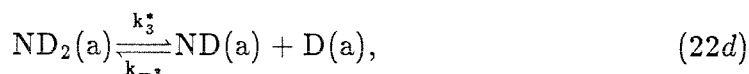
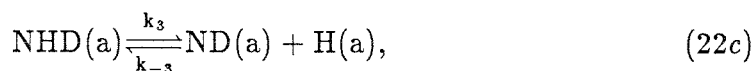
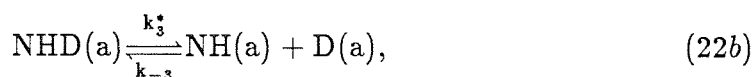
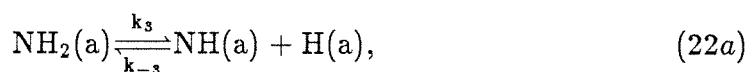
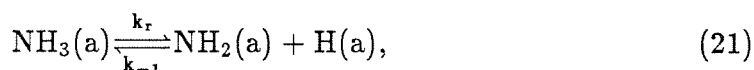
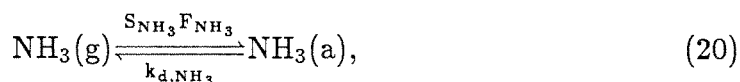
## VI. Conclusions

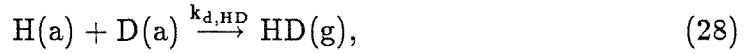
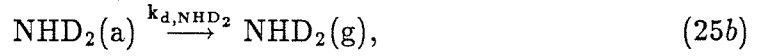
The isotopic exchange reaction between <sup>15</sup>NH<sub>3</sub> and deuterium for a partial pressure ratio of ammonia to deuterium of 4:1 with a total pressure of 2.5 x 10<sup>-6</sup> Torr produces all three exchange products on Ru(001) at temperatures between 380 and 720 K. The mechanism for exchange is dissociative. The exchange mechanism for ammonia and deuterium on platinum surfaces applies to the Ru(001) surface also. In particular, good agreement was obtained with the experimental data for the production of <sup>15</sup>NH<sub>2</sub>D, <sup>15</sup>NHD<sub>2</sub> and <sup>15</sup>ND<sub>3</sub>. The latter is produced from consecutive deuteration of surface nitrogen adatoms. A potential energy diagram is constructed for the synthesis of ammonia and the energy levels of and the activation barriers separating the chemisorbed intermediates in the ammonia decomposition and synthesis reactions, namely, NH<sub>3</sub>, NH<sub>2</sub> + H, NH + 2H, N + 3H are determined. The dissociative chemisorption of molecular nitrogen on Ru(001) is activated with an activation energy estimated to be approximately 5 kcal-mol<sup>-1</sup> in the limit of zero surface coverage of nitrogen adatoms.

*Acknowledgment.* This research was supported by the National Science Foundation under Grant No. CHE-8516615.

## Appendix

The reaction mechanism involving the production of  $\text{NH}_2\text{D}(\text{g})$  and  $\text{NHD}_2(\text{g})$  is the following:





where  $k_i^*$  is the rate coefficient of a surface reaction involving the cleavage of a N-D bond,  $k_i$  is the rate coefficient of a surface reaction involving the cleavage of a N-H bond, and  $E_i^* - E_i = 1.6 \text{ kcal}\cdot\text{mol}^{-1}$  [8]. With the mass balances for  $\text{NH}_2(\text{a})$ ,  $\text{NHD}(\text{a})$ ,  $\text{ND}_2(\text{a})$ ,  $\text{NH}(\text{a})$ ,  $\text{ND}(\text{a})$ ,  $\text{NH}_2\text{D}(\text{a})$  and  $\text{NHD}_2(\text{a})$ , one can iteratively solve for the rate of production of  $^{15}\text{NH}_2\text{D}$  and  $^{15}\text{NHD}_2$ .

## References

- [1] Ozaki A., Aika K. and Hori H., *Bull. Chem. Soc. Japan* **1971**, *44*, 3216.
- [2] Aika K., *Angew. Chem. Int. Ed. Engl.* **1986**, *25*, 558.
- [3] Uchiyama S., Hattori Y., Ozaki A. and Aika K., *Chem. Letters* **1981**, 1463.
- [4] Aika K., Hori H. and Ozaki A., *J. Catal.* **1972**, *27*, 424.
- [5] Urabe K., Aika K. and Ozaki A., *J. Catal.* **1974**, *32*, 108.
- [6] Urabe K., Aika K. and Ozaki A., *J. Catal.* **1975**, *38*, 430.
- [7] Aika K., Shimazki K., Hattori Y. and Ozaki A., *J. Catal.* **1985**, *92*, 296.
- [8] Tsai W. and Weinberg W.H., *J. Phys. Chem.* (submitted).
- [9] Vajo J.J., Tsai W. and Weinberg W.H., *J. Phys. Chem.* **1985**, *89*, 3243.
- [10] Tsai W., Vajo J.J. and Weinberg W.H., *J. Phys. Chem.* **1985**, *89*, 4926.
- [11] Vajo J.J., Tsai W. and Weinberg W.H., *J. Phys. Chem.* **1986**, *90*, 6531.
- [12] Ertl G., "Plenary Lecture," in *Proceedings of the 7th International Congress on Catalysis, Tokyo, 1980*.
- [13] Bozso F., Ertl G., Grunze M. and Weiss M., *J. Catal.* **1977**, *49*, 18.
- [14] Bozso F., Ertl G. and Weiss M., *J. Catal.* **1977**, *50*, 519.
- [15] Boudart M., *Catal. Rev.-Sci. Eng.* **1981**, *23*, 1.
- [16] Stoltze P., and Norskov J.K., *Phys. Rev. Lett.* **1985**, *55*, 2502; Bowker M., Parker I.B. and Waugh K.C., *Appl. Catal.* **1985**, *14*, 101.
- [17] Ertl G., in *Catalysis, Science and Technology*, Eds., Anderson J.R. and Boudart M., Vol. 4 (Springer-Verlag, Heidelberg, 1983), p. 210.
- [18] Scholten J.J.F., Zwietering P., Konvalinka J.A. and de Boer J.H., *Trans. Faraday Soc.* **1959**, *55*, 2166.
- [19] Taylor J.L., Ibbotson D.E. and Weinberg W.H., *J. Chem. Phys.* **1978**, *69*, 4298.
- [20] Thomas G.E. and Weinberg W.H., *J. Chem. Phys.* **1979**, *70*, 1437.
- [21] Ibbotson D.E., Wittrig T.S. and Weinberg W.H., *Surface Sci.* **1981**, *110*, 294.

- [22] Gland, J.L., and Kollin, E.B., Surface Sci. **1981**, 104, 478.
- [23] Kemball, C., Proc. R. Soc., Ser. A **1952**, 214, 413.
- [24] Danielson L.R., Dresser M.J., Donaldson E.E. and Dickinson J.T., Surface Sci. **1978**, 71, 599.
- [25] Benndorf C. and Madey T.E., Surface Sci. **1983**, 135, 164.
- [26] Tsai W., PhD Thesis, California Institute of Technology **1987**.
- [27] Shimizu H., Christmann K. and Ertl G., J. Catal. **1980**, 61, 412.
- [28] Tsai W., Vajo J.J. and Weinberg W.H., J. Phys. Chem. (submitted).
- [29] The probability of decomposition of ammonia on Ru(001) at 700 K is approximately 0.01 [8].
- [30] This is true only when the energy level of the barrier for the hydrogenation of N(a) to NH(a) is less than that for the hydrogenation of NH(a) to NH<sub>2</sub>(a), and this is confirmed in the present calculations.
- [31] Note that  $k_{-1}^{(0)}/k_{-3}^{(0)}$  was not adjustable while  $k_3^{(0)}$  and  $k_4^{(0)}$  are of "normal" magnitude.
- [32] Parmeter, J.E., Schwalke U. and Weinberg, W.H. (in preparation).
- [33] The apparent activation energy of decomposition at high temperatures,  $E_r - E_{d,NH_3}$ , was determined to be 5 kcal-mol<sup>-1</sup> from previous kinetic measurements [8].
- [34] DeFrees, D.J., Hehre, W.J., McIver, R.T. and McDaniel, D.H., J. Phys. Chem, **1979**, 83, 232.
- [35] Graham, W.R.M., Lew, H., Can. J. Phys. **1978**, 56, 85.
- [36] Selwyn, G.S. and Lin, M.C., Chem. Phys. **1982**, 67, 213.
- [37] Selwyn, G.S., Fujimoto, G.T. and Lin, M.C., J. Phys. Chem, **1982**, 86, 760.
- [38] Taylor K.C. and Klimisch R.L., J. Catal. **1973**, 30, 478.
- [39] Voorhoeve R.J.H. and Trimble L.E., J. Catal. **1975**, 38, 80.
- [40] The initial probability of dissociative adsorption of nitrogen can be written as  $k_s \exp(-E^{act}/k_B T)$ , where  $E^{act}$  is the activation energy of adsorption and  $k_s$  is given by  $k_a^{(0)}k_c^{(0)}/k_d^{(0)}$  [17].
- [41] There are numerous examples where the activation energy for the dissociative adsorption of nitrogen increases with coverage [13,14].

- [42] Emmett P.H., in *The Physical Basis for Heterogeneous Catalysis*, Eds., Drauglis E. and Jaffee R.I. (Plenum, New York 1975), p. 3.
- [43] Bond G.C., in *The Physical Basis for Heterogeneous Catalysis*, Eds., E. Drauglis and R.I. Jaffee (Plenum, New York 1975), p. 53.
- [44] Ozaki A., Taylor H. and Boudart M., Proc. R. Soc. London Ser. A **1960**, 258, 47.
- [45] Temkin M.I., Morozov N.M. and Shapatina E.M., Kinet. Catal. **1963**, 4, 260.
- [46] Nielsen A., Kjaer J. and Hansen B., J. Catal. **1964**, 3, 68.

TABLE 1. Kinetic Parameters for the Decomposition and Isotopic Exchange Reactions of Ammonia on Ru(001)

	Parameter	Value	Ref.
$S_{\text{NH}_3}^0$	Ammonia probability of adsorption	1	24,25
$k_{\text{d,NH}_3}^{(0)}$	Ammonia desorption preexponential factor	$1 \times 10^{14} \text{ s}^{-1}$	24,25
$E_{\text{d,NH}_3}$	Ammonia desorption activation energy	$19 \text{ kcal-mol}^{-1}$	8
$k_{\text{d,H}_2}^{(0)}, k_{\text{d,D}_2}^{(0)}$	Hydrogen desorption preexponential factor	$1 \times 10^{-3} \text{ cm}^2\text{-s}^{-1}$	26
$E_{\text{d,H}_2}, E_{\text{d,D}_2}$	Hydrogen desorption activation energy	$22 \text{ kcal-mol}^{-1}$	26
$S_{\text{D}_2}$	Deuterium probability of adsorption	0.25	27
$k_{\text{d,N}_2}^{(0)}$	Nitrogen desorption preexponential factor	$1.3 \times 10^{-3} \text{ cm}^2\text{-s}^{-1}$	8
$E_{\text{d,N}_2}$	Nitrogen desorption activation energy	$44.0 \text{ kcal-mol}^{-1}$	8
$k_{\text{r}}^{(0)}$	Surface reaction preexponential factor	$5 \times 10^{13} \text{ s}^{-1}$	
$E_{\text{r}}$	Surface reaction activation energy	$24 \text{ kcal-mol}^{-1}$	8
$k_{-2}^{(0)}$	Hydrogenation reaction preexponential factor	$3 \times 10^{-17} \text{ cm}^4\text{-s}^{-1}$	
$E_{-2}$	Surface hydrogenation activation energy	$40.5 \text{ kcal-mol}^{-1}$	
$n_s k_{\text{eff}}^{(0)}$	$n_s k_{-1}^{(0)} / k_2^{(0)}$	3000	
$E_{\text{eff}}$	$E_{-1} - E_2$	$6 \text{ kcal-mol}^{-1}$	

---

$k_3^{(0)}$	Surface reaction preexponential factor	$10^{11} \text{ s}^{-1}$
$E_3$	Surface reaction activation energy	$6 \text{ kcal-mol}^{-1}$
$k_4^{(0)}$	Surface reaction preexponential factor	$10^{13} \text{ s}^{-1}$
$E_4$	Surface reaction activation energy	$23 \text{ kcal-mol}^{-1}$
$k_{-1}^{(0)}$	Hydrogenation reaction preexponential factor	$0.3 \text{ cm}^2\text{-s}^{-1}$
$E_{-1}$	Surface hydrogenation activation energy	$12 \text{ kcal-mol}^{-1}$
$k_{-3}^{(0)}$	Hydrogenation reaction preexponential factor	$0.01 \text{ cm}^2\text{-s}^{-1}$
$E_{-3}$	Surface hydrogenation activation energy	$25 \text{ kcal-mol}^{-1}$
$n_s$	Surface atom density	$1.56 \times 10^{15} \text{ cm}^{-2}$

---

### Figure Captions

- Fig. 1: Rates of production of the products of the  $^{15}\text{NH}_3 + \text{D}_2$  exchange and decomposition reactions as a function of reciprocal temperature at a partial pressure ratio of  $^{15}\text{NH}_3$  to  $\text{D}_2$  of four and a total pressure of  $2.5 \times 10^{-6}$  Torr. Lines have been drawn through the data points for clarity.
- Fig. 2: Comparisons of model calculations with the experimental exchange and decomposition data for  $\text{N}_2$ ,  $^{15}\text{NH}_2\text{D}$ ,  $^{15}\text{NHD}_2$  and  $^{15}\text{ND}_3$ .
- Fig. 3: Potential energy diagram illustrating from right to left the catalytic decomposition of  $\text{NH}_3$  on  $\text{Ru}(001)$  where  $E_{\text{d,NH}_3} = 19 \text{ kcal-mol}^{-1}$ ,  $E_{\text{r}} = 24 \text{ kcal-mol}^{-1}$ ,  $E_{-1} = 12 \text{ kcal-mol}^{-1}$ ,  $E_3 = 6 \text{ kcal-mol}^{-1}$ ,  $E_{-3} = 25 \text{ kcal-mol}^{-1}$ ,  $E_4 = 23 \text{ kcal-mol}^{-1}$ ,  $E_{-2} = 40.5 \text{ kcal-mol}^{-1}$ ,  $\frac{3}{2}E_{\text{d,H}_2} = 33 \text{ kcal-mol}^{-1}$ , and  $\frac{1}{2}E_{\text{d,N}_2} = 22 \text{ kcal-mol}^{-1}$ . Note that the catalytic synthesis of  $\text{NH}_3$  from  $\text{N}_2$  and  $\text{H}_2$  is described by traversing this energy diagram from left to right. The model predicts an activation energy for dissociative adsorption of  $\text{N}_2$  of  $5 \text{ kcal-mol}^{-1}$ .

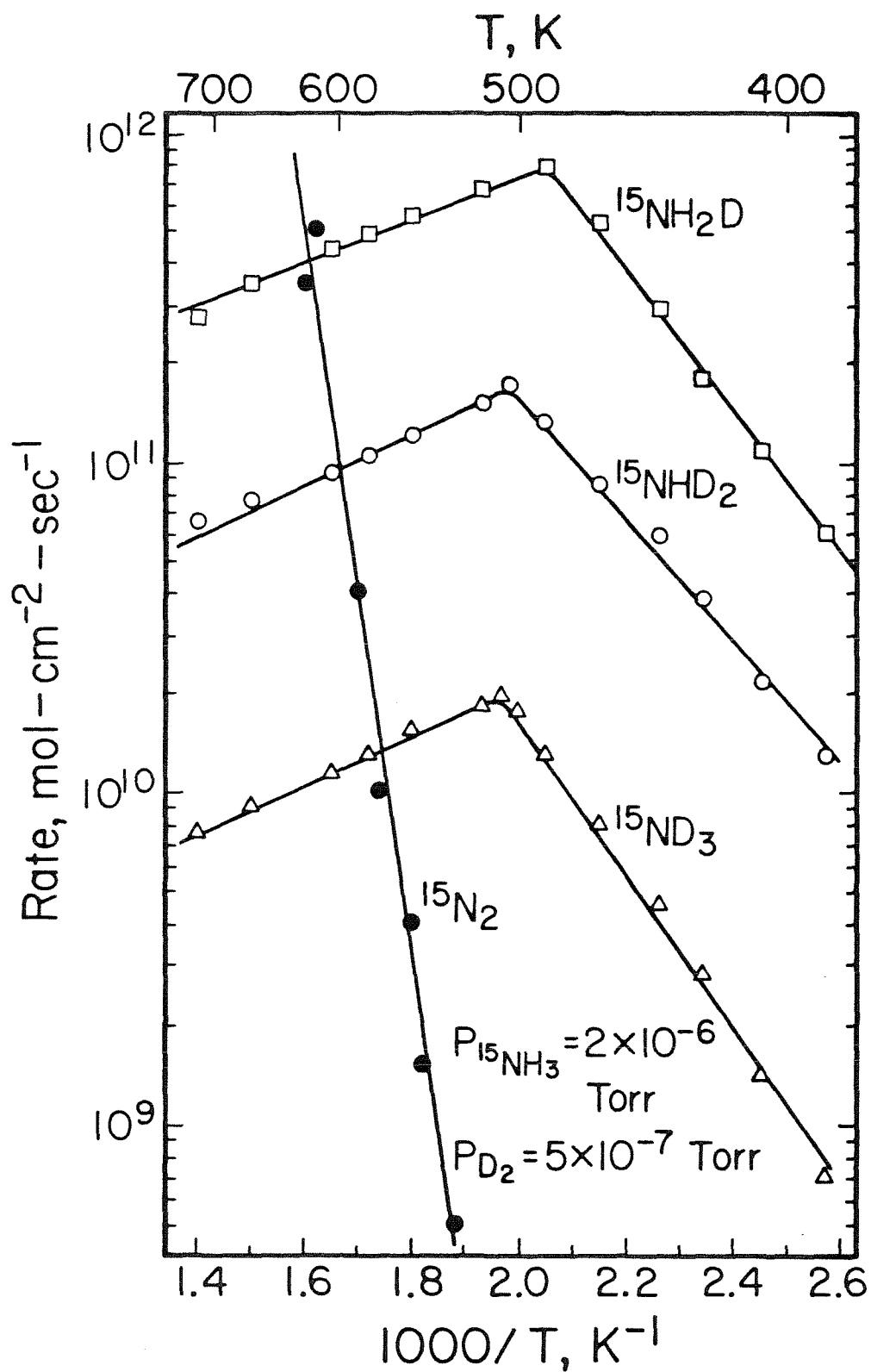


Figure 1

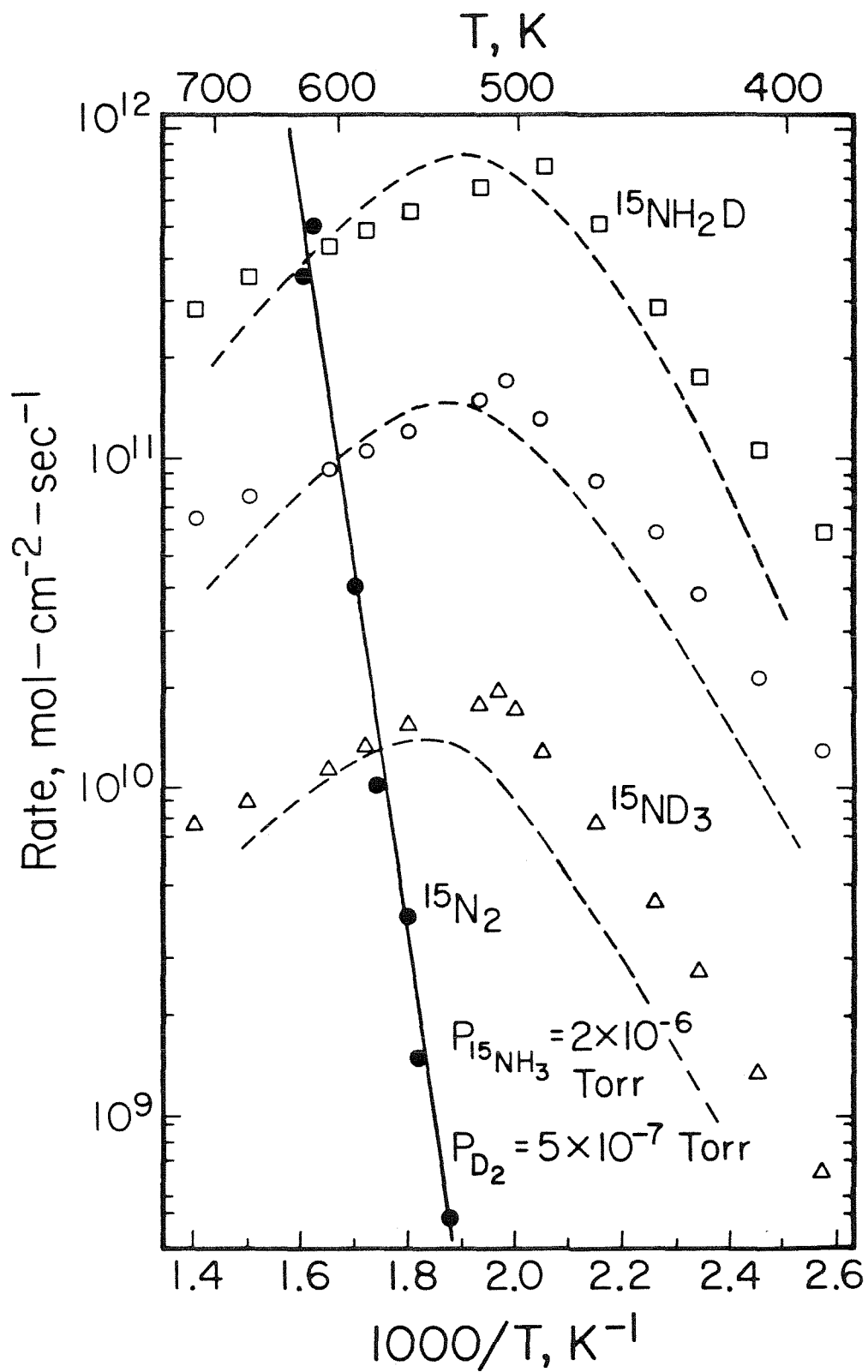


Figure 2

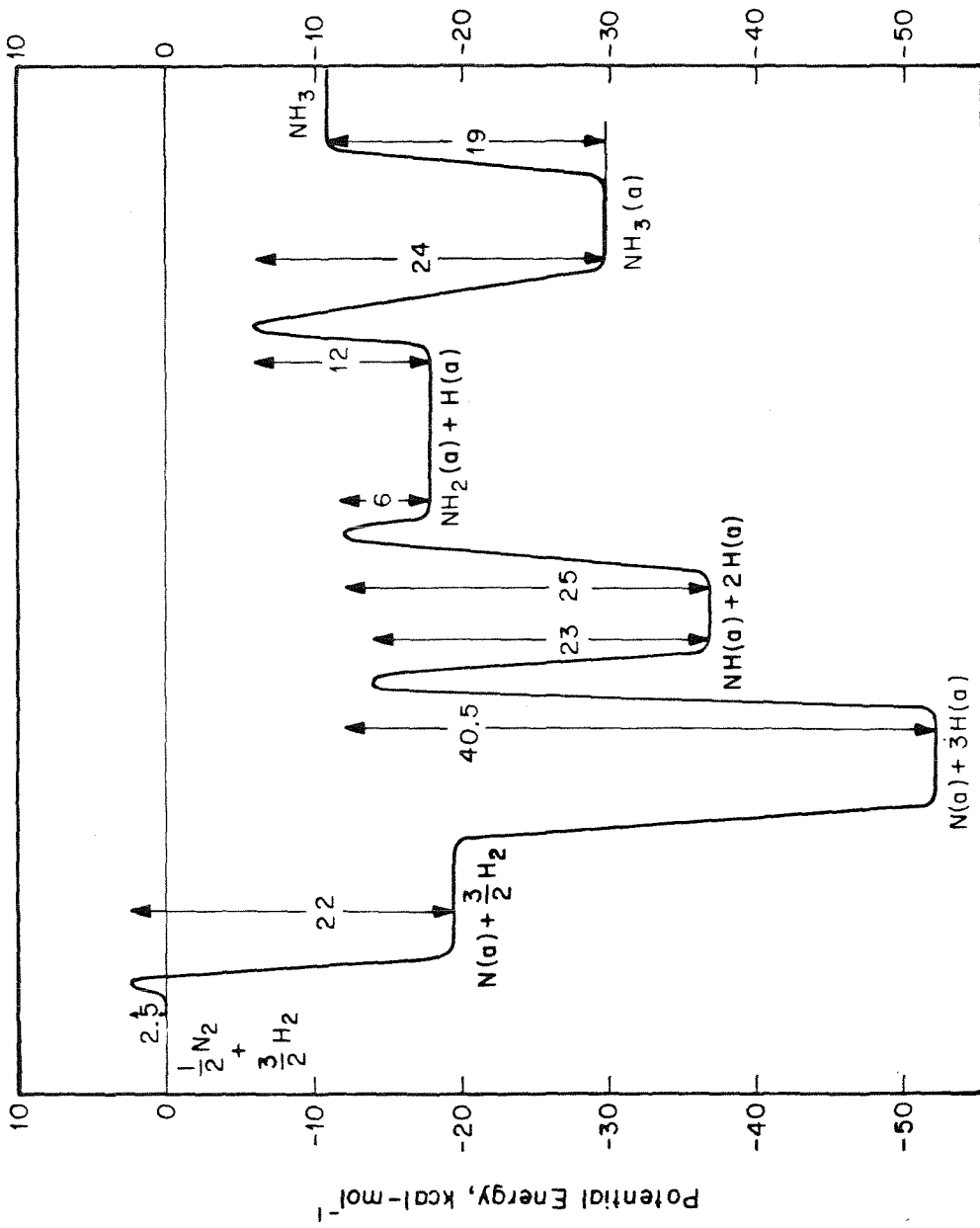


Figure 3

**Chapter 7.**

Conclusions

The catalytic decomposition of ammonia was found to proceed via the same reaction mechanism on polycrystalline platinum, Pt(110)-(1x2) and Ru(001) surfaces. Under conditions where the reaction rate is linearly dependent on ammonia pressure (at relatively lower pressures and/or higher temperatures), the rate of decomposition is controlled by a competition between the surface reaction that cleaves a N-H bond and the desorption of molecularly chemisorbed ammonia. When the rate of ammonia decomposition is independent of ammonia pressure (at relatively higher pressures and/or lower temperatures), the surface is nearly saturated with nitrogen adatoms, and the recombinative desorption of these nitrogen adatoms determines the rate of reaction. A mechanistic model that is embodied by a sequence of elementary reactions describes successfully both steady-state specific reaction rates and surface coverages over the wide range of pressures ( $5 \times 10^{-7}$ -0.6 Torr) and temperatures (400-1250 K) that were studied. In addition, the predicted coverage-dependence of the desorption rate coefficient of hydrogen on polycrystalline platinum during the decomposition of ammonia (with hydrogen inhibition) was experimentally observed from studies of chemisorption of deuterium on nitrogen-precovered Pt(110)-(1x2) surfaces. A comparison between activation barriers for the dissociative adsorption of nitrogen, estimated from mechanistic modeling of isotopic exchange reactions between ammonia and deuterium as well as the decomposition of ammonia on polycrystalline platinum and Ru(001) surfaces, indicates clearly that ruthenium is a superior catalyst to platinum for the synthesis of ammonia.

**Appendix 1.**

Versatile Microreactor for Studies of Gas-Surface  
Catalytic Reactions between  $10^{-7}$  and 1000 Torr

[Appendix 1 consists of an article coauthored with J.J. Vajo and W.H. Weinberg,  
which appeared in the *Review of Scientific Instruments* **1985**, **56**, 1439.]

# Versatile microreactor for studies of gas-surface catalytic reactions between $10^{-7}$ and 1000 Torr

J. J. Vajo, W. Tsai, and W. H. Weinberg

*Division of Chemistry and Chemical Engineering, California Institute of Technology, Pasadena, California 91125*

(Received 27 December 1984; accepted for publication 27 March 1985)

A microreactor system that is designed for studies of steady-state and batch heterogeneous reactions on a wire, foil, or single-crystal surface at pressures between  $10^{-7}$  and 1000 Torr is described. The applicability of the continuous stirred tank reactor approximation that facilitates the calculation of absolute reaction rates is discussed. Results for the decomposition of ammonia on a polycrystalline platinum wire are used to illustrate the performance of the microreactor.

## INTRODUCTION

Modern surface-science techniques have increased tremendously our understanding of the elementary steps associated with adsorption, desorption, and catalytic reactions occurring at solid surfaces. It is obviously desirable to be able to apply this extensive knowledge obtained at low pressures,  $10^{-10}$ – $10^{-6}$  Torr, to clarify the kinetic and mechanistic details of commercial catalytic reactions that occur at considerably higher pressures, typically 1–100 atmospheres. To apply this knowledge reliably requires a delineation of the mechanistic changes that accompany variations in pressure from ultrahigh vacuum to those employed commercially. Moreover, increasing the accessible pressure regime for which accurate kinetic data may be obtained increases the likelihood of interpreting the measured rate data mechanistically in terms of elementary reactions.

Recently, there have been several investigations of catalytically important reactions at pressures between  $10^{-8}$  Torr and several atmospheres.<sup>1–11</sup> Here, a microreactor is described that is capable of steady-state flow and batch heterogeneous reactions on a wire, foil, or single-crystal surface at pressures between  $10^{-7}$  and 1000 Torr. In particular, the performance of this reactor is illustrated by considering the decomposition of ammonia over a polycrystalline platinum wire.<sup>12</sup>

## I. REACTOR DESIGN AND OPERATION

The reactor consists of a high-vacuum section, a small reaction volume, and a sample manipulator, which is used to position the catalyst either in the high-vacuum region or in the reactor volume for experiments in different pressure regimes. Adapted from a design of Auerbach *et al.*,<sup>13</sup> the manipulator is comprised of a doubly differentially pumped housing, a shaft, which supports the catalyst sample, and three spring-loaded Teflon O-rings, which allow the shaft to be translated and rotated. A schematic of the manipulator is shown in Fig. 1. The housing is a stainless-steel tube that contains the O-rings and is welded to a 2½-in. flange for attachment to the reactor body. Two stainless-steel rings separate the O-rings and align them with two 0.46-cm pump-out ports. A removable top plate secures the O-rings in the housing. The first port is pumped by a mechanical pump, whereas

the second port is pumped by a Varian 2-in. diffusion pump with a chilled water-cooled baffle.

A mini-feedthrough (Ceramaseal 807B9299-2) welded to a stainless-steel tube comprises the manipulator shaft. This shaft provides support for the crystal, wire, or foil via two 0.24-cm OFHC copper wires, which are also used to heat the sample. Cooling is achieved by filling the hollow shaft with liquid nitrogen. Temperatures are measured with a 0.0075-cm-diameter W-5% Re/W-26% Re thermocouple, which is spot welded to the sample. Spring-loaded Teflon O-rings (Accratorics AR10400-206AC) are used to form a seal between the shaft and the manipulator housing. The shaft can be translated and rotated while maintaining a seal. All sealing surfaces are machined to obtain an optimum metal-to-Teflon seal.

Leakage past the O-rings and the degree to which the base pressure in the system is limited by this leakage may be calculated as follows. The pressure before a seal,  $P_a$ , is related to the pressure after the seal,  $P_b$ , by

$$P_a L = S P_b, \quad (1)$$

where  $L$  is the leak rate of the seal, and  $S$  is the speed at which gases are pumped away. The leak rate of a 14-in.-diameter seal is stated by Auerbach *et al.*<sup>13</sup> to be  $10^{-6}$  l/s. This corre-

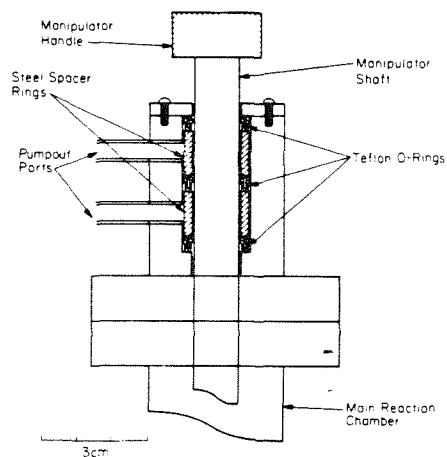


FIG. 1. Cross section of double differentially pumped sample manipulator.

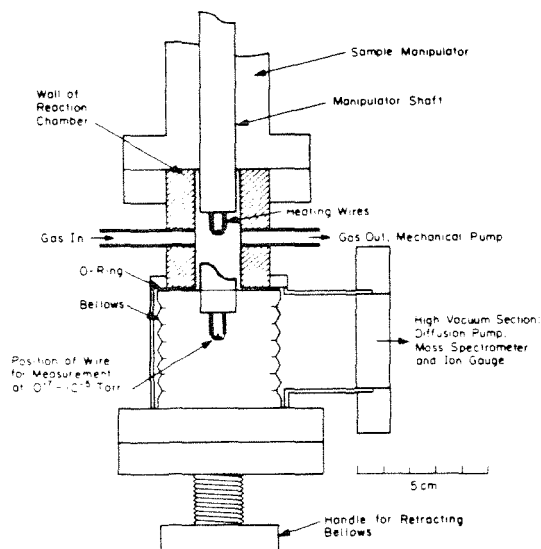


FIG. 2. Cross section of microreactor body, showing the wire in position for experiments at both  $10^{-4}$ –1000 Torr and  $<10^{-7}$ – $10^{-4}$  Torr. Ports for pressure measurement and the leak to the high-vacuum section, which are orthogonal to the inlet and outlet flow ports, are not shown. The volume of the baratron and the access ports, together with the shaded region, is the reactor volume,  $30 \text{ cm}^3$ .

sponds to  $3.6 \times 10^{-8} \text{ l/s}$  for a  $\frac{1}{8}$ -in.-diameter seal. Assuming atmospheric pressure before the first seal and a pumping speed of  $10^{-3} \text{ l/s}$  (certainly a lower limit), the pressure in the first section should be  $2.7 \times 10^{-2}$  Torr. Assuming the same pumping speeds in the second section and main reactor body results in a base pressure in the main chamber due to leakage that is below  $3.5 \times 10^{-11}$  Torr. Since this is below current limitations due to other factors, seal leakage does not limit the base pressure of the microreactor.

The main chamber of the microreactor consists of a modified right-angle ultrahigh-vacuum valve linked to a high-vacuum pumping section, as shown in Fig. 2. To increase the ratio of the catalytic surface area to the total gas volume and, consequently, increase the sensitivity, the port opposite the bellows was replaced with a tube of 13/16-in. internal diameter. This diameter is sufficiently large to accommodate the manipulator shaft and results in a reactor volume of  $10 \text{ cm}^3$ . Surfaces that are exposed to high pressures are plated with  $7.5 \times 10^{-5}$  in. of gold to suppress any reaction from occurring on the chamber walls.

Four ports of  $\frac{1}{16}$ -in. internal diameter, spaced  $90^\circ$  apart, provide for flow of reactant gases, pressure measurement, and detection of reaction products. The flow of gases is regulated by metering valves on the inlet and outlet flow lines. Flow rates can be varied from 0.1 to  $100 \text{ cm}^3/\text{s}$  by adjusting the calibrated inlet and outlet valves and the gas pressure behind the inlet valve. Mean residence times in the reactor under these conditions are adjustable between 0.1 and 10 s. Pressures are measured with MKS baratron gauges with sensitivities between either  $10^{-4}$  and 1 Torr,  $10^{-2}$  and 100 Torr, or  $10^{-1}$  and 1000 Torr, depending on the pressure at which the experiments are conducted. The additional volume of the baratron, together with the access ports, increases

the total reactor volume to  $30 \text{ cm}^3$ . Products are detected by a computer-interfaced EAI 1200 quadrupole mass spectrometer located in the high-vacuum section. Interchangeable pieces of Pyrex tubing with variable conductances provide a leak from the reactor to the high-vacuum section. The conductance of the Pyrex tubing is chosen to maintain a pressure of  $\sim 10^{-6}$  Torr at the mass spectrometer during a reaction. Cajon Ultra-Torr fittings are used to facilitate exchange of the Pyrex tubes. The base pressure of the micro-reactor, as it is currently pumped by a liquid-nitrogen-trapped Varian 2-in. diffusion pump, is below  $10^{-8}$  Torr.

An advantage of the compact design of this microreactor is the high sensitivity for reactions occurring over low area solids. A concomitant disadvantage, however, is that the surface cannot be examined spectroscopically either before, during, or after the catalytic reaction. Hence, a cleaning procedure for the particular surface under investigation must be formulated in a separate apparatus that does have such spectroscopic capabilities. An indication of the cleanliness of the surface may be ascertained *in situ* in the reactor via the thermal desorption spectra of probe molecules, e.g., hydrogen and carbon monoxide.

To conduct steady-state reactions between 0.01 and 1000 Torr, the sample is sealed in the reactor chamber, and the outflow of gases is pumped by a 75-l/min mechanical pump. A Pyrex tube provides the leak to the high-vacuum section. (For example, a 0.5-cm length of 0.0075-cm-i.d. tubing is used for reactions at 0.5 Torr.) For reactions at pressures between  $10^{-4}$  and  $10^{-2}$  Torr, the inlet metering valve is replaced by a 0.5-cm length, 0.008-cm-i.d. capillary tube to restrict inlet flow, and the outlet to the mechanical pump is sealed. The leak to the high-vacuum section is replaced with a tube of 0.46 cm i.d. which, in addition to providing a leak for product detection, provides for the outflow of gases pumped by the diffusion pump. Experiments at pressures between  $10^{-7}$  and  $10^{-5}$  Torr are conducted by opening the UHV right-angle valve and translating the catalyst directly into the high-vacuum section, as illustrated in Fig. 2. Batch reactions may also be performed by simply filling the reaction volume to the appropriate pressure and sealing the inlet and outlet flow lines. The leak to the mass spectrometer allows continuous monitoring of the accumulation of reaction products as a function of time.

To determine absolute reaction rates, the mass spectrometer is calibrated by flowing mixtures of products and reactants corresponding to different conversions through the reactor without a catalyst. Reaction rates are calculated under steady-state conditions at conversions below 10% using the continuous stirred tank reactor (CSTR) equation<sup>14,15</sup>

$$R = \frac{V}{\tau^{id} k_B T_g} (P_i - P_f), \quad (2)$$

where  $R$  is the reaction rate (molecules/ $\text{cm}^2 \text{ s}$ ),  $V$  is the reactor volume,  $\tau^{id}$  is the average residence time assuming CSTR conditions,  $k_B$  is the Boltzmann constant,  $T_g$  is the gas temperature, and  $P_i$  and  $P_f$  are the partial pressures in the reactor associated with the feed and with the steady-state reaction mixture, respectively. Average residence times are

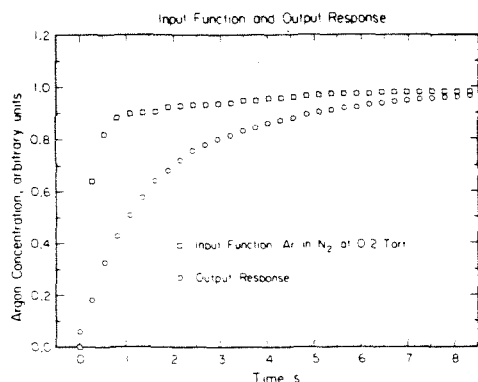


FIG. 3. Input function and output response for an approximate step function input of argon with nitrogen as a carrier gas at a pressure of 0.2 Torr. The average residence time for these conditions, determined using Eq. (4), is 1.42 s.

determined by filling the reactor with the outlet valve closed and monitoring the pressure rise as a function of time. Assuming that the gas obeys the ideal gas law and that at any time the pressure is constant throughout the reactor, the mass flow rate of gas into the reactor is given by

$$\frac{dn}{dt} = \frac{V}{k_B T_g} \frac{dP}{dt} \quad (3)$$

where  $n$  is the number of molecules and  $P$  is the reactor pressure. The average residence time for steady-state flow under CSTR conditions at a pressure  $P_0$  may be expressed as<sup>15</sup>

$$\tau^{id} \equiv \frac{n}{dn/dt} = \frac{P_0}{dP/dt_{P=P_0}} \quad (4)$$

The validity of assuming a CSTR model for the reactor has been investigated by a series of step response experiments, which are described and discussed in the next section.

## II. CSTR APPROXIMATION

Although continuous stirred tank conditions are frequently assumed for experiments in steady-state flow reactors,<sup>16-19</sup> the validity of the CSTR approximation has not been examined directly in these studies. The CSTR assumption is inaccurate when the reactor has an appreciable volume, which allows back-mixing, and when there are dead volumes where mixing occurs inefficiently. The microreactor described here has been designed to minimize these undesirable effects. To examine the validity of the CSTR approximation, a series of experiments has been conducted to characterize the response of the microreactor. A computer-controlled solenoid valve was used to generate approximate step function inputs of argon into the reactor with nitrogen as a carrier gas. The response of the reactor was monitored as a function of time using the mass spectrometer. Typical input and response data are shown in Fig. 3 for a pressure of 0.2 Torr. The input function was measured directly at the inlet stream via a bypass from the microreactor.

Using the response data, the residence time distribution (RTD)  $R(t)$  may be calculated. Here,  $R(t)dt$  is the fraction of effluent with a residence time in the reactor that is between  $t$

and  $t + dt$ . If the CSTR approximation is applicable, the experimentally determined RTD will resemble the RTD for a CSTR. The RTD for a CSTR may be written as<sup>14</sup>

$$R(t) = \frac{1}{\tau^{id}} \exp\left(-\frac{t}{\tau^{id}}\right), \quad (5)$$

where  $\tau^{id}$  is calculated from Eq. (4). In general, the actual RTD may be obtained from experimental response data by deconvoluting the linear response equation<sup>20</sup>

$$C_{out}(t) = \int_0^\infty C_{in}(t-t')R(t')dt', \quad (6)$$

where  $C_{in}(t)$  and  $C_{out}(t)$  are the concentrations of species entering and leaving the reactor, respectively. Various methods, including numerical integration and Fourier transformation, were used to compute  $R(t)$  from Eq. (6) for the data shown in Fig. 3. The result appears to be independent of the method employed, and the computed RTD is shown in Fig. 4. Also shown in Fig. 4 is the RTD for the CSTR model. Under these flow conditions,  $\tau^{id} = 1.42$  s was calculated using Eq. (4).

The CSTR approximation may be evaluated quantitatively by comparing the predicted average conversions based on the CSTR model and the actual RTD. For an arbitrary RTD, the average conversion may be expressed as<sup>14</sup>

$$\hat{x} = \int_0^\infty x(t')R(t')dt', \quad (7)$$

where  $x(t')$  is the integrated rate equation for a batch reaction. Assuming first-order kinetics,  $x(t)$  may be written as

$$x(t) = 1 - \exp(-kt), \quad (8)$$

where  $k$  is the reaction-rate coefficient. This expression simplifies at low conversions, where  $kt \ll 1$ , to

$$x(t) = kt. \quad (9)$$

Substituting Eq. (9) into Eq. (7) yields

$$\hat{x} = k \int_0^\infty t'R(t')dt'. \quad (10)$$

From Eq. (10) the average residence time may be defined as

$$\tau \equiv \int_0^\infty t'R(t')dt', \quad (11)$$

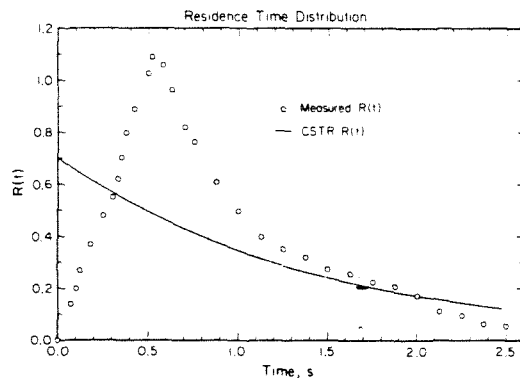


FIG. 4. Residence time distributions determined both experimentally from the data shown in Fig. 3 and computed assuming an ideal CSTR condition with  $\tau^{id} = 1.42$  s.

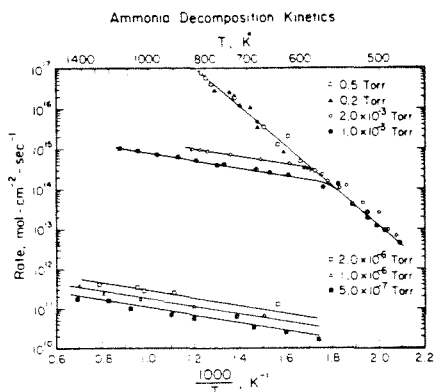


FIG. 5. Arrhenius plots of the rate of ammonia decomposition on platinum for ammonia pressures of 0.5, 0.2,  $2 \times 10^{-3}$ ,  $1 \times 10^{-3}$ ,  $2 \times 10^{-6}$ ,  $1 \times 10^{-6}$  and  $5 \times 10^{-7}$  Torr. Lines have been drawn through the data points as a visual aid.

assuming that  $R(t)$  is a normalized RTD. Thus, the average conversion for an arbitrary RTD and first-order kinetics at low conversions is

$$\hat{x} = k\tau. \quad (12)$$

Substituting Eq. (5) into Eq. (7) yields the following expression for the average conversion of a CSTR

$$\hat{x}^{id} = k\tau^{id}. \quad (13)$$

Consequently, comparing  $\tau$  and  $\tau^{id}$  determines quantitatively the error introduced by assuming ideal CSTR conditions. Using the RTD shown in Fig. 4,  $\tau$  computed from Eq. (11) is 1.47 s. Comparing this value to  $\tau^{id} = 1.42$  s indicates that under these conditions, the CSTR approximation is accurate to within 4% and hence may be used to compute absolute reaction rates. A similar result has been obtained for a range of flow rates at pressures between 0.1 and 10 Torr. For pressures below 0.1 Torr, the increased mean-free path of the gas molecules will improve agreement with the CSTR approximation, whereas for pressures above 10 Torr, further measurements would be necessary to examine the CSTR approximation.

### III. REACTOR PERFORMANCE

Absolute reaction rates determined for the decomposition of ammonia at steady state over a polycrystalline platinum wire are shown in Fig. 5. The production of nitrogen

was monitored mass spectrometrically, and  $P_{f,NH_3}$  in Eq. (2) was determined from the overall reaction stoichiometry. Residence times were  $\sim 1.5$  and 0.1 s for decomposition rates measured at pressures above  $1 \times 10^{-3}$  Torr and below  $2 \times 10^{-6}$  Torr, respectively. The range of observable rates, which already spans 7 orders of magnitude, may be extended further by increasing the residence time and by using a batch mode.<sup>21</sup> For the data of Fig. 5, average conversions were below 5%, except for temperatures above 800 K at pressures of  $1 \times 10^{-3}$  and  $2 \times 10^{-3}$  Torr, where average conversions were  $< 15\%$ . The observed kinetics suggest, however, that even for these rather high conversions, Eq. (9) remains applicable. This and other aspects of the decomposition kinetics displayed in Fig. 5 are discussed in detail elsewhere.<sup>12</sup>

### ACKNOWLEDGMENTS

This work was supported by the Army Research Office under Grant No. DAAG29-83-K-0094, and Central Research and Development Department of E. I. du Pont de Nemours and Company. The advice and assistance of Dr. Kurt Fickie, Dr. Charles Sobrero, and Dr. Jenna Zinck is very much appreciated.

- <sup>1</sup>D. W. Goodman, R. D. Kelly, T. E. Madey, and J. T. Yates, Jr., *J. Catal.* **63**, 226 (1980).
- <sup>2</sup>C. T. Campbell and D. W. Goodman, *Surf. Sci.* **123**, 413 (1982).
- <sup>3</sup>D. E. Peebles, D. W. Goodman, and J. M. White, *J. Phys. Chem.* **87**, 4378 (1983).
- <sup>4</sup>D. W. Goodman, *Acc. Chem. Res.* **17**, 94 (1984).
- <sup>5</sup>M. J. Mummey and L. D. Schmidt, *Surf. Sci.* **91**, 301 (1980).
- <sup>6</sup>M. J. Mummey and L. D. Schmidt, *Surf. Sci.* **109**, 29 (1981).
- <sup>7</sup>H. J. Krebs, H. P. Bonzel, and G. Gafner, *Surf. Sci.* **88**, 269 (1979).
- <sup>8</sup>B. Kasemo, K. E. Keck, and T. Högberg, *J. Catal.* **66**, 441 (1980).
- <sup>9</sup>J. Goschnick and M. Grunze, *J. Vac. Sci. Technol.* **18**, 561 (1981).
- <sup>10</sup>A. Vavere and R. S. Hansen, *J. Catal.* **69**, 158 (1981).
- <sup>11</sup>N. D. Spencer, R. C. Schoonmaker, and G. A. Somorjai, *J. Catal.* **74**, 129 (1982).
- <sup>12</sup>J. J. Vajo, W. Tsai, and W. H. Weinberg, *J. Phys. Chem.* (in press).
- <sup>13</sup>D. J. Auerbach, C. A. Becker, J. P. Cowin, and L. Wharton, *Rev. Sci. Instrum.* **49**, 1518 (1978).
- <sup>14</sup>J. M. Smith, *Chemical Engineering Kinetics*, 3rd ed. (McGraw-Hill, New York, 1981).
- <sup>15</sup>J. J. Carberry, *Chemical and Catalytic Reaction Engineering* (McGraw-Hill, New York, 1976).
- <sup>16</sup>D. G. Löffler and L. D. Schmidt, *J. Catal.* **41**, 440 (1976).
- <sup>17</sup>C. G. Takoudis and L. D. Schmidt, *J. Phys. Chem.* **87**, 958 (1983).
- <sup>18</sup>R. W. McCabe, *J. Catal.* **79**, 445 (1983).
- <sup>19</sup>W. L. Holstein and M. Boudart, *J. Catal.* **72**, 328 (1981).
- <sup>20</sup>O. Levenspiel, *Chemical Reaction Engineering*, 2nd ed. (Wiley, New York, 1972).
- <sup>21</sup>We estimate that the minimum detectable rate, for all pressures may be lowered by 1–2 orders of magnitude using the reactor in the batch mode.

**Appendix 2.**

Mechanistic Details of the Heterogeneous  
Decomposition of Ammonia on Platinum

[Appendix 2 consists of an article coauthored with J.J. Vajo and W.H. Weinberg, which appeared in the *Journal of Physical Chemistry* **1985**, 89, 3243.]

Reprinted from *The Journal of Physical Chemistry*, 1985, 89, 3243.  
Copyright © 1985 by the American Chemical Society and reprinted by permission of the copyright owner.

## Mechanistic Details of the Heterogeneous Decomposition of Ammonia on Platinum

J. J. Vajo, W. Tsai, and W. H. Weinberg\*

*Division of Chemistry and Chemical Engineering, California Institute of Technology,  
Pasadena, California 91125 (Received: December 26, 1984)*

Absolute reaction rates have been measured for the catalytic decomposition of  $\text{NH}_3$  and  $\text{ND}_3$  and for the  $\text{NH}_3 + \text{D}_2$  exchange reaction over a polycrystalline platinum wire at pressures between  $5 \times 10^{-7}$  and 0.5 torr and temperatures between 400 and 1200 K in a continuous flow microreactor. At relatively low pressures and/or high temperatures, a primary isotope effect was observed for the decomposition of  $\text{ND}_3$ , indicating that a surface reaction involving N-H bond cleavage is the rate-limiting step. Under these conditions, the order of the decomposition reaction is unity with respect to ammonia pressure with an apparent activation energy of 4.2 kcal/mol. As coverages increase, corresponding to relatively high pressures and/or low temperatures, the order of the decomposition reaction is zero with respect to ammonia, and the reaction rate becomes controlled by nitrogen desorption. In this case the apparent activation energy of the decomposition reaction is 22 kcal/mol. The kinetics of the  $\text{NH}_3 + \text{D}_2$  exchange reaction have been used, together with data concerning the adsorption-desorption parameters of  $\text{NH}_3$ ,  $\text{H}_2$ , and  $\text{N}_2$  as well as the reaction intermediates  $\text{NH}$  and  $\text{NH}_2$ , to develop a mechanistic model which describes the reaction rate over a wide range of experimental conditions and which includes the energetics of each intermediate step in the decomposition reaction. This model is discussed in terms of a potential energy diagram for ammonia decomposition on platinum.

### 1. Introduction

Interest in the catalytic decomposition of ammonia on transition-metal surfaces has been motivated by its relative simplicity as a heterogeneous reaction and by its relationship, via microscopic reversibility, to the synthesis of ammonia from nitrogen and hy-

drogen. Although the decomposition reaction on platinum surfaces has been examined extensively,<sup>1-7</sup> a detailed mechanism which

(1) Löffler, D. G.; Schmidt, L. D. *J. Catal.* **1976**, *41*, 440.

(2) Löffler, D. G.; Schmidt, L. D. *Surf. Sci.* **1976**, *59*, 195.

describes the reaction rate over a wide range of experimental conditions and which includes the energetics of individual reaction steps remains unformulated. Löffler and Schmidt have studied the decomposition kinetics on a platinum wire in a steady-state flow reactor with the ammonia pressure varying from 0.015 to 10.5 torr.<sup>1</sup> In the temperature range between 600 and 1700 K, they were able to fit their data accurately with a single Langmuir-Hinshelwood rate expression. However, the Langmuir-Hinshelwood rate expression provided no microscopic information concerning the individual, elementary reaction steps, and the lack of kinetic parameters for the adsorption and desorption of NH<sub>3</sub>, H<sub>2</sub>, and N<sub>2</sub> precluded a critical evaluation of particular kinetic models.

Recently, additional information has become available concerning the adsorption and desorption kinetics of NH<sub>3</sub>, H<sub>2</sub>, N<sub>2</sub>, and probable reaction intermediates (NH and NH<sub>2</sub>) on platinum surfaces. Thermal desorption mass spectrometry (TDS)<sup>3,8</sup> and electron energy loss spectroscopy<sup>9</sup> of ammonia chemisorbed on Pt(111) indicate the existence of two molecular states with desorption energies of 10–12 and 18–20 kcal/mol, respectively. The interaction of hydrogen with Pt(s)-9(111)×(111), i.e., the Pt(997) surface, has been elegantly studied by using helium beam scattering.<sup>10,11</sup> By monitoring the reduction in coherent helium scattering in the presence of disordered hydrogen adatoms, isosteric heats of adsorption of 22 and 19 kcal/mol were obtained for the step edges and the terraces, respectively. Since the activation energy for adsorption of hydrogen on platinum is known to be small,<sup>11,12</sup> at most 1 kcal/mol, the measured isosteric heats of adsorption are essentially equal to the activation energies of desorption. Moreover, "normal" values of the preexponential factor for a second-order desorption reaction of 10<sup>-3</sup>–10<sup>-2</sup> cm<sup>2</sup>/s were obtained.<sup>11</sup> The desorption of atomically adsorbed nitrogen as N<sub>2</sub> from a polycrystalline platinum ribbon has been investigated by using TDS.<sup>13</sup> Nitrogen desorption occurred with second-order kinetics, an activation energy of desorption of 19 kcal/mol, and a preexponential factor of the desorption rate coefficient of 4 × 10<sup>-8</sup> cm<sup>2</sup>/s. Both of these rate parameters were found not to vary with the fractional surface coverage of nitrogen.<sup>13</sup> The activation energy for dissociative adsorption of nitrogen on iron surfaces has been estimated to be ≤20 kcal/mol depending on surface orientation and nitrogen coverage.<sup>14</sup> Although the adsorption kinetics of N<sub>2</sub> on platinum surfaces have not been investigated directly, threshold ionization measurements have established the desorption of N<sub>2</sub><sup>\*</sup> from a platinum ribbon with 20 kcal/mol of vibrational excitation during ammonia decomposition at a pressure of 0.1–1.4 torr of ammonia and a temperature of 773–1373 K.<sup>15</sup> Laser-induced fluorescence has been used to determine an apparent activation energy of 63–69 kcal/mol for the desorption of NH radicals from a platinum wire in 0.1 torr of ammonia at 1200–1400 K.<sup>16,17</sup> The desorption of NH<sub>2</sub> radicals was not observed under similar conditions.

In the present work, we have measured absolute reaction rates for the catalytic decomposition of NH<sub>3</sub> and ND<sub>3</sub>, and for the NH<sub>3</sub>

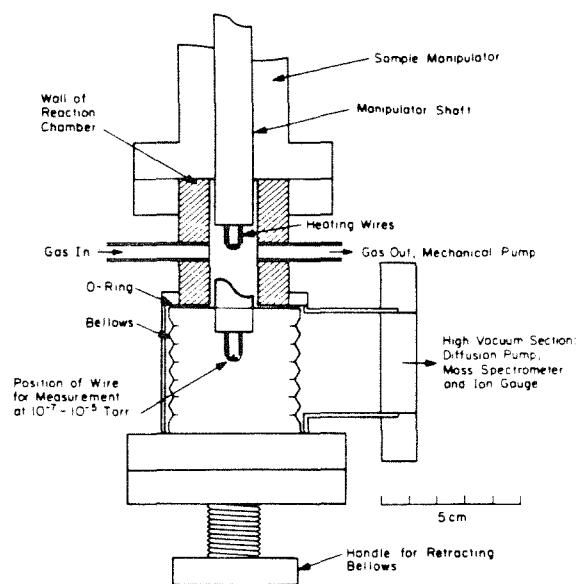


**Figure 1.** Cross section of microreactor body showing the wire in position for experiments at both  $10^{-3}$ –1 torr and  $10^{-7}$ – $10^{-5}$  torr. Ports for pressure measurement and the leak to the high vacuum section, which are orthogonal to the inlet and outlet flow ports, are not shown. The volume of the baratron and the access ports together with the shaded region is the reaction volume, 30 cm<sup>3</sup>. The sample manipulator is described in detail elsewhere.<sup>18</sup>

+ D<sub>2</sub> exchange reaction from 5 × 10<sup>-7</sup> to 0.5 torr in the temperature range between 400 and 1200 K. We have used these data, together with the aforementioned independently measured results, to clarify the detailed energetics of ammonia decomposition on platinum.

The organization of this paper is the following. In section 2, the experimental details are described. In section 3, the experimental data are presented. A mechanistic model is developed in section 4 and discussed in section 5. Finally, the results are summarized in section 6.

## 2. Experimental Procedures

The experiments were performed in a microreactor capable of steady-state flow and batch heterogeneous reactions on a wire, foil, or single crystal surface. A detailed description of the experimental system is reported elsewhere.<sup>18</sup> The decomposition experiments were carried out over resistively heated platinum wires in flowing ammonia over a range of  $P_{\text{NH}_3}$  from 5 × 10<sup>-7</sup> to 0.5 torr. A differentially pumped sample manipulator was used to translate and rotate the catalyst to different positions for experiments in various pressure regimes, as shown in Figure 1. Two 0.24-cm-diameter copper leads were used to support and heat the platinum, which was a 20-cm length of 0.0125-cm-diameter high purity (99.99%) polycrystalline wire wound into approximately 25 coils of 0.25-cm diameter. Temperatures were measured with a 0.0075-cm diameter W-5% Re/W-26% Re thermocouple, which was spot welded near the center of the wire.

The main chamber of the reactor, with a volume of 30 cm<sup>3</sup>, consists of a right-angle ultrahigh vacuum valve which is linked to a high vacuum section through a retractable bellows connection, as shown in Figure 1. The pressure in the reactor was measured with an MKS Baratron gauge. A capillary leak to an EAI 1200 quadrupole mass spectrometer in the high vacuum section enabled the product signal to be monitored continuously by a CP/M Z-80 based microcomputer. The base pressure of the high vacuum section, which is pumped by a liquid nitrogen trapped Varian 2-in. diffusion pump, is approximately 10<sup>-8</sup> torr.

- (3) Gland, J. L.; Kollin, E. B. *Surf. Sci.* **1981**, *104*, 478.
- (4) Guthrie, W.; Sokol, J.; Somorjai, G. A. *Surf. Sci.* **1981**, *109*, 390.
- (5) Robertson, A. J. B.; Willhoft, E. M. A. *Trans. Faraday Soc.* **1967**, *63*, 476.
- (6) Melton, C. E.; Emmett, P. H. *J. Phys. Chem.* **1964**, *68*, 3318.
- (7) Logan, S. R.; Kemball, C. *Trans. Faraday Soc.* **1960**, *56*, 144.
- (8) Gland, J. L. *Surf. Sci.* **1978**, *71*, 327.
- (9) Sexton, B. A.; Mitchel, G. E. *Surf. Sci.* **1980**, *99*, 523.
- (10) Poelsema, B.; Mechttersheimer, G.; Comsa, G. *Surf. Sci.* **1981**, *111*, 519.
- (11) Poelsema, B.; Mechttersheimer, G.; Comsa, G. *Surf. Sci.* **1981**, *111*, L728.
- (12) Christmann, K.; Ertl, G.; Pignet, T. *Surf. Sci.* **1976**, *54*, 365.
- (13) Wilf, M.; Dawson, P. T. *Surf. Sci.* **1976**, *60*, 561.
- (14) Grunze, M. In "The Chemical Physics of Solid Surfaces and Heterogeneous Catalysis"; King, D. A.; Woodruff, D. P., Eds.; Elsevier: Amsterdam, 1982, Vol. 4, p 150.
- (15) Foner, S. N.; Hudson, R. L. *J. Chem. Phys.* **1984**, *80*, 518.
- (16) Selwyn, G. S.; Lin, M. C. *Chem. Phys.* **1982**, *67*, 213.
- (17) Selwyn, G. S.; Fujimoto, G. T.; Lin, M. C. *J. Phys. Chem.* **1982**, *86*, 760.

- (18) Vajo, J. J.; Tsai, W.; Weinberg, W. H. *Rev. Sci. Instrum.*, in press.

## Decomposition of Ammonia on Platinum

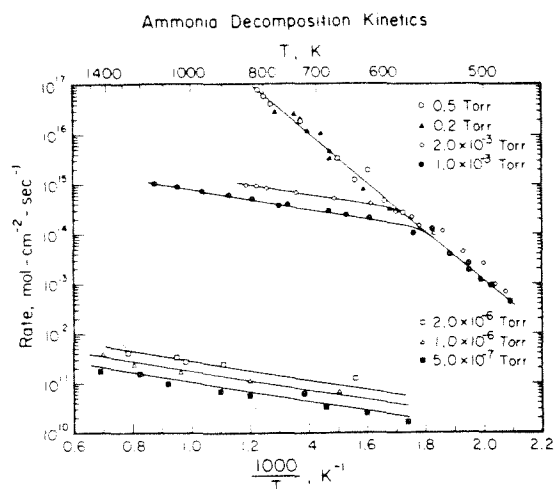


Figure 2. Arrhenius plots of the rate of ammonia decomposition on platinum for ammonia pressures of 0.5, 0.2,  $2 \times 10^{-3}$ ,  $1 \times 10^{-3}$ ,  $2 \times 10^{-6}$ ,  $1 \times 10^{-6}$ , and  $5 \times 10^{-7}$  torr. Lines have been drawn through the data points as a visual aid.

By manipulating the position of the wire, the flow rate of the gases, and the pumping speed, experiments were carried out at either  $10^{-3}$ –1 torr or  $10^{-7}$ – $10^{-5}$  torr. The flow rate could be varied from 0.1 to 100  $\text{cm}^3/\text{s}$  by adjusting the calibrated inlet and outlet valves. Mean residence times in the reactor under these conditions were adjustable between 0.1 and 10 s. Steady-state conversions were determined by monitoring the  $\text{N}_2$  signal with the mass spectrometer. The mass spectrometer was calibrated by flowing stoichiometric mixtures of  $\text{NH}_3$ ,  $\text{H}_2$ , and  $\text{N}_2$ , which corresponded to between 1% and 10% conversion, through the reactor over a room temperature platinum wire and monitoring the  $m/e$  28 signal with a total pressure of approximately  $10^{-6}$  torr in the vacuum chamber.

Reaction rates were calculated under steady-state conditions at conversions below 10% with the continuous stirred tank reactor (CSTR) equation<sup>19</sup>

$$R = (V/\tau k T_g)(P_{\text{NH}_3,i} - P_{\text{NH}_3,f}) \quad (1)$$

where  $R$  is the reaction rate (molecules/ $\text{cm}^2 \text{s}$ ),  $V$  is the reactor volume,  $\tau$  is the average residence time,  $k$  is the Boltzmann constant,  $T_g$  is the gas temperature, and  $P_{\text{NH}_3,i}$  and  $P_{\text{NH}_3,f}$  are the partial pressures of ammonia in the reactor associated with the feed and with the steady-state reaction mixture, respectively. The assumption of a CSTR model for the reactor was examined by a series of step-response experiments which indicated that the residence time distribution in the reactor was indeed approximated well by a CSTR.<sup>18</sup>

The ammonia used in this investigation was 99.99% anhydrous grade from Matheson and was purified further by freeze-thaw cycles in a dry ice/acetone bath. The deuterated ammonia was 99 atom % deuterium from Merck and was used without further purification.

Prior to the decomposition experiments, the platinum wire was heated in  $10^{-7}$ –0.1 torr of oxygen (99.99%) at 1100 K for 4 h and then reduced in  $10^{-7}$ –0.1 torr of hydrogen (99.99%) under the same conditions. (The actual pressures corresponded to the pressures at which the decomposition of ammonia was carried out subsequently.) This treatment led to reproducible decomposition rates of ammonia.

### 3. Experimental Results

3.1. *Decomposition of Pure  $\text{NH}_3$* . Absolute rates for the decomposition of ammonia are shown in Figure 2 as a function

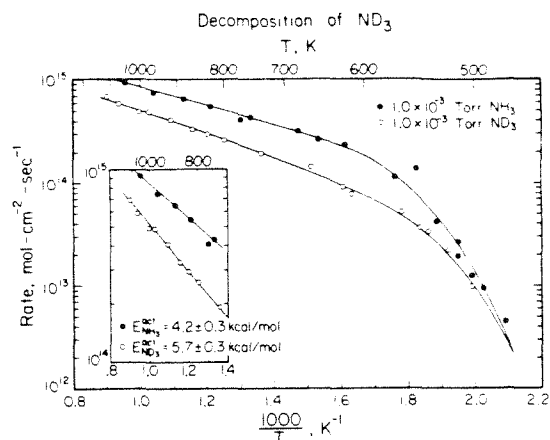


Figure 3. Comparison of the rate of decomposition of  $\text{ND}_3$  and  $\text{NH}_3$ , both at  $1 \times 10^{-3}$  torr. The inset shows the high-temperature region with an expanded scale illustrating the difference in activation energy for decomposition of  $\text{ND}_3$  and  $\text{NH}_3$ . Lines have been drawn through the data points for clarity.

of reciprocal temperature for ammonia pressures between 0.5 and  $5 \times 10^{-7}$  torr. At lower temperatures and higher pressures, the reaction rate becomes independent of ammonia pressure. For example, below approximately 550 K the decomposition rates at pressures of 0.5 and 10<sup>-3</sup> torr converge to a unique value, dependent only on the temperature, although the pressures differ by a factor of 500. Under these conditions the apparent activation energy is  $22 \pm 2$  kcal/mol, with an extrapolated intercept at  $1/T = 0$  of  $(6.4 \pm 5) \times 10^{22}$  molecules/ $\text{cm}^2 \text{s}$ .

At higher temperatures and lower pressures, the data show a transition from a zero order to a first-order dependence of the rate on ammonia pressure. This transition is seen explicitly in Figure 2 for decomposition at  $10^{-3}$  and  $2 \times 10^{-3}$  torr. At higher and lower pressures only the zero-order and first-order kinetics are observed, respectively. When the data for the three lowest pressures shown in Figure 2 are used, the order with respect to ammonia pressure is  $0.9 \pm 0.05$ . Concurrent with the increased dependence of the rate on ammonia pressure, the apparent activation energy decreases from 22 kcal/mol to a high temperature limit of  $4.2 \pm 0.3$  kcal/mol. The intercept at  $1/T = 0$  for the high temperature rate is dependent on the pressure. Assuming a first-order dependence and normalizing with respect to ammonia pressure yields a value for the intercept of  $(1.4 \pm 0.2) \times 10^{18}$  molecules/ $\text{cm}^2 \text{s torr}$ . The activation energies and orders of reaction with respect to ammonia pressure agree well with earlier results of Löffler and Schmidt,<sup>1</sup> although our absolute rates are a factor of 2–5 lower.

3.2. *Decomposition of Pure  $\text{ND}_3$* . Figure 3 shows the rate of decomposition of deuterated ammonia  $\text{ND}_3$ , together with the data for  $\text{NH}_3$ , both at  $10^{-3}$  torr. At low temperatures the rates converge, and the kinetics for  $\text{ND}_3$  decomposition appear almost identical with those for  $\text{NH}_3$ . However, at higher temperatures, as shown in the inset to Figure 3, the activation energy for decomposition of  $\text{ND}_3$  is  $5.7 \pm 0.3$  kcal/mol compared to  $4.2 \pm 0.3$  kcal/mol for  $\text{NH}_3$ . This difference in the activation energies is indicative of a primary isotope effect. A simple calculation assuming a vibrational frequency of  $3400 \text{ cm}^{-1}$  for the N–H bond predicts an increased activation energy of 1.3 kcal/mol. These results imply that, in the high-temperature (low activation energy) regime, a surface reaction involving the cleavage of at least one N–H bond is the rate-limiting step. Moreover, in regimes where the activation energy approaches 22 kcal/mol, the rate-limiting step apparently does not involve N–H bond cleavage.

3.3. *Isotope Exchange Reactions between  $\text{NH}_3$  and Deuterium*. The results of isotopic exchange experiments, performed to investigate reactions of possible surface intermediates (for example,  $\text{NH}_2$  and  $\text{NH}$  species, and N adatoms), are shown in Figure 4

(19) Smith, J. M. "Chemical Engineering Kinetics", 3rd ed.; McGraw-Hill: New York, 1981.

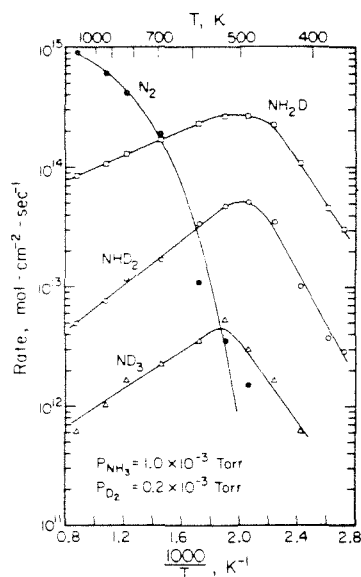


**Figure 4.** Rates of production of the products of the  $\text{NH}_3 + \text{D}_2$  exchange reaction as a function of reciprocal temperature at a partial pressure ratio of  $\text{NH}_3$  to  $\text{D}_2$  of 5. Lines have been drawn through the data points for clarity.

for a partial pressure ratio of ammonia to deuterium of 5:1 with a total pressure of  $1.2 \times 10^{-3}$  torr. Each of the three possible exchange products  $\text{NH}_2\text{D}$ ,  $\text{NHD}_2$ , and  $\text{ND}_3$  is observed. The ratio of the rates, calculated at the temperature corresponding to the maximum value of the rates, is 1.00:0.17:0.02 for  $\text{NH}_2\text{D}$ ,  $\text{NHD}_2$ , and  $\text{ND}_3$ , respectively. The values of the absolute rates are approximate; they have been determined relative to the absolute rate of nitrogen production by comparing the mass spectrometer sensitivity for nitrogen and  $\text{NH}_3$  and then using that value for the deuterated ammonia products. Hence the reaction rate for each of the exchange products was obtained by monitoring the parent ion peak intensity. On the basis of the measured fragmentation pattern of  $\text{NH}_3$ , the intensity of mass 18 was corrected for contributions due to cracking fragments of  $\text{ND}_3$  and  $\text{NHD}_2$ . At high temperatures the apparent activation energy, determined by using a least-squares analysis, for production of  $\text{NH}_2\text{D}$  is  $-2.3 \pm 0.1$  kcal/mol, while for  $\text{NHD}_2$  and  $\text{ND}_3$  the values are  $-4.4 \pm 0.3$  and  $-4.1 \pm 0.4$  kcal/mol, respectively. At lower temperatures the rate of production of all three species changes in a similar manner, and the apparent activation energies become  $8.4 \pm 0.4$ ,  $10.6 \pm 0.6$  and  $8.7 \pm 0.6$  kcal/mol for  $\text{NH}_2\text{D}$ ,  $\text{NHD}_2$ , and  $\text{ND}_3$ , respectively. The rate of ammonia decomposition, as determined from the rate of production of nitrogen, during the exchange reaction is also shown in Figure 4.

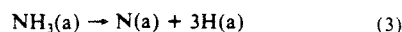
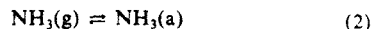
Similar experiments were conducted at partial pressure ratios of ammonia to deuterium of 2:1 and 1:1 with total pressures of  $1.5 \times 10^{-3}$  and  $2 \times 10^{-3}$  torr, respectively. The activation energies and position of the rate maxima are similar to those shown in Figure 4. The ratios of the rates, relative to  $\text{NH}_2\text{D}$ , were 1.00:0.28:0.04 and 1.00:0.50:0.07 for  $\text{NH}_2\text{D}$ ,  $\text{NHD}_2$ , and  $\text{ND}_3$  at pressure ratios of 2:1 and 1:1, respectively.

Steady-state rates for the decomposition of pure ammonia were, in all cases, achieved in a few seconds. In contrast, much longer times, often 5–10 min, were required for the exchange reactions. This observation may imply that ammonia and deuterium compete for the same adsorption sites on the platinum surface.<sup>20</sup>

#### 4. Mechanistic Modeling

**4.1. Simple Model for Decomposition of Pure  $\text{NH}_3$ .** The similarity between the apparent activation energy of 22 kcal/mol

determined at low temperatures and the nitrogen desorption energy of 19 kcal/mol,<sup>13</sup> together with the absence of an isotope effect at low temperatures, suggests that the rate-limiting step in the low-temperature, zero-order kinetic regime is the desorption of nitrogen. On the basis of this tenet, the decomposition reaction can be written mechanistically as



The decomposition rate of ammonia is given by

$$R_{\text{NH}_3} = 2k_{\text{d,N}_2}^0(n_s\theta_{\text{N}})^2 \exp(-E_{\text{d,N}_2}/kT) \quad (6)$$

where  $k_{\text{d,N}_2}^0$  and  $E_{\text{d,N}_2}$  are the preexponential factor and the activation energy of the desorption rate coefficient of nitrogen, respectively;  $n_s$  is the number of surface sites per  $\text{cm}^2$ , and  $\theta_{\text{N}}$  is the fractional surface coverage of nitrogen. This mechanism is expected to be valid far from overall equilibrium, under conditions where readsorption of hydrogen and nitrogen and the hydrogenation of surface nitrogen (the reverse of eq 3) can be neglected. The low conversion, <10%, maintained in our experiments satisfy these criteria.

To calculate reaction rates based on this mechanism, the following material balances for adsorbed ammonia and nitrogen were used

$$\begin{aligned} n_s(d\theta_{\text{NH}_3}/dt) &= (1 - \theta_{\text{N}} - \theta_{\text{NH}_3})S_{\text{NH}_3}^0F_{\text{NH}_3} - \\ &k_{\text{d,NH}_3}^0n_s\theta_{\text{NH}_3} \exp(-E_{\text{d,NH}_3}/kT) - k^0\theta_{\text{NH}_3}n_s \exp(-E_r/kT) = 0 \end{aligned} \quad (7)$$

$$\begin{aligned} n_s(d\theta_{\text{N}}/dt) &= \\ &-2k_{\text{d,N}_2}^0(n_s\theta_{\text{N}})^2 \exp(-E_{\text{d,N}_2}/kT) + k^0n_s\theta_{\text{NH}_3} \exp(-E_r/kT) = 0 \end{aligned} \quad (8)$$

where  $S_{\text{NH}_3}^0$  is the zero coverage limit for the adsorption probability of ammonia;  $F_{\text{NH}_3}$  is the molecular flux of ammonia to the surface; and  $k_{\text{d,NH}_3}^0$ ,  $k^0$ ,  $E_{\text{d,NH}_3}$ , and  $E_r$  are preexponential factors and activation energies for ammonia desorption and surface reaction rate coefficients, respectively. In these calculations we have employed the following assumptions: (1) the adsorption of ammonia is governed by first-order Langmuir kinetics; (2) the preexponential factors and activation energies are independent of coverage; and (3) the steady-state hydrogen coverage is small. The assumption of first-order Langmuir kinetics is valid when the lifetime of any precursor state to adsorption is short compared to the time characteristic of significant surface diffusion. For the high temperatures, greater than 500 K, where ammonia decomposition occurs, we expect this condition to be fulfilled. For example, if the binding energy of the  $\text{NH}_3$  precursor is on the order of 2 kcal/mol, then the surface residence time at 500 K implies a diffusion distance of only approximately 4 Å. The validity of the other two assumptions is discussed below.

Note that the steady states given in eq 7 and 8 are exact, since the data were obtained under steady-state flow conditions. When the values given in Table I are used, the calculated decomposition rates are in excellent agreement with the experimental values, as shown in Figure 5a–c. Although the desorption energy for nitrogen determined using TDS is 19 kcal/mol, to reproduce the observed activation energy at low temperatures it was necessary for  $E_{\text{d,N}_2}$  to be 22 kcal/mol. The kinetics observed at high temperatures were described accurately only when  $E_r$  and  $k^0$  were 16 kcal/mol and  $1.5 \times 10^{12} \text{ s}^{-1}$ , respectively. Thus, employing independently determined values for desorption of ammonia and nitrogen results in only two adjustable parameters. The systematic deviation of the model predictions from the experimental data for ammonia pressures of  $5 \times 10^{-7}$ ,  $1 \times 10^{-6}$ , and  $2 \times 10^{-6}$  torr is accounted for at least partially by the difficulty in calibrating the reactor for absolute rates at these low pressures. The agreement between the experimental data and the model calculation is obviously very good indeed.

(20) Klein, R. L.; Schmidt, L. D. *J. Chem. Phys.* **1982**, *76*, 3823.

## Decomposition of Ammonia on Platinum

TABLE I: Model Parameters for the Decomposition and Isotope Exchange Reactions of Ammonia on Platinum

parameter	value	ref	
$k_{d,NH_3}^0$	ammonia desorption preexponential	$1 \times 10^{14} \text{ s}^{-1}$	3, 8
$E_{d,NH_3}$	ammonia desorption energy	12 kcal/mol	3, 8
$S_{NH_3}^0$	ammonia probability of adsorption	1	3, 8
$k_{d,N_2}^0$	nitrogen desorption preexponential	$4 \times 10^{-8} \text{ cm}^2 \text{ s}^{-1}$	13
$E_{d,N_2}$	nitrogen desorption energy	22 kcal/mol	13
$k_{d,H_2}^0, k_{d,D_2}^0$	hydrogen desorption preexponential	$0.01 \text{ cm}^2 \text{ s}^{-1}$	10, 11
$E_{d,H_2}, E_{d,D_2}$	hydrogen desorption energy	19 kcal/mol	10, 11
$S_{D_2}^0$	deuterium probability of adsorption	0.1	10, 11
$k_r^0, k_1^0, k_2^0$	surface reaction preexponentials	$1.5 \times 10^{12} \text{ s}^{-1}$	
$E_r, E_1$	surface reaction activation energies	16 kcal/mol	
$E_{r,ND_3}$	surface reaction energy for $ND_3$	17.2 kcal/mol	
$k_{-2}^0$	hydrogenation reaction preexponential	$3 \times 10^{-17} \text{ cm}^4 \text{ s}^{-1}$	
$E_{-2}$	surface hydrogenation activation energy	28 kcal/mol	
$k_{-1}^0$	exchange reaction preexponential	$0.05 \text{ cm}^2 \text{ s}^{-1}$	
$E_{eff}$	$E_2 - E_{-1}$	4 kcal/mol	
$n_s$	surface atom density	$1 \times 10^{15} \text{ cm}^{-2}$	

The mechanism given by eq 2-5 describes successfully the transition from the zero-order, high activation energy regime to the first-order, low activation energy regime. Consideration of the high- and low-temperature limits of eq 6-8 will elucidate the origins of this transition. Analysis of the model indicates that when the activation energy is  $\geq 15$  kcal/mol,  $\theta_N > 0.9$ . Consequently, in this (low-temperature) case the surface is almost saturated with nitrogen. If we set  $\theta_N$  to unity, eq 6 becomes

$$R_{NH_3} = 2k_{d,N_2}^0 n_s^2 \exp(-E_{d,N_2}/kT) \quad (9)$$

and the rate is independent of ammonia pressure. In addition, from eq 9  $k_{d,N_2}^0$ , calculated from the extrapolated intercept at  $1/T = 0$  of  $(6.4 \pm 5) \times 10^{22}$  molecules/( $\text{cm}^2 \text{ s}$ ), is  $(3.2 \pm 2.5) \times 10^{-8} \text{ cm}^2/\text{s}$ . The remarkable agreement of this value with the value of  $4 \times 10^{-8} \text{ cm}^2/\text{s}$ , determined by TDS,<sup>13</sup> substantiates further the fact that the desorption of nitrogen controls the rate of reaction at low temperatures.

For high temperatures and/or low ammonia pressures, eq 6-8 may be simplified, by assuming that  $\theta_N$  and  $\theta_{NH_3}$  are small, and combined to give the rate expression

$$R_{NH_3} = \frac{k_r^0 S_{NH_3}^0 F_{NH_3} \exp(-E_r/kT)}{k_{d,NH_3}^0 \exp(-E_{d,NH_3}/kT) + k_r^0 \exp(-E_r/kT)} \quad (10)$$

from which the first-order dependence on ammonia pressure (flux) is established. Utilizing the values in Table I, we see that  $k_{d,NH_3}^0 \exp(-E_{d,NH_3}/kT) \gg k_r^0 \exp(-E_r/kT)$ . Thus, the apparent activation energy at high temperatures is given by  $E_r - E_{d,NH_3}$ . This expression illustrates clearly the origin of the isotope effect observed at high temperatures. Since the nonelementary surface reaction step, eq 3, involves dissociation of three N-H bonds, the activation energy for this step,  $E_r$ , should show an isotope effect. This is exactly what is observed. In order to model the data for  $ND_3$  accurately, it is necessary that  $E_{r,ND_3} = 17.2$  kcal/mol compared with 16 kcal/mol for  $NH_3$ . This increase of 1.2 kcal/mol compares well with the experimentally observed increase of 1.5 kcal/mol and with the theoretically predicted value of 1.3 kcal/mol; these three results are identical within experimental uncertainty.

Combining eq 7 with the relationship  $k_{d,NH_3}^0 \exp(-E_{d,NH_3}/kT) \gg k_r^0 \exp(-E_r/kT)$  implies almost a complete adsorption-desorption equilibrium for ammonia. Thus, only a fraction, approximately  $10^{-3}$  at 1000 K, of the adsorbed ammonia reacts; the

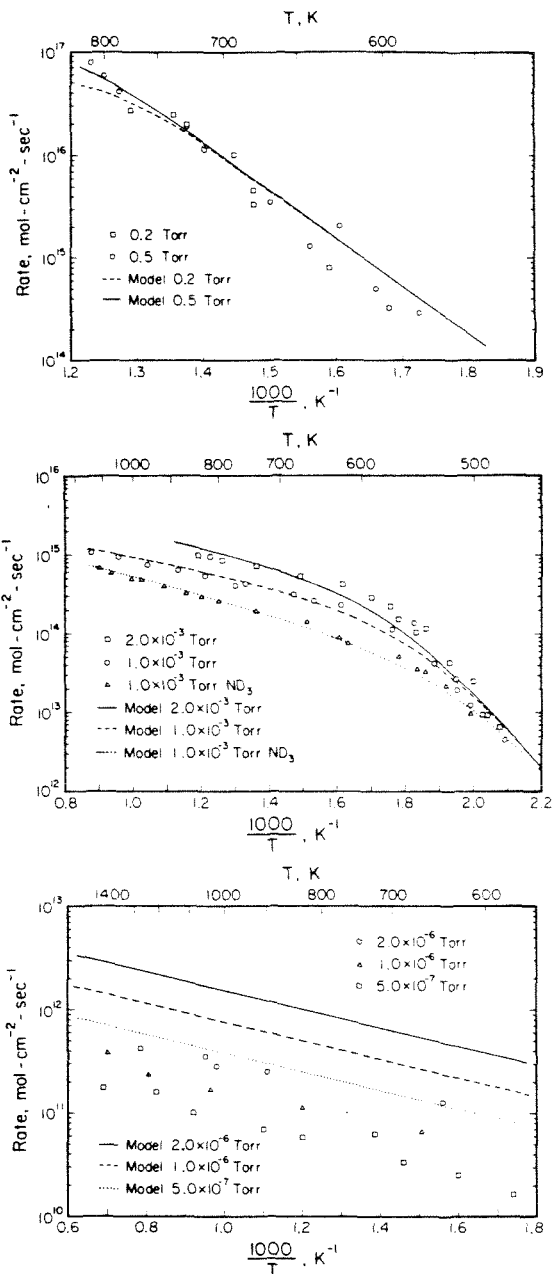


Figure 5. Comparison of calculations based on the mechanistic model described in the text with the experimental data for ammonia decomposition: (a) 0.5 and 0.2 torr; (b)  $2 \times 10^{-3}$ ,  $1 \times 10^{-3}$  torr, and  $1 \times 10^{-3}$  torr of  $ND_3$ ; (c)  $2 \times 10^{-6}$ ,  $1 \times 10^{-6}$ , and  $5 \times 10^{-7}$  torr.

remainder desorbs molecularly. In contrast, for ammonia decomposition on iron surfaces, it has been proposed that this equilibrium is not established.<sup>21</sup>

An analysis of the model indicates that any coverage dependence of the rate parameters describing eq 2-5, within reasonable limits, would not affect the calculated rates significantly. For low temperatures and/or high pressures, the rate is given by eq 6, where  $\theta_N$  is approximately unity. Thus, a variation of  $E_{d,N_2}$  with coverage would change the observed activation energy only slightly since

$\theta_N$  varies only slightly. Furthermore, both the observed linearity of the Arrhenius plots at low temperature and TDS results for nitrogen desorption from platinum<sup>13</sup> mitigate against any significant variation of  $E_{d,N}$  with coverage. Since the rate of ammonia decomposition under these conditions is given essentially by eq 9, the calculated decomposition rate is relatively insensitive to the rate parameters for eq 2 and 3, provided the rate of desorption and dissociation of ammonia does not become pathologically large or small, respectively. Therefore, a variation of  $E_{d,NH_3}$  and/or  $E_r$  with coverage would not change the calculated rates at low temperatures and/or high pressures.

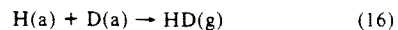
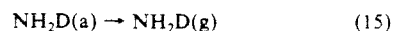
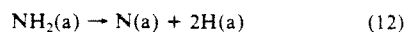
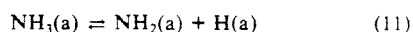
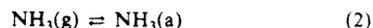
For high temperatures and/or low pressures, a similar argument may be expounded. Under these conditions the total surface coverage is small, and any changes in  $E_{d,NH_3}$  or  $E_r$  would be expected to be small. Moreover, since the rate of decomposition, which is accurately given by eq 10, is relatively insensitive to the kinetic parameters for nitrogen desorption, any variation in  $E_{d,N}$ , which occurs at these low coverages would not affect the calculated values. Thus, the assumption of coverage independent kinetic parameters is valid insofar as it does not significantly affect the model results.

**4.1.1. Comparison of Simple Model with Langmuir-Hinshelwood Rate Expression.** As mentioned previously, earlier data for ammonia decomposition under conditions similar to those of the present study were fit with a Langmuir-Hinshelwood (L-H) rate expression.<sup>1</sup> While the use of the L-H expression provides a consistent framework for discussion of a heterogeneous reaction, the inherent assumption of a chemisorption equilibrium and the lack of information pertaining to individual elementary steps can lead to various misconceptions. For example, a L-H analysis of the data for ammonia decomposition in the first-order (high-temperature) regime yields the heat of adsorption for ammonia. For ammonia decomposition on platinum, where we have seen that the equilibrium assumption is justified, the calculated value is 16.7 kcal/mol,<sup>1</sup> compared to 12–18 kcal/mol determined by TDS.<sup>3,8</sup> However, a similar analysis for ammonia decomposition on iron, where an adsorption-desorption equilibrium is believed not to exist,<sup>21</sup> leads to a value of 39 kcal/mol,<sup>22</sup> which is too large by a factor of 3 compared to direct determinations.<sup>23,24</sup> Moreover, the reaction rate coefficient in the L-H expression has been interpreted as the rate coefficient for the desorption of nitrogen.<sup>25</sup> This implies that the apparent activation energy observed at high temperature is due to the difference of the desorption energies of nitrogen and ammonia, a conclusion which is inconsistent with the isotope effect observed at high temperatures. Compared to the L-H expression, the steady-state, nonequilibrium approach adopted in the current model is able to describe both situations where chemisorption equilibrium either is or is not attained. Moreover, the high-temperature limit of the current model is consistent with the observed isotope effect.

**4.2. Kinetic Model for Isotope Exchange Reactions.** Although eq 3 represents the decomposition of adsorbed ammonia as a single kinetic step, we expect that eq 3 is actually composed of three elementary steps involving the sequential loss of hydrogen from ammonia, with  $NH_2(a)$  and  $NH(a)$  as intermediate species. Assuming that the formation of  $NH_2D$ ,  $NHD_2$ , and  $ND_3$  proceeds via the reverse of these three elementary dissociation reactions, the results of the isotope exchange reactions contain considerable information concerning the energetics of the intermediate species. It has been proposed that exchange of deuterium into ammonia on metal surfaces is a concerted reaction where N-H bond cleavage and N-D bond formation occur simultaneously.<sup>3,26</sup> On the basis of this idea, the exchange products would have evolved simply by sequential concerted reactions. In this case, the exchange kinetics would provide no information concerning the intermediate species of decomposition.

We believe, however, that the results shown in Figure 4 indicate a dissociative as opposed to a concerted reaction. Notice in Figure 4 that the energetics for production of all the exchange products are very similar. This implies that the mechanisms giving rise to the different exchange products have similar steps. These steps cannot be a series of concerted exchange reactions for the following reason. The maximum rate of production of  $NH_2D$  is approximately equal to the rate of ammonia decomposition at high temperatures. Therefore, the probability for an adsorbed molecule of ammonia to exchange is approximately equal to the probability for decomposition,  $10^{-3}$  at most. Neglecting the possibility that reaction of a singly deuterated ammonia could lead to no overall reaction, the probability for exchange of two deuterium atoms into ammonia is at most  $10^{-6}$ . Similarly, the probability for production of  $ND_3$  is  $10^{-7}$ . For this mechanism, the ratio of the rates would be  $1:10^{-3}:10^{-6}$  for  $NH_2D$ ,  $NHD_2$ , and  $ND_3$ , respectively. Since this ratio is inconsistent with the experimentally observed ratios, we favor a dissociative mechanism.

Since  $NH_2D$  is the major product of the exchange reaction, we have developed a model in which only the production of  $NH_2D$  is considered. Completely deuterated ammonia,  $ND_3$ , will be included later (in section 4.2.2) as a perturbation to the present model. Written mechanistically, the reaction steps are the following:



Assuming that the activation energies of desorption and the preexponential factors of the desorption rate coefficients for  $NH_2D$  and  $D_2$  are the same as for  $NH_3$  and  $H_2$ , respectively, the mass balance equations introduce six new parameters, namely,  $k^0_1$ ,  $k^0_2$ ,  $k^0_{-1}$ ,  $E_1$ ,  $E_2$ , and  $E_{-1}$ , which are the preexponential factors and activation energies for eq 11, 12, and 14, respectively. Furthermore, the kinetic parameters for the reverse of eq 11 are considered equal to those for eq 14, and vice versa. Consistent with the previous model, the adsorption of deuterium is assumed to be governed by second-order Langmuir kinetics, and the preexponential factors and activation energies are assumed to be independent of coverage. However, the fractional surface coverage of hydrogen is included in all calculations. The material balance equations indicate that the rates of reaction depend on  $E_2 - E_{-1}$  only and, therefore, we define an effective activation energy,  $E_{eff} \equiv E_2 - E_{-1}$ . However, the fractional surface coverage of  $NH_2$  depends on  $E_2$  and  $E_{-1}$  separately.

Rates of production of  $NH_2D$  and decomposition of  $NH_3$  (when the flux of deuterium is zero) were determined by solving iteratively the steady-state mass balance equations for  $\theta_{NH_3}$ ,  $\theta_D$ ,  $\theta_H$ , and  $\theta_N$ . To fit both the exchange data and the decomposition data for  $NH_3$ , the parameters  $k^0_1$ ,  $k^0_{-1}$ ,  $E_1$ , and  $E_{eff}$  were varied. All of the parameters used are shown in Table I. As in the case of the previous model, the values of  $k^0_1$  and  $E_{-1}$  given in Table I are required to fit the high-temperature data, while the kinetic parameters for the desorption of ammonia, nitrogen, and deuterium were obtained from direct independent measurements. The surface reaction preexponential factor  $k^0_2$  was arbitrarily, although reasonably, set equal to  $k^0_1$ . The match between the experimental results and the model predictions was less sensitive to the two remaining parameters,  $k^0_{-1}$  and  $E_{eff}$ . Their values were varied until the most accurate description of the data was obtained. Even in this (less sensitive) case, however, the permissible variation in

(22) Löffler, D. G.; Schmidt, L. D. *J. Catal.* **1976**, *44*, 244.

(23) Grunze, M.; Bozso, F.; Ertl, G.; Weiss, M. *Appl. Surf. Sci.* **1978**, *1*, 241.

(24) Weiss, M.; Ertl, G.; Nitschke, F. *Appl. Surf. Sci.* **1979**, *2*, 614.

(25) See ref 14, p 173.

(26) Kemball, C. *Proc. R. Soc., Ser. A* **1952**, *214*, 413.

## Decomposition of Ammonia on Platinum

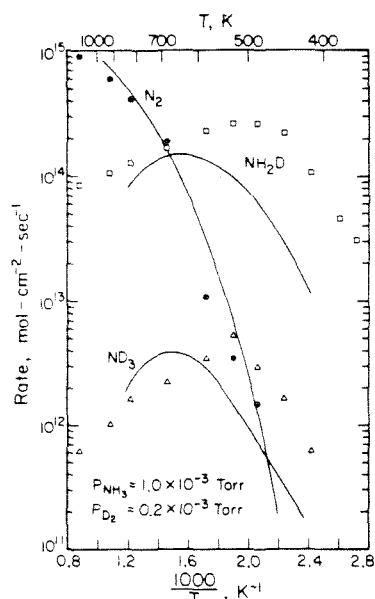


Figure 6. Comparison of model calculations with the experimental exchange data for  $N_2$ ,  $NH_2D$ , and  $ND_3$ .

$E_{\text{eff}}$  is only approximately 1 kcal/mol.

In Figure 6 both the calculated and the experimentally determined rates of  $NH_2D$  production are shown together with the rate of decomposition during the exchange reaction. Inspection of Figure 6 indicates that the energetics of the production of  $NH_2D$  are reproduced reasonably well by the model. However, the calculated rates are shifted to higher temperatures with respect to the experimental data. This shift may indicate the limitations of assuming that the preexponential factors and activation energies are constant. Indeed, a coverage-dependent activation energy and preexponential factor for the desorption of hydrogen is necessary in order to describe accurately the inhibition of the decomposition of ammonia by hydrogen. This inhibition as well as the effect of varying the rate parameters for hydrogen desorption on the calculated rate of production of  $NH_2D$  are discussed in detail elsewhere.<sup>27</sup> Also shown in Figure 6 is the rate of the decomposition of  $NH_3$  at  $1 \times 10^{-3}$  torr. Both the model predictions and the experimental data exhibit inhibition of the decomposition reaction in the presence of deuterium. Moreover, the model predicts accurately the observed inhibition. Inhibition of the decomposition of ammonia by a variety of partial pressures of deuterium and hydrogen has been investigated in detail and is reported elsewhere.<sup>27</sup>

When the mass balance equations for  $NH_2(a)$  and  $NH_2D(a)$  are used, the rate of production of  $NH_2D$  may be written as

$$R_{NH_2D} = \frac{k_{\text{eff}} k_1 \theta_{NH_3} \theta_D}{1 + k_{\text{eff}} (\theta_D + \theta_H)} \quad (17)$$

where  $k_{\text{eff}} = k_{-1}/k_2$  and  $k_1 = k_0^1 n_s \exp(-E_1/kT)$ , with similar expressions for  $k_2$  and  $k_{-1}$ . At high temperatures,  $k_{\text{eff}} (\theta_D + \theta_H) \ll 1$ , due to the low coverage of hydrogen and deuterium,  $< 10^{-3}$ . (For example,  $k_{\text{eff}} (\theta_D + \theta_H) = 0.15$  at  $T = 833$  K.) Consequently, in this limit the rate expression becomes

$$R_{NH_2D} = k_{\text{eff}} k_1 \theta_{NH_3} \theta_D \quad (18)$$

Analysis of the model results for  $\theta_{NH_3}$  and  $\theta_D$  shows that both ammonia and deuterium are within 0.1% of their respective adsorption-desorption equilibrium values. Therefore, the negative apparent activation energies observed at high temperatures result from decreasing equilibrium coverages of ammonia and deuterium

as the temperature is increased.

For low temperatures,  $1000/T > 2$ , we find that  $k_{\text{eff}} (\theta_D + \theta_H) \gg 1$  and  $\theta_D > 10 \theta_H$ . In this limit, the rate expression becomes

$$R_{NH_2D} = k_1 \theta_{NH_3} \quad (19)$$

This expression is similar to eq 10, which was derived for the decomposition reaction at high temperatures. However, in this case  $\theta_{NH_3}$  is not simply an equilibrium value since  $\theta_N$  in the ammonia mass balance, eq 7, is not negligible. On the basis of eq 19, the rate of exchange at low temperatures would be expected to show a primary isotope effect.

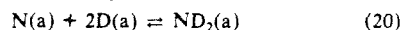
#### 4.2.1. Reduction of Exchange Model to Simple Decomposition.

By equating the flux of deuterium to zero, the above model reduces to a mechanistic model for the decomposition of pure  $NH_3$ . From the values given in Table I, the predicted rates are extremely close to those of the model discussed in section 4.1. The difference between the two models is approximately 5% at high and low temperatures, while the difference is largest, approximately 20%, at  $1000/T = 1.8$  for  $10^{-3}$  torr of ammonia.

Since hydrogen is explicitly included in the exchange model, we are able to evaluate our previous assumption of negligible hydrogen coverage. Analysis of the model indicates that the fractional coverage of hydrogen is at most 0.01. Therefore,  $\theta_H$  can safely be neglected.

In order for the exchange model to describe accurately the decomposition of pure ammonia, it was necessary to have  $E_1 = 16$  kcal/mol, which is equal to  $E_2$  of the previous model that was described in section 4.1. This agreement between  $E_1$  and  $E_2$  suggests that the isotope effect, observed at high temperatures, involves cleavage of the first N-H bond.

4.2.2. Production of  $ND_3$ . Since the fraction of adsorbed ammonia which exchanges to form  $NH_2D$  is less than  $10^{-3}$ , the same argument that mitigated against a concerted mechanism may be used to imply that consecutive dissociative exchanges would not lead to the observed rate of production of  $ND_3$ . A mechanism for the production of  $ND_3$  which involves consecutive dissociative exchanges of  $NH_2(a)$  to form  $ND_2(a)$  (subsequently  $ND_3$ ) with  $NH(a)$ ,  $NHD(a)$  and  $ND(a)$  as sequential intermediates cannot be ruled out on the basis of our experimental data. We cannot, however, assess critically this particular mechanism since imine species such as  $NH(a)$  and  $ND(a)$  have not been included in our mechanism. Therefore, we postulate that the formation of  $ND_3$  proceeds by successive deuteration of nitrogen adatoms. The complicating possibility of hydrogenation can be neglected because  $\theta_D > 10 \theta_H$ . This implies that the rate of addition of a hydrogen atom will be more than an order of magnitude lower than that for addition of a deuterium atom. Moreover, the rate of production of  $NH_2D$  exceeds that of  $ND_3$  by approximately a factor of 50. Hence the production of  $ND_3$  via deuteration of nitrogen adatoms may be treated as a perturbation on the exchange mechanism, where the calculated values of  $\theta_D$ ,  $\theta_N$ , and  $\theta_{NH_3}$  will not be affected significantly by including the mechanistic steps for the production of  $ND_3$ . The mechanism may be written as



where the (small) probability that adsorbed  $ND_3$  will decompose has been neglected. From the material balance equation for  $ND_2(a)$ , the rate may be expressed as

$$R_{ND_3} = \frac{k_{\text{eff}} k_{-2} \theta_N \theta_D^3}{1 + k_{\text{eff}} \theta_D} \quad (22)$$

where  $k_{-2} = k_0^{-2} n_s^3 \exp(-E_{-2}/kT)$  is the rate coefficient for eq 20. At high temperatures, eq 22 reduces to

$$R_{ND_3} = k_{\text{eff}} k_{-2} \theta_N \theta_D^3 \quad (23)$$

Differentiating the logarithm of  $R_{ND_3}$  with respect to  $\beta \equiv 1/kT$  yields the following expression

$$E_{-2} = -E_{\text{eff}} + \frac{\partial(\ln \theta_N)}{\partial \beta} + 3 \frac{\partial(\ln \theta_D)}{\partial \beta} - \frac{\partial(\ln R_{ND_3})}{\partial \beta} \quad (24)$$

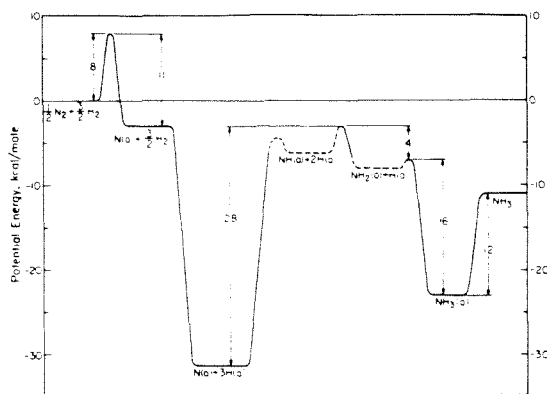


**Figure 7.** One-dimensional potential energy diagram illustrating from right to left the catalytic decomposition of  $\text{NH}_3$  over Pt where  $E_{d,\text{NH}_3} = 12$  kcal/mol,  $E_1 = 16$  kcal/mol,  $E_{\text{eff}} = E_2 - E_{-1} = 4$  kcal/mol,  $E_{-2} = 28$  kcal/mol, and  $1/2 E_{d,\text{N}_2} = 11$  kcal/mol. Note that the catalytic synthesis of  $\text{NH}_3$  from  $\text{N}_2$  and  $\text{H}_2$  is described by traversing this energy diagram from left to right. The model predicts an activation energy for adsorption of  $\text{N}_2$  molecules of 16 kcal/mol.

Using the value for  $E_{\text{eff}}$  from Table I, the experimental value for the term involving  $R_{\text{ND}_3}$ , and the model results for the terms involving  $\theta_{\text{N}}$  and  $\theta_{\text{D}}$ , we find that  $E_{-2} = 33$  kcal/mol. A similar analysis for the low-temperature data gives  $E_{-2} = 23$  kcal/mol. The difference between the high- and low-temperature values apparently suggests that  $E_{-2}$  varies with coverage. Since the activation energies have been assumed to be constant, we use an average of the high- and low-temperature values,  $E_{-2} = 28 \pm 5$  kcal/mol. Assuming the preexponential factor of the rate coefficient  $k_{-2}^0$  to be  $3 \times 10^{-17} \text{ cm}^4 \text{ s}^{-1}$  and using the values for  $\theta_{\text{N}}$  and  $\theta_{\text{D}}$  determined from the exchange model, the curve shown in Figure 6 was calculated for the production of  $\text{ND}_3$ . The agreement that is achieved between the model prediction and the experimental data is further evidence that  $\text{ND}_3$  is produced via deuteration of nitrogen adatoms.

## 5. Discussion

A one-dimensional potential energy diagram describing the decomposition (or synthesis) of ammonia on platinum is shown in Figure 7. This diagram was constructed from activation energies determined by using the kinetic models for the isotope exchange and decomposition reactions, and independently determined kinetic parameters for adsorption and desorption of nitrogen, hydrogen, and ammonia. An activation energy for desorption of ammonia of 12 kcal/mol was used for the model calculations. However, TDS indicates a second molecularly adsorbed state of ammonia with a desorption energy of 18 kcal/mol.<sup>3,8</sup> If 18 rather than 12 kcal/mol is used for the theoretical calculations, the value determined for  $E_1$  changes from 16 to 22 kcal/mol. This result indicates that the absolute level, with respect to nitrogen and hydrogen in their standard states, for the activation barrier to dissociation of the first hydrogen from ammonia is -7 kcal/mol, as shown in Figure 7, independent of  $E_{d,\text{NH}_3}$ .

Also shown in Figure 7 is  $E_{\text{eff}} = E_2 - E_{-1}$  which was found to be 4 kcal/mol. Since the calculated rates depend only on  $E_2 - E_{-1}$ , the potential energy level for  $\text{NH}_2(\text{a}) + \text{H}(\text{a})$ , which is equal to  $-E_{-1} - 7$  kcal/mol, cannot be determined from our kinetic model. This is indicated by a dashed curve in Figure 7. However, the desorption of  $\text{NH}_2$  radicals during ammonia decomposition was not detected experimentally by laser-induced fluorescence (LIF).<sup>16,17</sup> Therefore, we expect that  $E_{-1}$  is small, probably <5 kcal/mol; and consequently the fractional coverage of  $\text{NH}_2$  is small, below the (unknown) limit of detection. With a value of 44 kcal/mol for the heat of formation of  $\text{NH}_3$ ,<sup>28</sup> the potential

energy level for  $\text{NH}_2 + \text{H}(\text{a})$  is 34.5 kcal/mol. The heat of adsorption of the  $\text{NH}_2$  radical on the platinum surface is, therefore,  $E_{-1} + 41.5$  kcal/mol.

Although the rate of production of  $\text{NHD}_2$  was not analyzed in detail, the identical argument that was articulated above indicates that only the difference in energy between the barriers on each side of the  $\text{NH}(\text{a}) + 2\text{H}(\text{a})$  potential well would be obtained. The actual depth of the well cannot be determined. As mentioned previously, desorption of  $\text{NH}$  radicals during ammonia decomposition has been observed with an apparent activation energy of 63–69 kcal/mol.<sup>16</sup> To illustrate the relationship between the observed apparent activation energy and the actual activation energy for the desorption of  $\text{NH}$  radicals, consider the following argument. The rate of desorption of  $\text{NH}$  radicals may be written as

$$R_{d,\text{NH}} = k_{d,\text{NH}}^0 \theta_{\text{NH}} \exp(-E_{d,\text{NH}}/kT) \quad (25)$$

where  $k_{d,\text{NH}}^0$  and  $E_{d,\text{NH}}$  are the preexponential factor and the activation energy of the desorption rate coefficient for  $\text{NH}$  radicals. Differentiating the logarithm of  $R_{d,\text{NH}}$  with respect to  $\beta$  yields the negative of the observed activation energy

$$\frac{\partial(\ln R_{d,\text{NH}})}{\partial \beta} = \frac{\partial(\ln \theta_{\text{NH}})}{\partial \beta} - E_{d,\text{NH}} = -66 \pm 3 \text{ kcal/mol} \quad (26)$$

Thus only for the special case where  $\partial(\ln \theta_{\text{NH}})/\partial \beta = 0$  is the observed activation energy equal to the desorption energy. Since the reaction is carried out at steady state and low conversions where the reaction between  $\text{NH}(\text{a})$  and  $\text{H}(\text{a})$  to form  $\text{NH}_2(\text{a})$  can be neglected, the rate of production of  $\text{NH}(\text{a})$  is equal to the rate of decomposition of  $\text{NH}(\text{a})$ , and both these rates are equal to the rate of decomposition of ammonia. Therefore, at steady state

$$R_{\text{NH}_3} = k_{\text{NH}_3}^0 \theta_{\text{NH}} \exp(-E_{\text{NH}}/kT) \quad (27)$$

where  $k_{\text{NH}_3}^0$  and  $E_{\text{NH}}$  are the preexponential factor and the activation energy of the rate coefficient for the decomposition of  $\text{NH}(\text{a})$ . For the reaction conditions employed in the LIF study, the activation energy for the decomposition of ammonia, determined from the model described in section 4.2, is approximately 5 kcal/mol. Thus from eq 27

$$\frac{\partial(\ln R_{\text{NH}_3})}{\partial \beta} = \frac{\partial(\ln \theta_{\text{NH}})}{\partial \beta} - E_{\text{NH}} = -5 \text{ kcal/mol} \quad (28)$$

Combining eq 26 and 28, we obtain the activation energy for the desorption of  $\text{NH}$  radicals as  $61 \pm 3 + E_{\text{NH}}$  kcal/mol. To compare this value with the energy determined in the present study, we require a value for the absolute potential energy level of the barrier leading to decomposition of  $\text{NH}(\text{a})$  in order to express the desorption energy in terms of  $E_{\text{NH}}$ . Since the isotopic exchange data for the production of  $\text{NHD}_2$  have not been analyzed, this energy level may not be obtained from our kinetic model. We adopt the simplifying assumption that the  $\text{NH}(\text{a}) + 2\text{H}(\text{a})$  potential energy well is symmetrical. (Note that a more general case is shown in Figure 7.) As shown in Figure 7, the absolute potential energy level of the barrier for the hydrogenation of  $\text{NH}(\text{a})$  to  $\text{NH}_2(\text{a})$  is -3 kcal/mol. Therefore, assuming a symmetrical well, the absolute level for  $\text{NH}(\text{a}) + 2\text{H}(\text{a})$  is  $-E_{\text{NH}} - 3$  kcal/mol. Using a value of 85 kcal/mol for the heat of formation of  $\text{NH}$ ,<sup>29</sup> the potential energy level for  $\text{NH} + 2\text{H}(\text{a})$  is 66 kcal/mol, where we have used  $E_{d,\text{H}_2} = 19$  kcal/mol. Consequently, the activation energy for the desorption of  $\text{NH}$  radicals is  $69 + E_{\text{NH}}$  kcal/mol. This value agrees with the value determined via LIF within the experimental uncertainties.

The activation energy for hydrogenation of surface nitrogen,  $E_{-2} = 28$  kcal/mol, is shown also in Figure 7. Comparing this value with the activation energy for desorption of molecular nitrogen, 22 kcal/mol, shows that nitrogen desorption is favored energetically. Hydrogenation of surface nitrogen to form ammonia has been studied by Pirug and Bonzel on a polycrystalline platinum

(28) DeFrees, D. J.; Hehre, W. J.; McIver, R. T.; McDaniel, D. H. *J. Phys. Chem.* **1979**, *83*, 232.

(29) Graham, W. R. M.; Lew, H. *Can. J. Phys.* **1978**, *56*, 85.

## Decomposition of Ammonia on Platinum

foil by reaction of dissociatively adsorbed nitric oxide with hydrogen.<sup>30</sup> Although an activation energy for the hydrogenation reaction was not determined, an analysis of Pirug and Bonzel's data for the production of ammonia at a partial pressure ratio of hydrogen to nitric oxide of five (Figure 9 of ref 30) indicates almost quantitative agreement with our data for ND<sub>3</sub> production shown in Figure 4. The activation energy at high and low temperature as well as the temperature corresponding to the maximum rate are nearly identical. These results are consistent with a large energy barrier for the hydrogenation of nitrogen on platinum. Furthermore, since the ammonia produced in the NO + H<sub>2</sub> reaction necessarily results from hydrogenation of nitrogen adatoms, the agreement between the kinetics of ammonia production from NO + H<sub>2</sub> and the kinetics for ND<sub>3</sub> production from NH<sub>3</sub> + D<sub>2</sub> substantiates further the assertion that ND<sub>3</sub> results from deuteration of surface nitrogen.

Completion of the potential energy diagram using  $^{3/2}E_{d,H_2} = 28.5$  kcal/mol and  $^{1/2}E_{d,N_2} = 11$  kcal/mol results in an activation barrier for the dissociative adsorption of nitrogen of 8 kcal/mol on an atom basis or 16 kcal/mol for molecular nitrogen. The heat of adsorption of a nitrogen molecule adsorbed dissociatively on platinum is predicted to be exothermic by 6 kcal/mol. Evidently, the energetics for dissociative adsorption of nitrogen on platinum have not been examined directly. However, thermal desorption results have indicated an activated adsorption process.<sup>13,31</sup> Moreover, the probability of adsorption was observed to be independent of surface temperature over a range between 90 and 300 K.<sup>13</sup> This result indicates that in addition to being an activated process, the dissociative adsorption of nitrogen is apparently also a direct process,<sup>31</sup> in which *dissociation proceeds without prior thermal equilibration of the molecularly adsorbed species with the surface*. Direct dissociative adsorption of nitrogen on W(110) has been investigated by varying the incident translational energy of nitrogen with a helium-seeded molecular beam.<sup>32</sup> A simple analysis based on a one-dimensional potential energy barrier yielded a low coverage activation energy of 9.7 kcal/mol. Similar studies on platinum surfaces would be useful in elucidating the details of dissociative nitrogen adsorption.

Direct adsorption processes imply, through microscopic reversibility, direct desorption processes. Therefore it is energetically possible, during NH<sub>3</sub> decomposition, to desorb excited nitrogen molecules with excitation energies as large as the activation barrier for adsorption. The excitation energy may be translational and/or internal depending on the detailed shape of the potential energy surface. If only translational excitation is observed, the one-dimensional potential energy diagram shown in Figure 7 provides an adequate description of the process. If vibrational or rotational excitation is observed, the full potential energy surface must be taken into account. Vibrationally excited nitrogen with 20 kcal/mol of excess energy has been detected during ammonia decomposition on platinum.<sup>15</sup> The authors attribute this internal excitation to a recombination reaction involving adsorbed NH species. However, the observed vibrational energy may also be attributed to simple recombination of nitrogen adatoms, if the activation energy for adsorption is at least 20 kcal/mol. Considering the following argument, we believe that under the conditions where vibrational excitation was detected, the activation energy for adsorption may indeed be at least 20 kcal/mol. There are numerous examples where activation energies for adsorption increase sharply with coverage. For example, the activation energy for adsorption of nitrogen on Fe(100) has been shown to increase from an initial value of 2 to 11 kcal/mol at  $\theta_N = 0.2$ .<sup>33</sup> We

estimate that the fractional coverages of nitrogen were between 0.3 and 0.5 under conditions where vibrationally excited nitrogen was detected desorbing from platinum. Thus, postulating that the activation energy for dissociative adsorption of nitrogen has increased from an initial value of 16 to  $\geq 20$  kcal/mol is not at all unreasonable.

Observation of vibrationally excited nitrogen implies that the transition state for desorption occurs early, close to the reactants (nitrogen adatoms) on the nitrogen-platinum potential energy surface. For an accurate description of this type of adsorption/desorption process, a multidimensional potential energy surface, as opposed to a simple one-dimensional description, must be employed. Measurements of the angular dependence of the adsorption probability have cast doubt upon the validity of the one-dimensional activation barrier for dissociative nitrogen adsorption on W(110).<sup>32,34</sup> Comparing this result for adsorption on W(110) with desorption results obtained on platinum suggests that the processes on both surfaces are similar. If the transition state for desorption of nitrogen from tungsten also occurs early, the transition state for the adsorption reaction will occur late, where the adsorbing nitrogen resembles two nitrogen adatoms. Described in terms of a potential energy surface for an atom-diatom molecule collinear collision,<sup>35</sup> the hypothetical reactant particle must bend around into the product channel to reach the transition state. For nitrogen adsorption on tungsten, the incident translational energy must be converted into internal energy to bend around the potential surface and reach the transition state. Thus, the reaction probability as a function of incident translational energy does not have the simple step function form predicted by a one-dimensional model, and excitation of internal degrees of freedom near the transition state is important in surmounting the activation barrier for adsorption.

## 6. Synopsis

The results of this study may be summarized as follows:

1. For high temperatures and/or low pressures, a surface reaction involving the dissociation of the first N-H bond controls the rate of ammonia decomposition. The activation energy in this regime is  $4.2 \pm 0.3$  kcal/mol, and the rate of decomposition exhibits a primary isotope effect.
2. For low temperatures and/or high pressures, the surface is nearly saturated with nitrogen, and the rate of nitrogen desorption controls the rate of reaction. Consequently, the reaction rate is independent of ammonia pressure, and the observed activation energy,  $22 \pm 2$  kcal/mol, is equal to the activation energy for desorption of nitrogen.
3. The isotope exchange reaction, NH<sub>3</sub> + D<sub>2</sub>, produces all three exchange products. The mechanism for exchange is dissociative. In particular, reasonable agreement with the experimental data has been obtained assuming that ND<sub>3</sub> results from deuteration of surface nitrogen adatoms.
4. The kinetics of ammonia decomposition on platinum for a wide range of temperatures and pressures can be described remarkably well by coverage independent kinetic parameters.
5. The dissociative adsorption of molecular nitrogen on platinum is an activated process with an activation energy predicted to be approximately 16 kcal/mol in the limit of zero surface coverage of nitrogen adatoms.

*Acknowledgment.* We gratefully acknowledge the financial support of the Army Research Office under Grant No. DAAG29-83-K-0094, and the Central Research and Development Department of E. I. du Pont de Nemours and Company.

**Registry No.** NH<sub>3</sub>, 7664-41-7; Pt, 7440-06-4; D, 7782-39-0; H, 1333-74-0.

(30) Pirug, G.; Bonzel, H. P. *J. Catal.* **1977**, *50*, 64.

(31) For a recent review of activated adsorption, see: Morris, M. A.; Bowker, M.; King, D. A. In "Comprehensive Chemical Kinetics"; Bamford, C. H.; Tipper, C. F. H., Compton, R. G. Eds.; Elsevier: Amsterdam, 1984; Vol. 19.

(32) Lee, J.; Madix, R. J.; Schlaegel, J. E.; Auerbach, D. J. *Surf. Sci.* **1984**, *143*, 626.

(33) Bozso, F.; Ertl, G.; Grunze, M.; Weiss, M. *J. Catal.* **1977**, *49*, 18.

(34) Auerbach, D. J.; Pfnür, H. E.; Rettner, C. T.; Schlaegel, J. E.; Lee, J.; Madix, R. J. *J. Chem. Phys.* **1984**, *81*, 2515.

(35) Polanyi, J. C. *Acc. Chem. Res.* **1972**, *5*, 161.

**Appendix 3.**

The Chemisorption of Hydrogen on the (111) and (110)-(1x2)  
Surfaces of Iridium and Platinum

[Appendix 3 consists of an article coauthored with J.R. Engstrom and W.H. Weinberg.]

### Abstract

The chemisorption of hydrogen on both the Ir(111) and Pt(110)-(1x2) surfaces has been examined under ultrahigh vacuum conditions with thermal desorption mass spectrometry, LEED and contact potential difference measurements. No ordered adsorbate superstructures were observed on either surface at any fractional coverage and at surface temperatures from 100 to 700 K, and the (1x2) reconstruction of the Pt(110) surface was stable in all cases. Hydrogen adsorbs dissociatively on the Ir(111) surface, the adsorption reaction described by second-order Langmuir kinetics with an initial probability of adsorption of  $7 \times 10^{-3}$ . The rate parameters describing the second-order desorption reaction of hydrogen from the Ir(111) surface are weakly dependent on coverage between fractional coverages of 0.1 and 0.3, are given by  $E_d \simeq 12.6 \text{ kcal-mol}^{-1}$  and  $k_d^{(2)} \simeq 2 \times 10^{-6} \text{ cm}^2\text{-s}^{-1}$ . Beyond a fractional coverage of 0.3, however, both rate parameters decrease with increasing coverage. Hydrogen adsorbs dissociatively on the Pt(110)-(1x2) surface into two distinct adstates, the  $\beta_2$  and  $\beta_1$ , and the ratio of the saturation densities of these two states,  $\beta_2:\beta_1$ , is 1:2. Adsorption into the higher binding energy  $\beta_2$ -adstate is described by first-order Langmuir kinetics with an initial probability of adsorption of 0.46, whereas adsorption into the  $\beta_1$ -adstate is described by second-order Langmuir kinetics and an initial probability of adsorption of 0.022. The rate parameters describing the desorption reaction of hydrogen from the Pt(110)-(1x2) surface are *strongly* dependent on the coverage. In the coverage regime characteristic of the  $\beta_2$ -adstate ( $\theta \leq 0.32$ ) the rate parameters are approximately symmetric about one-half of saturation of this state. Specifically, from the values for the zero-coverage limit of  $E_d \simeq 18$

$\text{kcal}\cdot\text{mol}^{-1}$  and  $k_d^{(2)} \simeq 10^{-4} \text{ cm}^2\cdot\text{s}^{-1}$ , the parameters first increase to maximum values of  $E_d \simeq 26.5 \text{ kcal}\cdot\text{mol}^{-1}$  and  $k_d^{(2)} \simeq 0.3 \text{ cm}^2\cdot\text{s}^{-1}$  at  $\theta = 0.15$ , and subsequently decrease approximately to the values for the zero coverage limit at  $\theta = 0.32$ . In the coverage regime characteristic of the  $\beta_1$ -adstate ( $\theta > 0.32$ ), the activation energy decreases continuously with increasing coverage from a value of  $E_d \simeq 17 \text{ kcal}\cdot\text{mol}^{-1}$  at  $\theta = 0.35$ , whereas the preexponential factor remains essentially constant with a value of  $3 \times 10^{-4} \text{ cm}^2\cdot\text{s}^{-1}$ . The contact potential difference for hydrogen on Pt(110)-(1x2) increases continuously with coverage to a value of 0.17 eV at  $\theta = 0.30$ . As the coverage increases further, however, it decreases continuously approaching a value of -0.50 eV at saturation. Probable binding states for the  $\beta_2$ - and  $\beta_1$ -adstates on the Pt(110)-(1x2) surface are inferred from both the adsorption and desorption kinetics and the contact potential difference measurements. Comparisons of the results obtained on the (111) and (110)-(1x2) surfaces of both iridium and platinum suggest strongly that *local* surface structure (*e.g.*, "step" sites vs. terrace sites) has a profound influence on the kinetics of adsorption of hydrogen on these surfaces. Surface structure apparently also has a profound influence on the desorption kinetics of hydrogen via the mediation of adatom-adatom interactions. Whereas both attractive and repulsive interactions are clearly manifest within the  $\beta_2$ -adstates on the (110)-(1x2) surfaces, only repulsive interactions are apparent on the (111) surfaces and for the  $\beta_1$ -adstates on the (110)-(1x2) surfaces.

## I. Introduction

The study of the interaction of hydrogen with transition metal surfaces is of considerable fundamental importance. For example, hydrogen plays a central role in a multitude of technologically important catalytic reactions that occur on transition metal surfaces, such as hydrocarbon processing and Fischer-Tropsch synthesis. Other topics of technological interest include the embrittlement of materials by hydrogen and the possible use of transition metals as hydrogen storage media. Furthermore, the most reliable theoretical calculations can be carried out to describe these systems. Not surprisingly, a multitude of experimental investigations have been concerned with the chemisorption of hydrogen on various single crystalline surfaces of transition metals (1), including the Group VIII metals (2-22).

The primary thrust of the work described here is concerned with a detailed examination of the effects of surface structure on the dynamics of the elementary surface reactions that describe the adsorption and desorption of hydrogen. Previous studies have indicated that the presence of surface defects in the form of atomic steps can influence profoundly the kinetics of the adsorption and desorption reactions. For example, the initial probability of adsorption at step sites is nearly unity at surface temperatures of approximately 100 K and gas temperatures of approximately 300 K, whereas the corresponding probability on the "perfect" (111) surfaces of fcc transition metals is typically lower by an order of magnitude (2-17). Recent work on the Ni(111) surface and the considerably more corrugated Ni(110) surface indicates that the low probab-

ity of adsorption on the (111) surface can be explained by the presence of an activation barrier to dissociative adsorption, whereas adsorption on the (110) surface is essentially unactivated (16). The activation barrier on the Ni(111) surface is on the order of 2 kcal-mol<sup>-1</sup>, as judged by a continuous increase of the probability of adsorption with increasing normal translational energy of the H<sub>2</sub>. This viewpoint is supported by work examining the adsorption kinetics of hydrogen on the stepped Ni(997) surface (17). The effect of surface structure on the kinetics of the desorption reaction is manifest in a higher activation energy of desorption in the low coverage limit for hydrogen adsorbed at step sites, compared to hydrogen adsorbed at (111) terrace sites (3,9,13,15). Clearly, both the binding energy of the hydrogen adatom and the activation barrier of dissociative adsorption are influenced by the surface structure.

We present here new experimental data concerning the chemisorption of hydrogen on both the Ir(111) and the Pt(110)-(1x2) surfaces. These data are compared and contrasted both with data obtained previously in our laboratory concerning the chemisorption of hydrogen on the Ir(110)-(1x2) surface (18), and with data obtained by a number of investigators concerning the chemisorption of hydrogen on the Pt(111) surface (2-9,19-22). The comparison of the (111) and (110)-(1x2) surfaces of both iridium and platinum is motivated in part by similarities (in addition to the obvious differences) in the *local* surface structure between the two surfaces. In particular, the clean (110) surfaces of both iridium (23) and platinum (24) reconstruct to form (111) microfacets which are three atomic rows in width, and which are inclined at an angle of 109.5° with respect to one another (see Fig. 1). Consequently, the presence of structurally similar

threefold hollow adsites on each surface might be manifest in similar adsorption and desorption kinetics. However, the corrugated (110)-(1x2) surface possesses unique adsites as a consequence of its geometry (*e.g.*, high coordination "trough" sites, *cf.* site B of Fig. 1) which might influence greatly the rates of both the adsorption and desorption of hydrogen, especially at low surface coverages. For example, it has been observed that hydrogen prefers to reside in the highest coordination adsites that are available on a surface (1).

## II. Experimental Procedures

The experiments described here were performed in an ion pumped, stainless steel belljar that has been described in detail previously (25). The base pressure of the belljar is below  $5 \times 10^{-11}$  Torr of reactive gases. Facilities are available for experimental studies involving mass spectrometry, low-energy electron diffraction (LEED), contact potential difference measurements, X-ray and UV-photoelectron spectroscopies, and Auger electron spectroscopy. The Ir(111) and Pt(110) crystals were cut from single crystalline boules and were polished to within  $0.5^\circ$  of the appropriate orientations using standard metallographic techniques. The iridium (platinum) crystal was cleaned *in situ* by argon ion sputtering, heating in  $5 \times 10^{-7}$  Torr of oxygen at a temperature of 1100 K (700 K), and annealing to 1600 K (1400 K). Surface cleanliness was verified by Auger electron and X-ray photoelectron spectroscopies. Special care was taken to reduce the concentration of the silicon impurity in the platinum sample to a negligible level, since Niehus and Comsa (26) have shown that its presence is

related to the formation of a "subsurface oxide" on Pt(111).

Research grade (99.995%) hydrogen and deuterium were utilized without further purification. Deuterium was employed in a number of desorption experiments in order to increase the sensitivity (*i.e.*, the signal-to-noise ratio) of the mass spectrometric detection and to examine qualitatively the isotopic mixing of the adatoms on the surface. Exposures were effected either by backfilling the chamber or by employing a (calibrated) directional beam doser (27). The beam doser consists of a multichannel array of capillaries, and the gases are admitted to the dosing line behind this array via a separate capillary leak from a glass storage bulb. The gas pressure in the storage bulb (which determines the pressure at the doser) was monitored by a MKS Baratron gauge. A glass enclosure was installed around the ion source of the mass spectrometer for the thermal desorption mass spectrometric (TDMS) measurements (28). This glass enclosure permits the desorption products to be sampled preferentially from the front of the crystal, thus minimizing spurious signals originating from desorption from the edges of the crystal, the mounting wire leads and the manipulator.

The single crystals were spotwelded to tantalum wire leads which were mounted on a precision manipulator. Heating was effected by passing current through the wire leads/crystal circuit, while cooling was accomplished by conduction through the wire leads to support blocks that were in thermal contact with a reservoir of flowing liquid nitrogen. The temperature was measured by a W/5%Re-W/26%Re thermocouple spotwelded to the back of the crystal and referenced to an icepoint junction. Accurate temperature control was maintained by the use of an optimal control scheme, described elsewhere (29), which uti-

lizes a laboratory microcomputer as the control element. This control scheme is well-suited for the generation of linear temperature ramps that were used here in connection with the measurement of thermal desorption spectra. A wide range of heating rates can be realized, and the temporal temperature profiles are sufficiently reproducible to permit the averaging of spectra (following suitable baseline corrections) in order to increase the signal-to-noise ratio. The temperature control software has been designed both to control and to monitor the mass spectrometer, and a single routine provides data acquisition as well as control of the experiment (30).

Contact potential difference (CPD) measurements were made by employing the AC retarding potential technique of Nathan and Hopkins (31). A high-stability, low-noise and low-drift power supply (Kepco PCX 100-0.2MAT) was utilized to provide the appropriate potentials for the (LEED) electron gun (Varian 981-2125). A standard carbon battery provided the retarding bias, and a biquad band-pass filter (gain of 10, Q-factor of 100, tuned to 7 kHz) was used to condition the output from the collector (*i.e.*, the crystal). When tuned properly, noise margins were 5 mV, and the CPD measurements were reproducible to within less than 10 mV at a bandwidth of 10 Hz (beam energy  $\sim 45$  V and beam current  $\sim 0.1 \mu\text{A}$ ).

### III. Results

#### A. Hydrogen on Ir(111)

### 1. LEED Observations

Under all conditions examined, *i.e.*, at any fractional coverage and at surface temperatures as low as 100 K, no ordered adsorbate superstructures were observed, as judged by the absence of any fractional order LEED beams. This result is not surprising since ordered superstructures of hydrogen on hexagonally close-packed surfaces are rare [excluding the degenerate (1x1) overlayer, the presence of which has been inferred for hydrogen on Ru(001) (32), Pd(111) (13) and Pt(111) (33)]. A notable exception is the  $p(2 \times 2)$ -2H superstructure that has been observed for hydrogen on the Ni(111) surface (34,35). This submonolayer ( $\theta_H = 0.5$ ) superstructure might occur on Ni(111) due to the considerably smaller lattice constant characteristic of the first-row transition metals. Based solely on our (qualitative) LEED observations, we cannot rule out the possibility of an ordered (1x1) overlayer structure forming on the Ir(111) surface.

### 2. Desorption Kinetics

Thermal desorption spectra of H<sub>2</sub> from Ir(111), corresponding to ten different initial coverages that were obtained by varying the hydrogen exposure at 100 K, are shown in Fig. 2. The average heating rate  $\beta$  for each desorption spectrum was 20 K-s<sup>-1</sup> (37). Several qualitative features of the desorption kinetics are immediately apparent from Fig. 2. Consistent with the availability of only one high coordination adsite (38), the threefold hollow site, the desorption spectra exhibit one desorption feature or "state". The peak temperature is observed

to decrease continuously with increasing coverage, which is consistent with a second-order (adatom recombination) desorption reaction (39). Broadening of the desorption spectra (*i.e.*, the FWHM increases more than the maximum intensity) is clearly evident at the higher coverages corresponding to exposures above approximately 10–20 L (1L = 1 Langmuir  $\equiv 10^{-6}$  Torr-s), indicative of the presence of repulsive adatom-adatom interactions. These desorption spectra are qualitatively similar to those obtained on other hexagonally close-packed surfaces of the Group VIII metals, *e.g.*, Pt(111) (19), Rh(111) (40) and Ru(001) (41,42). However, the Ni(111) surface provides an exception, the desorption spectra from this surface “splitting” into two “states” for fractional coverages above one-half of a monolayer [*i.e.*, the coverage corresponding to an optimally ordered (2x2) superstructure] (35). Presumably, on Ni(111), the splitting of the desorption spectra and the formation of the submonolayer (2x2) superstructure are correlated.

The desorption kinetics were characterized quantitatively by employing an integral method involving variable heating rates (43). This method permits the assessment of the coverage dependence of the integral kinetic rate parameters, *i.e.*, the activation energy of desorption [ $E_d(\theta)$ ] and the (second-order) preexponential factor [ $k_d^{(2)}(\theta)$ ] of the desorption rate coefficient. The variation of the (linear) heating rate permits an evaluation of the rate of desorption [proportional to the mass spectrometric intensity for a chamber that is pumped sufficiently rapidly (39)] as a function of temperature at a *fixed coverage*, the latter of which is determined by integrating the mass spectrometric intensity versus time. Depending on the energetics of the desorption reaction and the

reproducibility of the temporal temperature profiles (which permits the averaging of spectra), varying the heating rate by 1–2 orders of magnitude is sufficient for the construction of a set of Arrhenius plots. The activation energy of the desorption reaction for a particular adsorbate coverage can be evaluated from the Arrhenius plot of the rate of desorption as a function of reciprocal surface temperature. By assuming an implicit coverage dependence (*i.e.*, order) for the desorption reaction, the preexponential factor of the desorption rate coefficient can also be evaluated as a function of adsorbate coverage. The major underlying assumption in this analysis is that the desorption reaction proceeds via a direct, one-step process, with the rate of this reaction specified completely by the surface temperature and the adsorbate concentration (44).

Arrhenius plots constructed from thermal desorption spectra of D<sub>2</sub> from Ir(111) that embodied two different fixed initial coverages and six different heating rates are shown in Fig. 3. Deuterium, which produces identical desorption spectra to those shown for hydrogen in Fig. 2, was employed to increase the sensitivity of the mass spectrometric detection (especially important at low heating rates). The heating rates were varied from 1.5 to 60 K-s<sup>-1</sup>. Two different initial coverages,  $\theta_0 = 0.15$  and  $\theta_0 = 0.47$ , were studied in order to emphasize two different coverage regimes. (An optimal signal-to-noise ratio is obtained by confining the analysis to the central part of the desorption peak, *i.e.*,  $0.2\theta_0 \leq \theta \leq 0.8\theta_0$ .) The former emphasized the low coverage limit, whereas the latter emphasized the low to moderate coverage regime. Higher coverages were not examined since contamination of the surface by background gases (primarily CO) became significant. This was due to a combination of the relatively high exposures necessary

to obtain a high coverage (exposures  $\geq 100$  L) and the low heating rates (total time for a complete spectrum  $\geq 200$  s) required by this method of analysis.

Making use of the data displayed in Fig. 3, the activation energy of desorption and the preexponential factor of the desorption rate coefficient have been evaluated as a function of coverage. These results are shown in Fig. 4. The preexponential factor was evaluated by assuming that saturation density of hydrogen is  $1.57 \times 10^{15}$  atoms-cm $^{-2}$  (the uncertainty associated with this assumption is negligible compared to other experimental uncertainties; see Sec. III.A.3) and that the desorption reaction is second-order in the fractional coverage of hydrogen adatoms.

The coverage dependence of the rate parameters is evident from an inspection of Fig. 4. For a fractional coverage below approximately 0.10, a significant variation in the rate parameters is observed—the activation energy of desorption decreases from 18 to 14 kcal-mol $^{-1}$ , whereas the preexponential factor decreases from  $1 \times 10^{-3}$  to  $1 \times 10^{-5}$  cm $^2$ -s $^{-1}$ . Between fractional coverages of approximately 0.1 and 0.3 the rate parameters are essentially independent of coverage and are given by  $E_d \simeq 12.6$  kcal-mol $^{-1}$  and  $k_d^{(2)} \simeq 2 \times 10^{-6}$  cm $^2$ -s $^{-1}$ . As the fractional coverage increases above 0.3, the rate parameters begin to decrease further. For coverages below approximately 0.1 and above approximately 0.3, a compensation effect is observed with the activation energy and preexponential factor varying in sympathy with coverage.

The strong coverage dependence of the rate parameters in the limit of low coverages is suggestive of the presence of a small concentration of defect sites at

which the binding energy of the hydrogen adatoms is *intrinsically* greater. Since the probability of adsorption at defect sites is significantly greater than that at perfect (111) sites, these defect sites will be populated preferentially at low coverages. Moreover, since hydrogen adatoms are bound more strongly at defect sites, diffusion between adsites will not act to remove this preferential population as molecules are desorbed in a TDMS experiment, *i.e.*, diffusion will act to populate defect sites as opposed to depopulating them. Thus, if defect sites are present, they will dominate the desorption kinetics at low coverages. This has been observed by Christmann and Ertl (3,45) who examined the chemisorption of hydrogen on Pt(111) and on a stepped Pt[9(111)x(111)] surface (*i.e.*, "defect site" density of 10%). Between fractional coverages of 0.2 and 0.5, both surfaces of platinum exhibited similar activation energies of desorption. However, at coverages below 0.2 the activation energy of desorption on the (111) surface remained virtually constant, whereas on the stepped 9(111)x(111) surface it increased approximately linearly to a value  $\sim 3 \text{ kcal}\cdot\text{mol}^{-1}$  greater than that observed on the (111) surface in the limit of zero coverage. Since the divergence in the kinetic parameters occurred at  $\theta = 0.2$  (*i.e.*, *not* 0.1), it is probable that there was significant mixing between (*i.e.*, recombination of) hydrogen adatoms at step sites and those at (111) terrace sites during the molecular desorption. This behavior of the kinetic parameters observed on the Pt[9(111)x(111)] surface is essentially identical to that observed here on the Ir(111) surface and suggests the presence of a small percentage of defect sites on this Ir(111) surface. Furthermore, the approximate linear decrease in the activation energy for  $\theta \leq 0.1$  on Ir(111) suggests that these defects may be step sites, as opposed to "point" defects for example. Scaling our results to those of Christmann and Ertl (3)

would suggest that this Ir(111) surface has a defect density on the order of  $\sim 5\%$ .

The decrease in the activation energy of desorption at coverages above approximately 0.3 is explained best by the occurrence of repulsive adatom-adatom interactions (presumably "through-metal") at these adsorbate concentrations. These interactions act to decrease the (average) binding energy of the hydrogen adatoms and, hence, the activation energy of desorption. The fact that these interactions appear to become significant at a fractional coverage of approximately 0.3 is of particular interest since the heat of adsorption of hydrogen on the Pt(111) surface is also essentially constant below this coverage (22). However, as the coverage increases beyond 0.3, the heat of adsorption decreases linearly. These results, for hydrogen on both Ir(111) and Pt(111) suggest that next-nearest neighbor interactions between hydrogen adatoms are relatively weak, whereas nearest neighbor interactions are repulsive on these surfaces. One can populate a hexagonally close-packed lattice [considering only one of the two inequivalent threefold hollow sites as an adsite (46)] at a fractional coverage of one-third such that no nearest neighbor adatom pairs exist. However, for fractional coverages above one-third, the adlayer must contain nearest neighbor pairs, Thus, and the occurrence of repulsive interactions between nearest neighbor hydrogen adatoms acts to decrease the (average) binding energy and, consequently, the activation energy of desorption.

The observation of a  $(\sqrt{3} \times \sqrt{3})R30^\circ$  LEED pattern near  $\theta = \frac{1}{3}$  would have lent considerable support to the above interpretation. However, no ordered hydrogen adatom superstructures have been observed on either Ir(111) or Pt(111)

(19) near a fractional coverage of one-third. This apparent discrepancy between the LEED observations and the measured energetics of desorption could be reconciled if both hcp and fcc threefold hollow sites are occupied at low (*i.e.*,  $\theta \leq \frac{1}{3}$ ) hydrogen coverages.

### 3. Adsorption Kinetics

The adsorption kinetics of hydrogen and deuterium on Ir(111) at 100 K have been characterized by integration of thermal desorption spectra such as those shown in Fig. 2. The integrated area of the mass spectrometric intensity with respect to time is proportional to the adsorbate coverage, and these data (the fractional coverage versus the exposure) represent an integrated form of the adsorption kinetics. The coverage dependence (which implies a mechanism) of the adsorption reaction can be deduced by comparing these integrated data with integrated functional forms of various assumed rate expressions, *e.g.*, Langmuir adsorption kinetics (47) and precursor-mediated adsorption kinetics (48). A quantitative assessment of the adsorption kinetics is dependent upon the assignment of an absolute coverage, which specifies the value of the initial probability of adsorption. We shall assume that the saturation density of hydrogen is equal to the metallic substrate density, *i.e.*,  $\theta_{\text{H}}^{\text{sat}} = 1$ , or  $n_{\text{b}}^{\text{sat}} = 1.57 \times 10^{15}$  atoms-cm<sup>-2</sup>. This value is reasonable when compared with values obtained under similar conditions on other hexagonally close-packed surfaces of the Group VIII metals, *e.g.*, 0.8–0.9 on Pt(111) (19,22) and  $0.85 \pm 0.15$  on Ru(001) (42). Since the measurement of the absolute initial probability of adsorption via TDMS is typically

accurate to only  $\sim 20\%$ , this additional uncertainty is of minor importance.

The relative fractional coverage is displayed as a function of exposure in Fig. 5 for (a) hydrogen and (b) deuterium. The solid lines represent the results of least-squares fits of the data to second-order Langmuir adsorption kinetics, *i.e.*, the probability of adsorption is proportional to the square of the fraction of vacant surface sites,  $(1 - \theta/\theta^{\text{sat}})^2$ . The adsorption of both hydrogen and deuterium is well represented by a second-order Langmuir model, and both exhibit, within experimental error, an identical initial probability of adsorption of  $7 \times 10^{-3}$ . This value of the initial probability of adsorption is significantly lower than values obtained on other hexagonally close-packed surfaces of the Group VIII metals, *e.g.*, 0.05 on Ni(111) (15), 0.65 on Rh(111) (40), 0.1–0.25 on Ru(001) (41,42) and 0.016–0.1 on Pt(111) (2,19,20). However it is *identical* to that found for the lower binding energy  $\beta_1$ -adstate on the Ir(110)-(1x2) surface that has been attributed to adsorption on the (111) microfacets of this reconstructed surface (18). Second-order Langmuir adsorption kinetics have been reported for hydrogen on Rh(111) (40), Ru(001) (41,42), Pt(111) (2,20) and for the  $\beta_1$ -adstate on Ir(110)-(1x2) (18). For small values of the initial probability of adsorption ( $s_0 \ll 1$ ), Kisliuk's second-order precursor model (48) reduces to  $s(\theta)/s_0 = (1 - \theta)^2/[1 + (K - 1)\theta]$ , where  $-s_0 \leq K \leq \infty$ . Thus, if the parameter  $K$  is approximately equal to unity, this second-order precursor model becomes equivalent to and experimentally indistinguishable from Langmuir adsorption kinetics. The parameter  $K$  is equal to unity if the rates of desorption and migration from the precursor state are independent of the occupation of the underlying site, *i.e.*, except for adsorption, the intrinsic and extrinsic precursor

states are equivalent. Since  $s_0$  is much less than unity in this case, we cannot rule out the possibility that the adsorption of hydrogen on Ir(111) proceeds through a weakly bound precursor state for which  $K \sim 1$ .

Consistent with the desorption kinetics discussed above, the adsorption kinetics also suggest the presence of a small fraction of defects on the Ir(111) surface studied here. These defect sites would be expected to increase the apparent probability of adsorption at low coverages. For example, Christmann and Ertl (3) have observed the initial probability of adsorption of hydrogen to increase by over a factor of three when comparing the stepped Pt[9(111)x(111)] surface ( $s_0 = 0.34$ ) to a "perfect" Pt(111) surface ( $s_0 \leq 0.1$ ), whereas above a fractional coverage of approximately 0.25, the two surfaces exhibited virtually identical (differential, *i.e.*,  $d\theta/d\epsilon$ ) adsorption kinetics. Examination of the complete data set for the adsorption of hydrogen on this Ir(111) surface reveals that the coverages observed at low exposures ( $\epsilon \leq 5$  L) are greater than those predicted from the "one-site" adsorption model. This is seen clearly for the low exposure data that are shown in Fig. 6. These data have been fit to a "two-site" adsorption model which is defined by

$$\theta = x_s \theta_s + (1 - x_s) \theta_f$$

and

$$d\theta/d\epsilon = x_s s_{0,s} (1 - \theta_s)^n + (1 - x_s) s_{0,f} (1 - \theta_f)^2,$$

where  $\epsilon \equiv 2F_{H_2}t/n_s$  is the exposure in units of atoms-site<sup>-1</sup>,  $x_s$  is the fraction of defect (*e.g.*, step) sites, and the subscripts "s" and "f" refer to "step" and "flat" (111) sites. If we assume that the defect sites exhibit behavior similar to that observed for the  $\beta_2$ -adstate on the Ir(110)-(1x2) surface (18), namely an

initial probability of adsorption of unity (*i.e.*,  $s_{0,s} = 1$ ), the data are in excellent *quantitative* agreement with the two-site adsorption model by assuming either first- or second-order Langmuir adsorption kinetics for the step sites (*i.e.*,  $n = 1$  or  $2$ ) (49). This agreement is shown explicitly in Fig. 6, where an optimum fit to the data was obtained with a fraction of defect sites of 0.025. (Note that if  $s_{0,s} = 0.5$  and  $x_s = 0.05$  are assumed, for example, the resulting fit is *considerably* worse.) The data for deuterium were not fit to the "two-site" model since the scatter in these data was greater due to a fewer number of data points for deuterium [*e.g.*, the data for hydrogen displayed in Figs. 5(a) and 6 represent the average values of a number (two to three) of separate experiments]. Due to both the quantitative nature of this analysis and the use of only one assumption (*i.e.*,  $s_{0,s} = 1$ ) a defect density of 2.5% is more reliable than the value of 5% implied by the previously discussed behavior of the desorption parameters.

In concluding, we note that a determination of the defect density in and of itself is not particularly interesting. Rather, knowledge of the relative population of defect sites is often crucial to a more complete understanding of results obtained concerning other fundamental gas-surface interactions, *e.g.*, heterogeneous catalysis. For example, the product distribution from the hydrogenolysis of *n*-butane over iridium surfaces has been found to depend sensitively on the concentration of step sites (low-coordination-number metal surface atoms) (50), whereas these same sites are apparently also necessary for the relatively facile activation of C-H bonds in saturated hydrocarbons on iridium (51).

## B. Hydrogen on Pt(110)-(1x2)

### 1. LEED Observations

As in the case of the Ir(111) surface, no ordered adsorbate superstructures were observed under any conditions examined, and the (1x2) LEED pattern representative of the clean surface was always present. These observations are in agreement with those reported previously for the adsorption of hydrogen on the structurally similar Ir(110)-(1x2) surface (18).

### 2. Desorption Kinetics

Thermal desorption spectra of D<sub>2</sub> from Pt(110)-(1x2) for nine different initial coverages are shown in Fig. 7. The linear heating rate produced by employing the digital temperature controller for each spectrum was 3.0 K-s<sup>-1</sup>. As for the Ir(111) surface, hydrogen and deuterium produce thermal desorption spectra that are identical within experimental error. Unlike the Ir(111) surface, however, two distinct desorption peaks, or "states", are clearly apparent in Fig. 7. Previous work (2,52) did not resolve these two desorption features clearly due to the high heating rates that were employed in those studies ( $\beta \geq 40$  K-s<sup>-1</sup>). The state desorbing at approximately 300 K, which we label the  $\beta_2$ -adstate [consistent with previous work on the Ir(110)-(1x2) surface (18)], saturates at low exposures (*i.e.*, a high probability of adsorption). The narrow width of the thermal desorption peaks from this  $\beta_2$ -adstate (FWHM  $\sim 30$  K; compare Fig. 7 with Fig. 2) suggests the presence of *attractive* adatom-adatom interactions (39). The state desorbing near 200 K, which we label as the  $\beta_1$ -

adstate, saturates at much larger exposures compared to the  $\beta_2$ -adstate, and the peak temperature decreases continuously with increasing coverage, indicative of second-order desorption. Broadening of the desorption peaks of the  $\beta_1$ -adstate is apparent also, quite similar to that observed on Ir(111) (*cf.* Fig. 2), and this suggests the presence of repulsive adatom-adatom interactions. The ratio of the saturation densities of the two adstates,  $\beta_2:\beta_1$ , is approximately 1:2. These thermal desorption spectra are *very* similar to those obtained on the Ir(110)-(1x2) surface (18).

Deuterium and hydrogen were adsorbed sequentially to determine the approximate extent of exchange between the two adstates. Thermal desorption spectra of  $D_2$ , HD and  $H_2$  (not corrected for differences in pumping speeds or mass spectrometric sensitivities), obtained at a heating rate of  $3.0 \text{ K}\cdot\text{s}^{-1}$  following the sequential exposures of 0.64 L of  $D_2$  and 8.5 L of  $H_2$ , are shown in Fig. 8. This exposure of  $D_2$  populates approximately 85% of the  $\beta_2$ -adstate, whereas the additional exposure of  $H_2$  fills the remainder of the  $\beta_2$ -adstate and populates approximately 35% of the  $\beta_1$ -adstate (see Fig. 11 below). Thus, the initial coverage of hydrogen adatoms and deuterium adatoms is approximately equal. There is significant exchange between the two adstates during the course of the TDMS measurements, occurring at temperatures as low as 200 K. Similar thermal desorption spectra are obtained if the exposure sequence is reversed. These results are in (qualitative) agreement with results obtained from similar isotopic exchange experiments carried out on the Ir(110)-(1x2) surface (18).

The desorption kinetics were characterized quantitatively by employing the integral method involving variable heating rates described above. In this

case, the heating rates were varied from 2 to 25 K-s<sup>-1</sup>. Three to four spectra were measured at each heating rate and summed to increase the signal-to-noise ratio. Two different initial coverages,  $\theta_0 = 0.37$  and  $\theta_0 = 0.70$ , were employed in order to examine two different coverage regimes: in this case, the  $\beta_2$ - and  $\beta_1$ -adstates. In particular, the lower initial coverage was utilized to examine fractional coverages below approximately 0.35, and the higher initial coverage was employed to examine fractional coverages between approximately 0.35 and 0.65. We note that *serious* errors could arise if the *entire* coverage range were examined by utilizing a single high initial coverage, since two distinct "states" are clearly apparent in this case. These errors would arise from the decreasing resolution of the two desorption features at high heating rates ( $\beta \gg 3$  K-s<sup>-1</sup>), as observed in previous work (2,52). Since desorption from the  $\beta_1$ -adstate is characterized by a lower activation energy (lower desorption temperature), the  $\beta_1$  peak will shift upward in temperature more than the  $\beta_2$  peak as the heating rate is increased, resulting in a mixing of the two desorption features at intermediate coverages (*i.e.*,  $0.2 \leq \theta \leq 0.45$ ). This can be avoided, at least for desorption from the  $\beta_2$ -adstate, by employing an initial coverage representative of (essentially) only the  $\beta_2$ -adstate, *i.e.*,  $\theta_0 = 0.37$ .

Making use of data from Arrhenius plots similar to those shown in Fig. 3, the activation energy of desorption and the preexponential factor of the desorption rate coefficient have been evaluated as a function of surface coverage. These results are shown in Fig. 9. The preexponential factor was evaluated by assuming that the saturation density of hydrogen is  $1.60 \times 10^{15}$  atoms-cm<sup>-2</sup> (see Sec. III.B.3) and that the desorption reaction is second-order. The rate pa-

rameters are strongly dependent on coverage for desorption from the  $\beta_2$ -adstate. In addition, a compensation effect is clearly apparent for desorption from the  $\beta_2$ -adstate, both rate parameters first increasing and then decreasing with coverage. In particular, from a zero coverage limit of approximately  $18 \text{ kcal-mol}^{-1}$ , the activation energy of desorption first increases to a value of  $26.5 \text{ kcal-mol}^{-1}$  at a fractional coverage of 0.15 and then decreases to a value of approximately  $18 \text{ kcal-mol}^{-1}$  as the coverage increases to a value of 0.32, *i.e.*, saturation of the  $\beta_2$ -adstate. Concomitantly, from a zero coverage limit of approximately  $10^{-4} \text{ cm}^2\text{-s}^{-1}$ , the preexponential factor of the desorption rate coefficient first increases to a value of  $0.3 \text{ cm}^2\text{-s}^{-1}$  and then decreases to a value of approximately  $10^{-3} \text{ cm}^2\text{-s}^{-1}$ . The approximate symmetry of the rate parameters about a fractional coverage of  $\theta \sim 0.15$  (*i.e.*, one-half of saturation of the  $\beta_2$ -adstate) is provocative.

The initial increase in the activation energy of desorption as the fractional coverage increases to a value of 0.15 is due to attractive adatom-adatom interactions at these adsorbate concentrations. The presence of attractive interactions in the adlayer was implied by the narrow width of the  $\beta_2$ -adstate desorption peak. These interactions act to increase the (average) binding energy of the hydrogen adatoms and, hence, the activation energy of desorption, since there is no activation energy of adsorption for the  $\beta_2$ -adstate (adsorption probability near unity; see Sec. III.B.3). An initial increase in the activation energy of desorption has been observed also for hydrogen on the (110) surfaces of both iridium (18) and nickel (somewhat less pronounced) (14). The fact that these attractive interactions are much more apparent on fcc (110) surfaces, compared

to fcc (111) surfaces, for example, implies that surface structural effects are important.

The (110) surfaces of fcc metals consist of close-packed rows of atoms separated by one-dimensional channels (see Fig. 1). The probable location of the low coverage  $\beta_2$ -adstate of hydrogen is the pseudo-fourfold hollow "trough" sites on the Ir(110)-(1x2) surface (18). The saturation density of the  $\beta_2$ -adstate on the Pt(110)-(1x2) surface is approximately equal to the density of these "trough" sites, *i.e.*, one hydrogen adatom per fourfold hollow site at saturation. It appears that these one-dimensional channels can mediate particularly well "through lattice" attractive adatom-adatom interactions between *next*-nearest neighbors along the [001] channel direction. From this point of view, the decrease in the activation energy of desorption between fractional coverages of approximately 0.15 and 0.30 is due to the occurrence of *repulsive* adatom-adatom interactions between *nearest* neighbors. If both attractive next-nearest neighbor and repulsive nearest neighbor interactions occur, one might expect to observe ordering in one-dimension along the [001] direction at a fractional coverage corresponding to one-half saturation of the  $\beta_2$ -adstate (*i.e.*,  $\theta = 0.15$ ). However, if the interaction *between* adjacent channels were sufficiently weak that ordering in *two*-dimensions did not occur (*i.e.*, no correlation between the one-dimensional channels), one would not expect to observe a new LEED pattern different from the clean surface (1x2) pattern. Since no new LEED patterns were observed, we can exclude *two*-dimensional ordering in the  $\beta_2$ -adstate, whereas *one*-dimensional ordering remains a distinct possibility.

The coverage dependence of the kinetic rate parameters of the  $\beta_1$ -adstate

is also apparent from an inspection of Fig. 9. The activation energy of desorption decreases approximately linearly with increasing coverage from a value of 17 kcal-mol<sup>-1</sup> at  $\theta = 0.35$  to a value of 13 kcal-mol<sup>-1</sup> at  $\theta = 0.65$ , whereas the preexponential factor maintains an essentially constant value of approximately  $3 \times 10^{-4}$  cm<sup>2</sup>-s<sup>-1</sup>. The decrease of the activation energy is again due to the occurrence of repulsive adatom-adatom interactions which act to decrease the binding energy of the hydrogen adatoms. It is important to note that desorption from the  $\beta_1$ -adstate occurs in the presence of a fully occupied  $\beta_2$ -adstate. Thus, in addition to interactions *within* the  $\beta_1$ -adstate, interactions *between* the  $\beta_1$ - and  $\beta_2$ -adstates may contribute also to the repulsive energy which leads to a decrease in the activation energy of desorption from the  $\beta_1$ -adstate.

### 3. Adsorption Kinetics

The adsorption kinetics of hydrogen and deuterium on Pt(110)-(1x2) at 120 K have been characterized by integration of thermal desorption spectra similar to those shown in Fig. 7. The fractional coverage of deuterium adatoms is displayed as a function of exposure in Fig. 10, and hydrogen exhibits identical adsorption kinetics. The absolute coverage has been assigned by comparing the integrated intensities of thermal desorption spectra corresponding to saturated overlayers at 120 K and at 170 K. The saturation density of deuterium adatoms at 170 K has been measured to be  $1.07 \pm 0.1 \times 10^{15}$  atoms-cm<sup>-2</sup> (36). We find that the saturation density at 120 K is  $1.60 \times 10^{15}$  atoms-cm<sup>-2</sup>. As may be seen in Fig. 10, the adsorption kinetics are represented by two distinct regimes

corresponding to the  $\beta_2$ - and  $\beta_1$ -adstates. Since the two adstates exhibit vastly different adsorption kinetics, they can be examined separately.

The fractional coverages, relative to each of the adstate saturation values, are displayed as a function of exposure in Fig. 11 for (a) the  $\beta_2$ - and (b) the  $\beta_1$ -adstate ( $n_s^{\text{sat}} = 0.52 \times 10^{15}$  atoms-cm $^{-2}$  for the  $\beta_2$ -adstate, and  $n_s^{\text{sat}} = 1.08 \times 10^{15}$  atoms-cm $^{-2}$  for the  $\beta_1$ -adstate).

The solid lines represent the results of least-squares fits of the data to (a) first-order and (b) second-order Langmuir adsorption kinetics. The adsorption of deuterium into the  $\beta_2$ -adstate is characterized by an initial probability of adsorption of 0.45, whereas the corresponding probability for the  $\beta_1$ -adstate is considerably smaller, 0.024. Analysis of the adsorption kinetics of hydrogen results in values for the initial probability of adsorption of 0.46 for the  $\beta_2$ -adstate and 0.022 for the  $\beta_1$ -adstate, *i.e.*, experimentally indistinguishable from deuterium.

Since the adsorption of hydrogen is dissociative, the observation of *first-order* Langmuir adsorption kinetics [ $s(\theta/\theta^{\text{sat}})/s_0 = (1 - \theta/\theta^{\text{sat}})$ ] for the  $\beta_2$ -adstate is somewhat unexpected. However, the  $\beta_2$ -adstate on the structurally similar Ir(110)-(1x2) surface exhibits first-order Langmuir adsorption kinetics (18). First-order adsorption kinetics have been reported also for hydrogen on the (111) and (100) surfaces of nickel (14). The initial probability of adsorption of 0.46 for the  $\beta_2$ -adstate compares well to both the value of 0.33 reported previously by Lu and Rye (2) for the Pt(110) surface and the value of 0.34 attributed to adsorption at step sites on the Pt[9(111)x(111)] surface (3).

As for the  $\beta_1$ -adstate on Pt(110)-(1x2), second-order Langmuir adsorption kinetics have been reported both for the  $\beta_1$ -adstate on the Ir(110)-(1x2) surface, as well as for the hexagonally close-packed surfaces of Rh (40), Ru (41,42), Pt (2,20) and Ir (this work). The value of 0.022 for the initial probability of adsorption compares well to the value of 0.016 reported by Lu and Rye for hydrogen adsorption on Pt(111) (2), supporting the proposition that, as for the Ir(110)-(1x2) surface (18), the  $\beta_1$ -adstate can be attributed to adsorption on the (111) microfacets of the reconstructed Pt(110)-(1x2) surface. Finally, as for the Ir(111) surface, second-order Langmuir adsorption kinetics, characterized by a small initial probability of adsorption, cannot be distinguished by these experiments from precursor-mediated kinetics in which the precursor state interacts weakly with the surface.

#### 4. Contact Potential Difference Measurements

Contact potential difference (CPD) measurements have been carried out in order to evaluate the work function change ( $\Delta\varphi$ ) upon adsorption of hydrogen on the Pt(110)-(1x2) surface. These measurements can provide information concerning electron transfer between the adsorbate and the substrate, *i.e.*, the dipole moment of the adsorbate-substrate complex. For the data presented here, the CPD has been measured as a function of time while the surface was exposed to a constant partial pressure of hydrogen. Since the adsorption kinetics of hydrogen on the Pt(110)-(1x2) surface are characterized by two distinct regimes, a relatively lower partial pressure was employed to examine the CPD for the  $\beta_2$ -

adstate (approximately  $2 \times 10^{-8}$  Torr), whereas a higher one was employed for the  $\beta_1$ -adstate (approximately  $5 \times 10^{-7}$  Torr). Making use of the coverage versus exposure relationships shown in Figs. 11(a) and (b), the CPD was evaluated as a function of coverage.

The CPD for hydrogen adsorbed on the Pt(110)-(1x2) surface at 120 K is shown in Fig. 12 as a function of the (total) fractional coverage. Adsorption into the  $\beta_2$ -adstate results in an increase in the CPD, reaching a maximum of 0.17 eV at a coverage of 0.3. As the coverage increases beyond 0.3, characteristic of adsorption into the  $\beta_1$ -adstate, the CPD decreases, approaching a value of -0.50 eV at saturation. For coverages below approximately 0.2 and above approximately 0.4 the CPD varies linearly with coverage, indicating that the dipole moment of the adsorbed hydrogen adatoms is constant at these concentrations (*i.e.*, depolarization effects are small). The calculated values for the dipole moments ( $\mu$ ) are +0.12 D for the  $\beta_2$ -adstate ( $\theta \leq 0.2$ ), and -0.17 D for the  $\beta_1$ -adstate ( $\theta \geq 0.4$ ), where 1 D  $\equiv$  1 esu-cm. The nonlinear variation in the CPD at the intermediate coverages between 0.2 and 0.4 is due primarily to the partial filling of the  $\beta_1$ -adstate prior to the filling of the  $\beta_2$ -adstate, and, possibly, the occurrence of depolarization effects within the  $\beta_2$ -adstate. Note that depolarization effects are absent in the  $\beta_1$ -adstate as the coverage approaches saturation.

An initial *increase* in the CPD, followed by a continuous *decrease* has been observed for hydrogen adsorbed on both the Ir(110)-(1x2) surface (18) and the stepped Pt[9(111)x(111)] surface (3). On the structurally similar Ir(110)-(1x2) surface, the CPD increases linearly to a maximum of 0.30 eV at a coverage

of 0.33 ( $\mu = +0.14$  D), corresponding to the filling of the higher binding energy  $\beta_2$ -adstate. As the lower binding energy  $\beta_1$ -adstate populates, the CPD decreases and approaches a saturation value of -0.14 eV. On Pt[9(111)x(111)], the CPD increases to a maximum of 0.02 eV at a coverage of 0.25, and then decreases continuously to a value of -0.36 eV at saturation coverage. For fractional coverages above 0.7, the CPD of this stepped platinum surface becomes indistinguishable from that obtained on the Pt(111) surface, where the CPD is observed to decrease continuously from zero coverage (19,21).

The apparent disparity in the sign of the dipole moment for the low coverage, higher binding energy states {the  $\beta_2$ -adstates on the (110)-(1x2) surfaces of Pt and Ir, and the "step sites" on Pt[9(111)x(111)]} and the lower binding energy states [the  $\beta_1$ -adstates and/or the (111) "terrace sites"] can be explained by the following arguments. Clearly, the continuous decrease in the CPD observed on Pt(111) (19,21) is due to electron donation from the hydrogen adatoms to the metal surface. Since we attribute the  $\beta_1$ -adstates to adsorption on the (111) microfacets of the (110)-(1x2) surfaces, this explanation holds also for the observed decrease in the CPD for the filling of the  $\beta_1$ -adstates. The increase in the CPD for the  $\beta_2$ -adstates can be interpreted as either (i) electron donation from the metal surface to the hydrogen adatoms, assuming the adatoms lie above the image dipole plane of the surface, or (ii) electron donation from the hydrogen adatoms to the metal surface (as for the  $\beta_1$ -adstates) with the adatoms lying *below* the image plane (*e.g.*, the pseudo-fourfold hollow "trough" sites, *cf.* Fig. 1). The latter viewpoint, the  $\beta_2$ -adstate being located in the troughs, was adopted previously to explain the CPD behavior on the Ir(110)-(1x2) surface on

the basis of adsorption-induced changes in the UV photoelectron spectra (18). We believe this interpretation is also applicable to the results obtained here on the Pt(110)-(1x2) surface {and elsewhere on the Pt[9(111)x(111)] surface (3), adsorption at the inner corner of the steps being below the image plane (54)}. Indeed, the proposition of the pseudo-fourfold hollow adsite for the  $\beta_2$ -adstate is consistent with the observation that hydrogen tends to adsorb preferentially at high coordination surface sites (1).

#### 4. Coadsorption of CO and H<sub>2</sub>

The coadsorption of hydrogen and carbon monoxide on the Pt(110)-(1x2) surface was studied in order to examine the perturbations by CO on the adsorption and desorption of hydrogen. It is of interest to review briefly the results obtained previously concerning the coadsorption of CO and H<sub>2</sub> on the structurally similar Ir(110)-(1x2) surface (55). The adsorption of hydrogen on an Ir(110)-(1x2) surface exposed previously to CO results in less hydrogen occupying the high binding energy  $\beta_2$ -adstate, and occupation of the  $\beta_1$ -adstate at a lower surface coverage of hydrogen. The post-adsorption of CO on a hydrogen precovered surface causes a preferential shift of the hydrogen from the  $\beta_2$ - to the  $\beta_1$ -adstate. In both cases, the adsorption of one-half of a monolayer of CO poisons or displaces completely all of the hydrogen chemisorbed in the  $\beta_2$ -adstate, shifting the occupancy to the  $\beta_1$ -adstate.

Thermal desorption spectra of H<sub>2</sub> from Pt(110)-(1x2), corresponding to the same initial coverage of hydrogen ( $\epsilon_{\text{H}_2} = 0.39 \text{ L}$ ,  $\theta_{\text{H}} = 0.26$ , *i.e.*, 80% of

saturation of the  $\beta_2$ -adstate) and six different subsequent exposures of CO at 120 K, are shown in Fig. 13(A) ( $\theta_{\text{CO}} = 1$  is saturation and is equal to  $0.92 \times 10^{15}$  molec-cm $^{-2}$  (53)). Since the linear heating rate was 15 K-s $^{-1}$ , the spectra are shifted to slightly higher temperatures with respect to those shown in Fig. 7 for the clean surface (where  $\beta = 3.0$  K-s $^{-1}$ ). In all cases, H $_2$  desorption was complete prior to any desorption of CO ( $T \geq 400$  K). For exposures of CO below approximately 1 L, desorption from the  $\beta_2$ -adstate is suppressed progressively with increasing CO exposures, whereas desorption between 200 and 300 K (characteristic of the  $\beta_1$ -adstate on the clean surface) increases concomitantly. For exposures above 1 L, the H $_2$  thermal desorption peak downshifts further in temperature to approximately 200 K. Integration of these thermal desorption spectra indicates that displacement of hydrogen from the surface at 120 K has not occurred for these exposures of CO. In addition, no new LEED patterns were observed for these exposure sequences for temperatures between 120 and 300 K (56). This observation, coupled with the fact that H $_2$  desorption from the  $\beta_2$ -adstate is extinguished completely at fractional coverages of CO below 0.5, indicates that (long-range) adsorbate segregation is not occurring, which, for example, does occur on the Rh(111) surface (58).

Three desorption regimes, dependent upon the CO postexposure, are apparent in Fig. 13(A). At zero postexposure, desorption is exclusively from the  $\beta_2$ -adstate. For postexposures between approximately 0.5 and 1 L, the  $\beta_2$ -adstate has been virtually extinguished, and the desorption peaks are very similar to those expected if the hydrogen adatoms were merely displaced [*i.e.*, no additional CO(a)-H(a) interactions] to the  $\beta_1$ -adstate (*cf.* Fig. 7 and  $\epsilon_{\text{D}_2} = 8$

L). For postexposures above 1 L, this " $\beta_1$ -like" adstate is suppressed, and a new "state" with a peak temperature of approximately 200 K begins to dominate the desorption spectra. If exposures below  $\sim 1$  L displace completely hydrogen adatoms to the  $\beta_1$ -adstate, it is reasonable to assume that exposures above 1 L ( $\theta_{\text{CO}} \geq 0.4$ ) may lead to repulsive interactions between the CO admolecules and the hydrogen adatoms. These interactions would explain the observed splitting and shift in the desorption peak to lower temperature.

Contact potential difference measurements were carried out to test the above hypothesis concerning the effects of coadsorbed CO on the chemisorption of hydrogen. Since the two clean surface adstates of hydrogen are characterized by dipole moments of opposite sign (*cf.* Fig. 12), displacement of adatoms from one adstate to the other should result in large changes in the CPD, whereas (non-displacing) interactions between the CO admolecules and the hydrogen adatoms may only marginally affect the CPD (assuming we can account for the CPD that is due solely to the CO). An experiment was conducted in order to measure the CPD for the exposure sequence represented by the thermal desorption spectra shown in Fig. 13(A). Specifically, the CPD was measured as a function of time while the clean Pt(110)-(1x2) surface was exposed to 0.39 L of hydrogen, followed by a constant partial pressure of CO of  $5 \times 10^{-8}$  Torr. These data are shown in Fig 13(B). The CPD for CO adsorbed on the clean surface is shown also for reference purposes. (Within experimental error, the adsorption kinetics of CO were found to be identical for the clean surface and for this precoverage of hydrogen.) From Fig. 13(B) we see that the CPD decreases precipitously upon the initial exposure of CO, decreasing to  $\sim -0.02$  eV at an exposure of 0.3 L

and to  $\sim -0.21$  eV at 1 L. Above exposures of approximately 1 L, the CPD is essentially constant at  $\sim -0.22$  eV.

These results for the CPD are entirely consistent with the above interpretation concerning the thermal desorption spectra. For exposures below approximately 1 L, the CPD decreases rapidly as the hydrogen adatoms are displaced to the  $\beta_1$ -adstate. However, for exposures above approximately 1 L, little change in the CPD is observed, consistent with the occurrence of (non-displacing) interactions between the CO admolecules and the hydrogen adatoms which lead to the observed changes in the thermal desorption spectra.

The effect of preadsorbed CO on the chemisorption of hydrogen on the Pt(110)-(1x2) surface was studied briefly. It was found that an exposure of 1.1 L of CO ( $\theta_{\text{CO}} \sim 0.4$ ) blocked completely the adsorption of H<sub>2</sub> into the  $\beta_2$ -adstate. The resulting adsorption into the  $\beta_1$ -adstate was characterized by an initial probability of adsorption of 0.016 and second-order Langmuir kinetics, *i.e.*, very similar to the clean surface on which  $s_0 = 0.022$  and second-order Langmuir kinetics applied also. The thermal desorption spectra from this CO precovered surface were found to be similar to those expected for hydrogen adatoms which were merely displaced to the  $\beta_1$ -adstate, *e.g.*, spectrum d in Fig. 13(A). Finally, adsorption of hydrogen on this CO precovered surface resulted in a continuous decrease in the CPD, consistent with preferential adsorption into the  $\beta_1$ -adstate.

In summary, the post- or preadsorption of CO on the Pt(110)-(1x2) surface poisons hydrogen adsorption into the  $\beta_2$ -adstate and shifts its occupation to the  $\beta_1$ -adstate, consistent with earlier work on the structurally similar Ir(110)-

(1x2) surface (55). At low to moderate coverages of CO ( $\theta_{\text{CO}} \leq 0.4$ ) the CO acts merely to displace the hydrogen adatoms from the  $\beta_2$ - to the  $\beta_1$ -adstate. However, at CO coverages above one-half of a monolayer, repulsive interactions between the CO admolecules and the hydrogen adatoms leads to a reduced binding energy of the hydrogen adatoms and, hence, a lower desorption temperature of hydrogen.

#### IV. Discussion

The results obtained here concerning the chemisorption of hydrogen on both the Ir(111) and Pt(110)-(1x2) surfaces have illustrated clearly the importance of surface structure and its influence on the rates of both adsorption and desorption. The initial probability of adsorption can vary by as much as two orders of magnitude when comparing the close-packed (111) and the corrugated (110)-(1x2) surfaces of both iridium and platinum. However, the adsorption kinetics characteristic of the lower binding energy  $\beta_1$ -adstates on the (110)-(1x2) surfaces are virtually identical to those observed on the corresponding (111) surfaces. The desorption kinetics are also influenced strongly by the surface structure. The (110)-(1x2) surfaces possess unique adsites as a consequence of their geometry, and these sites are related directly to the observation of an additional [with respect to the (111) surfaces] higher binding energy  $\beta_2$ -adstate. Furthermore, these (110)-(1x2) surfaces apparently mediate particularly well attractive adatom-adatom interactions between the hydrogen adatoms in this higher binding energy  $\beta_2$ -adstate. As in the case of the adsorption kinetics, the

desorption kinetics characteristic of the lower binding energy  $\beta_1$ -adstates on the (110)-(1x2) surfaces are very similar to those observed on the corresponding (111) surfaces. In the discussion that follows, we shall quantify these comparisons of the adsorption and desorption kinetics of hydrogen on the (111) and (110)-(1x2) surfaces of both iridium and platinum.

The adsorption kinetics of hydrogen on the (111) and (110)-(1x2) surfaces of both iridium and platinum are summarized in Table 1 in terms of the initial probabilities of adsorption ( $s_0$ ) and the functional dependence of the reaction on the fractional coverage  $[f(\theta)]$  (59). In all cases, the kinetics were evaluated at surface temperatures between 100 and 150 K, and for gas temperatures of approximately 300 K. The dominant role of the surface structure in determining the rate of the adsorption reaction is clearly apparent. Adsorption into the  $\beta_2$ -adstates of both iridium and platinum is characterized by near unity initial probabilities of adsorption and first-order Langmuir adsorption kinetics. These values of  $s_0$  imply that adsorption into the  $\beta_2$ -adstates is not activated.

The importance of the *local* surface structure is supported by the observation of both essentially identical values of the initial probabilities of adsorption and identical second-order Langmuir kinetics for adsorption on the (111) surfaces and into the  $\beta_1$ -adstates on the (110)-(1x2) surfaces. The striking similarity of the adsorption kinetics for these two adstates on macroscopically distinct surfaces is due to the presence of structurally similar threefold hollow adsites. This result was not totally unexpected; however, it is somewhat surprising that (111) microfacets which are only three atomic rows in width exhibit essentially identical rates of adsorption as a "perfect" (111) surface. The low values observed for

the initial probabilities of adsorption on the (111) surfaces could be explained by the presence of an activation barrier for dissociative adsorption. Previous work employing molecular beam techniques has suggested that this barrier is on the order of 0.4–1.5 kcal-mol<sup>-1</sup> on the Pt(111) surface (7,8). As discussed above, more recent work on the adsorption of hydrogen on the Ni(111) surface (16) implicates the presence of an activation barrier of approximately 2 kcal-mol<sup>-1</sup> on this structurally similar close-packed surface. In addition, in agreement with our point of view (*i.e.*, unactivated adsorption into the low-coverage  $\beta_2$ -adstates on the (110)-(1x2) surfaces), adsorption on the Ni(110) surface was found to be essentially unactivated.

The kinetic parameters which describe the desorption reaction (the activation energy of desorption and the second-order preexponential factor of the desorption rate coefficient) are displayed as a function of surface coverage in Fig. 14 for iridium and in Fig. 15 for platinum (activation energy only) (60) for both the (111) surface and the  $\beta_1$ -adstate on the (110)-(1x2) surface. The abscissae have been scaled such that the *absolute* adsorbate concentrations are equal for the two adstates on any vertical line.

For coverages above approximately 0.1, the kinetic parameters for each adstate on the iridium surfaces are given by similar values. However, in the limit of zero coverage, the kinetic parameters characteristic of this Ir(111) surface are closer to the zero coverage limit on the Ir(110)-(1x2) surface, which is characteristic of the  $\beta_2$ -adstate. This observation supports the proposition argued above that the desorption kinetics at coverages below 0.1 are dominated by the presence of defect sites (*e.g.*, step sites) participating in the desorption reaction.

Consequently, the zero coverage limit on a perfect Ir(111) surface might be expected to be characterized by the (coverage-independent) values measured here for coverages between 0.1 and 0.3, *i.e.*,  $E_d \simeq 12.6 \text{ kcal-mol}^{-1}$  and  $k_d^{(2)} \simeq 2 \times 10^{-6} \text{ cm}^2\text{-s}^{-1}$ . Note that the former is close to the value of  $\sim 13.5 \text{ kcal-mol}^{-1}$  for the zero coverage limit of the  $\beta_1$ -adstate on the Ir(110)-(1x2) surface.

For fractional coverages above approximately one-third of a monolayer, the activation energy of desorption on the Ir(111) surface begins to decrease. We believe this is due to the occurrence of repulsive adatom-adatom interactions between nearest neighbors which decrease the (average) binding energy of the hydrogen adatoms and, hence, the activation energy of desorption. However, for the  $\beta_1$ -adstate on the Ir(110)-(1x2) surface, a continuous decrease in the activation energy is observed. This result could be explained also by the occurrence of repulsive interactions between the adatoms. For example, since desorption from the  $\beta_1$ -adstate occurs in the presence of a fully occupied  $\beta_2$ -adstate, the two adstates being essentially nearest neighbors (*cf.* Fig. 1), repulsive interactions between adatoms in the  $\beta_1$ -adstate and those in the  $\beta_2$ -adstate could occur.

As may be seen in Fig. 15, on the platinum surfaces, the activation energies of desorption vary with the surface coverage in a manner similar to that observed on the iridium surfaces. For fractional coverages below 0.3, the activation energy of desorption on the Pt(111) surface is essentially independent of the coverage. In addition, although it was not investigated quantitatively, Norton *et al.* (22) found evidence for hydrogen that was more strongly bound at coverages below approximately 0.05, presumably due to defect sites. As the coverage increases beyond 0.3, the activation energy of desorption decreases due

to the occurrence of repulsive interactions between nearest neighbor hydrogen adatoms. For the  $\beta_1$ -adstate on the Pt(110)-(1x2) surface, the activation energy of desorption decreases continuously with increasing coverage, indicative of the occurrence of repulsive interactions at all adsorbate concentrations for which the  $\beta_2$ -adstate probably plays a role (*e.g.*, via a direct interaction with the  $\beta_1$ -adstate). In the limit of zero coverage the two adstates exhibit a similar activation energy of desorption of approximately 16 kcal-mol<sup>-1</sup>, emphasizing again the similarity of the two adstates.

The kinetic parameters which describe the desorption of hydrogen from the (110)-(1x2) surfaces of both iridium and platinum are displayed in Fig. 16 as a function of surface coverage. The dominant influence of the surface structure is clearly apparent. For both surfaces, the parameters vary sympathetically with surface coverage, first increasing and subsequently decreasing, in the coverage regime characteristic of the  $\beta_2$ -adstate ( $\theta \leq 0.33$ ). The activation energies of desorption for the  $\beta_1$ -adstates ( $\theta \geq 0.33$ ) decrease continuously with increasing coverage, whereas the preexponential factors remain essentially constant. The rate parameters for the Pt(110)-(1x2) surface are symmetric about a coverage equal to one-half of saturation of the  $\beta_2$ -adstate. This result has been interpreted as a manifestation of the occurrence of attractive adatom-adatom interactions between next-nearest neighbors and repulsive interactions between nearest neighbors which, in this case, are apparently of approximately equal strength. The rate parameters for the Ir(110)-(1x2) surface appear to be asymmetric in the  $\beta_2$ -adstate coverage regime. However, these results should be treated with some caution, since a single high initial coverage ( $\theta=0.8$ ) was used

to evaluate the entire coverage regime displayed in Fig. 16. It is probable that at the high heating rates (as large as  $110 \text{ K-s}^{-1}$ ) employed to evaluate the parameters, significant mixing occurred between the  $\beta_1$ - and  $\beta_2$ -adstates in the intermediate coverage regime ( $0.2 \leq \theta \leq 0.45$ ). On the other hand, a mismatch in the strength of the attractive and repulsive interactions could contribute also to the observed asymmetry. In any case, the interpretation involving attractive adatom-adatom interactions at low coverages and repulsive interactions as the  $\beta_2$ -adstate approaches saturation remains valid also for the Ir(110)-(1x2) surface.

## V. Conclusions

The major conclusions of this work examining the chemisorption of hydrogen on both the Ir(111) and the Pt(110)-(1x2) surfaces can be summarized as follows:

1. Hydrogen adsorbs dissociatively on the Ir(111) surface, the adsorption reaction described by second-order Langmuir kinetics with an initial probability of adsorption of  $7 \times 10^{-3}$ .
2. The rate parameters describing the desorption of hydrogen from the Ir(111) surface are weakly dependent on coverage between fractional coverages of 0.1 and 0.3 and are given by  $E_d \simeq 12.6 \text{ kcal-mol}^{-1}$  and  $k_d^{(2)} \simeq 2 \times 10^{-6} \text{ cm}^2\text{-s}^{-1}$ . The activation energy of desorption decreases continuously with coverage above  $\theta = 0.3$ , indicative of the occurrence of repulsive interactions between nearest neighbor hydrogen adatoms.
3. Both the variation in the desorption rate parameters at coverages below approximately 0.1 and the observation of an apparently higher probability of adsorption for this same coverage regime suggest that the Ir(111) surface examined here may contain a fraction of defect sites on the order of 2.5–5.0%.
4. Hydrogen adsorbs dissociatively on the Pt(110)-(1x2) surface into two distinct adstates which are designated as the  $\beta_2$  and  $\beta_1$ . The ratio of the saturation densities of the two adstates,  $\beta_2:\beta_1$ , is 1:2. Adsorption into the higher binding energy  $\beta_2$ -adstate is described by first-order Langmuir kinetics with an initial probability of adsorption of 0.46. Adsorption into the  $\beta_1$ -adstate is described by second-order Langmuir kinetics with an "initial" probability of adsorption of 0.022.
5. The rate parameters describing the desorption of hydrogen from the  $\beta_2$ -adstate on the Pt(110)-(1x2) surface depend strongly on the coverage. From the values for the zero coverage limit given by  $E_d \simeq 18 \text{ kcal-mol}^{-1}$  and  $k_d^{(2)} \simeq 10^{-4} \text{ cm}^2\text{-s}^{-1}$ , the rate parameters first increase to maximum values given by  $E_d \simeq 26.5$

kcal-mol<sup>-1</sup> and  $k_d^{(2)} \simeq 0.3 \text{ cm}^2\text{-s}^{-1}$  at  $\theta = 0.15$ , and subsequently decrease to approximately the values for the zero coverage limit at  $\theta = 0.32$ , *i.e.*, saturation of the  $\beta_2$ -adstate. The variation of the parameters in this coverage regime is symmetric about a coverage equal to one-half of saturation of the  $\beta_2$ -adstate, implicating the occurrence of attractive adatom-adatom interactions between next-nearest neighbors and repulsive interactions between nearest neighbor hydrogen adatoms. In the coverage regime characteristic of the  $\beta_1$ -adstate, the activation energy decreases linearly with increasing coverage from  $E_d \simeq 17 \text{ kcal-mol}^{-1}$  at  $\theta = 0.35$ , whereas the preexponential factor maintains a constant value of  $k_d^{(2)} \simeq 3 \times 10^{-4} \text{ cm}^2\text{-s}^{-1}$ .

6. Adsorption of hydrogen on the clean Pt(110)-(1x2) surface results in a continuous increase in the CPD, reaching a maximum value of 0.17 eV at a coverage of  $\theta = 0.30$ , *i.e.*, nearly saturation of the  $\beta_2$ -adstate. Adsorption into the  $\beta_1$ -adstate results in a continuous decrease in the CPD, approaching a value of -0.50 eV at saturation. The initial increase in the CPD is attributed to the  $\beta_2$ -adstate being located below the image dipole plane of the surface, in the pseudo-fourfold hollow "trough" sites.
7. The pre- or postadsorption of CO on the Pt(110)-(1x2) surface poisons hydrogen adsorption into the  $\beta_2$ -adstate, shifting preferentially its occupation to the  $\beta_1$ -adstates.
8. Surface structure has been found to have a profound influence on the kinetics of the adsorption of hydrogen. Comparisons of the results obtained on the (111) and (110)-(1x2) surfaces of both iridium and platinum suggest strongly that the *local* surface structure is the major determining factor. This viewpoint is supported by the striking similarities observed between the adsorption kinetics for the (111) surfaces and for the  $\beta_1$ -adstates on the (110)-(1x2) surfaces of both iridium and platinum, the latter adstates attributed to adsorption on the (111) microfacets of these reconstructed surfaces.

9. The desorption kinetics have also been found to be influenced profoundly by the surface structure. The (110)-(1x2) surfaces of both iridium and platinum possess unique [with respect to the (111) surfaces] psuedo-fourfold hollow ad-sites that are associated with the higher binding energy  $\beta_2$ -adstates which are not observed on the (111) surfaces. Whereas both attractive and repulsive adatom-adatom interactions within the  $\beta_2$ -adstates are mediated by the (110)-(1x2) surfaces, only repulsive interactions are apparent on the (111) surfaces and for the  $\beta_1$ -adstates on the (110)-(1x2) surfaces.

### Acknowledgement

This work was supported by the National Science Foundation under Grant No. CHE-8516615.

**References**

1. Z. Knor, in: *Catalysis: Science and Technology*, Eds. J. R. Anderson and M. Boudart, Springer-Verlag, Berlin, Vol. 3, p. 231 (1982).
2. K. E. Lu and R. R. Rye, *Surface Sci.* **45**, 677 (1974).
3. K. Christmann and G. Ertl, *Surface Sci.* **60**, 365 (1976).
4. B. E. Nieuwenhuys, *Surface Sci.* **59**, 430 (1976).
5. R. W. McCabe and L. D. Schmidt, Proc. 7<sup>th</sup> Intern. Vac. Congr. and 3<sup>rd</sup> Intern. Conf. Solid Surfaces (Vienna 1977) p. 1201.
6. D. M. Collins and W. E. Spicer, *Surface Sci.* **69**, 85 (1977); D. M. Collins and W. E. Spicer, *Surface Sci.* **69**, 114 (1977).
7. R. J. Gale, M. Salmeron and G. A. Somorjai, *Phys. Rev. Letters* **38**, 1027 (1977); M. Salmeron, R. J. Gale and G. A. Somorjai, *J. Chem. Phys.* **67**, 5324 (1977).
8. M. Salmeron, R. J. Gale and G. A. Somorjai, *J. Chem. Phys.* **70**, 2807 (1979).
9. B. Poelsma, G. Mechttersheimer and G. Comsa, *Surface Sci.* **111**, L728 (1981); B. Poelsma, G. Mechttersheimer and G. Comsa, *Surface Sci.* **111**, 519 (1981).
10. G. E. Gdowski, J. A. Fair and R. J. Madix, *Surface Sci.* **127**, 541 (1983).
11. B. E. Nieuwenhuys, D. I. Hagen, G. Rovida and G. A. Somorjai, *Surface Sci.* **59**, 155 (1976).
12. J. M. Derocette and J. Marien, *Phys. Stat. Solidi (a)* **39**, 281 (1977).
13. H. Conrad, G. Ertl and E. E. Latta, *Surface Sci.* **41**, 435 (1974).
14. K. Christmann, O. Schober, G. Ertl and M. Neumann, *J. Chem. Phys.* **60**, 4528 (1974).
15. A. Winkler and K. D. Rendulic, *Surface Sci.* **118**, 19 (1982).
16. H. J. Robota, W. Vielhaber, M. C. Lin, J. Segner and G. Ertl, *Surface Sci.* **155**, 101 (1985).
17. H. Karner, M. Luger, H. P. Steinruck, A. Winkler and K. D. Rendulic, *Surface*

- Sci. **163**, L641 (1985).
18. D. E. Ibbotson, T. S. Wittrig and W. H. Weinberg, *J. Chem. Phys.* **72**, 4885 (1980).
  19. K. Christmann, G. Ertl and T. Pignet, *Surface Sci.* **54**, 365 (1976).
  20. R. W. McCabe and L. D. Schmidt, *Surface Sci.* **65**, 169 (1977).
  21. P. R. Norton and J. W. Goodale, *Solid State Commun.* **31**, 223 (1979).
  22. P. R. Norton, J. A. Davies and T. E. Jackman, *Surface Sci.* **121**, 103 (1982).
  23. C.-M. Chan, M. A. Van Hove, W. H. Weinberg and E. D. Williams, *Solid State Commun.* **30**, 47 (1979); C.-M. Chan, M. A. Van Hove, W. H. Weinberg and E. D. Williams, *Surface Sci.* **91**, 430 (1980).
  24. See *e.g.*, G. L. Kellogg, *Phys. Rev. Letters* **55**, 2168 (1985); H. Niehus, *Surface Sci.* **145**, 407 (1984); A. M. Lahee, W. Allison, R. F. Willis and K. H. Rieder, *Surface Sci.* **126**, 654 (1983).
  25. J. L. Taylor, D. E. Ibbotson and W. H. Weinberg, *J. Chem. Phys.* **69**, 4298 (1978).
  26. H. Niehus and G. Comsa, *Surface Sci.* **102**, L14 (1981); H. Niehus and G. Comsa, *Surface Sci.* **93**, L147 (1980).
  27. D. E. Ibbotson, T. S. Wittrig and W. H. Weinberg, *Surface Sci.* **110**, 294 (1981).
  28. P. Feulner and D. Menzel, *J. Vacuum Sci. Technol.* **17**, 662 (1980).
  29. J. R. Engstrom and W. H. Weinberg, *Rev. Sci. Instrum.* **55**, 404 (1984).
  30. J. R. Engstrom, PhD Thesis, California Institute of Technology, 1987.
  31. R. Nathan and B. J. Hopkins, *J. Phys. E* **7**, 851 (1974).
  32. P. Hoffmann and D. Menzel, *Surface Sci.* **152/153**, 382 (1985).
  33. J. Lee, J. P. Cowin and L. Wharton, *Surface Sci.* **130**, 1 (1983); I. Batra, *Surface Sci.* **87**, L97 (1984).
  34. J. Behm, K. Christmann and G. Ertl, *Solid State Commun.* **28**, 763 (1978).
  35. M. A. Van Hove, G. Ertl, K. Christmann, J. Behm and W. H. Weinberg, *Solid State Commun.* **28**, 373 (1978).

36. K. Christmann, J. Behm, G. Ertl, M. A. Van Hove and W. H. Weinberg, J. Chem Phys. **70**, 4168 (1979).
37. The digital temperature controller was not employed in the measurement of these spectra.
38. In actual fact, there are two inequivalent threefold hollow sites when the second substrate layer is taken into account.
39. C.-M. Chan, R. Aris and W. H. Weinberg, Appl. Surface Sci. **1**, 360 (1978); C.-M. Chan and W. H. Weinberg, Appl. Surface Sci. **1**, 377 (1978).
40. J. T. Yates, P. A. Thiel and W. H. Weinberg, Surface Sci. **84**, 427 (1979).
41. J. A. Schwarz, Surface Sci. **87**, 525 (1979).
42. H. Shimizu, K. Christmann and G. Ertl, J. Catal. **61**, 412 (1980).
43. J. L. Taylor and W. H. Weinberg, Surface Sci. **78**, 259 (1978).
44. This assumption may break down, for example, if (i) desorption precedes through a precursor state. That is, the kinetics of the rate of exchange between the precursor state and the chemisorbed state can influence the apparent rate of desorption; see *e.g.*, D. A. King, Surface Sci. **64**, 43 (1977), and R. Gorte and L. D. Schmidt, Surface Sci. **76**, 559 (1978).
45. Although the values of the kinetic parameters reported by Christmann and Ertl (**3**) have been questioned insofar as their *quantitative* accuracy is concerned (**9,22**), a *qualitative* (internal) comparison of the results obtained on the two surfaces is nonetheless pedagogical. Indeed, both Christmann and Ertl (**3**) and Comsa *et al.* (**9**) report a difference in the activation energies of desorption from defect (step) sites and (111) terrace sites of  $E_d^{\text{step}} - E_d^{(111)} \sim 3 \text{ kcal-mol}^{-1}$ .
46. Hydrogen apparently adsorbs preferentially on the hcp-type site (*i.e.*, the threefold hollow site directly above a second-layer substrate metal atom) on Pt(111) at  $\theta = 1$  (**33**), whereas both inequivalent threefold hollow sites are populated on Ni(111) at  $\theta = 0.5$  (**34,35**).
47. I. Langmuir, Chem. Rev. **6**, 451 (1929); J. B. Taylor and I. Langmuir, Phys. Rev. **44**, 423 (1933).

48. P. Kisliuk, J. Phys. Chem. Solids **3**, 95 (1957); **5**, 78 (1958).
49. The relative disagreement between the "one-" and "two-site" adsorption models becomes progressively smaller as the coverage increases. Note that the *integral* adsorption kinetics (*i.e.*,  $\theta$  vs.  $\epsilon$ ) still differ appreciably at  $\theta \sim 0.15$ , whereas the *differential* kinetics (*i.e.*,  $d\theta/d\epsilon$  vs.  $\epsilon$ ) are nearly identical for  $\theta \geq 0.05$ .
50. J. R. Engstrom, D. W. Goodman and W. H. Weinberg, J. Am. Chem. Soc. **108**, 4653 (1986).
51. P. D. Szuromi, J. R. Engstrom and W. H. Weinberg, J. Chem. Phys. **80**, 508 (1984).
52. R. W. McCabe and L. D. Schmidt, Surface Sci. **60**, 85 (1976).
53. T. E. Jackmann, J. A. Davies, D. P. Jackson, W. N. Unertl and P. R. Norton, Surface Sci. **120**, 389 (1982).
54. This adsorption site, the bridge site in the inner corner of the step (which is equivalent to the psuedo-fourfold hollow designation used here) is supported by high-resolution electron energy loss spectra of hydrogen adsorbed on a Pt[6(111)x(111)] surface; see, *e.g.*, A. M. Baro and H. Ibach, Surface Sci. **92**, 237 (1980).
55. D. E. Ibbotson, T. S. Wittrig and W. H. Weinberg, Surface Sci. **97**, 297 (1980).
56. Carbon monoxide forms ordered phases on the Pt(110)-(1x2) surface at temperatures above 300 K for  $\theta \geq 0.5$  [(1x1) LEED pattern] and  $\theta \geq 0.9$  [(2x1)p1g1 LEED pattern] (**53**). At temperatures below 250 K, a metastable c(8x4) superstructure has been reported also for a saturation coverage ( $\theta = 1$ ) of CO (**57**).
57. T. E. Jackman, J. A. Davies, D. P. Jackson, P. R. Norton and W. N. Unertl, J. Phys. C **15**, L99 (1982).
58. E. D. Williams, P. A. Thiel, W. H. Weinberg and J. T. Yates, Jr., J. Chem. Phys. **72**, 3496 (1980).
59. There is considerable disagreement in the literature concerning the adsorption kinetics of hydrogen on the Pt(111) surface. As shown in Table 1, Lu and

Rye (2) report second-order Langmuir kinetics and an initial probability of adsorption of 0.016. However, neither Christmann *et al.* (19) nor McCabe and Schmidt (20) could fit the kinetics to any "one-site" models and reported an initial probability of adsorption of 0.1. It is of interest to note that for fractional coverages greater than approximately 0.2, the data of Christmann *et al.* (19) are described well by second-order Langmuir kinetics with an "initial" probability of adsorption of 0.024.

60. An *approximate* heat of adsorption of  $D_2$  on the Pt(111) surface was measured by Norton *et al.* (22). The values that were reported (and used here) were approximate since a fixed gas temperature was employed. Nonetheless, the effects of a fixed gas temperature and the probable presence of an activation barrier to dissociative adsorption (on the order of  $1 \text{ kcal}\cdot\text{mol}^{-1}$ ) are within other experimental uncertainties such that we may equate the heat of adsorption and the activation energy of desorption.

**Table 1**Hydrogen Adsorption Kinetics on Iridium and Platinum <sup>a)</sup>

	Iridium			Platinum		
	$s_0$	$f(\theta)$	Ref.	$s_0$	$f(\theta)$	Ref.
(111)	$7 \times 10^{-3}$	$(1 - \theta)^2$	b)	0.016	$(1 - \theta)^2$	<b>(2,59)</b>
(110)-(1x2) $\beta_1$ -adstate	$7 \times 10^{-3}$	$(1 - \theta)^2$	<b>(18)</b>	0.022	$(1 - \theta)^2$	b)
(110)-(1x2) $\beta_2$ -adstate	1.0	$(1 - \theta)$	<b>(18)</b>	0.46	$(1 - \theta)$	b)

a) In all cases, the kinetics were evaluated at surface temperatures of 100 to 150 K, and for gas temperatures of approximately 300 K.

b) This work.

## Figure Captions

- Figure 1. Structural models for the (110)-(1x2) and (111) surfaces of iridium and platinum. A and B represent two probable locations for the hydrogen adatoms in the higher binding energy  $\beta_2$ -adstates observed on the (110)-(1x2) surfaces (see text), A being a twofold bridge site, and B being a pseudo-fourfold hollow site. C and D denote the preferred hydrogen binding sites both on the (111) surfaces and for the  $\beta_1$ -adstates on the (110)-(1x2) surfaces which, on both surfaces, are inequivalent threefold hollow sites.
- Figure 2. Thermal desorption spectra of hydrogen from the Ir(111) surface parametric in exposure of hydrogen. The surface temperature during adsorption was 100 K, and the average heating rate ( $\beta$ ) for each spectrum was 20 K-s<sup>-1</sup> (37).
- Figure 3. Arrhenius plots obtained for deuterium desorption from the Ir(111) surface by varying the heating rate and maintaining a constant initial coverage of (a), 0.15; and (b), 0.47.
- Figure 4. Activation energy ( $E_d$ ) and second-order preexponential factor ( $k_d^{(2)}$ ) of the desorption rate coefficient for D<sub>2</sub> desorption from Ir(111) as a function of fractional surface coverage. The squares were obtained from the data presented in Fig. 3(a) ( $\theta_0 = 0.15$ ), the circles from Fig. 3(b) ( $\theta_0 = 0.47$ ).
- Figure 5. The coverage-exposure relationship for (a) hydrogen and (b) deuterium on the Ir(111) surface. The solid curves represent least-squares fits of the data to second-order Langmuir kinetics with an initial probability of adsorption of (a)  $7.1 \times 10^{-3}$  for H<sub>2</sub>, and (b)  $7.0 \times 10^{-3}$  for D<sub>2</sub>.
- Figure 6. The coverage-exposure relationship for low exposures of hydrogen to the Ir(111) surface. In this coverage regime, the "two-site" adsorption model (*i.e.*, the fraction of defect sites  $x_s = 0.025$ , and  $n = 1$  or  $2$ ; see text) provides a superior fit of the data with respect to the "one-site" model (*i.e.*,  $x_s = 0.0$ ) (49).
- Figure 7. Thermal desorption spectra of deuterium from the Pt(110)-(1x2) surface para-

metric in exposure of deuterium. The surface temperature during adsorption was 120 K, and the linear heating rate for each spectrum was  $3.0 \text{ K-s}^{-1}$ . The ratio of the saturation densities of the two adstates,  $\beta_2:\beta_1$ , is approximately 1:2.

Figure 8. Thermal desorption spectra of  $\text{D}_2$ , HD and  $\text{H}_2$  from a coadsorbed overlayer of hydrogen and deuterium. In this experiment, 0.64 L of  $\text{D}_2$  was exposed first, populating approximately 85% of the  $\beta_2$ -adstate, and, subsequently, 8.5 L of  $\text{H}_2$  was exposed. The surface temperature during adsorption was 120 K, and the linear heating rate was  $3.0 \text{ K-s}^{-1}$ .

Figure 9. Activation energy ( $E_d$ ) and second-order preexponential factor ( $k_d^{(2)}$ ) of the desorption rate coefficient for  $\text{D}_2$  desorption from Pt(110)-(1x2) as a function of fractional surface coverage.

Figure 10. The coverage-exposure relationship for deuterium on the Pt(110)-(1x2) surface. The solid curve has been drawn to facilitate the presentation. The coverage regimes representative of the  $\beta_2$ - and  $\beta_1$ -adstates are marked to emphasize the vastly different kinetics exhibited by the two states.

Figure 11. Analytic fits to the adsorption kinetics of  $\text{D}_2$  on the Pt(110)-(1x2) surface derived from the data shown in Fig. 10. (a) The adsorption kinetics for  $\text{D}_2$  into the  $\beta_2$ -adstate fit to a first-order Langmuir model with an initial probability of adsorption of 0.45. The coverage has been normalized to saturation of the  $\beta_2$ -adstate. (b) The adsorption kinetics for  $\text{D}_2$  into the  $\beta_1$ -adstate fit to a second-order Langmuir model with an initial probability of adsorption of 0.024. The coverage has been normalized to saturation of the  $\beta_1$ -adstate.

Figure 12. The CPD of hydrogen on the Pt(110)-(1x2) surface as a function of fractional coverage at 120 K. The coverage regimes representative of the  $\beta_2$ - and  $\beta_1$ -adstates are marked to emphasize the (apparently) different charge transfer characteristics of the two adstates.

Figure 13. (A) Thermal desorption of  $\text{H}_2$  from preadsorbed hydrogen (0.39 L;  $\theta_{\text{H}} = 0.26$ ) exposed to varying amounts of CO (0–4.4 L CO;  $\theta_{\text{CO}} = 0$ –0.8). The surface

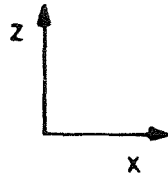
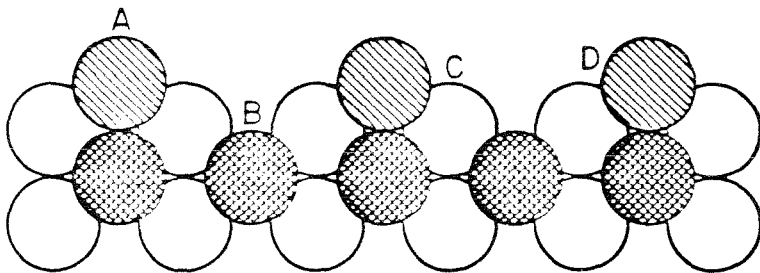
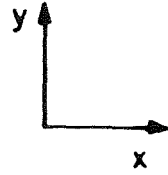
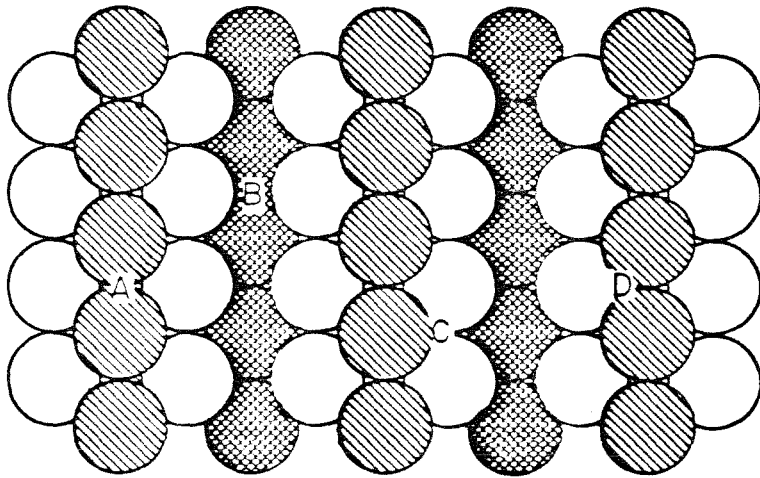
temperature during adsorption was 120 K, and the linear heating rate was 15 K-s<sup>-1</sup>. The coverage of hydrogen was constant with these CO exposures. (B) The CPD for the exposure sequence represented by the thermal desorption spectra given in (A). The surface was exposed to 0.39 L of H<sub>2</sub>, followed by a constant partial pressure of CO of 5 x 10<sup>-8</sup> Torr. The dashed line in (B) represents the CPD for CO exposed to a *clean* Pt(110)-(1x2) surface.

Figure 14. Comparison of the desorption rate parameters, the activation energy ( $E_d$ ) and the second-order preexponential factor ( $k_d^{(2)}$ ), for hydrogen on the Ir(111) surface and for the  $\beta_1$ -adstate on the Ir(110)-(1x2) surface as a function of fractional coverage. The abscissae have been scaled such that the absolute adsorbate concentrations are equal for the two adstates. The zero coverage limit for the Ir(110)-(1x2) surface is shown for reference purposes. The data for the Ir(110)-(1x2) surface are from Ibbotson *et al.* (18).

Figure 15. Comparison of the activation energies of desorption ( $E_d$ ) for deuterium on the Pt(111) surface and for the  $\beta_1$ -adstate on the Pt(110)-(1x2) surface as a function of fractional coverage. The abscissae have been scaled such that the absolute adsorbate concentrations are equal for the two adstates. The data for the Pt(111) surface are from Norton *et al.* (22,60).

Figure 16. Comparison of the desorption rate parameters, the activation energy ( $E_d$ ) and the second-order preexponential factor ( $k_d^{(2)}$ ), for hydrogen on the (110)-(1x2) surfaces of both iridium and platinum as a function of fractional coverage. The data for the Ir(110)-(1x2) surface are from Ibbotson *et al.* (18).

## Ir, Pt (II) - (1x2)



## Ir, Pt (III)

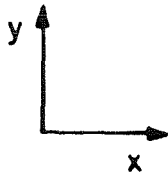
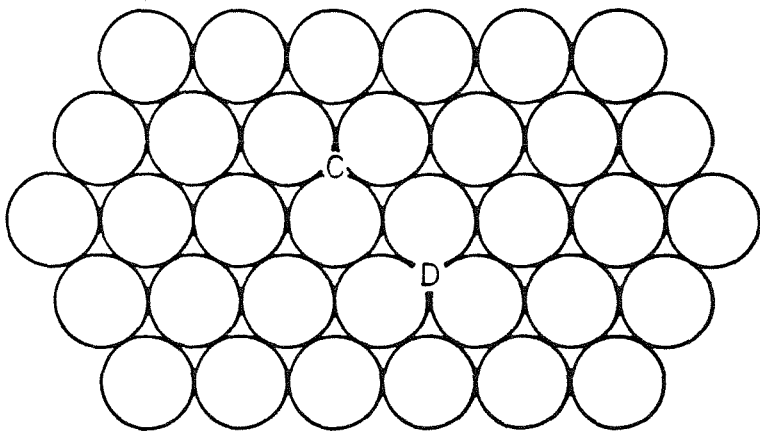


Figure 1

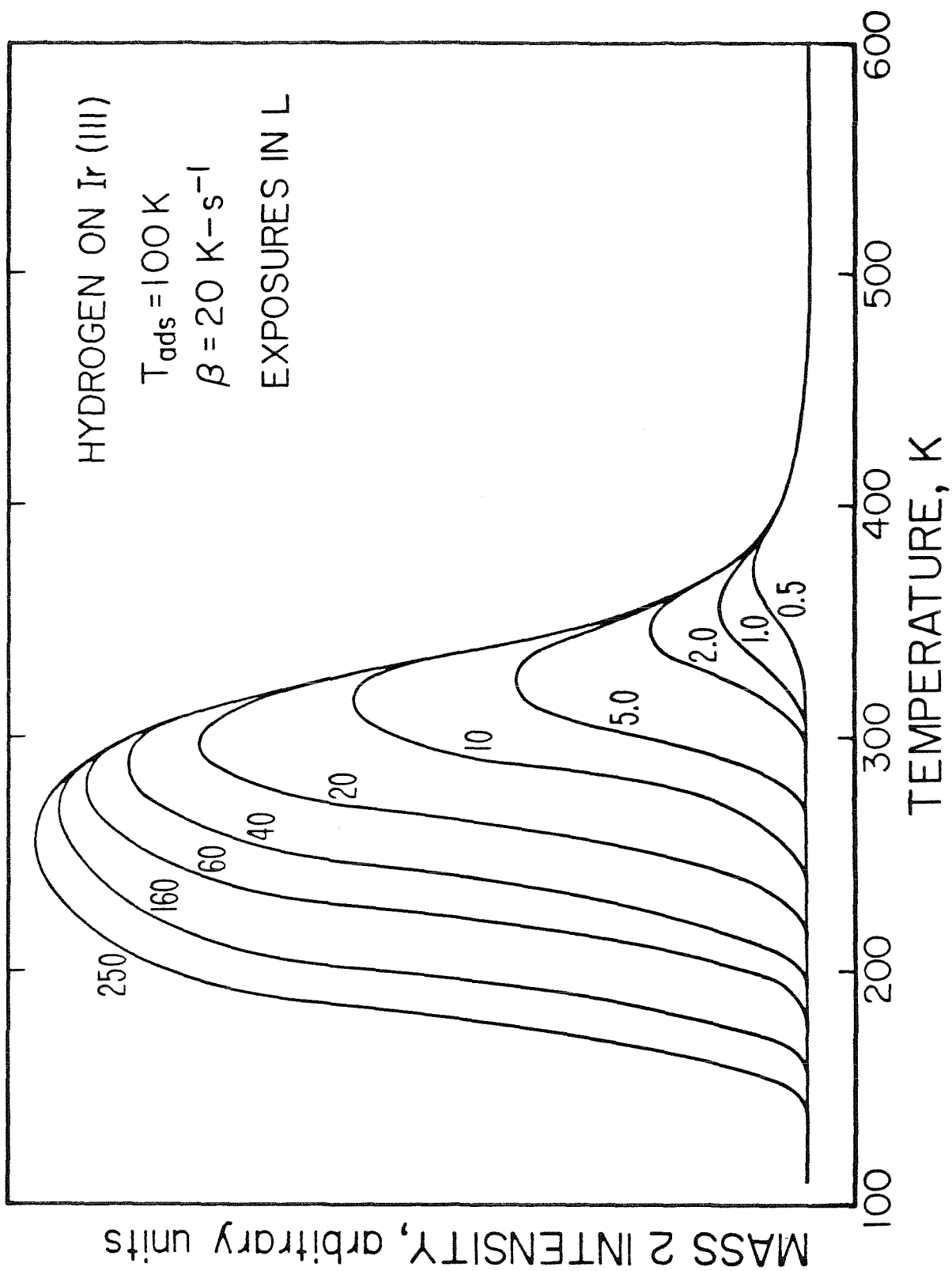


Figure 2

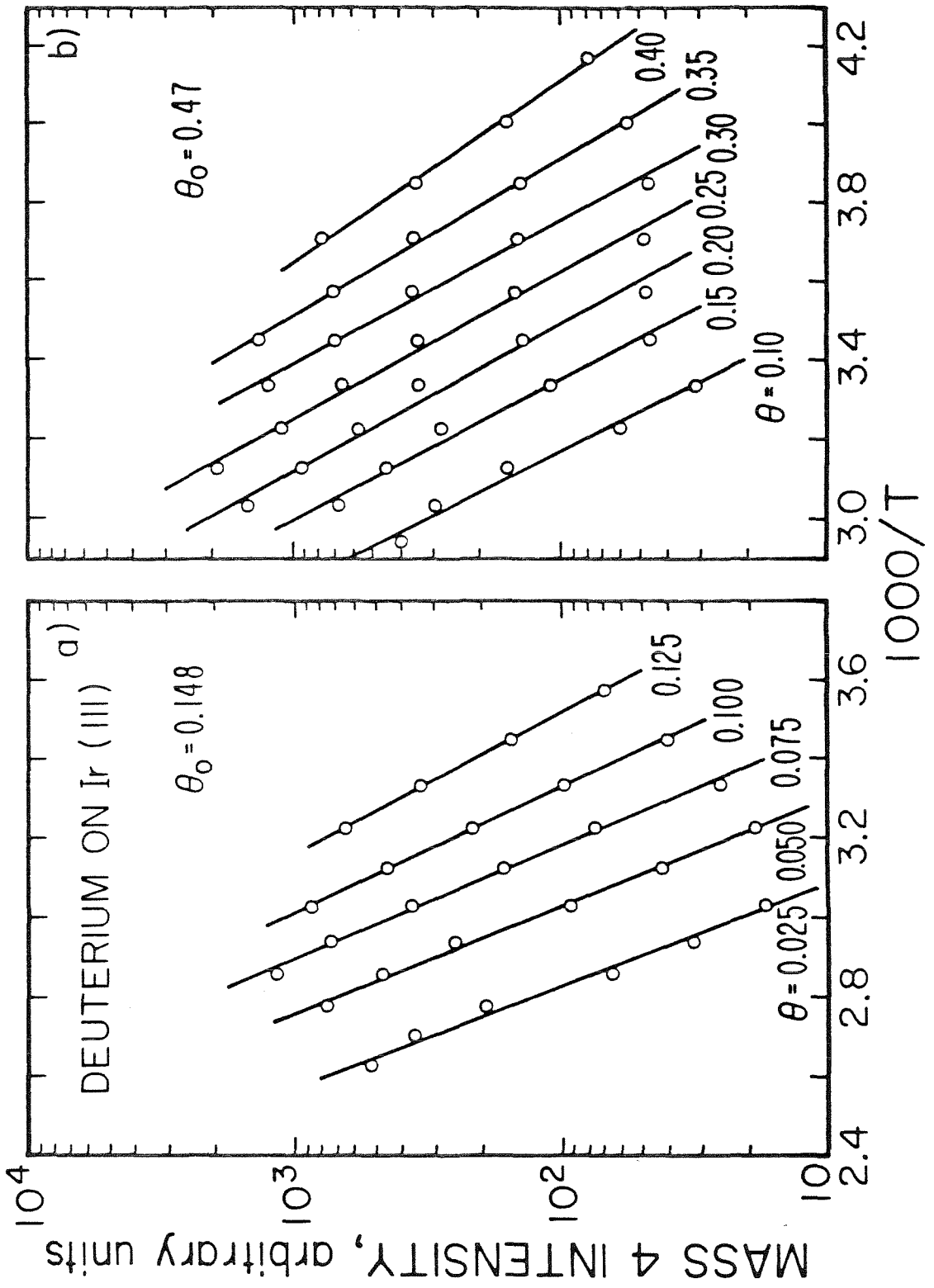


Figure 3

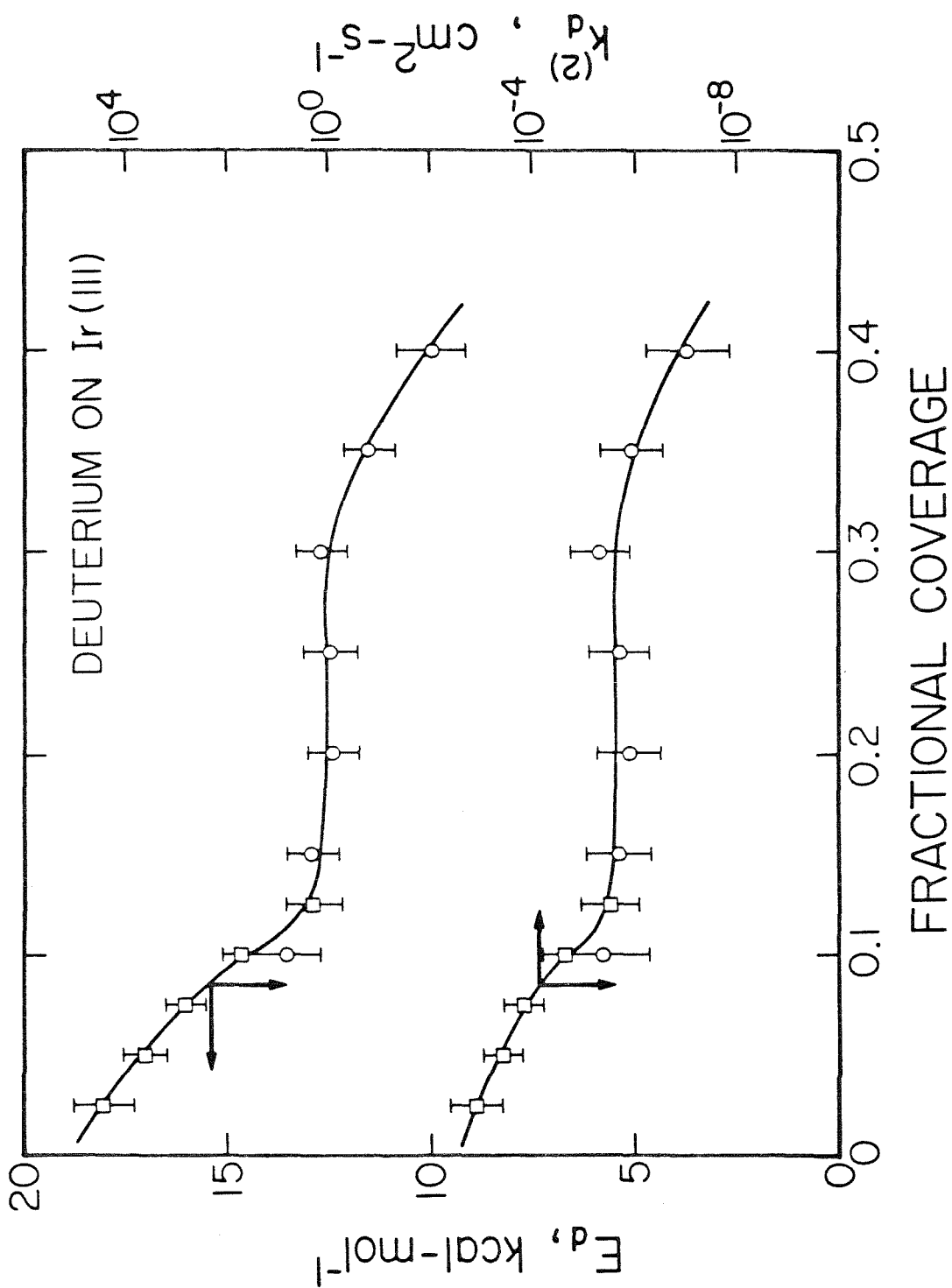


Figure 4

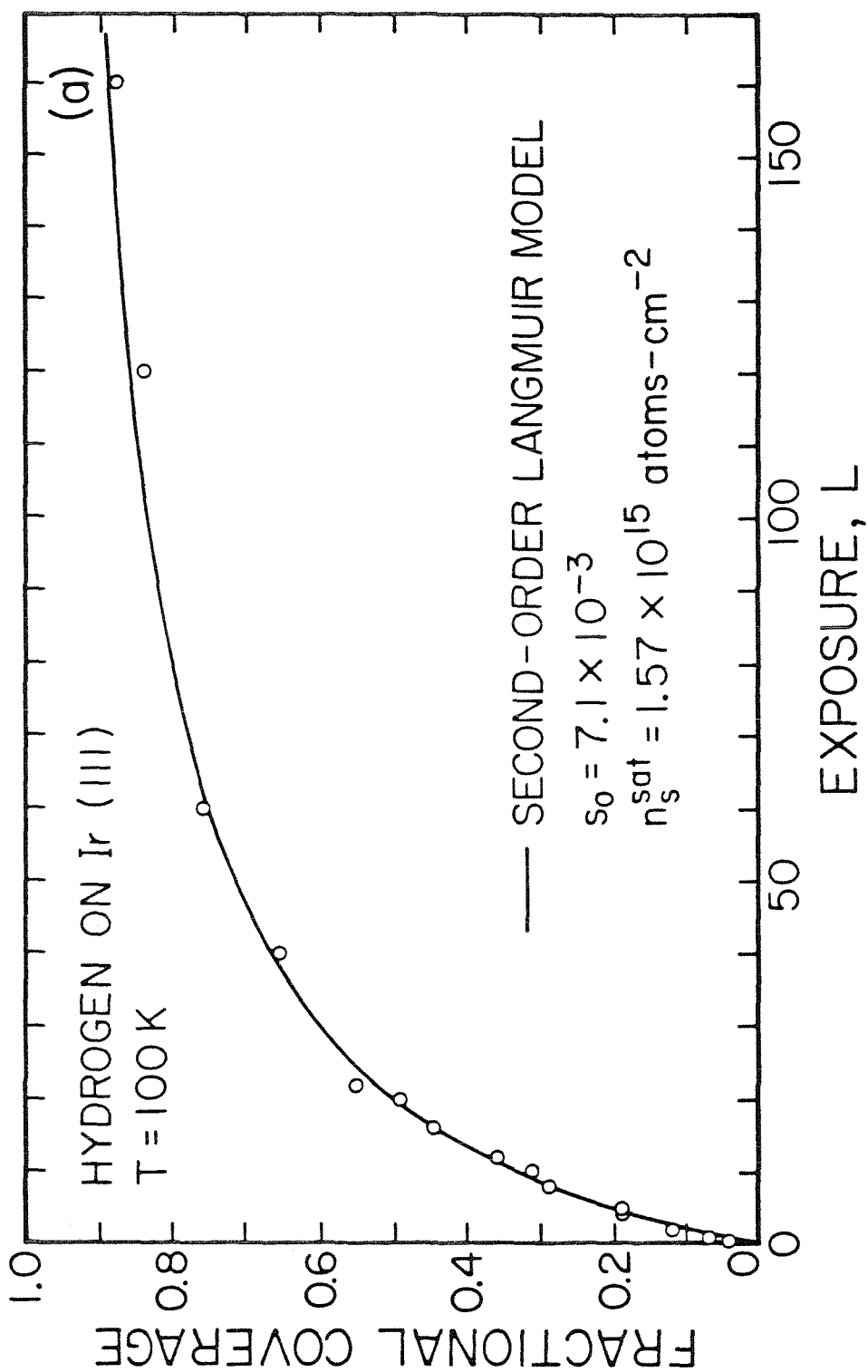


Figure 5(a)

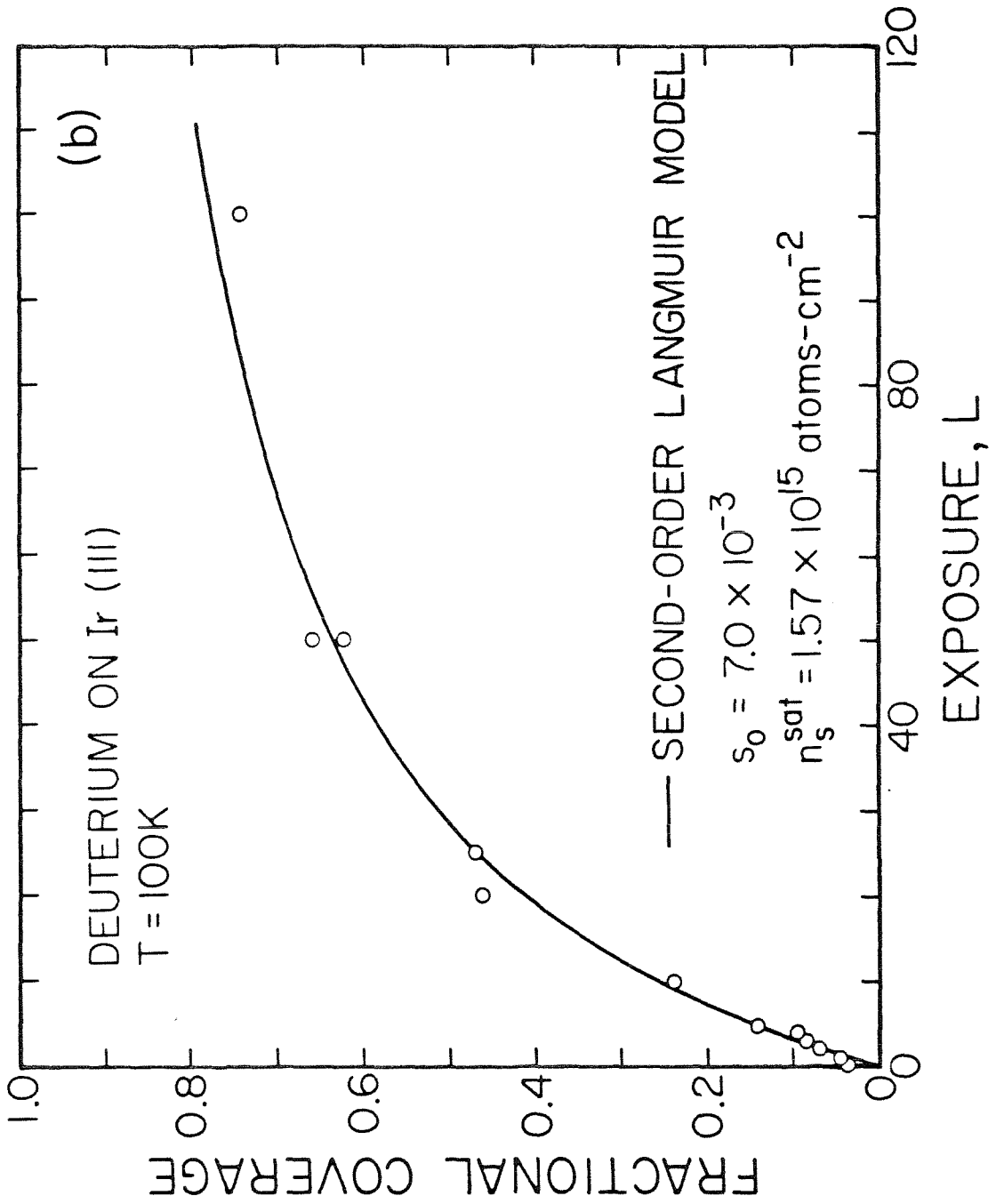


Figure 5(b)

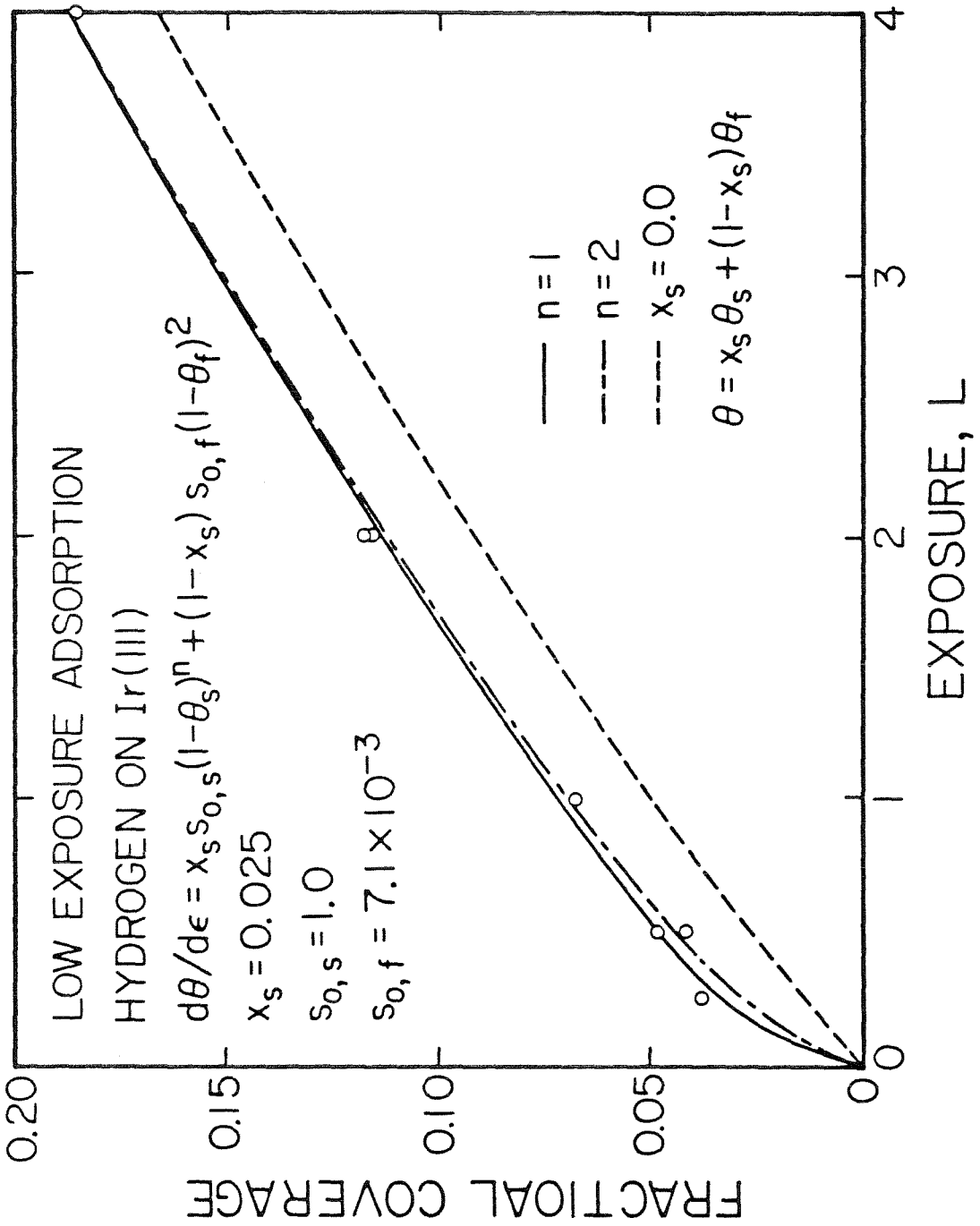


Figure 6

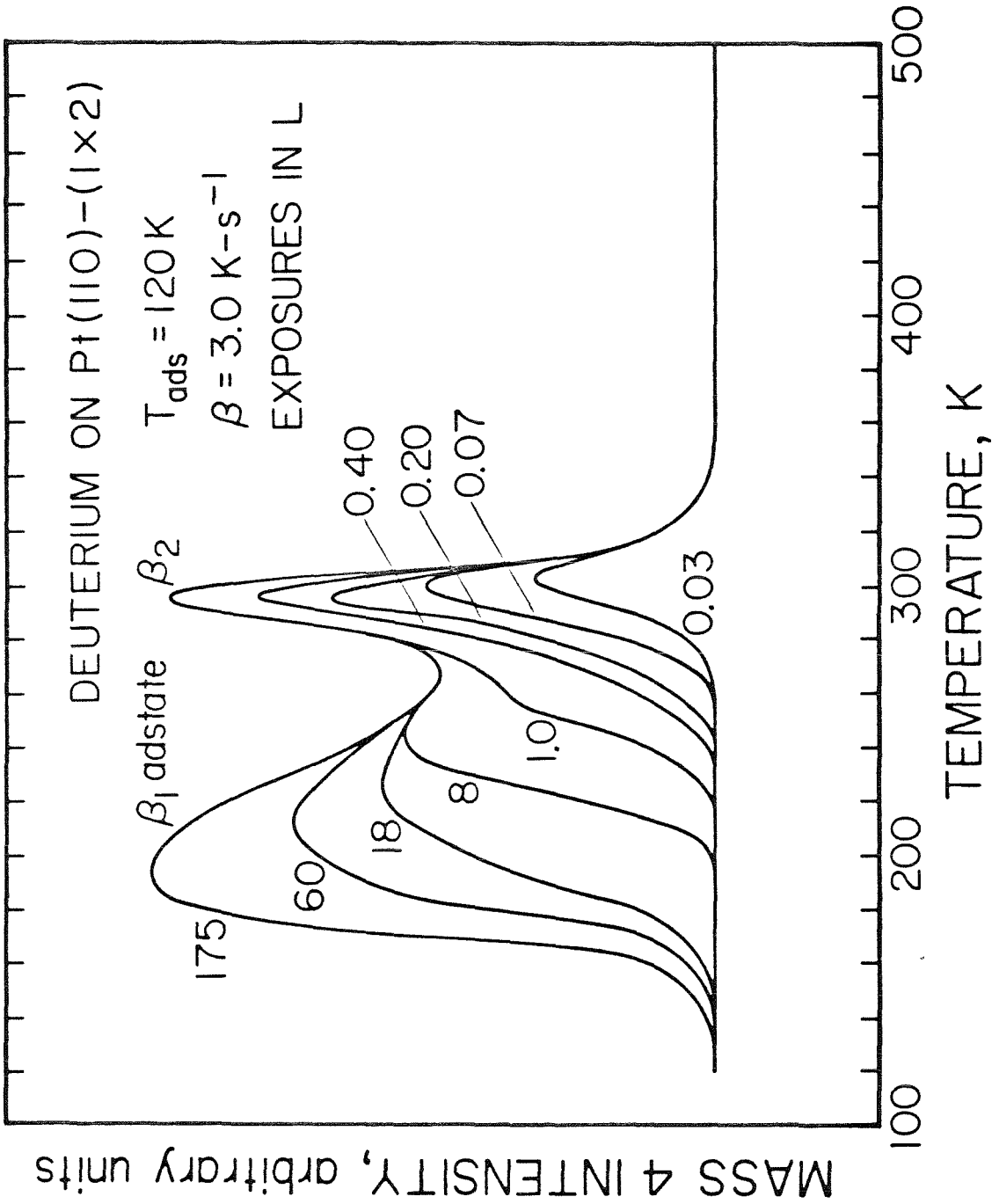


Figure 7

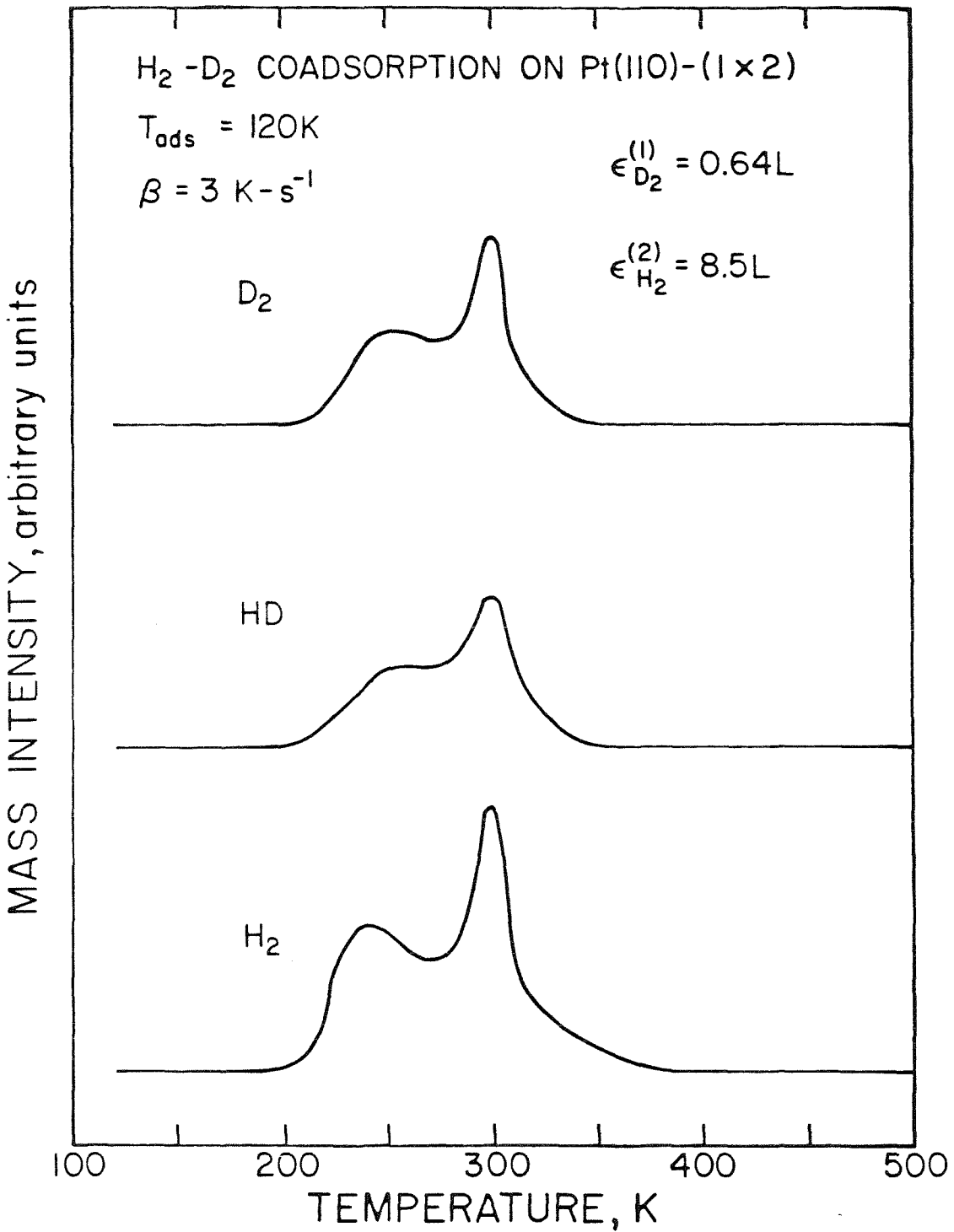


Figure 8

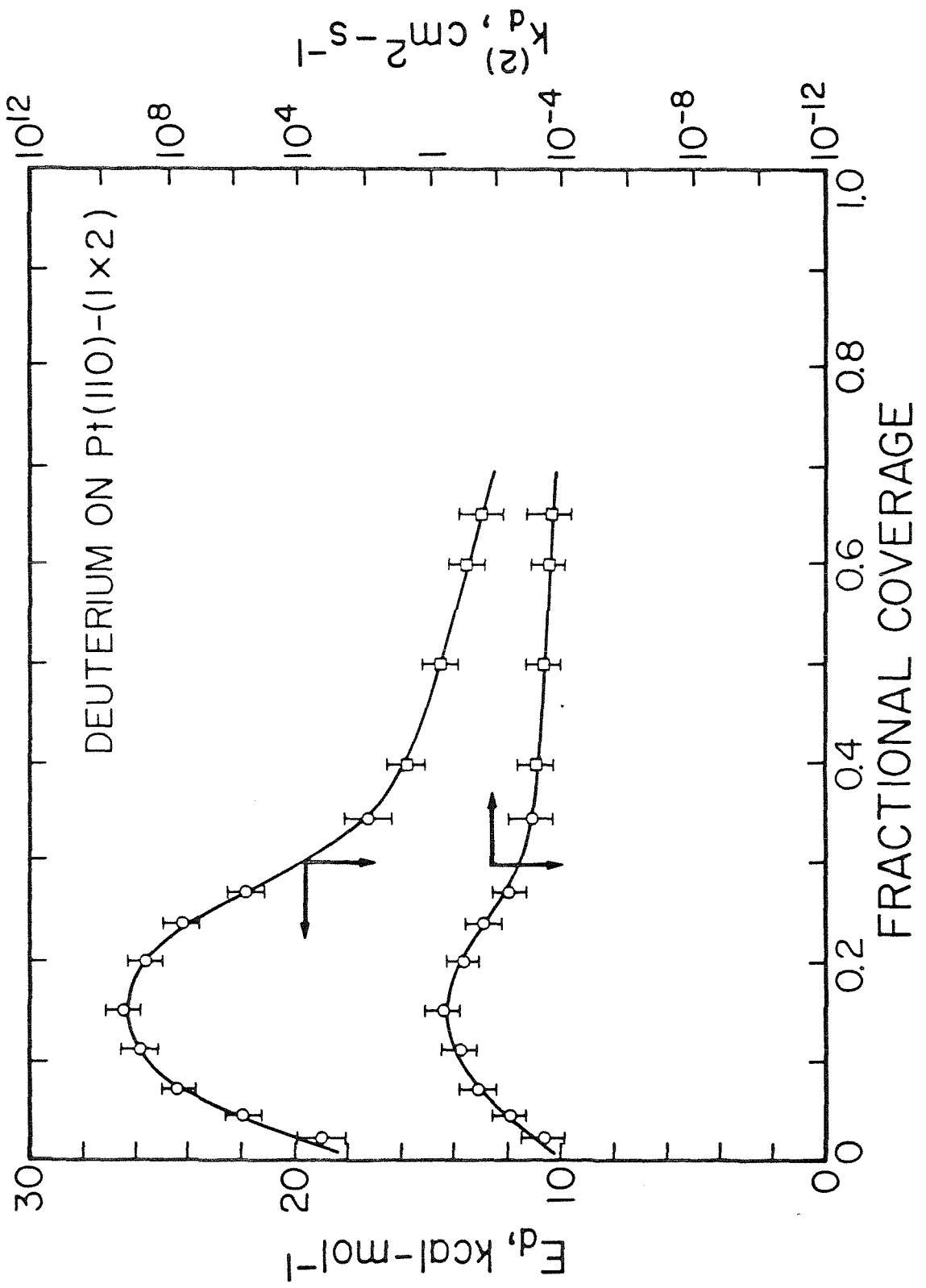


Figure 9

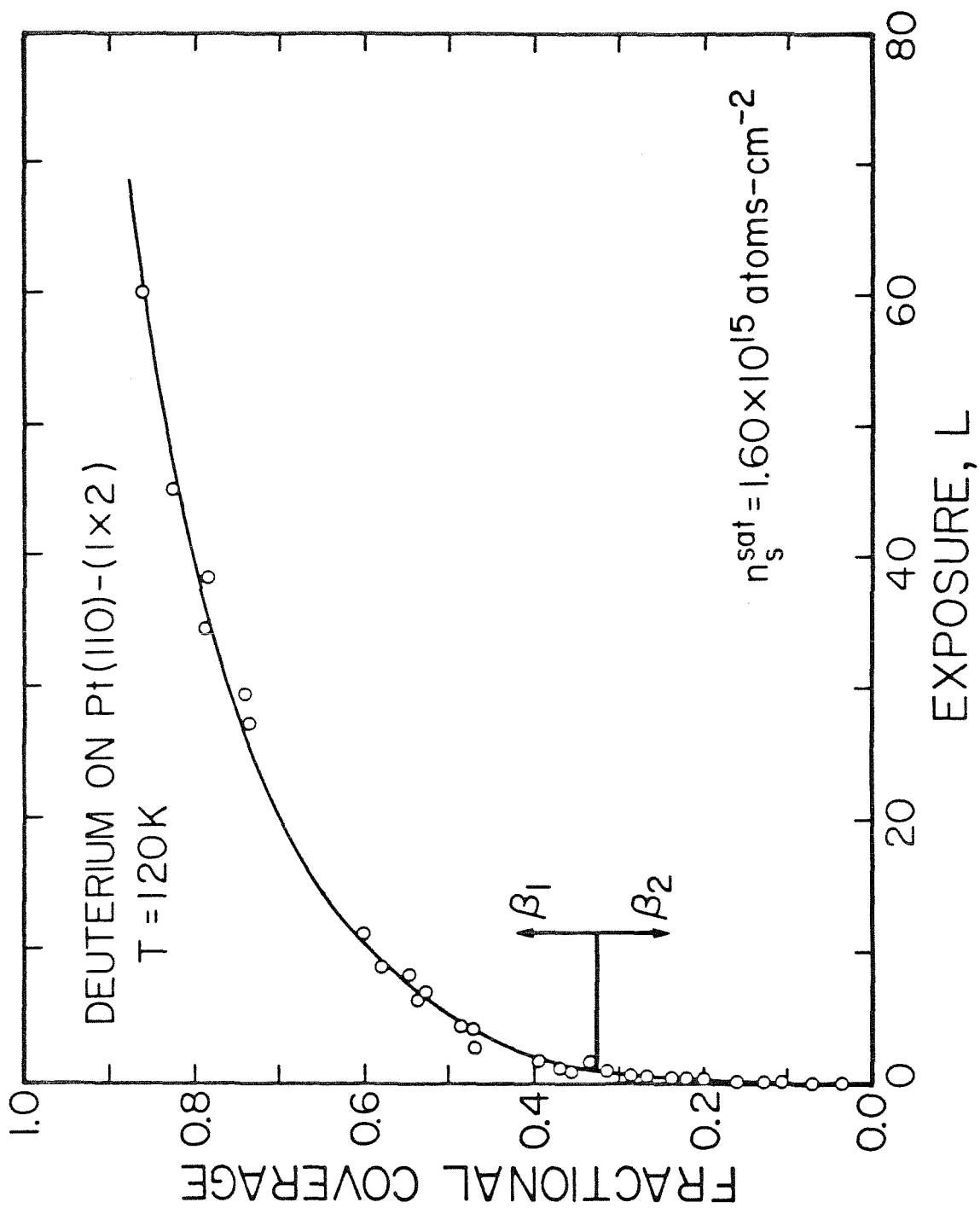


Figure 10

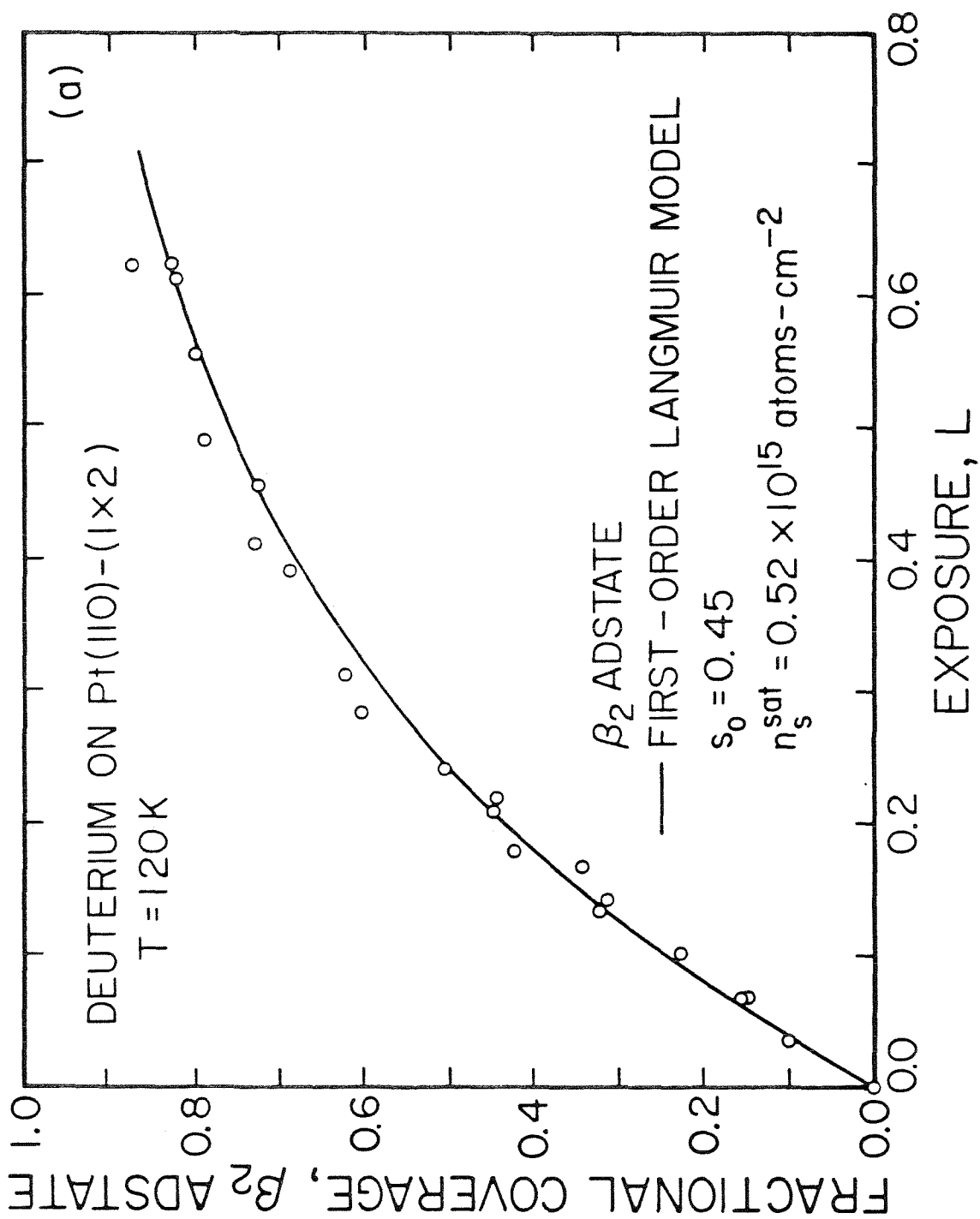


Figure 11(a)

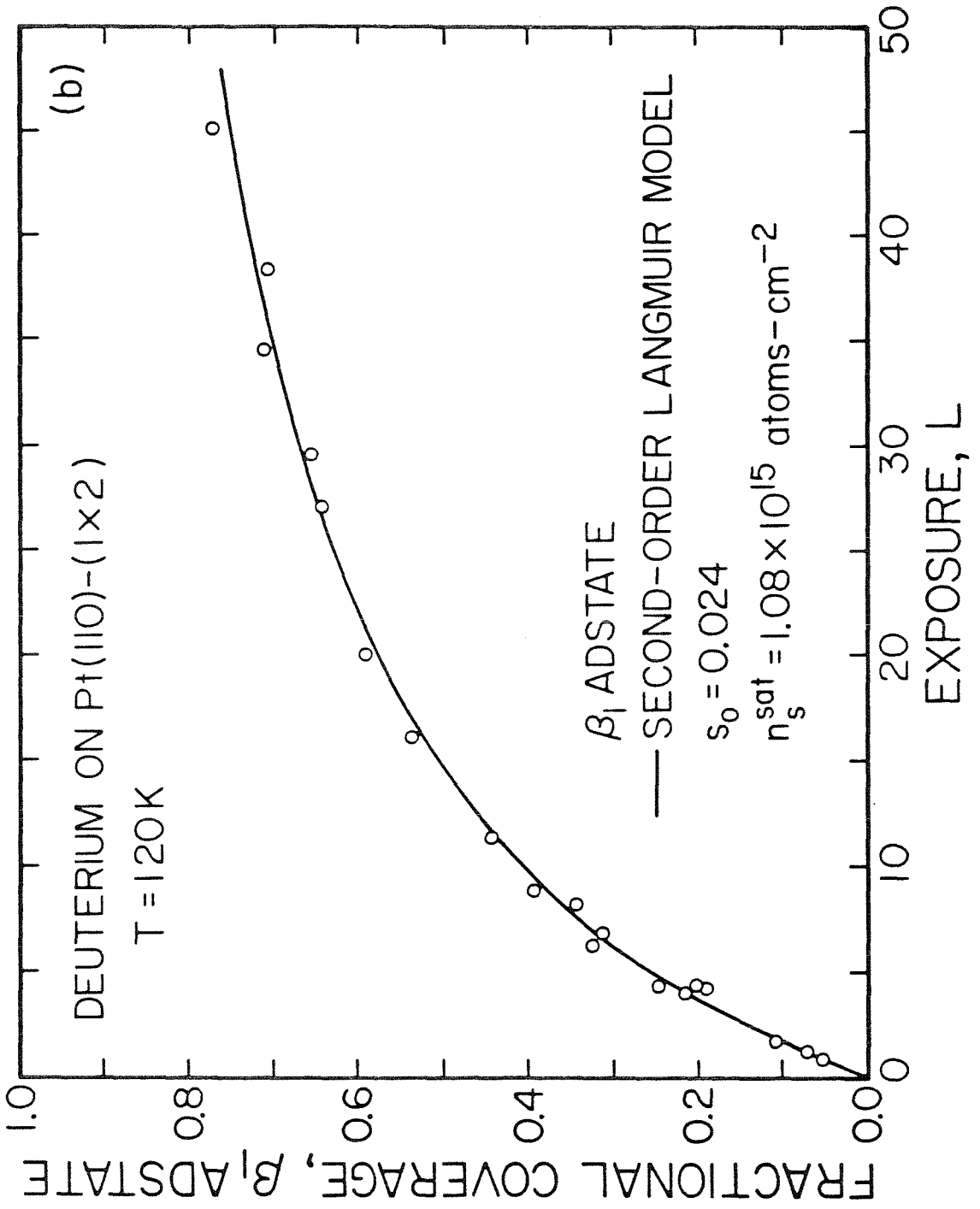


Figure 11(b)

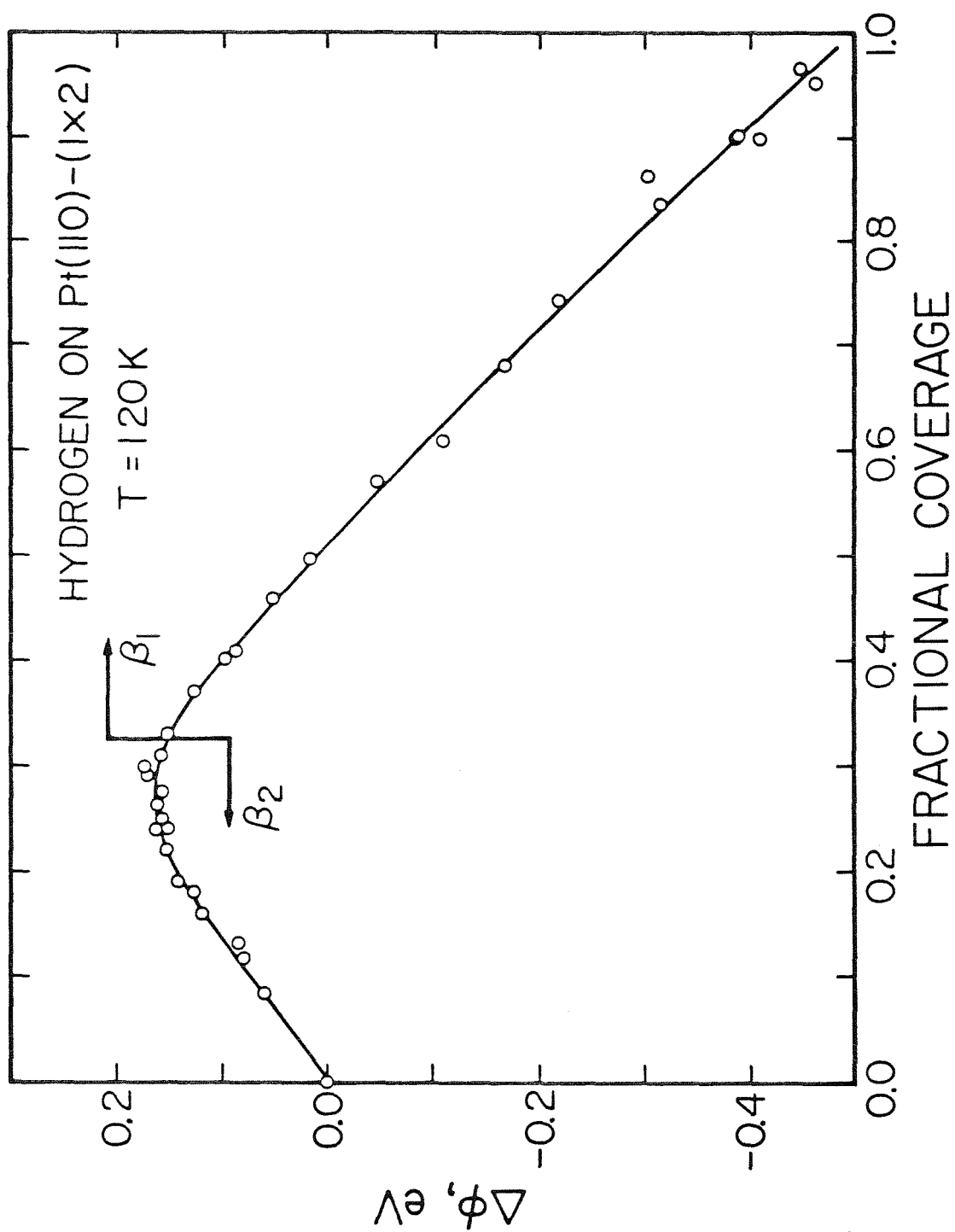


Figure 12

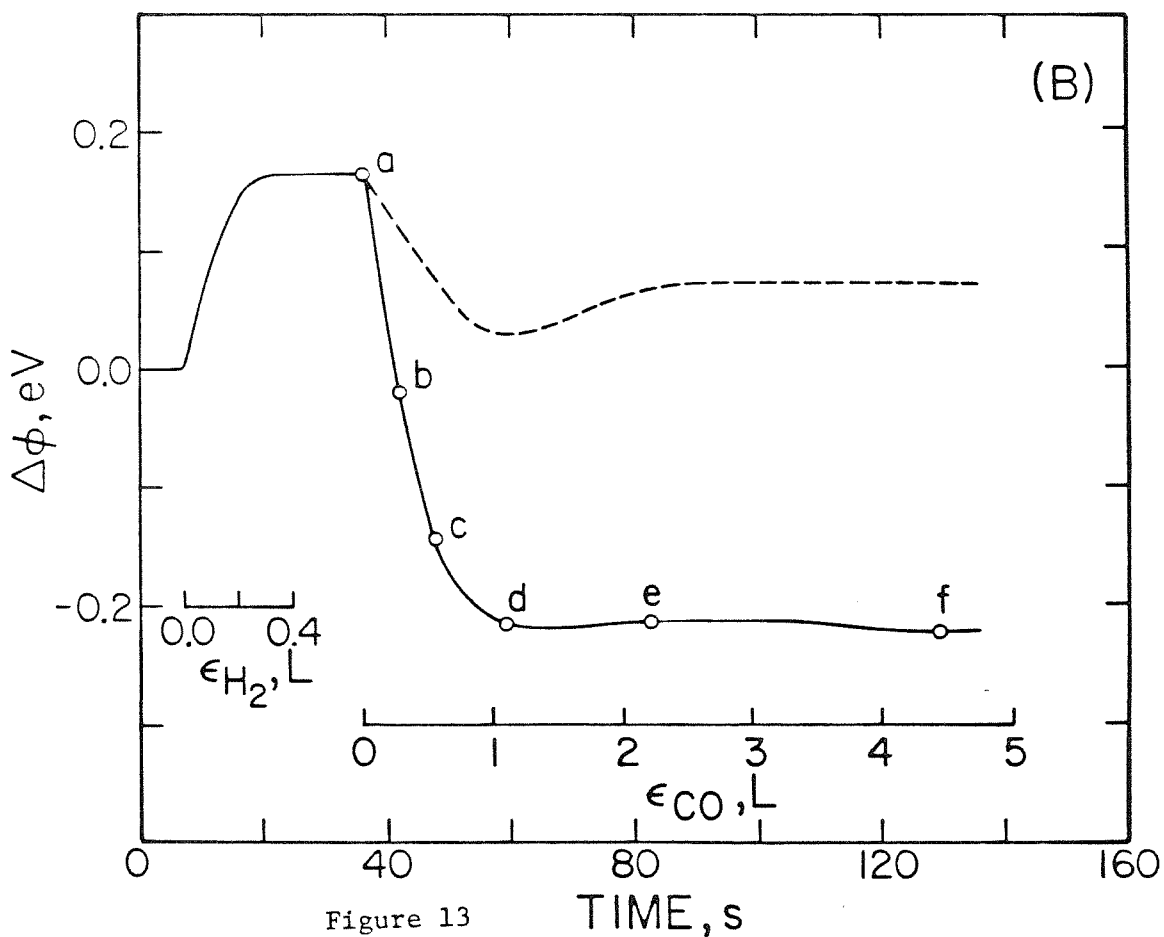
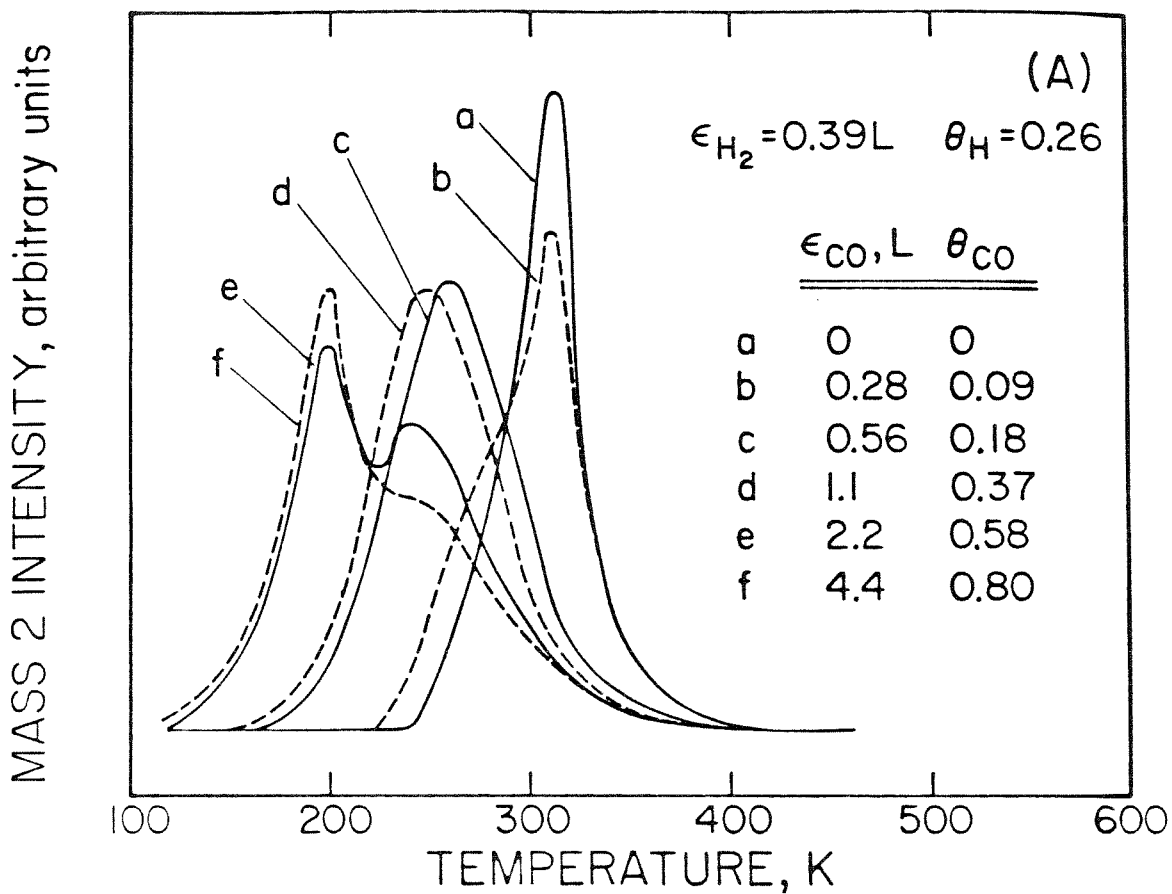


Figure 13

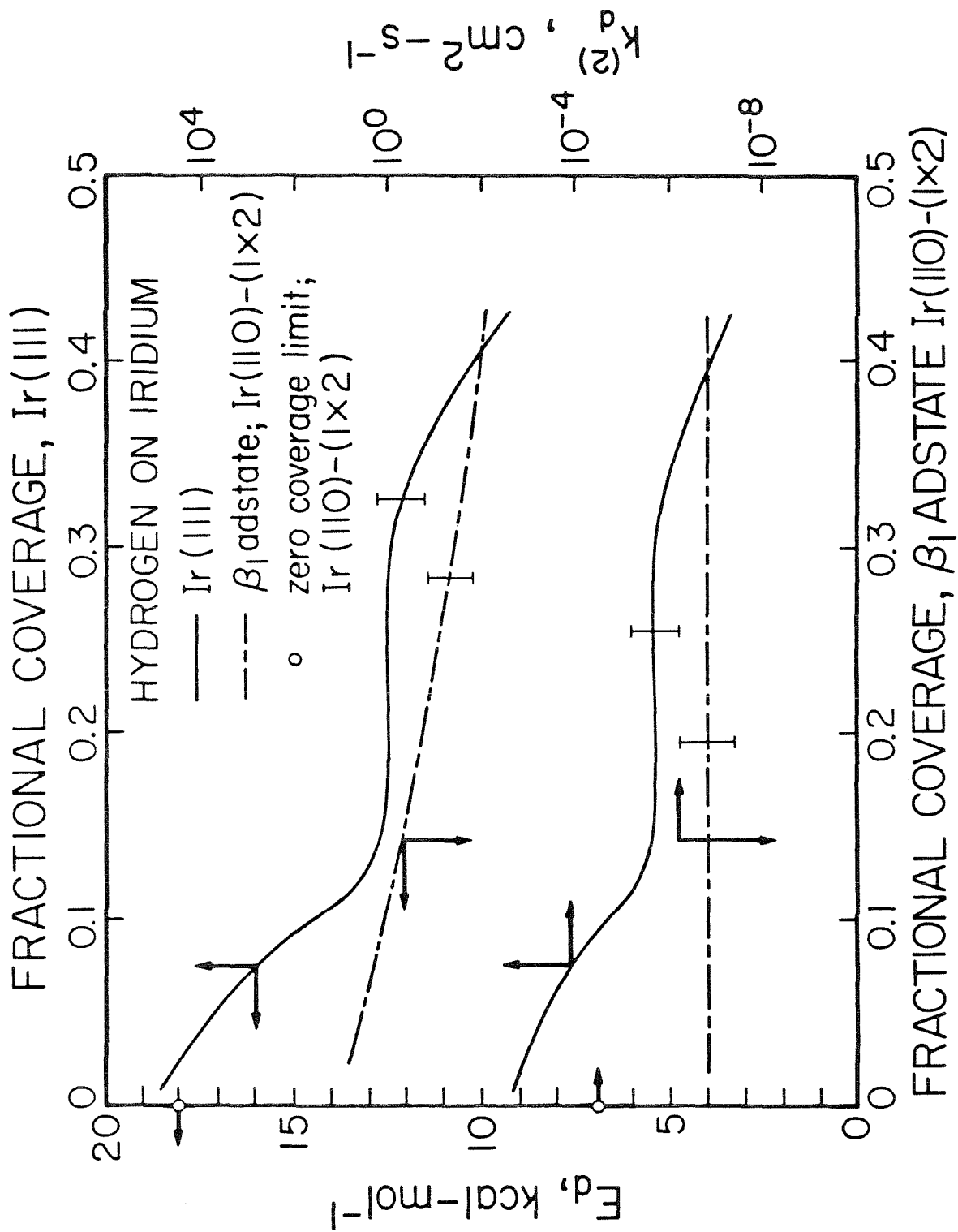


Figure 14

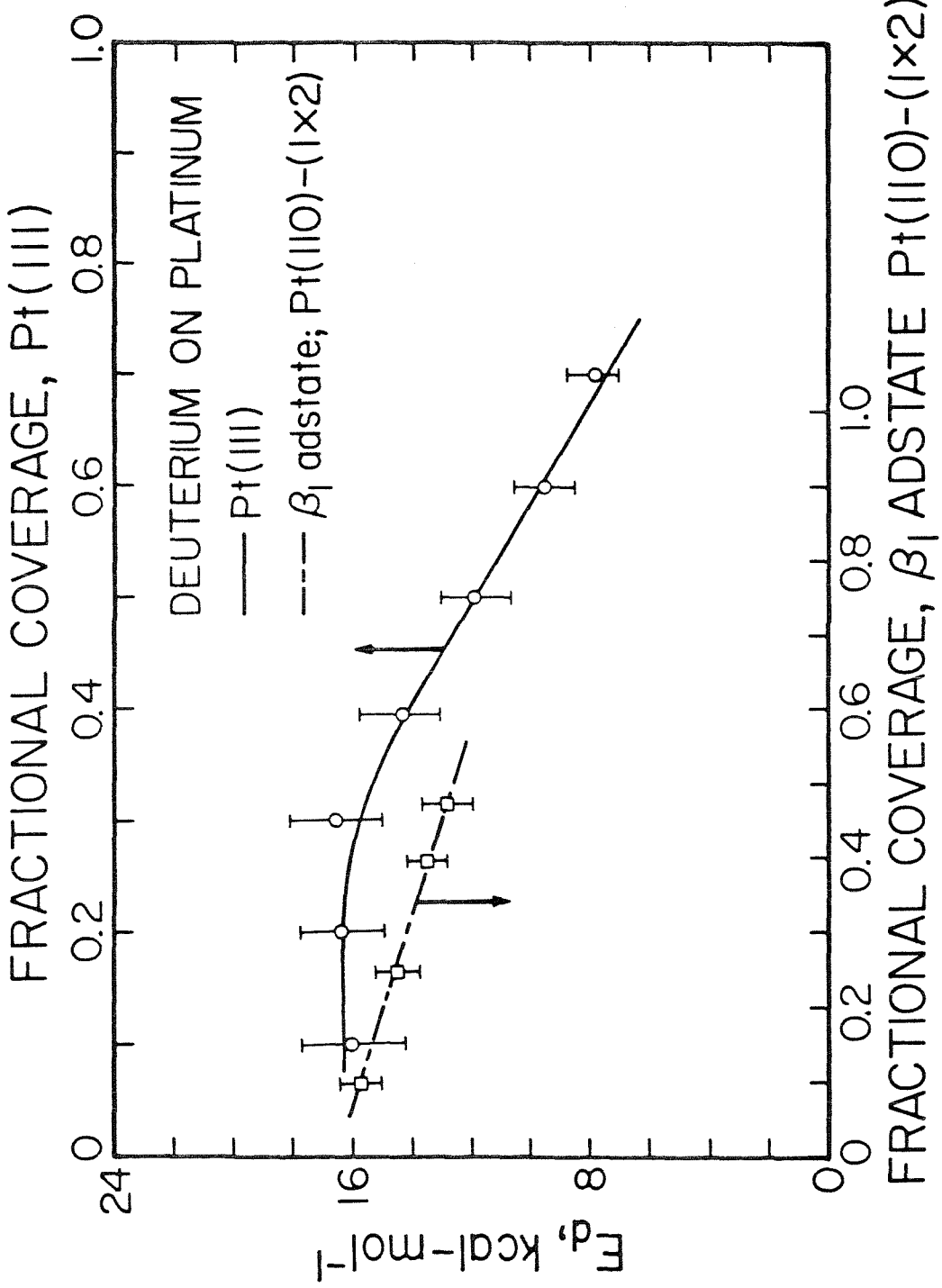


Figure 15

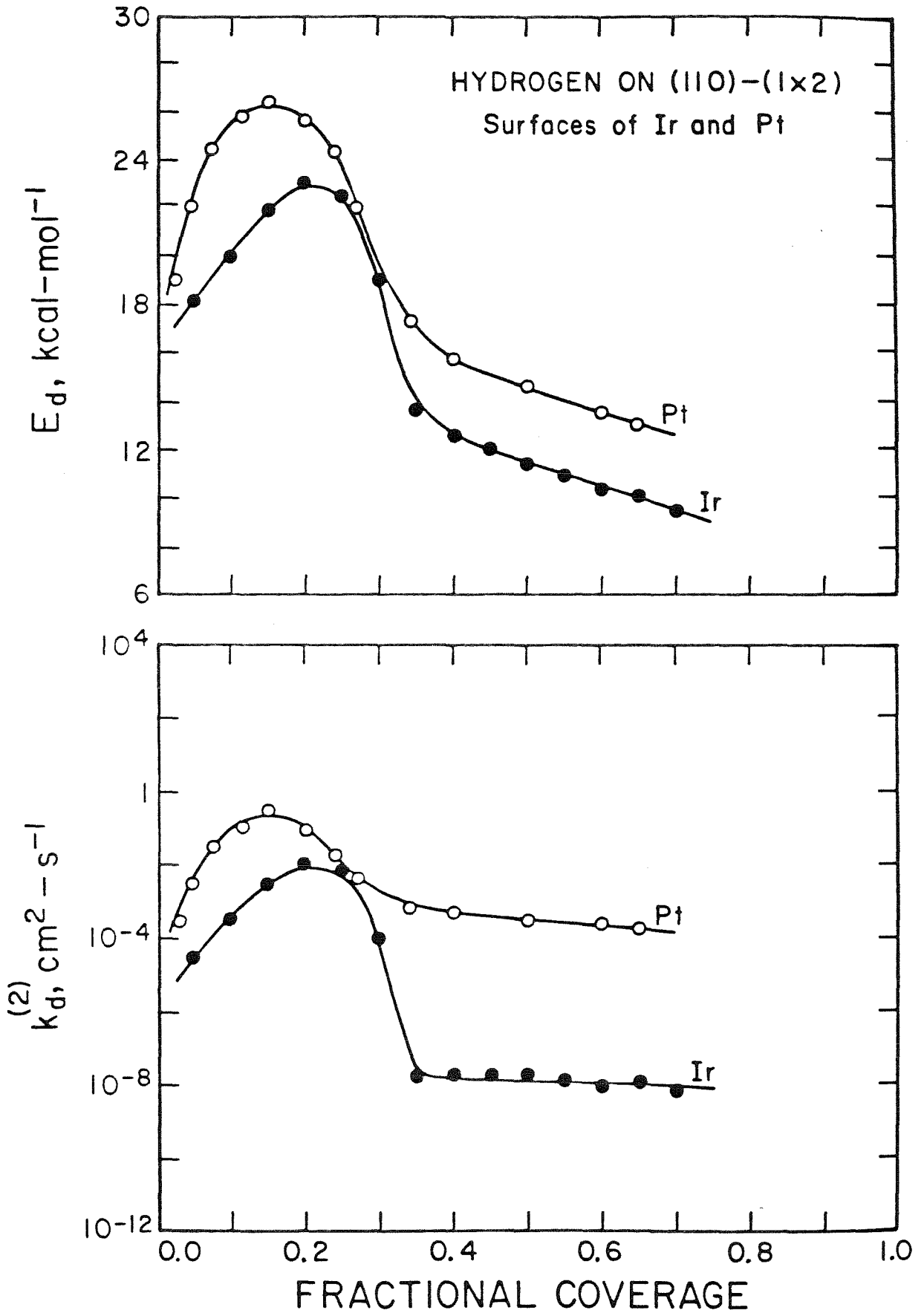


Figure 16

**Appendix 4.**

Steady-State Decomposition of Ammonia on the Pt(110)-(1x2) Surface

[Appendix 4 consists of an article coauthored with J.J. Vajo and W.H. Weinberg, which appeared in the *Journal of Physical Chemistry* **1986**, 90, 6531.]

## Steady-State Decomposition of Ammonia on the Pt(110)-(1 × 2) Surface

J. J. Vajo, W. Tsai, and W. H. Weinberg\*

*Division of Chemistry and Chemical Engineering, California Institute of Technology,  
 Pasadena, California 91125 (Received: July 22, 1986)*

Steady-state absolute reaction rates are reported for the catalytic decomposition of ammonia on the Pt(110)-(1 × 2) single-crystalline surface at pressures between  $1 \times 10^{-6}$  and  $2.6 \times 10^{-6}$  Torr and at temperatures between approximately 350 and 900 K. For temperatures below 475 K the apparent activation energy is  $24 \pm 4$  kcal/mol, and the reaction rate approaches zero order in ammonia pressure. At higher temperatures the activation energy decreases, becoming  $1 \pm 1$  kcal/mol for temperatures above 550 K. Under these conditions the rate of decomposition is linearly dependent on ammonia pressure. The surface composition at  $2 \times 10^{-6}$  Torr and temperatures between 350 and 600 K was measured by thermal desorption experiments conducted during the steady-state decomposition of ammonia. The results indicate that nitrogen adatoms are the predominant surface species and that the activation energy for nitrogen desorption is 24–26 kcal/mol, independent of the nitrogen coverage. A mechanistic model that had been developed previously [Vajo, J. J.; Tsai, W.; Weinberg, W. H. *J. Phys. Chem.* 1985, 89, 3243] was found to describe accurately the pressure and temperature dependence of both the decomposition kinetics and the measured steady-state coverage of nitrogen adatoms. Both the experimental measurements and the mechanistic model indicate that molecular nitrogen is produced by the recombinative desorption of nitrogen adatoms on the platinum surface.

### I. Introduction

The decomposition of ammonia on platinum surfaces has been studied extensively by a variety of experimental techniques.<sup>1–8</sup> While the steady-state decomposition kinetics on polycrystalline platinum surfaces have been firmly established for a wide range of pressure and temperature,<sup>1–4</sup> the important surface intermediates and surface reactions, although suggested,<sup>3,7,8</sup> have not been determined unequivocally. Threshold ionization measurements have established the desorption of  $N_2^*$  with 20 kcal/mol of vibrational excitation during ammonia decomposition at a pressure of 0.1–1.4 Torr on a polycrystalline platinum ribbon at temperatures between 773 and 1373 K.<sup>7</sup> On the basis of these results, the authors suggested that (at least under these conditions) the bimolecular reaction of two adsorbed NH species is the dominant reaction producing molecular nitrogen and controlling the rate of ammonia decomposition. Indeed, NH radicals have been observed by laser-induced fluorescence (LIF) to desorb from a polycrystalline platinum wire in 0.1 Torr of ammonia at 1200–1400 K.<sup>8</sup> Although nitrogen adatoms were believed to be at least an order of magnitude more abundant for all the experimental conditions studied, the lack of an appropriate calibration precluded any estimate of the NH surface concentration.

In a recent study in our laboratory, absolute reaction rates were measured for ammonia decomposition by a polycrystalline platinum wire over a wide range of pressure and temperature.<sup>3</sup> The results were interpreted in terms of a steady-state, nonequilibrium mechanistic model embodied by elementary surface reactions. A quantitatively accurate description of the experimental data was obtained for the entire range of conditions studied ( $5 \times 10^{-7} \leq p_{NH_3} \leq 0.5$  Torr and  $400 \leq T \leq 1200$  K) with independently measured adsorption-desorption parameters for  $NH_3$ ,  $N_2$ , and  $H_2$ . The model implies that at low temperatures and/or high pressures, nitrogen adatoms are the dominant surface species and that the recombinative desorption of nitrogen controls the observed rate of reaction. At high temperatures and/or low pressures, the surface coverage of all species is low and a competition between the desorption of molecular ammonia and the cleavage of an N–H

bond of molecularly adsorbed ammonia controls the rate of ammonia decomposition.

In the present study, absolute reaction rates have been measured for the steady-state decomposition of ammonia by a Pt(110)-(1 × 2) surface at pressures between  $1 \times 10^{-6}$  and  $2.6 \times 10^{-6}$  Torr and temperatures between 350 and 900 K. Thermal desorption measurements, conducted during the steady-state decomposition, were used to determine the composition, coverage, and kinetics of desorption of the adsorbed species that are present during the ammonia decomposition reaction. These results are used to evaluate the generality of our previously proposed mechanistic model<sup>3</sup> and to explore the surface structural dependence of the ammonia decomposition reaction on platinum.

### 2. Experimental Procedures

The measurements were performed in an ion-pumped, stainless steel bell jar that has been described in detail previously.<sup>9</sup> The base pressure of the bell jar was below  $1 \times 10^{-10}$  Torr of reactive gases. The Pt(110) crystal was oriented and cut from a single-crystalline boule of platinum and was polished to within  $0.5^\circ$  of the (110) orientation by standard metallographic techniques. The crystal was etched in aqua regia and cleaned in situ by argon ion sputtering at 1200 K, heating in  $5 \times 10^{-7}$  Torr of oxygen at 800 K, and annealing to 1400 K. Auger electron spectroscopy was used to verify surface cleanliness. Special care was taken to reduce the bulk concentration of silicon impurity, since it has been shown that its presence is related to the formation of a "subsurface oxide" on Pt(111).<sup>10</sup> After cleaning and annealing, the (1 × 2) LEED pattern that is characteristic of the clean, reconstructed Pt(110) surface was observed.

Since decomposition of ammonia occurred readily on the hot filament of the mass spectrometer, the steady-state decomposition experiments were carried out with a directional beam doser consisting of a multichannel array of capillaries.<sup>11</sup> This provided a beam pressure to background pressure ratio of greater than 100:1 at the platinum surface. In addition, the crystal manipulator was cooled to approximately 100 K with liquid nitrogen, which reduced further the background ammonia pressure. Absolute "beam" fluxes were determined by measuring the rate of pressure decrease in the doser reservoir. Absolute reaction rates were determined by replacing the ammonia in the doser reservoir with nitrogen (the

(1) Löffler, D. G.; Schmidt, L. D. *J. Catal.* 1976, 41, 440.  
 (2) Löffler, D. G.; Schmidt, L. D. *Surf. Sci.* 1976, 59, 195.  
 (3) Vajo, J. J.; Tsai, W.; Weinberg, W. H. *J. Phys. Chem.* 1985, 89, 3243.  
 (4) Tsai, W.; Vajo, J. J.; Weinberg, W. H. *J. Phys. Chem.* 1985, 89, 4926.  
 (5) Gland, J. L.; Kollin, E. B. *Surf. Sci.* 1981, 104, 478.  
 (6) Sexton, B. A.; Mitchell, G. E. *Surf. Sci.* 1980, 99, 523.  
 (7) Foner, S. N.; Hudson, R. L. *J. Chem. Phys.* 1984, 80, 518.  
 (8) Selwyn, G. S.; Lin, M. C. *Chem. Phys.* 1982, 67, 213.

(9) Taylor, J. L.; Ibbotson, D. E.; Weinberg, W. H. *J. Chem. Phys.* 1978, 69, 4298.

(10) Niehus, H.; Comsa, G. *Surf. Sci.* 1981, 102, L14.

(11) Ibbotson, D. E.; Wittig, T. S.; Weinberg, W. H. *Surf. Sci.* 1981, 110, 294.

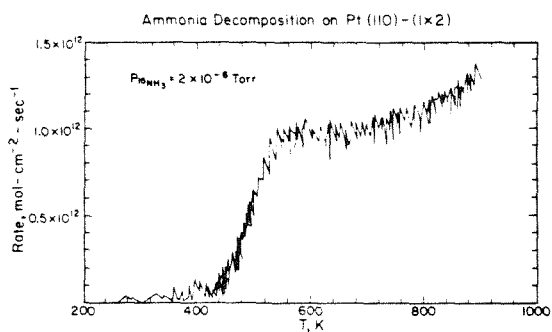


**Figure 1.** Steady-state decomposition of  $^{15}\text{NH}_3$  on Pt(110)-(1  $\times$  2) at  $2 \times 10^{-6}$  Torr. The surface was exposed to a continuous flux of  $^{15}\text{NH}_3$  at an initial temperature of 900 K and then cooled at a rate of 2–3 K/s while recording the  $^{15}\text{N}_2$  mass spectrometric signal.

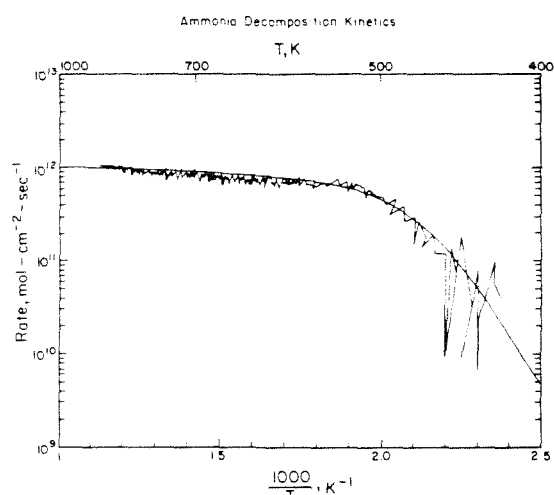


**Figure 2.** Arrhenius plots of the data shown in Figure 1. The continuous line represents the result of model calculations, as discussed in the text.

reaction product) and calibrating the mass spectrometer with the known flux from the capillary array.

Both  $^{15}\text{NH}_3$  (99 atom %  $^{15}\text{N}$ ) and  $^{15}\text{ND}_3$  (99 atom %  $^{15}\text{N}$ , 99 atom % deuterium) were obtained from MSD Isotopes and were used without further purification. Their purities were verified in situ mass spectrometrically.

### 3. Experimental Results

**3.1. Steady-State Decomposition of  $^{15}\text{NH}_3$ .** Absolute reaction rates for the decomposition of  $^{15}\text{NH}_3$  by the Pt(110)-(1  $\times$  2) surface are shown in Figure 1 as a function of temperature at an effective pressure of ammonia of  $2 \times 10^{-6}$  Torr. These data were obtained by exposing the clean surface at 900 K to a continuous flux of  $^{15}\text{NH}_3$ . The surface was then cooled at a rate of 2–3 K/s while recording the  $^{15}\text{N}_2$  mass spectrometric intensity.<sup>12</sup> Identical results were obtained by monitoring the  $\text{H}_2$  product. The data displayed in Figure 1 are shown as a function of reciprocal temperature in Figure 2. In this representation, the two different kinetic regimes, which have been observed previously for ammonia decomposition by platinum,<sup>1–3</sup> are quite evident. For temperatures below approximately 475 K, the apparent activation energy is  $24 \pm 4$  kcal/mol; at higher temperatures, the activation energy decreases, becoming approximately  $1 \pm 1$  kcal/mol for temperatures above 550 K.

(12) The results presented in Figure 1 are independent of cooling rate for rates less than 20 K/s, the highest rate used. This indicates that steady-state rates are established quickly compared to these rates of cooling.

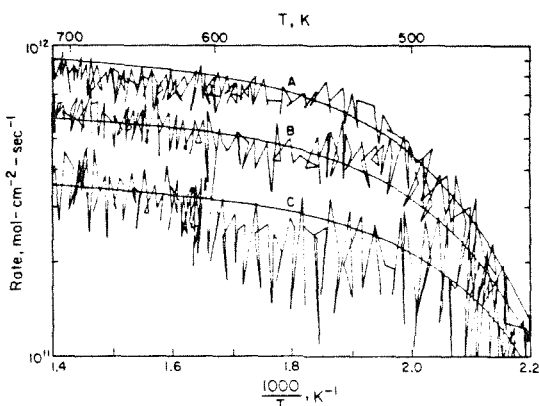


**Figure 3.** Steady-state decomposition of ammonia on Pt(110)-(1  $\times$  2): (A)  $2.6 \times 10^{-6}$  Torr, (B)  $1.7 \times 10^{-6}$  Torr, and (C)  $1 \times 10^{-6}$  Torr. The continuous lines represent the results of model calculations, as discussed in the text.

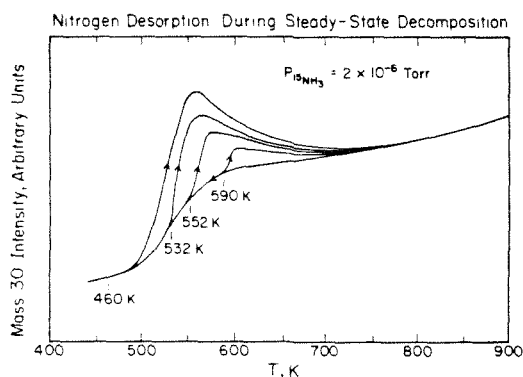


**Figure 4.** Thermal desorption of  $^{15}\text{N}_2$  from Pt(110)-(1  $\times$  2) during the steady-state decomposition of  $^{15}\text{NH}_3$  at  $2 \times 10^{-6}$  Torr. The temperatures indicated in the figure represent the temperatures at which the desorption was begun. The data have been smoothed as a visual aid.

The dependence of the reaction rate on ammonia pressure is shown in Figure 3 for ammonia pressures of  $1 \times 10^{-6}$ ,  $1.7 \times 10^{-6}$ , and  $2.6 \times 10^{-6}$  Torr. For temperatures above approximately 550 K, the dependence of the reaction rate on ammonia pressure is nearly first order, while for temperatures below 500 K the reaction rates begin to converge, approaching zero order in ammonia pressure.

**3.2. Surface Composition and Coverage during Ammonia Decomposition.** The  $^{15}\text{N}_2$  mass spectrometric intensity is shown as a function of temperature in Figure 4 for several cooling and heating cycles during a continuous exposure of the Pt(110)-(1  $\times$  2) surface to  $^{15}\text{NH}_3$  at an effective pressure of  $2 \times 10^{-6}$  Torr. For each cycle, the initial surface temperature was 900 K. The surface was then cooled at a rate of 2–3 K/s to a specified temperature that was maintained for 30 s.<sup>13</sup> Thereafter, the surface temperature was increased at a rate of 5 K/s to 900 K. The cooling part of each cycle reflects the steady-state rate of decomposition of  $^{15}\text{NH}_3$ , as shown also in Figure 1. Each heating curve reflects, however, both the steady-state rate of decomposition and the thermal desorption of nitrogen from the surface.

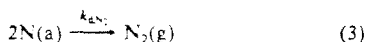
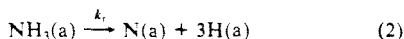
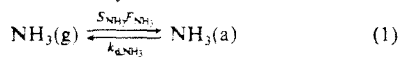
In addition to the monitoring of the production of  $^{15}\text{N}_2$ , as shown in Figure 4, the  $\text{H}_2$  (or  $\text{D}_2$  during the decomposition of  $^{15}\text{ND}_3$ ) mass spectrometric signal was also recorded. For each cycle, only the steady-state rate of decomposition was observed regardless

(13) The surface temperature was held constant to ensure a steady-state rate of decomposition, although steady states are attained much more rapidly; see ref 12.

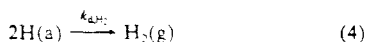
TABLE I: Model Parameters for the Decomposition of Ammonia on Pt(110)-(1 × 2)

symbol	parameter	value	ref
$S_{\text{NH}_3}^0$	ammonia probability of adsorption	1	3
$k_{\text{d,NH}_3}^{(0)}$	ammonia desorption preexponential	$1 \times 10^{14} \text{ s}^{-1}$	3
$k_r^{(0)}$	surface reaction preexponential	$1.3 \times 10^{11} \text{ s}^{-1}$	
$E_r - E_{\text{d,NH}_3}$	difference between surface reaction and desorption activation energies	0.5 kcal/mol	
$k_{\text{d,N}_2}^{(0)}$	nitrogen desorption preexponential	$4 \times 10^{-8} \text{ cm}^2/\text{s}$	
$E_{\text{d,N}_2}$	nitrogen desorption activation energy	24.5 kcal/mol	
$k_{\text{d,H}_2}^{(0)}$	hydrogen desorption preexponential	$3 \times 10^{-4} \text{ cm}^2/\text{s}$	15
$E_{\text{d,H}_2}$	hydrogen desorption activation energy	19 kcal/mol	15

Briefly, this model is based on a series of elementary (or "almost elementary") reactions, namely



and



where  $S_{\text{NH}_3}$  is the probability of molecular adsorption of ammonia,  $F_{\text{NH}_3}$  is the flux of ammonia to the surface, and  $k_{\text{d,NH}_3}$ ,  $k_r$ ,  $k_{\text{d,N}_2}$ , and  $k_{\text{d,H}_2}$  are the rate coefficients of the four surface reactions. Each of these rate coefficients may be written as  $k_i = k_i^{(0)} \times \exp[-E_i/k_B T]$  with (assumed) coverage-independent preexponential factors  $k_i^{(0)}$  and activation energies  $E_i$ .

The steady-state rate of decomposition of ammonia is determined by solving the material balance equation for each adsorbed species. This model description of the measured rates of ammonia decomposition, utilizing the parameters listed in Table I is indicated by the continuous lines in Figures 2 and 3. Obviously, the model accurately describes both the temperature and the pressure dependence of the reaction rate.

The model embodied by eq 1-4 has been used successfully to describe the decomposition of ammonia by polycrystalline platinum at pressures between  $5 \times 10^{-7}$  and 0.5 Torr and temperatures between 400 and 1200 K.<sup>3</sup> Independently measured values were used for the adsorption and desorption rate parameters of ammonia, nitrogen, and hydrogen. To describe the decomposition of ammonia on the Pt(110)-(1 × 2) surface, the values of the initial probability of adsorption of ammonia and the preexponential factors of the rate coefficients for the desorption of both ammonia and nitrogen were the same as those employed previously.<sup>3</sup> The desorption parameters for hydrogen on Pt(110)-(1 × 2) have been measured independently.<sup>15</sup> For the model results shown in Figures 2 and 3,  $E_{\text{d,N}_2} = 24.5$  kcal/mol. However, essentially identical results were obtained with either  $E_{\text{d,N}_2} = 24$  kcal/mol and  $k_{\text{d,N}_2}^{(0)} = 3 \times 10^{-8} \text{ cm}^2/\text{s}$  or  $E_{\text{d,N}_2} = 26$  kcal/mol and  $k_{\text{d,N}_2}^{(0)} = 2 \times 10^{-7} \text{ cm}^2/\text{s}$ . This range of  $E_{\text{d,N}_2}$  was measured directly during ammonia decomposition on Pt(110)-(1 × 2), as shown in Figure 6. This model thus contains two adjustable parameters, namely  $k_r^{(0)}$  and  $E_r - E_{\text{d,NH}_3}$ .<sup>3</sup> The measured rates at high temperatures were described best by  $E_r - E_{\text{d,NH}_3} = 0.5$  kcal/mol. For comparison,  $E_r - E_{\text{d,NH}_3} = 4$  kcal/mol is required to describe the decomposition of ammonia on a polycrystalline platinum wire.<sup>3</sup> The difference in these values reflects the structural sensitivity of ammonia decomposition on platinum, an issue that is discussed in section 4.3.

In addition to the absolute rate of ammonia decomposition, the model embodied by eq 1-4 yields the steady-state coverage of each adsorbed species. As expected, the calculated steady-state coverages of both molecular ammonia and atomic hydrogen are small (<0.01) for all the reaction conditions studied. The calculated fractional surface coverage of nitrogen adatoms as a function of

reciprocal temperature is shown in Figure 5, together with the measured coverage, each at an ammonia pressure of  $2 \times 10^{-6}$  Torr. The agreement between the calculated and the measured steady-state nitrogen coverages is excellent (using the same set of independently determined model parameters). The recombination of nitrogen adatoms is the only reaction that gives rise to molecular nitrogen in this mechanistic model. Therefore, the agreement between the calculated and the measured surface coverages of nitrogen implies that the recombinative desorption of nitrogen is certainly the dominant (and arguably the only) mechanism of nitrogen production.

Vibrationally excited molecular nitrogen with 20 kcal/mol of excess energy has been detected during ammonia decomposition on polycrystalline platinum.<sup>7</sup> This internal excitation was attributed to a recombination reaction involving two adsorbed NH species. However, the observed vibrational energy may alternatively be attributed to the recombination of nitrogen adatoms, if the activation energy for the dissociative adsorption of molecular nitrogen is at least 20 kcal/mol. On the basis of a mechanistic model for the  $\text{NH}_3 + \text{D}_2$  exchange reaction on a polycrystalline platinum wire, the dissociative adsorption of nitrogen is predicted to be an activated process, with an activation energy of approximately 16 kcal/mol in the limit of zero surface coverage.<sup>3</sup> Using model parameters appropriate for a polycrystalline surface, we estimate that the fractional coverage of nitrogen was between 0.3 and 0.5 under the experimental conditions where vibrationally excited nitrogen was detected desorbing from platinum. Postulating that the activation energy for the dissociative adsorption of nitrogen has increased from an initial (zero coverage) value of 16 kcal/mol to  $\geq 20$  kcal/mol at these surface coverages is certainly not unreasonable.

**4.3. Surface Structural Dependence of Ammonia Decomposition on Platinum.** The decomposition of ammonia has been examined previously on a polycrystalline platinum wire that was cleaned by oxidation, reduction, and annealing cycles at 1100 K.<sup>3</sup> Extensive annealing of a polycrystalline platinum ribbon at 1400 K for 12 h has been shown to produce a surface with predominantly (111) orientation.<sup>18</sup> Assuming that the platinum wire consists of (111)-oriented microfacets enables comparisons to be made with the Pt(110)-(1 × 2) surface used in the present study. However, the presence of a large number of defect sites on the "oriented" polycrystalline surface must be considered in any comparison. Under conditions where the surfaces are nearly saturated with nitrogen adatoms, the observed activation energies for the decomposition of ammonia on polycrystalline platinum and Pt(110)-(1 × 2) are  $22 \pm 2^3$  and  $24 \pm 4$  kcal/mol, respectively. Although these values are identical within experimental uncertainties, the best model description of the measured rates was obtained with  $E_{\text{d,N}_2} = 22$  and 24.5 kcal/mol for the polycrystalline platinum and the Pt(110)-(1 × 2) surfaces, respectively. Since the recombinative desorption of nitrogen controls the rate of ammonia decomposition under these conditions, it follows that the desorption of nitrogen at high surface coverages of nitrogen adatoms is, at most, only slightly sensitive to the structure of the platinum surface. Similar results have been obtained for ammonia decomposition on a polycrystalline platinum disk and a Pt(210) surface.<sup>2</sup> The influence of defect sites, which should be less prevalent on the Pt(110)-(1 × 2) surface, is of minor importance during ammonia decomposition under these conditions of high surface coverage. Previously, the activation energy for the dissociative adsorption of nitrogen on a polycrystalline platinum surface was estimated to be 16 kcal/mol.<sup>3</sup> However, the similarity of  $E_{\text{d,N}_2}$  for both the polycrystalline platinum surface and the Pt(110)-(1 × 2) surface does not imply that the activation energies for the dissociative adsorption of nitrogen are also the same on these two surfaces.

When the rate of ammonia decomposition is first order in ammonia pressure (high surface temperatures), the observed activation energies are  $4.2 \pm 0.3$  and  $1 \pm 1$  kcal/mol for the polycrystalline platinum<sup>3</sup> and the Pt(110)-(1 × 2) surfaces, re-

(18) Lambert, R. M.; Comrie, C. M. *Surf. Sci.* 1974, 46, 61.

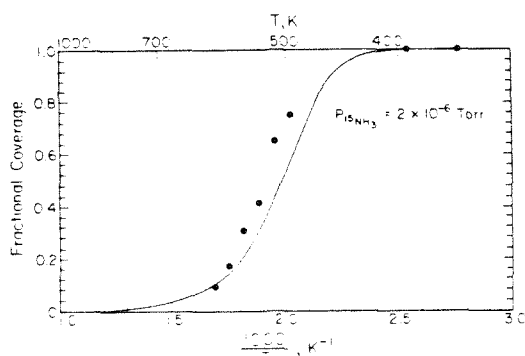
Decomposition of  $\text{NH}_3$  on the Pt Surface

Figure 5. Steady-state fractional coverages of  $^{15}\text{N}$  on  $\text{Pt}(110)-(1 \times 2)$  during the decomposition of  $^{15}\text{NH}_3$  at  $2 \times 10^{-6}$  Torr. The continuous line represents the results of model calculations, as discussed in the text.

of whether the surface was being heated or cooled; i.e., unlike the case of  $\text{N}_2$  shown in Figure 4, no hysteresis was observed for temperatures above 350 K.<sup>14</sup> Since we estimate the mass spectrometric detection limit with this procedure to be less than 0.05 monolayer, the ratio of the steady-state coverage of nitrogen atoms to that of hydrogen atoms on the surface at temperatures between 350 and 600 K is greater than 20:1. This important result clearly establishes that during the steady-state decomposition of ammonia at  $2 \times 10^{-6}$  Torr and above 350 K the most abundant intermediate on the  $\text{Pt}(110)-(1 \times 2)$  surface is nitrogen adatoms.

Since these thermal desorption measurements, carried out during the steady-state ammonia decomposition reaction, showed only nitrogen desorption, the area between each heating and cooling curve (e.g., in Figure 4) is a measure of the concentration of nitrogen adatoms present during the steady-state decomposition of ammonia at the particular temperature where the heating was begun. Steady-state fractional surface coverages of nitrogen for ammonia decomposition at  $2 \times 10^{-6}$  Torr and temperatures between 350 and 600 K were measured in this way and are shown in Figure 5. In order to obtain these fractional coverages, the data were normalized to the saturation coverage of nitrogen adatoms that was obtained at temperatures below 400 K.

A comparison of the fractional coverages of nitrogen shown in Figure 5 with the steady-state reaction rate shown in Figure 2 reveals that the increase in the apparent activation energy observed below approximately 500 K is associated with the accumulation of nitrogen on the surface. Hence, as the fractional coverage of nitrogen approaches unity, the recombinative desorption of molecular nitrogen controls the rate of the ammonia decomposition reaction and the observed activation energy is the activation energy for the desorption of nitrogen. With selection of an initial temperature at which the surface is saturated with nitrogen (i.e., below 400 K) and variation of the heating rate from 3 to 25 K/s, the activation energy of the desorption rate coefficient of nitrogen may be evaluated as a function of fractional nitrogen coverage. For a rapidly pumped system (in which the rate of pumping is much greater than the rate of desorption), the desorption rate is proportional to the partial pressure (i.e., the ion current of the mass spectrometer) and the coverage at any point in a desorption spectrum may be obtained from the time-integrated product signal. With variation of the heating rate with a constant initial coverage, i.e., a particular steady-state temperature, the spectra can be used to construct Arrhenius plots of the desorption rate at constant coverages of which the slope is  $-E_{\text{a},\text{N}_2}(\theta_{\text{N}})/k_{\text{B}}$ .<sup>16</sup> With this procedure, the activation energy for the desorption of nitrogen from the  $\text{Pt}(110)-(1 \times 2)$  surface during the ammonia

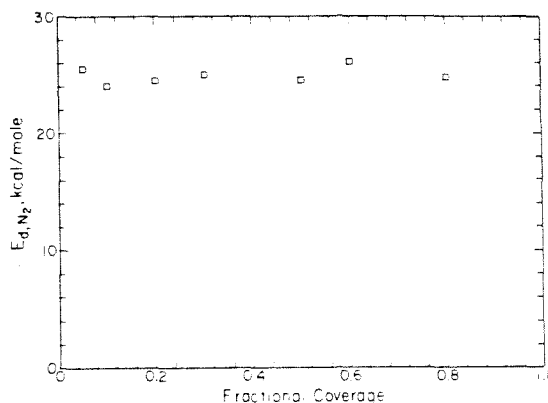


Figure 6. Activation energy as a function of coverage for the thermal desorption of  $^{15}\text{N}_2$  from  $\text{Pt}(110)-(1 \times 2)$ , determined by varying the heating rate from 3 to 25 K/s at an initial temperature of 400 K during the steady-state decomposition of  $^{15}\text{NH}_3$  at  $2 \times 10^{-6}$  Torr.

decomposition reaction has been measured and is shown as a function of fractional nitrogen coverage in Figure 6. It is apparent that this activation energy is 24–26 kcal/mol and is independent of nitrogen coverage. The preexponential factor of the desorption rate coefficient of nitrogen is approximately  $4 \times 10^{-8}$   $\text{cm}^2/\text{s}$ .

#### 4. Discussion

##### 4.1. Surface Composition during Ammonia Decomposition.

The thermal desorption measurements conducted during the steady-state decomposition of ammonia on the  $\text{Pt}(110)-(1 \times 2)$  surface at  $2 \times 10^{-6}$  Torr show clearly that nitrogen adatoms are the dominant surface species over the entire range of temperatures studied. For steady-state reaction temperatures below 400 K, the nitrogen overlayer corresponds to essentially saturation coverage.<sup>17</sup> At higher reaction temperatures, the steady-state fractional coverage of nitrogen decreases, becoming less than 0.1 for temperatures above 600 K. The steady-state concentrations of adsorbed species such as  $\text{NH}$  or  $\text{NH}_2$  are at least a factor of 20 lower than that of nitrogen adatoms for temperatures above 350 K. This result is consistent with the LIF measurements described in section 1.<sup>8</sup> Although the desorption of  $\text{NH}$  radicals from a platinum wire was observed during the steady-state decomposition of ammonia at 1200–1400 K and 0.1 Torr, the concentration ratio of  $\text{N}(\text{a})$  to  $\text{NH}(\text{a})$  was estimated to be  $>10:1$ .

The activation energy for the recombinative desorption of molecular nitrogen from the  $\text{Pt}(110)-(1 \times 2)$  surface during the steady-state decomposition of ammonia was found to be 24–26 kcal/mol, which agrees with the observed activation energy of  $24 \pm 4$  kcal/mol for the steady-state decomposition of ammonia under conditions where the fractional surface coverage of nitrogen approaches unity, cf. Figures 2 and 5. Moreover, both of these values agree with the activation energy of  $24 \pm 2$  kcal/mol for the thermal desorption of nitrogen, determined independently, following the dissociative adsorption of ammonia at 400 K.<sup>15</sup> In these experiments, the surface was cooled to 300 K and the system evacuated prior to the thermal desorption measurements. These results imply that when the surface concentration of nitrogen adatoms approaches saturation, the desorption of nitrogen controls the rate of ammonia decomposition.

4.2. Mechanistic Modeling. A microscopic description of the catalytic decomposition of ammonia on a polycrystalline platinum surface has recently been presented and discussed in detail.<sup>3</sup>

(14) If the surface was cooled to below 300 K during exposure to  $^{15}\text{NH}_3$  and subsequently heated, a small thermal desorption peak of  $\text{H}_2$  was observed near 300 K. This is due entirely to hydrogen desorption from the  $\text{Pt}(110)-(1 \times 2)$  surface and is unrelated to any adsorbed  $\text{NH}_x$  species.<sup>15</sup>

(15) Tsai, W.; Vajo, J. J.; Weinberg, W. H., in preparation.

(16) Taylor, J. L.; Weinberg, W. H. *Surf. Sci.* **1978**, *78*, 259.

(17) The kinetic parameters for the desorption of molecular ammonia and hydrogen from the  $\text{Pt}(110)-(1 \times 2)$  surface have been measured independently.<sup>15</sup> On the basis of these results, the steady-state fractional coverages of both molecular ammonia and hydrogen adatoms at temperatures near 400 K and an ammonia pressure of  $2 \times 10^{-6}$  Torr are predicted to be  $<10^{-3}$ , i.e., approximately 3 orders of magnitude lower than the measured coverage of nitrogen.

spectively. Using the measured range of 0–2 kcal/mol for the activation energy for ammonia decomposition on Pt(110)-(1 × 2) yields a reaction probability of  $(1-2.8) \times 10^{-3}$  at  $1/T = 0$ . The measured reaction probability at  $1/T = 0$  for the polycrystalline platinum surface is  $(2.4-3.3) \times 10^{-3}$ .<sup>3</sup> On the basis of the model embodied by eq 1–4, the rate of ammonia decomposition in this regime is controlled by a competition between the rate of cleavage of an N–H bond and the rate of desorption of molecularly adsorbed ammonia. The observed activation energy is therefore given by  $E_r - E_{d,NH_3}$ .<sup>3</sup> Values for  $E_r$  and/or  $E_{d,NH_3}$ , individually accurate to within the measured difference in activation energy of approximately 3 kcal/mol, are not available. Thus a determination of the relative contributions from changes in  $E_r$  and/or  $E_{d,NH_3}$  is precluded. The observed difference in activation energies and the similarity of the reaction probabilities at  $1/T = 0$  indicate, however, that for finite temperatures ( $1/T > 0$ ) where the rate of decomposition is linearly dependent on ammonia pressure the reaction probability on the Pt(110)-(1 × 2) surface is greater than that on the polycrystalline surface. For example, at  $2 \times 10^{-6}$  Torr and 800 K, the reaction probabilities are  $1.6 \times 10^{-3}$  and  $2.0 \times 10^{-4}$  on the Pt(110)-(1 × 2) and the polycrystalline platinum surfaces, respectively.

##### 5. Synopsis

The results of this study may be summarized as follows:

1. The steady-state decomposition kinetics of ammonia on Pt(110)-(1 × 2) are qualitatively similar to those observed on a polycrystalline platinum surface. Under conditions where the reaction rate is linearly dependent on ammonia pressure, the observed activation energy is  $1 \pm 1$  kcal/mol. For conditions where the rate of decomposition becomes independent of ammonia pressure, the observed activation energy increases to  $24 \pm 4$  kcal/mol.

2. Nitrogen adatoms are the predominant surface species during ammonia decomposition at  $2 \times 10^{-6}$  Torr. For temperatures below 400 K, the Pt(110)-(1 × 2) surface is saturated with nitrogen adatoms. At higher temperatures, the fractional coverage of nitrogen adatoms decreases, becoming  $< 0.1$  for temperatures above 600 K.

3. The mechanistic model developed previously for the decomposition of ammonia on a polycrystalline platinum wire<sup>3</sup> describes accurately the pressure and temperature dependence of the reaction rate and the measured steady-state coverage of nitrogen adatoms on the Pt(110)-(1 × 2) surface.

4. The recombinative desorption of nitrogen is the major reaction mechanism producing molecular nitrogen during ammonia decomposition at  $2 \times 10^{-6}$  Torr.

*Acknowledgment.* This research was supported by the National Science Foundation under Grant No. CHE-8516615.

**Appendix 5.**

Data Acquisition and Real-time Control Computer Station

An IBM-XT system with a Data Translation 2805 12-bit A/D board was used to automate the routine of data acquisition and real-time control of experimental variables such as substrate temperature and mass flow rate of gaseous reactants. A list of the developed software are as follows:

- [1]. AUGER.FOR - automation of routine Auger spectra acquisition.
- [2]. DA.FOR - function as a 2 channels preselected voltage output (channel 0-1 jumpered at 0 to +10V).
- [3]. AD.FOR - function as an 8 channels meter for measuring input voltage (differentially bipolar jumpered, channel 2- +/- 1V gain of 10, channel 1- +/- 10V gain of 1).
- [4]. TDMS.FOR - automation of temperature control of the substrate (linear ramp and step) as well as data acquisition of thermocouple and mass spectrometer (M.S.) signals). Software require system characterization as well as optically-isolated programmable power supply.
- [5]. MASS.FOR - automation of data acquisition of any two system variables (eg, M.S. and temperature) without feedback control. Users are allowed to select the time-step and total duration.
- [6]. WORK.FOR - automation of data acquisition for work function measurement.
- [7]. SCAN.FOR - automation of background scanning for M.S. as well as sweeping of the electron multiplier.
- [8]. TMMS.FOR - automation of frequency response measurement of the sinusoidal perturbation experiment.
- [9]. XPS.BAS - automation of XPS spectra acquisition & analysis utilizing Metrabyte CTM-05 pulse counter interface.

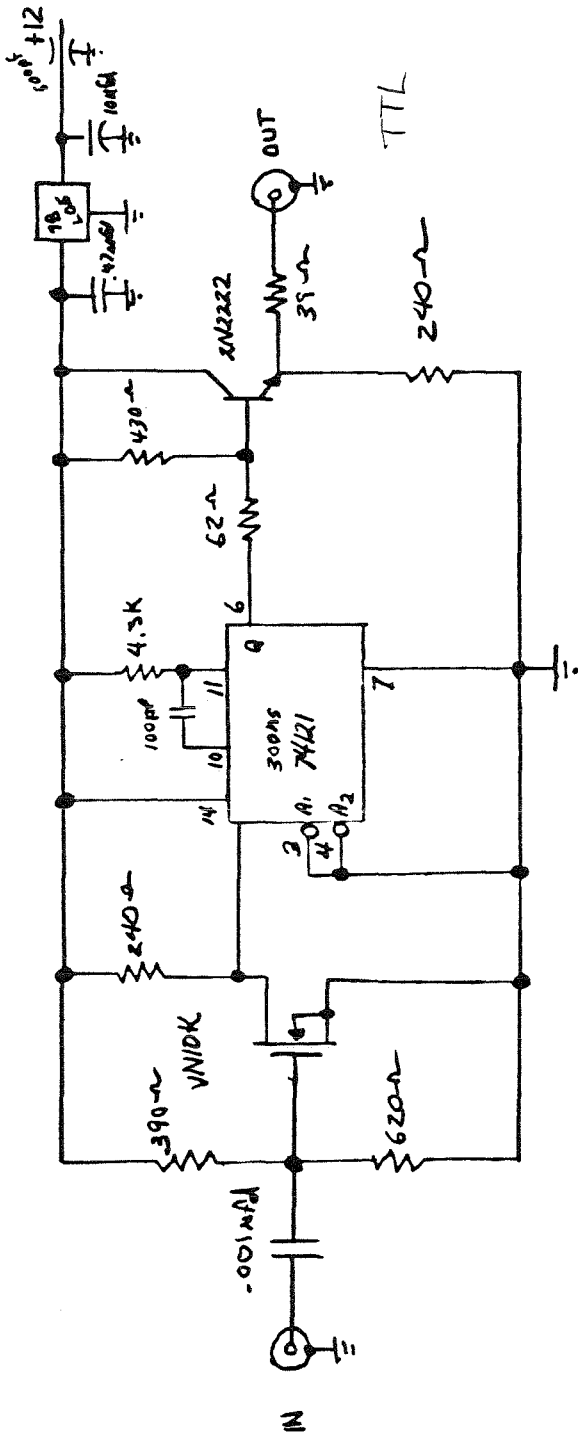
Further features of the supporting software under MS-DOS are:

- [10]. MSKERMIT.EXE - function as a fast transfer of data as well as binary codes through the CIT-NETWORK
- [11]. V.BAT & VAX.EXE - same

as above except incorporating an high resolution graphics features for xhmeia using the Hercules Graphics card. [12]. PLOT.EXE - graphics software for data plotting.

The central development of the IBM-XT working station is the series of 8088 assembler program and subroutines that were used in the actual interfacing of the DT 2805 and the CTM-05. For instances, routine XAV function as a single channel A to D conversion at about 1 MHz turn over frequency. XDV function as a single channel D to A conversion. Multi-channels using Direct Memory Access are also available for high speed scanning.

In addition, an IBM-XT interfaced pulse counter system was constructed via utilizing a Metrabyte CTM-05 (5 channel counter-timer interface) and the Princeton SSR model 1120 amplifier/discriminator. The power supply of the 1120 is placed in a separate module which deliver a 12.5V, 60mA output. The sensitivity of the discriminator is up to 2mV for a minimum width of 300ns pulse with the threshold level set at the maximum sensitivity. The digitized ECL output is then transformed into a TTL logic through a level converter (see Schematics) before entering the CTM-05 counter. An basic-8086 assembler program is written for the direct counting of the signal pulses as well as the actual data acquisition of the XPS spectra (see XPS.BAS). Moreover, a Metrabyte DAC-02 board is used for the creation of the necessary voltage ramp for the energy scanning.



TTL LEVEL  
CONVERTER  
T DUNN  
1284